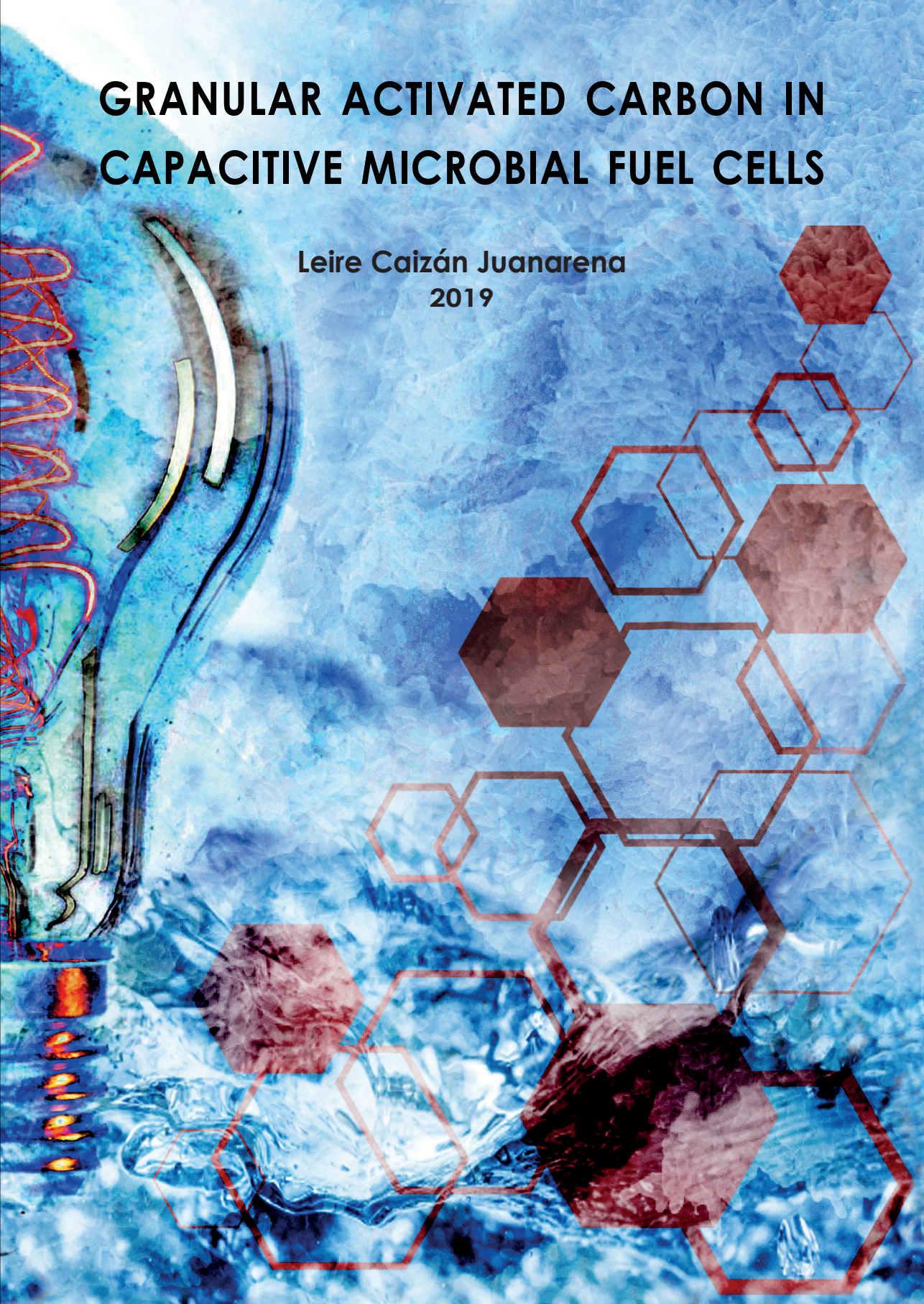


GRANULAR ACTIVATED CARBON IN CAPACITIVE MICROBIAL FUEL CELLS

Leire Caizán Juanarena
2019



Propositions

1. The study of single activated carbon granules cannot predict their performance on up-scaled reactors.
(this thesis)
2. Bacterial activity, rather than electrode properties, determines the performance of capacitive bioanodes.
(this thesis)
3. A good research question saves time and money.
4. Complex scientific research can only be explained in a simplified way when well understood.
5. Scientific research is often driven by *fashionable* topics.
6. Surrounding yourself with people who challenge you is crucial for personal development and self-improvement.
7. The illusion of choice is a delusion of freedom.

Propositions belonging to the thesis, entitled
“Granular Activated Carbon in Capacitive Microbial Fuel Cells”

Leire Caizán Juanarena

Wageningen, 14 June 2019

Granular Activated Carbon in Capacitive Microbial Fuel Cells

Leire Caizán Juanarena

Thesis committee

Promotor

Prof. Dr C.J.N. Buisman

Professor of Biological Recovery and Reuse Technology

Wageningen University & Research

Co-promotor

Dr A. ter Heijne

Assistant Professor, Department of Environmental Technology

Wageningen University & Research

Other members

Prof. Dr A.J.M. Stams, Wageningen University & Research

Dr A.W. Jeremiasse, MAGNETO Special Anodes B.V., Schiedam

Dr F. Harnisch, Helmholtz Centre for Environmental Research- UFZ, Germany

Dr M.A. Pereira, University of Minho, Portugal

This research was conducted under the auspices of the Graduate School for Socio-Economic and Natural Sciences of the Environment (SENSE).

Granular Activated Carbon in Capacitive Microbial Fuel Cells

Leire Caizán Juanarena

Thesis

submitted in fulfilment of the requirements for the degree of doctor
at **Wageningen University**

by the authority of the Rector Magnificus,

Prof. Dr A.P.J. Mol,

in the presence of the

Thesis Committee appointed by the Academic Board

to be defended in public

on Friday 14 June 2019

at 11 a.m. in the Aula.

Leire Caizán Juanarena

Granular Activated Carbon in Capacitive Microbial Fuel Cells, 198 pages.

PhD thesis, Wageningen University, Wageningen, the Netherlands (2019).

With references, with summaries in English, Spanish and Basque.

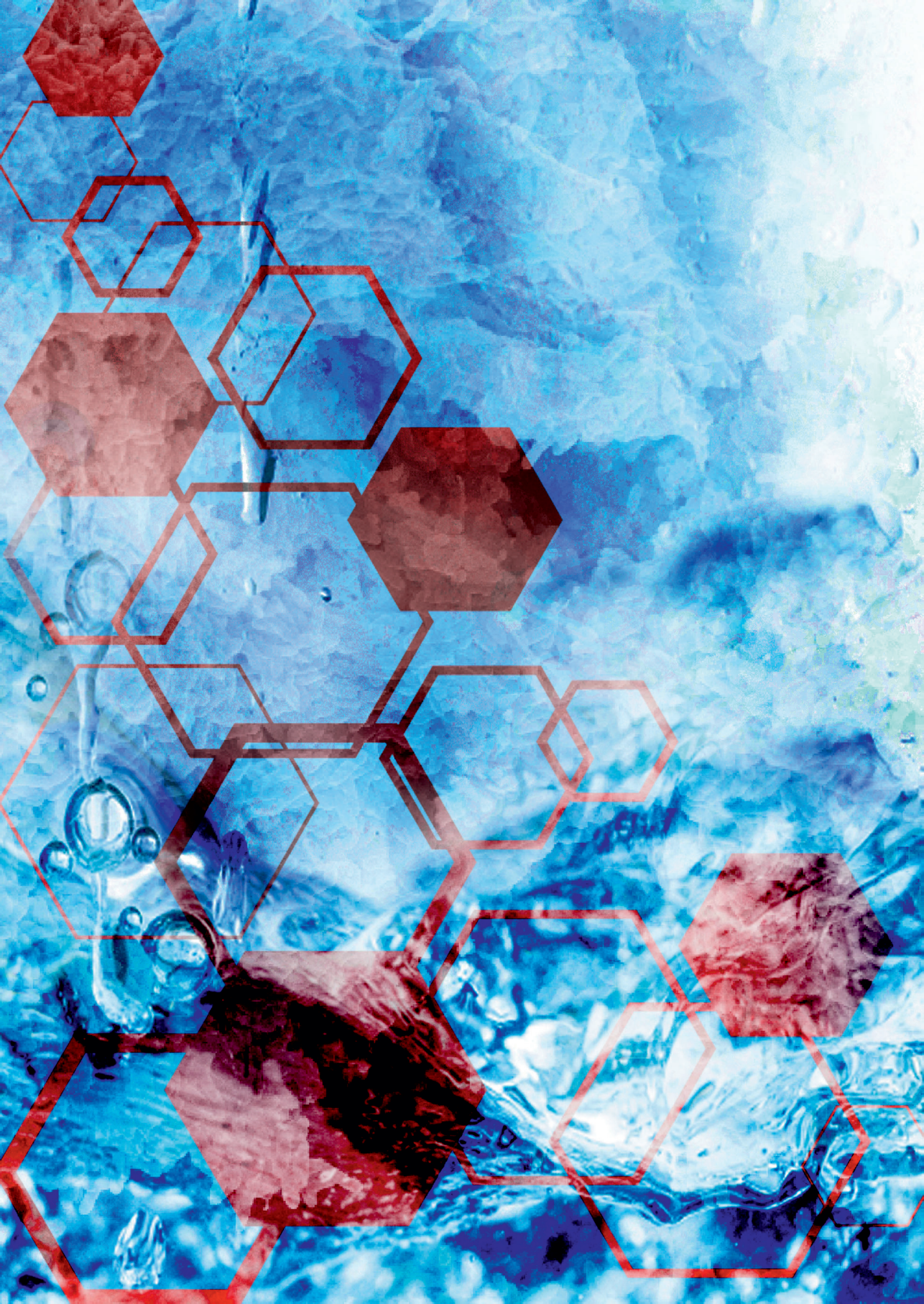
ISBN: 978-94-6343-978-7

DOI: <https://doi.org/10.18174/477215>

Nire gurasoei

Table of Contents

Chapter 1	General Introduction	9
Chapter 2	Combination of bioelectrochemical systems and electrochemical capacitors: Principles, Analysis and Opportunities	29
Chapter 3	Electrochemical and microbiological characterization of single carbon granules in a multi-anode Microbial Fuel Cell	55
Chapter 4	3D biofilm visualization and quantification on granular bioanodes with Magnetic Resonance Imaging	77
Chapter 5	Screening for electrical conductivity in anaerobic granular sludge from full-scale wastewater treatment plants	101
Chapter 6	General Discussion	121
References		149
Summary/Resumen/Laburpena		181
Acknowledgments		195



Chapter 1

General Introduction



1. Renewable energy

Fossil fuels such as oil, coal and natural gas are nowadays the major suppliers of energy worldwide, with a contribution of about 81.4% in 2015 (International Energy Agency, 2017). However, the rising world energy consumption, the depletion of fossil fuels and the increasing environmental concerns have led to the necessity of alternative energy sources that are clean and renewable. Energy obtained from natural sources such as solar, wind, water, geothermal or biomass would meet those criteria (Ellabban et al., 2014). According to the International Renewable Energy Agency, energy from biomass (i.e. bioenergy, either as solid, liquid or gaseous fuel) is the responsible for half of the renewable energy consumption, four times more than solar photovoltaic (PV) and wind combined in 2017 (International Energy Agency, 2018). In the same year, renewable energy contributed to three main sectors: 24% to electricity production, 10% to air/water heating and 3% to transportation (fuels) (International Energy Agency, 2018). Energy supply and climate change are two of the sustainable development goals the European Union to be tackled in the coming years (European Commission, 2019). However, only 17% of Europe's total energy consumption comes from renewable energy sources (International Energy Agency, 2018). Therefore, a rapid transition needs to take place from fossil fuels towards the implementation of renewable energy. The energy transition will come along with a socio-technical transition, where the existence of a diversity of new technologies need to be stimulated in order to compete with well-established technologies (Papachristos, 2017).

The research in relation to renewable energy covers many different aspects, including the search for novel sources, assessment of sustainability, production methods, management, energy storage, and others (Jha et al., 2017). Specially energy storage is an important issue that the renewable energy sector faces, as electricity produced from renewable sources like sun and wind is difficult to predict, variable in time and depends on the weather conditions (Andoni et al., 2019). Another aspect to consider is the optimized use of resources, which is necessary to reduce the carbon footprint and emission of greenhouse gases (GHG). In this context, the concept of circular economy is gaining much attention, where the main goal is to close the lifecycle of materials and products (Tomić & Schneider, 2018). Using biomass from waste streams can be a solution to close energy, water and nutrient cycles (Wielemaker et al., 2018) and provides a solution for the waste biomass produced in cities, such as municipal solid waste, urban green residues or food processing waste (Jiang et al., 2017). Additionally, one of the largest renewable energy contributors, i.e. bioenergy, is mainly produced from first generation biofuels (e.g. starch, sugar, animal fats, vegetable oil), which comes along with low conversion efficiencies, large need for transportation and fuel-food competition of crops (Gasparatos et al., 2013). Therefore, extracting energy from waste streams is of great importance, as it is the case of wastewater, explained in the following section (Mo & Zhang, 2013).

2. Wastewater

Wastewater from industries (food and beverage, textile), agriculture (irrigation, brines) and households (urine, faeces, kitchen waste) are valuable sources of energy as they contain compounds such as organics (measured as chemical oxygen demand or COD) and nutrients (N, P, K) that can be recovered or converted into valuable products (e.g. methane, chemicals). The ultimate goal of wastewater treatment is to achieve a high-quality water output that will allow for its remediation and reuse (as e.g. drinking water, irrigation, industry), but also to protect water resources, the environment and public health (Almuktar et al., 2018). For example, an excess of nutrient (N, P) discharge to the environment can cause eutrophication, an excess of algae growth and consequently oxygen depletion in water (Nixon, 1995). Removing polluting components from wastewater is therefore essential, and when this process is combined with the reuse and formation of valuable products, wastewater changes from waste stream into resource. As an example, the nutrients present in the wastewater from households (domestic wastewater) in the Netherlands could cover 25-59% of the synthetic fertilizer demand in Dutch agriculture, while its COD could cover 59% of the natural gas demand for cooking in the form of methane (Zeeman & Kujawa-Roeleveld, 2011).

However, the composition of the many different wastewater streams is complex and variable, which could condition their treatment and final product. Table 1 is an example of some of the compounds that can be found in different types of wastewater. To use the highest potential from the different waste streams, source-separation based on their composition might be favorable (Zeeman & Kujawa-Roeleveld, 2011). This could be the case for domestic wastewater, which compiles streams from toilet (urine and faeces), water bath and wash water, kitchen waste (solid organics) and rain water (Kujawa-Roeleveld & Zeeman, 2006).

Table 1. A list of some compounds and the type of wastewater where they are present (Tchobanoglous & Burton, 1991).

	COMPOUND	WASTEWATER TYPE
ORGANIC	Carbohydrates	Domestic; Commercial; Industrial
	Fats, oil, grease	Domestic; Commercial; Industrial
	Pesticides	Agricultural
	Phenols	Industrial
	Proteins	Domestic; Commercial; Industrial
	Surfactants	Domestic; Commercial; Industrial
	Volatile components	Domestic; Commercial; Industrial
INORGANIC	Chlorides	Domestic
	Heavy metals	Industrial
	Nitrogen	Domestic; Agricultural
	Phosphorous	Domestic; Commercial; Industrial
	Sulphur	Domestic; Commercial; Industrial

Current wastewater treatment plants (WWTPs) are energy intensive, thus an increase in energy efficiency together with resource recovery (energy generation, water reuse and nutrient recycling) are some of the main improvements needed in WWTPs (Mo & Zhang, 2013). Usually, there is a primary treatment to remove floating and settleable solids that is based on physical operations such as screening and sedimentation. There is also a secondary treatment that includes a biological process and is meant to remove biodegradable organics and suspended solids, aerobically and/or anaerobically (Tchobanoglous & Burton, 1991). The aerobic process is highly efficient for the removal of a large range of pollutants thanks to the formation of activated sludge, which can also trap particles that don't necessarily need to be broken down. However, half of the energy (~ 0.3 kWh per m^3 of wastewater) goes for aeration in the system (McCarty et al., 2011) and the amount of sludge remaining after the treatment is high (over 50% of the COD input in kg), which requires further treatment and thus also economic investment. On the contrary, the anaerobic process (or digestion) does not need aeration and can effectively convert organic pollutants to biogas (a mixture of CH_4 and CO_2), as explained in section 2.1. In this way, biogas production can be the main energy contributor in a WWTP with a reduction of the 40% of its energy consumption (Y. Gu et al., 2017). The major drawbacks of this technology are its highly dependence towards temperature and the high concentration of nutrients (e.g. N and P) in the effluent, which can be even higher than in the influent (Chernicharo et al., 2015). An additional treatment, the so-called tertiary or advanced treatment, which removes compounds of concern (e.g. organics, nutrients, toxics) that are left after the secondary treatment. It is meant to achieve high-quality water, sometimes for specific purposes (e.g. industrial cooling tower, groundwater recharge), and includes very varied treatment technologies such as chemical coagulation or reverse osmosis (Tchobanoglous & Burton, 1991).

Biological treatments that can recover energy from the wastewater treatment process are, among others, anaerobic digestion and microbial fuel cells (MFCs).

2.1. Anaerobic digestion

The best known anaerobic wastewater treatment system is the up-flow anaerobic sludge bed reactor (UASB), developed in the Netherlands in the early seventies (Lettinga et al., 1980). Other forms of anaerobic digesters have also gained popularity, such as the expanded granular sludge bed reactor (EGSB) or internal circulation reactor (IC) (Van Lier, 2008). All these systems are based on microbial granules, i.e. aggregates of microorganisms with a high density, which allow for a high upwards influent flow while retaining a high amount of biomass in the reactor. The combination of high biomass densities and tall reactors allows the treatment of large amount of wastewater on a small surface area, making them ideal for industrial and area-limited applications (Van Lier et al.,

2008). The organic material is biologically converted to a variety of end products, among which the main gaseous compounds are methane (CH_4) and carbon dioxide (CO_2). Figure 1 shows a scheme of all the possible metabolic pathways for anaerobic biological degradation of complex organics. First, these are hydrolyzed to more simple molecules (monomers/oligomers) by fermentative bacteria (a), which further ferment them to low-molecular-weight compounds such as organic acids and alcohols. The production of acetate and hydrogen (H_2) from these intermediates, called acetogenesis, is done by hydrogen-producing acetogenic bacteria (b). Acetogenesis also includes acetate production from H_2 and CO_2 by acetogens and homoacetogens (c). Methanogenesis includes the processes by which hydrogenotrophic acetogens (d) convert H_2 to CH_4 and acetoclastic methanogens (e) convert acetic acid to CH_4 . The former bacteria (c) usually have a syntrophic association with hydrogen-producing acetogenic bacteria (b), as they keep the H_2 partial pressure low and thus thermodynamically favor the acetogenesis. This process is known as interspecies hydrogen transfer (IHT) (Angenent, Karim, et al., 2004). The more complex composition the wastewater has, the more limitation and competitive pathways will be present until more simple molecules are reached (Van Lier et al., 2008).

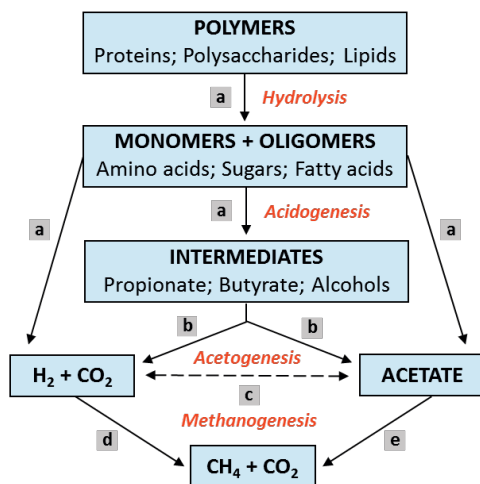


Figure 1. Methanogenic anaerobic digestion of complex organic polymers with the following trophic groups of microorganisms working together: a) fermentative (acidogenic) bacteria; b) hydrogen-producing acetogenic bacteria; c) acetogens and homoacetogens; d) hydrogenotrophic acetogens; and e) acetoclastic methanogens. Figure modified from (Angenent, Karim, et al., 2004).

2.2. Microbial Fuel Cells

A potential alternative to the common biological treatments in WWTPs is the so-called Microbial Fuel Cell (MFC), a technology that extracts electricity from the degradation of organics in wastewater by the use of electrodes catalyzed by bacteria (P. Aelterman et al., 2006; Kim et al., 2010; S. T. Oh et al., 2010; Pant et al., 2012). These bacteria are known

as electrochemically active bacteria or electrogens (see section 3.1). A typical MFC has two electrode compartments (anode and cathode), separated by a membrane, and an external electric circuit. Bacteria are attached to the anode, where they oxidize the organics present in wastewater and simultaneously extract electrons, together with producing protons and CO_2 (see Figure 2). Electrons are transferred from the bacteria to the anode, and then to the cathode via an external circuit (harvested as electricity). Protons and other positively charged ions pass through the membrane and react with electrons and final electron acceptors in the cathode (Du et al., 2007; Santoro, Arbizzani, et al., 2017; Slate et al., 2019). Usually acetate oxidation in the anode is combined with oxygen reduction in the cathode, giving a theoretical working cell voltage of 1.1 V (vs NHE) (Rozendal et al., 2008). The combination with H_2 production in the cathode is also possible, requiring external power, which is commonly known as a Microbial Electrolysis Cell (MEC) (Call & Logan, 2008; Heidrich et al., 2013).

Different electrode materials can be used in the anode and in the cathode, such as metals (e.g. stainless steel, titanium, platinum) or carbon electrodes (e.g. graphite, carbon brush). Especially carbonaceous materials are widely used in MFC anodes as they have good biocompatibility and chemical stability, high conductivity and low cost (Call & Logan, 2008). Chemical and physical properties of electrode materials is of great importance, as they will determine crucial processes in MFCs such as microbial attachment, electron transfer or electrode surface reactions (Heidrich et al., 2013). For example, it has been proven that a larger electrode surface area can increase microbial attachment and MFC power densities (Di Lorenzo et al., 2010). Membranes are beneficial for MFCs, as there is no cross-contamination of compounds (e.g. acetate, hydrogen, oxygen) between the anode and cathode chambers that might lead to pollution of the system and reduction of electron recovery (i.e. Coulombic efficiency). Therefore, in terms of efficiency, it is better to include a membrane, even though it represents one of the most expensive constituents of an MFC (Rozendal et al., 2008).

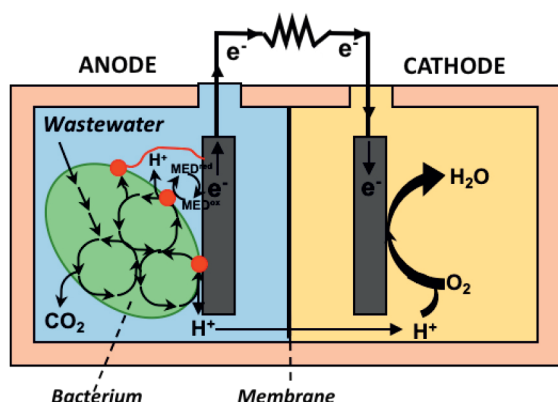


Figure 2. A conventional MFC for wastewater treatment with the different electron transfer mechanisms between bacteria and electrode. Modified from (Logan et al., 2006).

As previously seen, wastewater is a mixture of several compounds and can carry some toxic substances for bacteria (H_2S , heavy metals). Therefore, in the same way as for anaerobic digestion, a pre-treatment previous to the MFC may be necessary to remove toxic materials but also fats and solids that are not degradable by the bacteria. In addition, complex wastewater comes along with a wide diversity of microorganisms with different metabolic pathways as those shown in Figure 1. Microorganisms that are not effective in current production may negatively influence MFC performance, especially when they are attached to the anode surface. Production of methane, for example, will compete for the hydrogen and acetate with electrogens and can hinder the production of current and overall power output of the MFC (Lovley, 2008; Rozendal et al., 2008). In fact, it has been observed that the performance of MFCs with wastewaters is lower than that with water of pure components (Van Ginkel et al., 2005), and that low substrate loading rates are preferable to avoid microbial competition (Sleutels et al., 2016). In order to be able to focus on certain important factors of MFCs, such as electrode properties or cell design, the use of real wastewater not recommended but instead pure compounds such as acetate and optimum conductions like high ionic conductivity.

Compared to conventional wastewater treatment, MFC can recover the chemical energy from wastewater without demanding energy for aeration (Rabaey & Verstraete, 2005), reducing sludge production (Pham et al., 2009) and can work at low COD loading rates (Pham et al., 2006). It also produces electricity directly, and not through intermediate components as it is the case for CH_4 . The power output of a MFC is the product of cell voltage (E_{cell}) and current (I) (Sleutels et al., 2012), while for anaerobic digestion power output is the result of methane production and its combustion efficiency to electricity (Ter Heijne et al., 2011). MFCs are considered to be a promising and energy-efficient technology for wastewater treatment (H. Liu et al., 2004; Rabaey & Rozendal, 2010; Rozendal et al., 2008), where COD removal efficiencies and the ability to produce a clean water effluent is of utmost importance. Table 2 gives an overview of the performance of activated sludge (aerobic treatment), anaerobic digestion and MFCs in terms of loading rates, removal efficiencies, sludge production, nutrient removal and energy balance.

Table 2. Performance and efficiencies in three different wastewater treatments. Volumes refer to the reactor volume. ¹(Rozendal et al., 2008); ²(Rabaey & Verstraete, 2005); and ³(Van Lier et al., 2008).

	Volumetric loading rate (kg COD m ⁻³ day ⁻¹)	Sludge production	Nutrient removal	Energy consumption (kWh kg ⁻¹ COD)	Energy production (kW m ⁻³)	COD removal efficiency
Activated sludge	0.5 – 2 ¹	High	High	1 (aeration) ³	-	High
Anaerobic digestion	10 – 20 ²	Low	Low	Low	0.5 - 1 (CH ₄) ²	Low
Microbial Fuel Cell	0.1 – 10 ²	Low	Low	Low	0.01 1.25 ²	Low

3. Performance of MFCs

3.1. Electrochemically active bacteria

Electrochemically active bacteria (EAB) are microorganisms capable of extracellular electron transfer (EET), which can occur in different manners: i) indirectly, via mediators (small, redox reactive molecules) that can ‘shuttle’ electrons from the bacteria to the electrode, and ii) directly, via membrane proteins such as cytochromes or other redox active components like conductive pili (i.e. nanowires) (Cheng Li et al., 2017). In 1911, M.C. Potter was the first to discover the ability of bacteria to transfer electrons, and since then many studies and technologies have made use of it. One example are MFCs, where EAB colonize the anode electrode to form the so-called bioanode. Here, electrons are transferred from the bacteria to the solid surface as shown in Figure 2 (Lovley, 2008; Pham et al., 2009). *Geobacter spp.*, the most studied species growing in the anode, has proven to use the electrode as the final electron acceptor by direct electron transfer mechanisms (DIET), i.e. without any mediator (Bond & Lovley, 2003; Koch & Harnisch, 2016). While in bioanodes electron transfer occurs in the micro-meter scale, long distance electron transfer (in the order of centimeters) has also been observed in marine sediments by filamentous bacteria (Malvankar et al., 2015; Pfeffer et al., 2012). Microorganism can also be present in the cathode, forming a biocathode, which have shown to enhance oxygen reduction reaction (ORR) in MFCs and to carry several reduction reactions (e.g. H_2 or CH_4 formation) in other bioelectrochemical systems (BESs). Nevertheless, the electron transfer mechanism from the cathode to the microorganisms is not completely understood and several possible pathways are under discussion (Patil et al., 2012; Villano et al., 2010).

Another place where EAB are present and that is recently taking more attention is in anaerobic granular sludge. During the anaerobic digestion of wastewater treatment, microbial aggregates are being formed, which are mainly composed of syntrophic microorganisms able to degrade the complex substrates present in the wastewater. Therefore, the formation of granular sludge does not only give advantages in terms of settleability but also allows for physically close metabolic pathways that can perform interspecies electron transfer (IET) (Stams et al., 2006; Stams & Plugge, 2009). Figure 3 shows a scheme where the degradation of complex organics in such aggregates occur. The most common and well-described IET mechanism is by means of soluble molecules (mediators), such as H_2 , formate or other electron shuttles (e.g. flavins), which can be transferred from some microbial species to others. However, DIET has recently being proposed as an alternative mechanism, meaning microorganisms can transfer electrons directly via pili (nanowires), cytochromes or conductive materials (e.g. minerals) within the aggregates (Dubé & Guiot, 2015; Shrestha et al., 2013). Apart from *Geobacter spp.* present in anaerobic granules, some methanogens that are the ultimate electron acceptors for the production of methane in anaerobic digestion have been shown to perform DIET (Rotaru, Shrestha, Liu, Shrestha, et al., 2014; Wegener et al., 2015). The research on determining

electron transfer mechanisms between microorganisms in anaerobic granular sludge is generally done in experimental settings with pure substrates and microbial strains and under very controlled environmental conditions. Electrical conductivity (Cheng Li et al., 2017) and the microbial community (Shrestha et al., 2014) are parameters that have been related to DIET in anaerobic granular sludge.

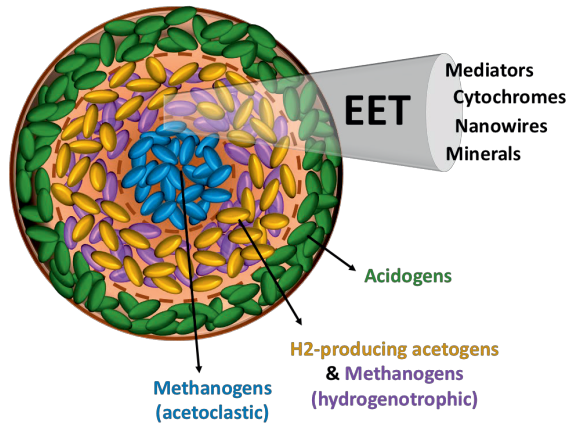
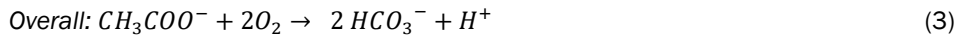
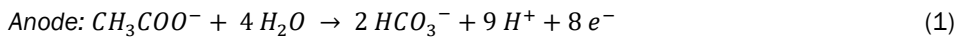


Figure 3. A representation of an anaerobic granule formed in anaerobic wastewater treatment that can degrade complex organics by the use of a varied range of microbial community. Interspecies electron transfer (IET) occurs among the syntrophic communities within the granule. Modified from (Dubé & Guiot, 2015).

3.2. Electrochemical reactions

The reactions at the anode and cathode determine the thermodynamics in MFCs. The energy recovery of the cell in the form of electricity will depend on the potential difference between the bioanode (lower) and the cathode (higher). The reactions occurring in the cell are presented based on acetate as the simplified substrate in the anode (Eq. 1), and oxygen reduction in the cathode (Eq. 2), which is the most common reaction. Combining these two reactions, the overall redox reaction in MFCs is obtained (Eq. 3).



The Gibbs free energy (ΔG_r , r standing for reaction) is the maximum energy that can be extracted from a thermodynamically closed system. In the case of an MFC, the Gibbs free energy is negative ($\Delta G_r = -847.60 \text{ kJ mol}^{-1}$) and the reaction is spontaneous, meaning that energy is released (Rozendal et al., 2008). It can be calculated as in Eq. 4, where ΔG^0_r is the Gibbs energy under standard conditions ($T = 298 \text{ K}$, 1 bar pressure and 1 M concentration of all species) and R is the gas constant ($8.314 \text{ J K}^{-1} \text{ mol}^{-1}$).

$$\Delta G_r = \Delta G^0_r + RT \ln \frac{[\text{HCO}_3^-]^2 [\text{H}^+]}{p\text{O}_2 [\text{CH}_3\text{COO}^-]} \quad (4)$$

However, the amount of energy produced from the chemical reaction in MFCs is better expressed as the overall electromotive force (E_{emf}), measured in volts, which is calculated from the Gibbs energy as follows:

$$E_{\text{emf}} = -\frac{\Delta G_r}{nF} \quad (5)$$

Where n is the number of electrons per mol reaction and F is the Faraday's constant (96485 C mol^{-1}). Now, this E_{emf} can be calculated as reduction potentials for the anode (written as reduction reaction) and cathode separately, combining equation 4 and 5 (see below).

$$E_{\text{an}} = E_{\text{an}}^0 - \frac{RT}{nF} \ln \frac{[\text{CH}_3\text{COO}^-]}{[\text{HCO}_3^-]^2 [\text{H}^+]^9} \quad (6)$$

$$E_{\text{cat}} = E_{\text{cat}}^0 - \frac{RT}{nF} \ln \frac{1}{p\text{O}_2 [\text{H}^+]^8} \quad (7)$$

The standard electrode potentials (vs NHE) are $+0.187 \text{ V}$ for the anode and $+1.229 \text{ V}$ for the cathode. However, the resulting electrode potentials under specific conditions are -0.296 V for the anode (assuming 5 mM of HCO_3^- and CH_3COO^- , and $\text{pH}=7$) and $+0.805 \text{ V}$ for the cathode (assuming $p\text{O}_2 = 0.2$ and $\text{pH}=7$). This results in a cell voltage of 1.1 V , calculated in Eq. 8, which is usually presented as the maximum cell voltage to achieve in an MFC with these electron donor and acceptors.

$$E_{\text{emf}} = E_{\text{cat}} - E_{\text{an}} = 0.805 \text{ V} - (-0.296 \text{ V}) = 1.101 \text{ V} \quad (8)$$

3.3. Main limitations

3.1.1. Overpotentials

As seen in the previous section, bacteria can gain energy from the transfer of electrons from a reduced substrate (e.g. acetate) with a lower potential than the oxidizing agent (e.g. the electrode or O_2). Depending on the substrate, the oxidation potentials will vary and thus the theoretical cell voltage (E_{emf}) as shown in Eq. 8. The larger the potential difference between the electron donor (anode) and acceptor (cathode), the more energy can be extracted in MFCs. However, the practical cell voltage is usually far from the theoretical one (around 0.6 to 0.8 V) as consequence of the many resistances within the cell, which

translates into potential losses. On the one hand, overpotentials refer to potential losses occurring in each of the electrodes, as consequence of mass-transfer and charge-transfer resistances. In the case of bioanode, there are also resistances related to the growth and maintenance of bacteria that can cause overpotentials. On the other hand, there are potential losses at other parts of the cell, such as ionic loss due to ionic resistances in the anode and the cathode electrolytes, or transport loss across the membrane due to ion transport resistances (pH gradient). Figure 4 illustrates the overpotentials (η) and potential losses (E_{ion} and E_{tran}) that can be found in an MFC. By reducing them, the voltage efficiency can increase, leading to an increased cell voltage and also power output (Sleutels et al., 2009).

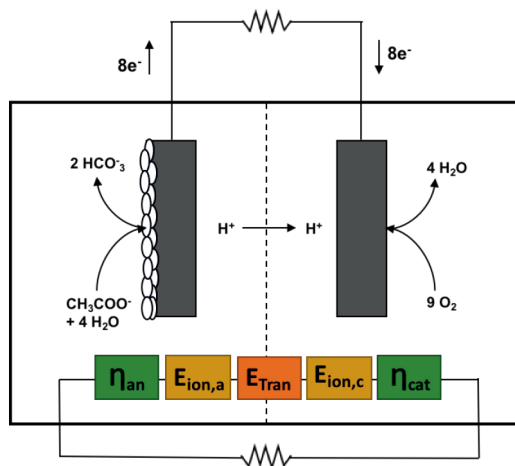


Figure 4. Overpotentials occurring in an MFC. η_{an} = anode overpotential; $E_{\text{ion,a}}$ = ionic loss in the anode; E_{tran} = transport losses through the membrane; $E_{\text{ion,c}}$ = ionic loss in the cathode; and η_{cat} = cathode overpotential. Modified from (Sleutels et al., 2009).

3.1.2. Low power output

The power output reported for MFCs is quite comparable with that achieved with anaerobic digestion, as seen in Table 2 (Rabaey & Verstraete, 2005). However, these values are reached at laboratory-scale, where the experimental conditions are controlled and optimal (Fan et al., 2008; Yang & Logan, 2016). When scaling-up, less favorable conditions are expected, such as complex substrates, changes in temperature or increased internal resistances. These might lead to a further decrease of power outputs and hence make the competition of MFCs more difficult in terms of energy production with other existing wastewater treatment technologies (Ter Heijne et al., 2011). In fact, Logan and collaborators (Logan et al., 2015) showed a stagnating power production trend for MFCs in the last decades (up to $\sim 5 \text{ W m}^{-2}$ cathode surface area). It is known that the type of substrate, choice of electrode material and potential (Sleutels et al., 2011) cell configuration and operational conditions (Du et al., 2007) directly affect the power output

of MFCs. Therefore, many research studies focus on finding ways of increasing it (Shuiliang Chen et al., 2019; Fan et al., 2007; Pham et al., 2009; Younggy et al., 2011).

One option that is recently gaining interest is the combination MFCs with electrochemical capacitors (EC) (W. Chen et al., 2018; Santoro et al., 2015; Y. Wang et al., 2016). Electrochemical capacitors, also known as supercapacitors, are widely used for short-term energy storage in electronic devices and have two different charge storage principles: i) electrostatic charge, where charge is stored by the formation of an electrical double layer (EDL) on the electrode/electrolyte interface; and ii) electrochemical charge or pseudocapacitance, where charge is stored by the adsorption/desorption of cations or/and intercalation/de-intercalation coupled with reversible redox reactions of metal ions at the electrode/electrolyte interface (Jayalakshmi & Balasubramanian, 2008; Sharma & Bhatti, 2010). Due to the ability of ECs to store charge, MFCs can be operated intermittently and deliver higher current densities during discharge (A Dewan et al., 2009). In addition, the use of electrodes with capacitive properties that can form the EDL leads to lower overpotentials and therefore higher cell voltages (Santoro et al., 2019). These properties make the combination of EDLCs and MFCs, referred to as capacitive MFCs, suitable to reach higher power outputs.

4. Capacitive Microbial Fuel Cells

EDLCs can be placed externally (A Dewan et al., 2009; Walter et al., 2014), connected to the external circuit of the MFC, or internally (Deeke et al., 2012), by using electrode materials with high specific surface area (i.e. capacitive electrodes) (Candelaria et al., 2012). Carbonaceous materials are commonly used as capacitive electrodes due to their high conductivity, high surface area (up to 2000 m² g⁻¹), good corrosion resistance, high temperature stability, and low cost. Among them, activated carbon is widely used (Pandolfo & Hollenkamp, 2006).

4.1. Activated carbon properties

Activation of carbon is the process by which the surface area (and porosity) of a carbon precursor is increased. Common precursors of activated carbon are biomass (e.g. wood, nut cells), coals, petroleum coke or selected polymers (e.g. polyvinylidene chloride). These precursors usually have relatively low porosity and blocked pore entrances. Therefore, the activation process opens these existing pores but also creates new ones, so the total pore volume of the material is higher after activation (Pandolfo & Hollenkamp, 2006). Activation processes can be divided in two main groups: i) physical activation, where the carbonization of precursors is first done in an inert atmosphere to remove non-carbonaceous elements, followed by the development of porosity with oxidizing gases like O₂, CO₂ or steam, at a controlled temperature range of 600-1200°C; and ii) chemical activation, carried out by mixing the precursors with chemical activating agents like

phosphoric acid (H_3PO_4), zinc chloride (ZnCl_2) and potassium hydroxide (KOH), followed by the carbonization at 400-900°C (J. Wang & Kaskel, 2012). Depending on the carbon precursor and activation conditions (mostly temperature, time and gaseous environment), the resulting properties of the activated carbon will vary and can also be controlled to some extent (Pandolfo & Hollenkamp, 2006).

Pores of activated carbon materials can be classified into three main size-ranges: micropores (<2 nm), mesopores (2-50 nm) and macropores (>50 nm) (J. Lee et al., 2006). Because micropores have the highest surface-area-to-volume ratio, when present in significant proportions, they are the ones contributing most to the surface area of activated carbons. Due to their small size, they can be very useful for diffusion (restricted) selectivity. Mesopores also contribute to the surface area and provides wider transport pores for diffusion and better accessibility of ions/molecules. As for macropores, they usually don't contribute to the surface area of porous carbon, and their main function is to be the transport path into the interior of carbon particles (Han et al., 2014; Pandolfo & Hollenkamp, 2006). Characterization of the pore size distribution (PSD) of activated carbon can be done by different techniques. Mercury (Hg) and helium (He) displacements are usually used to determine the total pore volume ($\text{cm}^3 \text{g}^{-1}$), while the adsorption with CO_2 or N_2 gases are respectively used to determine the volume of narrow micropores (< 0.7 nm) wider pores. The cumulative pore volume of both mesopores and macropores can also be obtained by mercury porosimetry (Pastor-Villegas & Durán-Valle, 2002).

4.2. Double-layer capacitance

Capacitance is the measure of charge storage, in Farads (F). Capacitance of carbon electrodes will largely depend on the surface area of the material, which allows for electrical double layer (EDL) formation and thus charge storage. Figure 5 illustrates the EDL formation of an activated carbon granule with EAB growing on its surface, which convert acetate to electrons that are been released and transferred to the carbon structure. At the same time, protons and other cations present in the solution (e.g. H^+ , Na^+ , K^+), counterbalance the negative charges maintaining electroneutrality. This layer of negative and positive charges in the carbon electrode/electrolyte interface is the same charging principle previously explained of EDL capacitors. Therefore, the AC granule here acts as an energy harvester and also as an energy storage system. Theoretically, an approximated capacitance value of 100 F g^{-1} for $1000 \text{ m}^2 \text{ g}^{-1}$ of carbon surface area is expected (Kötz & Carlen, 2000). However, it was proven that a stronger activation process, leading to an increased surface area of the carbon, does not necessarily come along with an increase in capacitance (Pandolfo & Hollenkamp, 2006).

BET (Brunauer-Emmett-Teller) surface area, determined by N_2 adsorption, is traditionally used to define the sorption capacity of electrode materials (Han et al., 2014). However, the area accessed by N_2 gas is usually less restricted than that accessed by the electrolyte, as N_2 gas is less susceptible to the carbon properties (Frackowiak & Béguin,

2001). One example for this is the PSD of the carbon previously mentioned. It has been determined that micropores are the pores contributing most to the capacitance, e.g. in aqueous electrolytes (H_2SO_4) the optimum range was found to be 0.8–2 nm (Pandolfo & Hollenkamp, 2006). However, in general, narrow micropores will lead to restricted electrolyte diffusion and so the movement rate of ions into and outside the pores will be restricted during charge and discharge cycles. As an example, it was calculated that pores bigger than 1.1 nm could be accessed by the electrolyte in less than 0.1 s, while pores of about 0.6 nm could only be accessed after 5 s (Frackowiak & Béguin, 2001). Mesopores also contribute to the capacitance, although to a lower extent than micropores, and are known to improve the accessibility and transport of ions. As for macropores, they don't contribute much to the capacitance but, same as for mesopores, they act as transport channels to smaller pores (Pandolfo & Hollenkamp, 2006). Therefore, micropores are needed for charge storage but wider pores are necessary to improve the accessibility of ions and thus deliver high energy at high rate. Therefore, not only the pore size but the network connection between large and small pores is thus of great importance (Frackowiak & Béguin, 2001). Other factors, such as carbon morphology (e.g. size, shape), surface chemistry (e.g. oxygen functional groups), electrical conductivity of the carbon or the electrochemical techniques used to calculate capacitance, will also influence the measurement of the capacitance (Pandolfo & Hollenkamp, 2006).

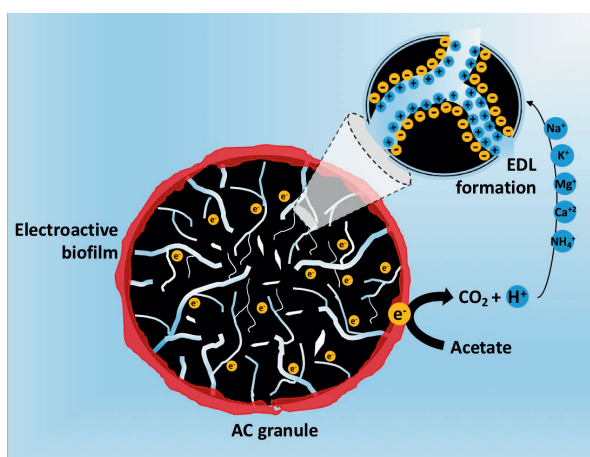


Figure 5. Single activated carbon (AC) granule with electroactive biofilm growing around it. Faradaic current is that produced by EAB from substrate oxidation, while capacitive current is that stored as charge in the electrical double layer (EDL). Modified from (Borsje et al., 2016).

4.3. Intermittent operation mode

The use of porous electrodes (capacitive) have proven to increase Coulombic efficiencies (Di Lorenzo et al., 2010), current densities and stored charge (Deeke et al., 2012) compared to non-porous electrodes (non-capacitive). Similarly, the ability to store charge

allows for intermittent operation mode of MFCs, which means they can carry out charge and discharge processes physically but also temporarily separated. On the one hand, higher current densities can be achieved during discharge as the stored charge is much higher than in non-capacitive materials. Similarly, charge can be released more efficiently as there is a higher local conductivity due to the formation of EDL, which helps keeping the electroneutrality during discharge and hence reducing overpotentials. On the other hand, a physical separation of these two processes, as it can happen in fluidized bed reactors (Deeke et al., 2015), allows for the treatment of larger wastewater volumes, avoiding clogging issues that otherwise would be present with flat electrodes with little space between them. In addition, the discharge cell can have on the contrary a small volume that can be beneficial to reduce material (e.g. catalyst, membrane) cost.

One of the easiest ways to understand the differences between capacitive and non-capacitive electrodes in MFCs is to analyze their current and potential responses during charge/discharge cycles, as shown in Figure 6 (one cycle). During charge, the cell is in open circuit (no current) while EAB are oxidizing the substrate and thus charging the electrode, which reduces its potential to the open cell potential value (-0.296 V vs NHE in the case of acetate). The change in potential occurs gradually in the case of capacitive electrodes as the EDL is being formed, while the potential decreases at a faster rate in the case of non-capacitive electrodes where non or little charge storage is possible. During discharge, in this case at a constant applied potential, there is first a peak in current that gradually decreases until reaching a steady-state current, which is the faradaic current produced by bacteria at that specific potential. The potential difference between the charged electrode and the applied anode potential gives the driving force needed for the stored charge to be released. The current peak is thus related to the release of charge stored in the EDL, referred to as capacitive current. This current peak is much smaller for non-capacitive electrodes, which also can (or not) have lower faradaic currents. It is important to realize that, during discharge, EAB still produce electrons and so there is a combined response of the capacitive and faradaic currents. By subtracting the faradaic current to the total produced current, the capacitive current can be determined, which directly relates to the capacitance of the electrode.

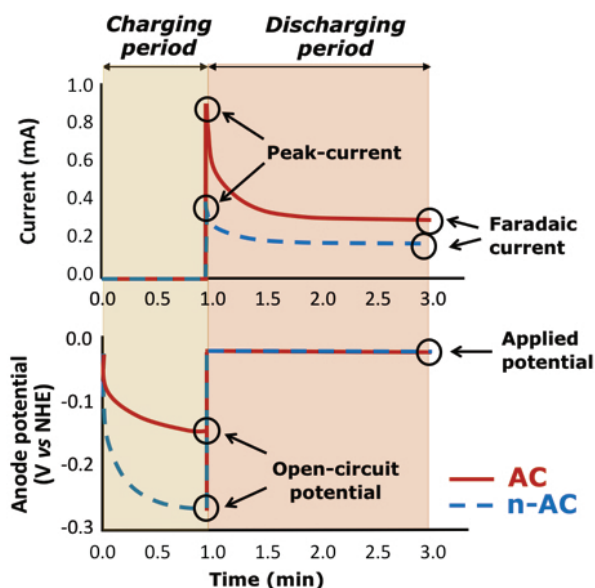


Figure 6. Example of current (up) and potential (down) responses of activated carbon (AC, red) and non-activated carbon (n-AC, blue) during a charge/discharge cycle. Modified from (Borsje et al., 2016).

4.4. Single AC granules

Bacterial growth is a very important aspect to consider when optimizing the current production and Coulombic efficiency of the system. Therefore, studying biofilm formation, determining capacitive electrode properties and most importantly understanding the biofilm-electrode interaction is of upmost importance to achieve high MFC performance. To this end, the study of single AC granules (Borsje et al., 2016; Rodrigo-Quejigo et al., 2018) have shown to provide valuable information for their further implementation in larger scale systems such as packed (Rabaey et al., 2005) or fluidized bed reactors (Deeke et al., 2015).

In this thesis, two types of activated carbon (AC) granules are used: GAC, produced from coal as precursor, and PK, produced from peat as precursor. One type on non-activated carbon granule, made of graphite (GG), is also used. Table 3 shows their pores sizes and volumes which were determined in a previous study by N_2 adsorption (Borsje et al., 2016). The percentage of micropores (< 2 nm) and mesopores (2-50 nm) is also shown. The skeletal volume, which belongs to the carbon structure, was determined by He adsorption. By summing up the total pore volume and skeletal volume, the envelop density ($g\ cm^{-3}$) and specific surface area (SSA, $m^2\ g^{-1}$) of all carbon granules were determined.

Table 3. Information about the size, density, surface area, pore volume and size of the activated carbon granules (GAC 830W and PK 1-3) and non-activated carbon granules (GG) used in this thesis. Modified from (Borsje et al., 2016).

	Pore size (nm)	Pore Volume (cm ³)	Pore size (nm)	Pore volume (cm ³)	Micropores- Mesopores (%)	Skeletal volume (cm ³)
GG	0.3 - 35.84	0.0018	35.8 - 361.3	0.0017	4-96	2.870
GAC 830W	0.3 - 4.5	0.47	4.5 - 339	0.01	80-20	1.363
PK 1-3	0.3 - 24.56	0.46	24.8 - 245.9	0.04	60-40	0.930

5. Thesis objective

Wastewater represents a renewable source of bioenergy that is present all over the world from households, agricultural and industrial operations, and that must be cleaned before releasing it to the environment. In this context, the present study assesses and combines two of the major problems, i.e. electricity production and wastewater treatment, with the use of Microbial Fuel Cells (MFCs). Classical MFCs have limitations like energy losses in the anode/cathode and low power output, among others. Capacitive MFCs are a potential solution to these problems by the use of capacitive electrodes that are conductive and provide a large (porous) surface area for charge storage and biofilm growth.

The aim of this thesis is to investigate single activated carbon (AC) granules as capacitive material for bioanodes, to assess the potential for their application in large-scale MFCs.

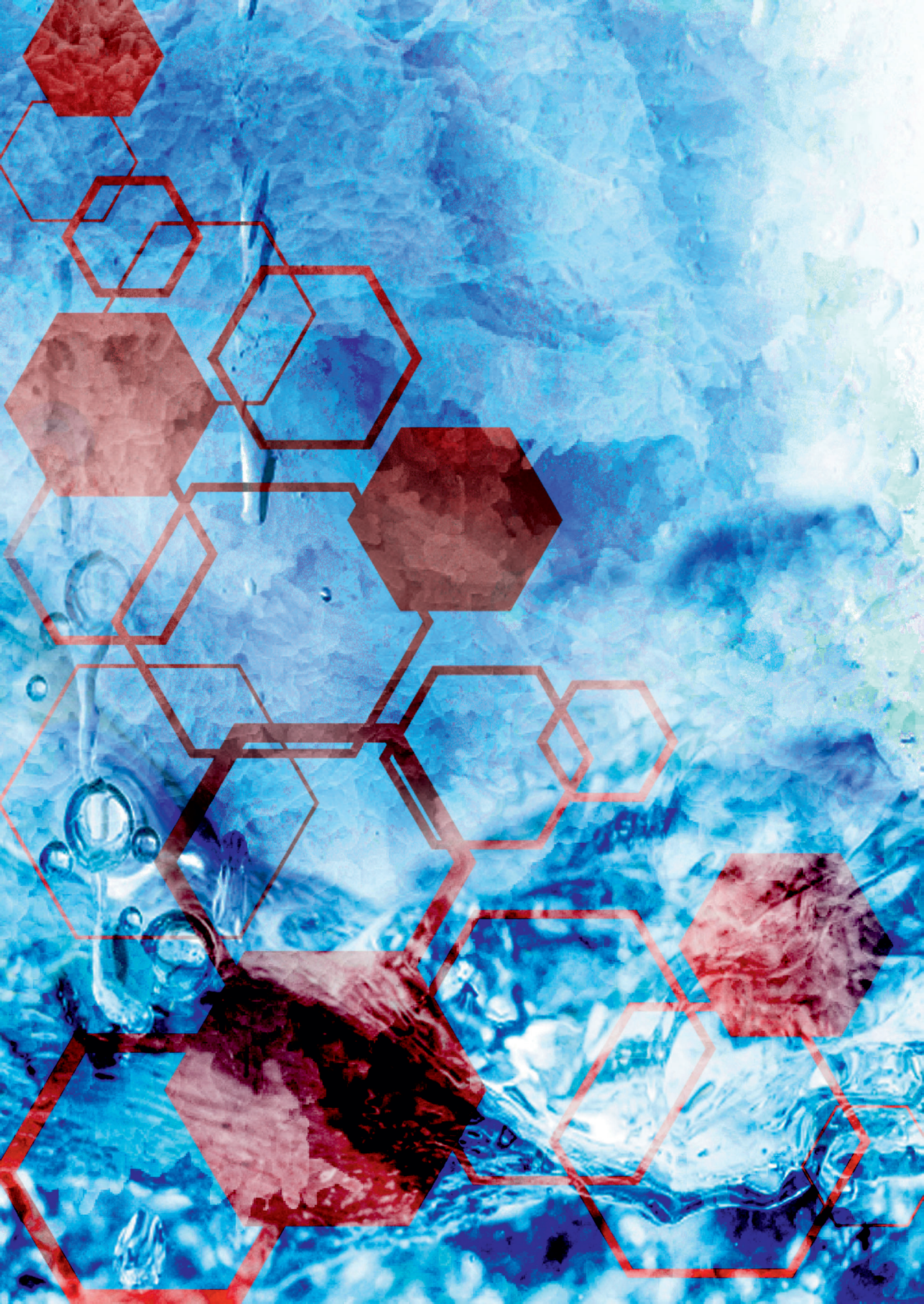
The first chapter of this thesis focuses on a literature review of the use of MFCs in combination with electrochemical capacitors, with special emphasis on the use of capacitive materials in the anode and cathode electrodes. The theory of capacitance is explained in more detail, and it is demonstrated how the capacitance of AC granules can be determined with different electrochemical techniques. The effect of biofilm growth on the capacitance of AC granules is also reported and discussed. The state-of-the-art use of capacitive electrodes, their charge-discharge behavior, applications, and most important challenges are addressed.

The second chapter of this thesis studies continuous and intermittent performance of single activated carbon granules as bioanodes in acetate-fed MFCs. Regarding the continuous performance, current production of two types of AC granules and 3 different granule sizes is monitored under controlled conditions. After the growth period, total produced charge was calculated, biofilm growth was quantified, microbial community of the biofilm was analyzed, and SEM images were used to study biofilm growth. Regarding intermittent performance, charge/discharge experiments were done to determine charge

storage of two types of AC granules as a function of discharge anode potential and charge/discharge cycle duration.

The third chapter of this thesis focuses on determining biofilm growth and distribution on single AC granules by the use of an advanced analytical technique: Magnetic Resonance Imaging (MRI). Granules were continuously monitored for current production and collected from the reactor at different growth stages. By differentiating the distribution of hydrogen nuclei in the biofilm and the bulk water, 3D images of the biofilm are taken and further processed to obtain the total biofilm volume. The same granules were further analyzed for total nitrogen content, which allows for a comparison of MRI results with chemical analysis. This is the first time MRI is applied for biofilm quantification on granular carbon electrodes.

The fourth and last chapter of this book focuses on the measurement of electrical conductivity of anaerobic granular sludge from a wide variety of wastewater treatment plants. Electrical conductivity of biological samples has been measured for bioanodes, but also the presence of electrochemically active bacteria in anaerobic granules that contain complex syntrophic microbial communities is believed to result in electrical conductivity. Electrical conductivity may be linked to the capability of electron transfer within anaerobic granules and the aim of this study was to assess if electrical conductivity is a widespread phenomenon in anaerobic granular sludge. We aimed to link electrical conductivity to other chemical and biological analyses of the different types of granular sludge.



Chapter 2

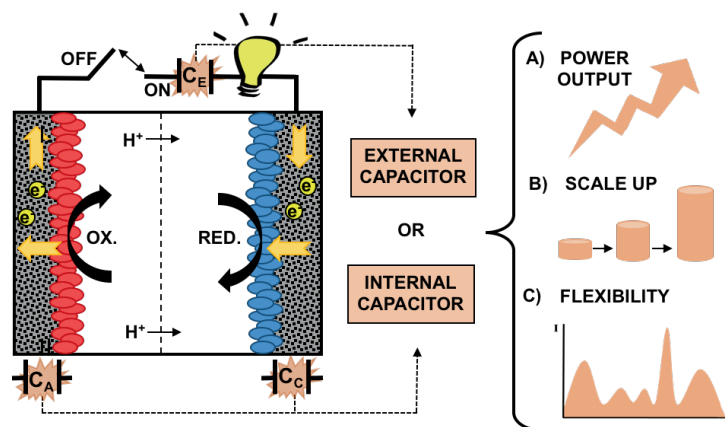
Combination of bioelectrochemical systems and electrochemical capacitors: Principles, Analysis and Opportunities

Leire Caizán-Juanarena, Casper Borsje, Tom Sleutels, Doekle Yntema, Carlo Santoro, Ioannis Ieropoulos, Francesca Soavi, Annemiek ter Heijne

Abstract

Bioelectrochemical systems (BES) combine electrodes and reactions driven by microorganisms for many different applications. The conversion of organic material in wastewater into electricity occurs in microbial fuel cells (MFCs). The power densities produced by MFCs are still too low for application. One way of increasing their performance is the use electrochemical capacitors, widely used for charge storage. Capacitive MFCs, i.e. the combination of capacitors and MFCs, allow for energy harvesting and storage and has shown to result in improved power densities, which facilitates the up-scaling and application of the technology. This review summarizes the state-of-the-art of combining capacitors with MFCs, starting with the theory and working principle of electrochemical capacitors. We address how different electrochemical measurements can be used to determine (bio)electrochemical capacitance and show how the measurement data can be interpreted. In addition, we present examples of the combination of capacitors, both internal and external, that have been used to enhance MFC performance. Finally, we discuss the most promising applications and the main existing challenges for capacitive MFCs.

Capacitive BES = Harvesting + Storage



Keywords: microbial fuel cells; capacitance; electrical double-layer; up- scaling; supercapacitor; power output.

1. Introduction

1.1. Bioelectrochemical systems for current generation

Bioelectrochemical systems (BESs) employ microorganisms that catalyze an electrochemical reaction either at the anode, cathode or both. Since the rediscovery of microorganisms capable of extracellular electron transfer, after its first discovery by M.C. Potter, the research into BESs has exploded (Potter, 1911)(Santoro, Arbizzani, et al., 2017). The electron transfer mechanism itself, being either direct (via cytochromes, mediators or extracellular structures) or indirect (via excreted or added electron shuttles) has led to numerous publications (Busalmen et al., 2008; Kracke et al., 2015; Lovley, 2006; Nielsen et al., 2009; Patil et al., 2012; Reguera et al., 2005, 2006; Schröder, 2007). Additionally, application of BESs has grown in a variety of fields, such as wastewater treatment, bioremediation, desalination, resource recovery of nutrients and biosensors. Several reviews have already focused on organic carbon (Pant et al., 2010), nitrogen (Kelly & He, 2014; Rodríguez-Arredondo et al., 2015), sulphur (Rabaey, 2009) and metal (Nanchaiah et al., 2015) as possible electron donors and acceptors in BESs. Regarding the conversion of organic waste into electricity, the primary objective is to efficiently produce current from the available substrate (Pham et al., 2009). Highest current densities are produced in anodes where most of the available biomass is attached to the electrode and not suspended as planktonic biomass (Franks et al., 2010; Khan et al., 2016). The combination of biofilm and electrode is generally referred to as bioanode, which is the responsible electrode for substrate oxidation. On the cathode, protons and electrons converge and a (bio)electrochemical reduction reaction occurs. In the case of microbial fuel cells (MFCs), a reactant, usually oxygen, is reduced to water or hydroxide ions depending on the electrolyte pH (Kinoshita, 1992; Slate et al., 2019). In the case of microbial electrolysis cells (MECs), hydrogen or methane is produced as final product through an external applied voltage (Call & Logan, 2008; M. C. A. A. Van Eerten-Jansen et al., 2012).

The performance of an MFC is determined by the Coulombic efficiency, cell voltage, and current. The Coulombic efficiency describes which part of electrons from the substrate end up in the electrical circuit. It is lower than 100% when competing (microbial) conversions, like methanogenesis or sulphate reduction, take place or when electrons are consumed for biomass formation (Sleutels et al., 2011). Therefore, Coulombic efficiency has an effect on the energy efficiency of the system. This energy efficiency is also affected by the cell voltage, which is a function of current in practice. The thermodynamic cell voltage at neutral pH is ≈ 1100 mV, which is the difference between the cathode and anode potentials. The anode equilibrium potential is -496 mV (vs Ag/AgCl 3M KCl) for the acetate/ CO_2 redox couple ($[\text{HCO}_3^-] = 5$ mM, $[\text{CH}_3\text{COO}^-] = 5$ mM, pH = 7), and the cathode equilibrium potential is $+605$ mV (vs Ag/AgCl 3M KCl) for oxygen reduction ($p\text{O}_2 = 0.2$, pH = 7)(Logan et al., 2006).

At open circuit conditions, when no current is flowing, the measured cell voltage should theoretically match the thermodynamic cell voltage. Under fully anaerobic conditions, in

the presence of a sufficiently high acetate concentration and with a well-developed electroactive biofilm, the anode open circuit potential (OCP) approaches the thermodynamic one. On the contrary, in neutral media, the cathode OCP can be significantly lower than the theoretical one for the redox couple O_2/H_2O (at pH 7). Platinum has shown a strong oxygen reduction reaction (ORR) catalysis activity and has been largely used in the past. However, over time platinum has been replaced by alternative catalyst (e.g. platinum alloys, transition metal oxides) due to its high cost and low stability with components present in real wastewater (Santoro et al., 2019; Z. Wang et al., 2014). Usually, the cathode potential is 300 mV lower when platinum or iron-based catalysts are used and becomes even lower (400-500 mV) with carbonaceous metal-free materials (Kodali et al., 2017; Santoro, Serov, et al., 2016). When the external circuit is closed and the MFC is connected to an external load, the actual cell voltage becomes lower than the open circuit voltage. The cell voltage decreases because part of the energy is dissipated in resistive contributions of the electrochemical cell components and processes; the internal resistances (Shuiliang Chen et al., 2019; Fan et al., 2008). The internal resistance includes (i) the electronic resistance of current collectors and electrode materials, (ii) the ionic resistance that depends on wastewater conductivity, (iii) membrane resistance (if applicable), and (iv) the charge transfer resistances that are directly related to the kinetics of redox reactions. Electrode kinetics include the activation overpotential related to electron transfer, and the mass transport losses that are related to i.e. diffusion, depletion or accumulation of the chemical species involved in the reactions (Bard & Faulkner, 2001; Jeremiasse et al., 2009). At the bioanode, voltage losses due to internal resistance occur because of the complex nature of the anode electron transfer mechanisms. These electron transfer mechanisms, via direct electron transfer or mediators, are extensively discussed in literature (Kumar et al., 2017; Patil et al., 2012; Schröder, 2007). At the cathode, voltage losses occur for the ORR. As the ORR at the cathode takes place in neutral media, the concentrations of both H^+ and OH^- , reagents for the ORR, are at the lowest value and lead to diffusion limitations. Many researchers aim to reduce the losses related to oxygen reduction, utilizing low-cost, environmentally friendly and durable (biological) catalysts, as described above (Kinoshita, 1992; Santoro, Babanova, et al., 2016; Santoro, Serov, et al., 2016).

1.2. Limited power density for commercialization of MFCs

For MFCs to become competitive with a mature, commercially available wastewater treatment technologies like anaerobic digestion, a power density of 1000 W m^{-3} would be required (Arends & Verstraete, 2012; Ter Heijne et al., 2011). Power densities of MFCs have shown a stagnating trend over the last years (Logan et al., 2015), with a maximum value of 200 W m^{-3} of reactor volume or $2\text{-}3\text{ W m}^{-2}$ of projected membrane surface area. It is important to note that reported power densities are generally obtained in lab-scale systems, mostly under optimized conditions, with model substrates and considerable

amounts of added salts and buffer and at high operating temperature (Fan et al., 2008; Yang & Logan, 2016). Especially for application in wastewater treatment, electrolyte conductivity is low, pH is not controlled, temperature varies significantly being generally lower than in lab-scale experiments, and system clogging is a risk. All these factors reduce the power density compared to optimized conditions. Moreover, when scaling up MFCs, the limitations encountered at lab-scale become more prominent and additional limitations, like energy losses due to pressure drop, increase of contact resistance, requirement of higher system mechanical integrity and use of highly conductive and thus expensive materials, appear (Dekker et al., 2009; Heidrich et al., 2013; Rodenas Motos et al., 2017; Rossi et al., 2019; Zamora et al., 2017).

An alternative for scaling up, well known from chemical fuel cells and battery applications, is through the stacking of the different cells, which can be connected in series or parallel (Peter Aelterman et al., 2006; Ioannis Ieropoulos et al., 2008; Z. Liu et al., 2008; Shin et al., 2006). This configuration increases the complexity of control and equipment required to operate the overall system. In fact, a risk of stacking cell pairs is the occurrence of cell reversal, which decreases the performance of the full stack (S. E. Oh & Logan, 2007). Another approach for scaling up is to increase the number of separate modules used (I. A. Ieropoulos et al., 2013; Kim et al., 2010), which may take away some of the disadvantages of larger-scale operation. However, separate modules often require more materials (connections, tubing, feed troughs) than stacked cells.

1.3. Exploiting electrochemical capacitive properties in BESs

Recently, it was demonstrated that the use of materials with electrochemical capacitive properties can enhance the power density of MFCs (Feng et al., 2014; Houghton et al., 2016; Lv et al., 2014, 2012; Santoro, Kodali, et al., 2017; Soavi et al., 2016). Capacitive materials are materials with a high specific surface area that allows for charge storage. The use of capacitive materials was first explored for the so-called “biosupercapacitors”, which combined capacitive materials with enzymatic fuel cells (Agnès et al., 2014; Pankratov, Blum, et al., 2014; Pankratov et al., 2016; Pankratov, Falkman, et al., 2014). Already in these early studies, increased current/power densities were reported compared to non-capacitive materials. The use of capacitors in combination with BESs has two advantages: ability of (i) enhanced power density and (ii) flexibility of operation (Deeke et al., 2015; H. Wang et al., 2015). The enhanced power density is the result of the high specific surface area, which decreases the local current density and thus overpotentials, and increases current. Several studies have shown that intermittent operation mode of a capacitive MFCs, both internal (Deeke et al., 2012) and external (A Dewan et al., 2009; Walter et al., 2014) can lead to an increased power output compared to a continuous external load. Under intermittent mode, energy is delivered at high rate only for short periods (lower than minutes) thanks to the high charge density (and counter ions) stored within the electrical double layer (EDL). This results in higher power densities compared to non-capacitive

systems. Finally, capacitive BESs can buffer discontinuities of current in the small-time scale and deliver on-demand energy. This feature is extremely useful in the context of energy storage of renewable energy, which usually cannot provide a constant power generation. Due to their flexible and dynamic electrochemical response, capacitive BESs can be combined with batteries or with other energy harvesters (e.g. fuel cells, solar cells) (H. Wang et al., 2015).

So far, over 200 papers have been published describing the combined use of capacitors and BESs. Figure 1 shows the most relevant applications of BES that use capacitors either in the external circuit (e.g. robotics (I. A. Ieropoulos et al., 2012; Walters et al., 2013), biosensor (B. Liu et al., 2015; F. Zhang et al., 2011), benthic MFCs (Arias-Thode et al., 2017; Tender et al., 2008)) or integrated in the electrochemical cell (e.g. desalination (Meng et al., 2017; Stoll et al., 2015)). The study of power management systems and energy harvesting systems to optimize the power output of MFCs, which usually include a capacitor, is also extensive (include electronic circuits with all kind of transformers, converters and boosters) (Erbay et al., 2014; Park & Ren, 2012a). Other energy harvesting strategies include the use of external capacitors to e.g. avoid voltage reversal (Papaharalabos et al., 2017), the use of intermittent energy harvesting operation mode (Walter et al., 2014) or the optimization of external resistances to enhance cell performance (Pinto et al., 2011). As for internal capacitors, many studies focus on the modification of electrode materials to develop/increase their capacitive properties to integrate them in BESs (W. Chen et al., 2018; Feng et al., 2014). Similarly, the application of capacitive materials as electrodes is extensively used in MFCs mostly in the anode (Y. Wang et al., 2018, 2016) but also in the cathode (Ansari et al., 2016; Santoro, Kodali, et al., 2017).

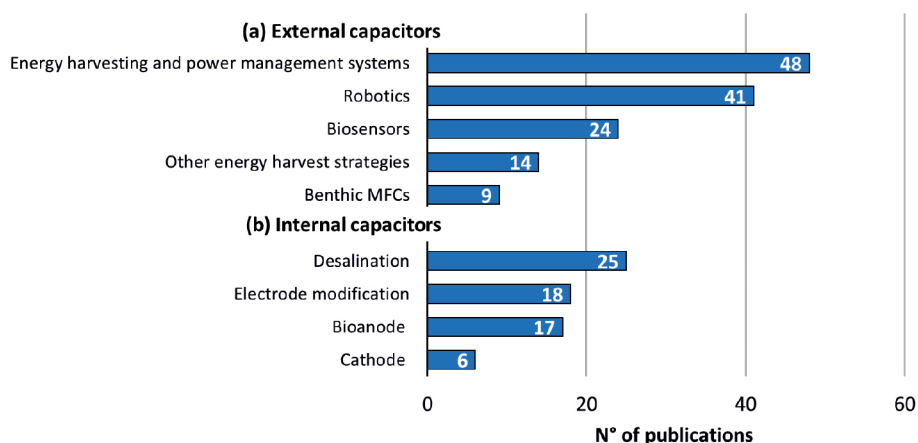


Figure 1. Number of publications, ordered from high to low, related to the use of capacitors in combination with BES. Publications are classified based on the type of capacitor involved, i.e. (a) external (outside in the circuit) or (b) internal (inside the cell).

When internal capacitors are used in MFCs, they exploit inherent or additional capacitive features of anode and/or cathode. In this review, we discuss the use of electrochemical capacitors and capacitive electrodes in BESs with focus on power produced in MFCs. First, an overview of the theory on electrochemical capacitors is provided (section 2), followed by how capacitance can be measured with the use of different electrochemical techniques (section 3). After, the integrated use of electrochemical capacitors in MFCs, both in anodes and cathodes, is explained, with focus on capacitive materials and examples of applications (section 4). The use of external capacitors is then addressed, where their behaviour under cell intermittent operation mode and their use on the research field of robotics is explained (section 5). A future outlook on the combination of BESs and electrochemical capacitors is finally presented (section 6).

2. The electrical double layer and BES

The capacitance of a material reflects the ability to store charge, and thus understanding of capacitance is crucial to get insight in how such materials can be combined with MFCs. The value of capacitance, expressed in Farad (F), corresponds to the amount of charge (Q) that can be stored over a potential difference (ΔV) of 1 V, and for ideal systems is a constant, i.e.:

$$C = \frac{dQ}{dV} \quad (1)$$

When a porous electrode is polarized, charge carriers can distribute into the bulk of the electrode over a relatively large distance (screening length) that is inversely related to the charge-carrier density; such region is called space-charge region (SCR) and ranges between a few angstroms to several thousands of angstroms in semiconductors but it is negligible in metals (Bard & Faulkner, 2001). On the electrolyte side, the formation of a compact layer of ions of the same charge (but different sign with respect to the electrode surface), the Inner Helmholtz Plane (IHP), forms at the closest distance from the electrode while a diffuse layer, the Outer Helmholtz Plane (see Figure 2) forms at largest distance from the electrode.

With the formation of an electrical double-layer in the solid part of the interface and in the electrolyte, charge is distributed and potential gradients develop in the SCR, IHP and OHP regions. These three potential gradients (Φ_C , Φ_H , Φ_{diff}) make up three capacitive components (C_C , C_H , C_{diff}) that are connected in series and contribute to the electrode double-layer capacitance (C_{dl}) as follows:

$$\frac{1}{C_{dl}} = \frac{1}{C_C} + \frac{1}{C_H} + \frac{1}{C_{diff}} \quad (2)$$

where C_C is the SCR capacitance, C_H is the capacitance related to the compact layer and C_{diff} is the capacitance of the diffuse layer. Hence, C_{dl} will be determined by the smallest of the capacitive components. In the case of EDL capacitors (EDLCs), high conductive

electrodes and concentrated solutions are used, hence C_C and C_{diff} are high and EDL formation is only driven by C_H .

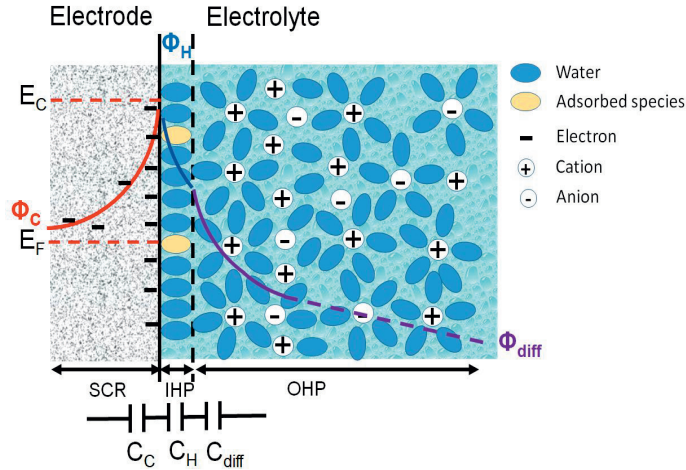


Figure 2. Scheme of the electrical double-layer at the solid-electrode/electrolyte interface with the formation of the space-charge region (SCR) in the solid electrode, the Inner Helmholtz Plane (IHP) and diffuse layer (Outer Helmholtz Plane, OHP) in the electrolyte. The potential trend within the three regions (Φ_C , Φ_H , Φ_{diff}) and the equivalent circuit that models the three capacitive components (C_C , C_H , C_{diff}) of the interfaces are reported. E_C and E_F are the electrode conduction and Fermi level, respectively. The Fermi level is the equilibrium potential of the electrons.

According to the Helmholtz model, for concentrated solutions (typically 1M for EDLCs) the capacitance C_H at each electrode interface is related to the surface area of the electrode (A) according the following equation:

$$C_H = \frac{k_0 \varepsilon A}{\delta_{dl}} \quad (3)$$

where k_0 is the vacuum permittivity ($8.85 \cdot 10^{-12} \text{ F m}^{-1}$), ε is the dielectric constant of the electrical double-layer region (that depends on solvent chemistry), and δ_{dl} is the thickness of the double-layer (δ_{dl} ; in the order of 10^{-10} m). Carbon electrodes, that have up to $2000 \text{ m}^2 \text{ g}^{-1}$ of surface area (A) in contact with the electrolyte, have a high specific double layer capacitance in the order of $100\text{-}150 \text{ F g}^{-1}$. Pore size and distribution of the porous electrode plays an important role in the formation of EDL. An optimal combination of micropores ($<2 \text{ nm}$), mesopores ($2\text{-}50 \text{ nm}$) and macropores ($>50 \text{ nm}$) in the electrode structure will minimize transport resistances of ions and maximize formation of EDL. In the same way, ionic composition and concentration of the electrolyte should be such so their availability does not limit EDL formation (Béguin et al., 2014; Conway, 1999).

The maximum practical cell voltage (V_{max}), together with the capacitance (C) and the internal resistance (i.e. the equivalent series resistance, ESR) of the capacitor, will determine the performance of EDLCs that can be analyzed in terms of energy and power

densities. The capacitance results from the series combination of the two electrode capacitances.

$$C = \left(\frac{1}{C_{\text{negative electrode}}} + \frac{1}{C_{\text{positive electrode}}} \right)^{-1} \quad (4)$$

Therefore, in order to achieve high cell capacitance, both electrodes have to feature high capacitance values. In case of unbalanced values of electrode capacitance, the cell response will be driven by the lowest capacitive electrode.

High specific energy of EDLCs (Eq. 5) is achievable by high values of C and V_{max} , which are dependent on the carbon electrode porosity and nanostructure and the electrochemical stability window of the electrolyte, respectively (Béguin et al., 2014; Conway, 1999). Indeed,

$$E = \frac{1}{2} \frac{C (V_{\text{max}})^2}{m_{\text{sc}}} \quad (5)$$

High specific power (Eq. 6) is achieved at low ESR, which in turn depends on: i) the conductivity of the electrolyte; ii) the electronic resistance of electrode materials; iii) the interfacial resistance between the electrode and the current-collector; and iv) the ionic resistance of ions migrating/diffusing through the small pores of porous architectures of the electrode.

The best performing commercially available EDLCs operate in organic electrolytes and feature $E_{\text{max}} < 5 \text{ Wh kg}^{-1}$, $P_{\text{max}} < 10 \text{ kW kg}^{-1}$ and $V_{\text{max}} < 2.7 \text{ V}$ (Béguin et al., 2014).

$$P = \frac{1}{4} \frac{(V_{\text{max}})^2}{\text{ESR } m_{\text{sc}}} \quad (6)$$

where E is the specific energy (Wh kg^{-1}), P is the specific power (W kg^{-1}), C is the capacitance (F), V_{max} is the maximum cell voltage (V), ESR is the internal resistance, which is equal to the equivalent series resistance (ESR) (Ω), and m_{sc} is the mass (kg) of the EDLC.

Materials that feature fast and reversible redox processes and exhibit a linear dependence of the charge stored with the potential can be termed pseudocapacitive electrodes (Brousse et al., 2015). In pseudocapacitive and other redox materials (i.e. materials that undergo faradic reactions but that cannot be termed pseudocapacitive), the faradic processes involve the bulk material and not only the surface. Therefore, charge accumulation at the IHP is higher with respect to EDLCs carbon electrodes, which increases the capacity and energy storage capability of the cells.

The integration of an EDLC with an MFC is the results of the combination of electrostatic and irreversible electrochemical (faradaic) processes that convert chemical energy into electric energy. This concept notably differs from the working principle of hybrid, asymmetric or pseudocapacitors that work with reversible electrochemical processes. In most of the studies, the anode serves as a growth surface for electroactive bacteria, which release electrons to the anode via the bioelectrochemical oxidation of a substrate. This faradic process is then the responsible for the electrochemical double-layer formation at the anode/wastewater interface, where the surface negative charges are balanced by

counter ions (cations) in the wastewater. The same process, but with opposite polarity, takes place at the cathode. These are charged positively due to reduction reactions (biological or chemical) occurring at the electrode, and balanced out by ions (anions) naturally occurring in the wastewater. Therefore, at the shortest times, the two electrodes work like the negative (anode) and positive (cathode) electrodes of an electrochemical capacitor that store charge and energy, by electrostatic charge separation at the two electrode EDLs (Figure 3A). When the circuit of the MFC is closed, charges accumulated on the interface of both electrodes are released to the electrolyte (Figure 3B). After discharge, the external load is disconnected and the MFC is in open circuit conditions. Under these conditions, the anode is charged by the electro-active biofilm until it reaches the equilibrium potential, while the double-layer is formed. In other words, the internal capacitor is charged via the (bio)electrochemical reactions occurring at anode and cathode.

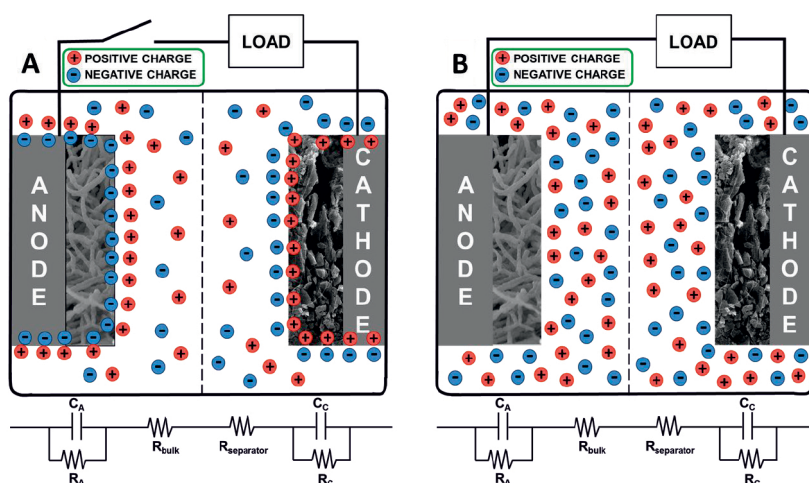


Figure 3. MFC with a capacitive bioanode and a capacitive cathode. A) Charge storage in form of electrical double layer in each of the electrodes while an open circuit. B) Charge release from electrode/electrolyte interface to the electrolyte in a closed circuit. C_A and C_C refer to anode and cathode capacitances, respectively, and R_A and R_C refer to anode and cathode resistance, respectively. R_{bulk} refers to the resistance of the electrolyte and $R_{separator}$ to the resistance of the membrane.

Figure 4 shows the response of current and voltage of an EDLC-MFC during one self-charge/galvanostatic discharge cycle. The response of anode and cathode potentials are also shown. At open cell, there is no current flowing through an external load, and both electrodes are polarized to a certain potential value resulting in a specific open cell voltage (OCV). When closing the circuit, the discharge occurs and both the capacitive and faradaic currents are measured. The anode potential will gradually increase (release of negative charges), while the cathode potential will decrease (release of positive charges). The

change in potential consists of both the ohmic drop (related to the internal resistance of the system) and the capacitance of the electrode (under fast discharge current regime). As a result of the changes in anode and cathode potential, the cell voltage will decrease during discharge. While the open cell voltage (OCV) refers to the voltage at open circuit conditions, the useful cell voltage for power output will be that after the ohmic drop, referred to as V_{cell} . In the discharging phase, the capacitive bioanode will deliver the stored charge and will be simultaneously charged by the electroactive bacteria.

In the charging phase, the anode and cathode potentials will be restored to their original level, driven by the faradaic current produced by the electroactive bacteria at the anode, and by the presence of oxygen at the cathode. This will result in an increase in cell voltage until again reaching the OCV.

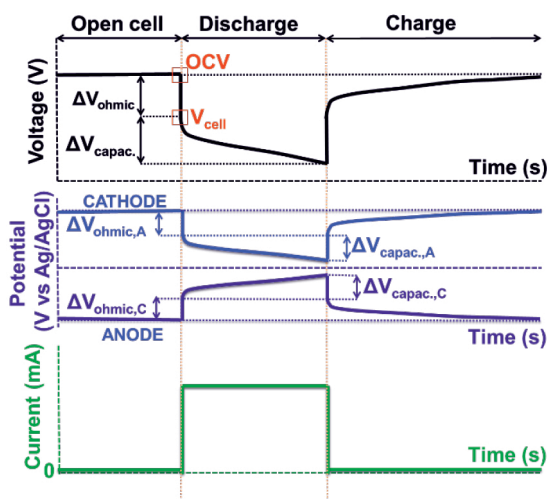


Figure 4. Cell voltage (up) and current (bottom) responses of a fully capacitive MFC during a charge/discharge cycle after a period of open cell. In the middle, the potential response of the cathode and anode electrodes. ΔV refers to the change in voltage that relates to two processes: the ohmic drop (ΔV_{ohmic}) and the change due to capacitance ($\Delta V_{\text{capac.}}$).

Alternatively to internal EDLCs, external capacitors can also be connected to MFCs (see section 5). Both for internal and external EDLCs, the evaluation of the capacitive response has to consider the parallel faradaic processes taking place during the discharge of EDLC-MFC systems.

If no additional external load is connected, the current generated by the MFC (I_{MFC}) charges the external EDLC up to a voltage that, in absence of leakage currents, corresponds to the highest voltage of the MFC exhibited in open circuit, referred before as V_{max} . The EDLC can then deliver the stored charge both disconnected (as in external capacitors) or while being connected to the MFC (as internal capacitors). In the former case, the discharge profile will be that characteristic of a conventional EDLC (and related

to its ESR and C). For an EDL galvanostatic discharge at the set current I_{EDLC} , the delivered charge is:

$$Q = I_{EDLC} dt \quad (7)$$

When the EDLC is discharged while being connected with the MFC, the discharge behavior will be different as the EDLC will deliver energy at the set current I_{EDLC} while being simultaneously recharged by the MFC (I_{MFC}). The charge delivered by the EDLC-MFC when being connected is the following:

$$Q = I dt = (I_{MFC} + I_{EDLC}) dt \quad (8)$$

and the system features an apparent capacitance C' that can be calculated as:

$$C' = \frac{dQ}{dV} = (I_{MFC} + I_{EDLC}) \frac{dt}{dV} \quad (9)$$

which is higher than that exhibited by the EDLC alone (see eq. 7). The apparent capacitance concept applies even for other kinds of systems where an energy harvested is integrated with EDLC, and was introduced by Intermite et al. (2017) (Intermite et al., 2017) for a solar cell-EDLC integrated device. Electrostatic and faradic processes have typically different rates and kinetics, with the latter being typically slower than the formers. Therefore, it has to be expected that the apparent capacitive response of MFC-EDLC systems and/or of the capacitive electrodes of MFCs might be different at different current regimes. While at fast discharge currents and short times, the cell response is mainly driven by the EDLC behavior, at low currents and longer time, the MFC redox processes mainly affect performance.

3. Measurement of capacitance using electrochemical techniques

Measurement of capacitance is crucial to determine how much charge can be stored by the electrode materials used in an MFC. Several electrochemical measurement techniques are available to determine the capacitance of electrodes and electrodes combined with microorganisms. It is important to underline that the evaluation of single electrode capacitance requires the use of a reference electrode (3-electrode mode). When the tests are performed in 2-electrode mode, the overall cell response is evaluated and in this case the capacitance that is measured is that of the cell.

To illustrate the current-potential behavior of capacitive electrodes, a 3-electrode setup was used. The working electrode was an activated carbon granule (weight= 1.03 mg, SSA= 764 m² g⁻¹), connected to a titanium wire as current collector. The reference electrode was an Ag/AgCl, 3M KCl electrode and the counter electrode was a graphite felt. The anolyte consisted of 50 mM phosphate buffer, a concentration that is relevant for BES, although different from that usually used during supercapacitor testing (often 0.1 or 1 M in acid or alkaline solutions). The cathode, separated from the anolyte by a cation exchange membrane (CEM), had 100mM of [Fe(CN)₆]³⁻ as electrolyte. The electrochemical response

of this capacitive granule (anode) was measured using the three electrochemical measurement techniques: (i) chronopotentiometry; where current is controlled at negative and positive levels, (also known as galvanostatic mode) (ii) chronoamperometry; where the electrode potential is controlled at fixed levels (also known as potentiostatic mode), and (iii) Cyclic Voltammetry (CV), where the electrode potential is changed linearly with time. All techniques were set up in a way that they followed a similar time response regime, meaning each cycle had a duration of about 10 minutes with similar scan rates and currents.

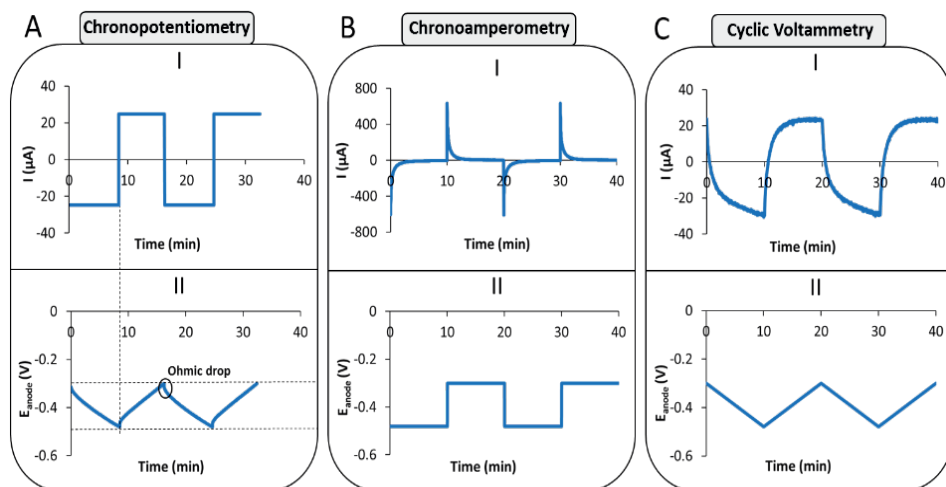


Figure 5. Current (I) and potential (II) responses of a capacitive anode (single activated carbon granule) during charge/discharge cycles (3 in total) with different electrochemical techniques: A) Chronopotentiometry; B) Chronoamperometry and C) Cyclic Voltammetry. The horizontal dotted lines mark the potential range at which the measurements were set, while the vertical dotted line points the end of a charge/discharge cycle in both current and potential graphs. The black circle shows the ohmic (potential) drop when the cycle is changed.

Figure 5A shows the results obtained with chronopotentiometry measurements. At $t = 0$, a current of $-25 \mu\text{A}$ was applied; electrons are transported into the granule and as a consequence the potential of the granule decreases, finally to a (set) level of -0.48 V . When this occurs, at around $t = 10$ minutes, the current was changed to $+25 \mu\text{A}$, and as a result, electrons are transported from the granule to the counter electrode, leading to an increase of its potential (up to -0.3 V). The measured change in potential consists of two contributions: i) the ohmic potential drop that is related to the internal resistance and ii) the potential that is related to the capacitance. The ohmic drop can be seen in the graphs as an immediate steep change in potential (dV) when the current direction is altered. From that value, the ohmic resistance can be calculated by the potential change divided by the momentary current change ($\text{ESR} = dV/dI$). Strategies to diminish the ohmic drop can be to use a lower current, or to use a small pause in between current alteration that results in a

potential without the ohmic drop. The total change in charge is calculated as the integral of current over time.

Figure 5B shows the results obtained with chronoamperometry measurements. At designated times (every 10 minutes in this case) a potential difference was applied between the granule and the reference electrode, which leads to transport of electrons into or out of the granule. While the potential values are steady, the current has a relatively high peak (I_p) when the potential level changes, which is around 20 times higher than the current applied/achieved with the other two techniques. The vertical amplitude of the current is therefore much higher, which means the current changes much faster and thus its measurement resolution is much lower, being more prone to errors even with higher data sampling rates. The applied potential divided by the peak current will give the value of the ohmic resistance ($I_p = V/ESR$).

Another way to calculate capacitance is to use Eq. 10, which represents the current curve during chronoamperometry measurements.

$$I = \frac{V}{ESR} e^{-\frac{t}{\tau}} \quad (10)$$

where τ is the EDLC time constant, i.e. the time required for 63% charge/discharge of the EDLC and t is the time (s). The capacitance can be derived by obtaining the value of τ from the measurement graph and dividing it by the ohmic resistance ($C = \tau/ESR$).

Finally, Figure 5C shows the results obtained with cyclic voltammetry measurements. To allow comparison with the other measurements, the cyclic voltammogram is split in such a way that current and potential responses are plotted separately as a function of time. At $t = 0$ the voltage is altered at a specific rate, in this case 0.3 mV s^{-1} , so that the set potential range (-0.3 V to -0.48 V) is covered in 10 minutes. The potential changes linearly between these two limits, while the current changes fast right after one cycle and reaches a steady value towards the end of a cycle. The current is then directly proportional to the rate of the potential change and the capacitance value ($I = C \times dV/dt$). Here, the shape of the curve is also influenced by the ohmic drop: it can be seen as the non-ideal block-shaped graph of the current. However, the value of the ohmic drop (and thus ohmic resistance) is more difficult to extract from the graph.

From the discharge cycles ($n = 3$), the capacitance, defined as the total change in charge (dQ) during discharge, divided by the change in potential (dV ; Eq. (1)), was determined for each electrochemical technique. Figure 6A shows that the highest capacitance was obtained for the chronoamperometry measurements ($88 \pm 0.05 \text{ mF}$), followed by chronopotentiometry ($69.1 \pm 0.5 \text{ mF}$), and cyclic voltammetry measurements ($66 \pm 0.2 \text{ mF}$). Thus, capacitance values have to be interpreted with care, as the measurement method used will influence the outcomes.

Determining electrode capacitance becomes more complicated when a biofilm is present. When an electroactive biofilm grows on a capacitive electrode (bioanode), the bacteria will release electrons to the anode via the bioelectrochemical oxidation of the

substrate (electron donor). This faradaic process is then the driver for the EDL formation at the solid-electrode/electrolyte interface, where the charge carriers are compensated by ions of opposite charge in the wastewater, as shown in Figure 2. To determine the combined capacitance of the electrode and biofilm, the apparent capacitance can be calculated with the sum of I_{EDLC} and I_{MFC} , as shown in Eq. 9. However, to study the effect of biofilm growth on electrode capacitance, the I_{MFC} must be subtracted. Of all techniques, only chronoamperometry allowed to do so, as the potential was maintained at fixed potential (at -0.3 V) during discharge and thus I_{MFC} was determined based on the steady-state current. Figure 6B shows the capacitance values of discharge cycles ($n=3$) for chronoamperometry under abiotic conditions (day 0, same as Figure 6A) and under biotic conditions (days 6, 18 and 35 after bacterial inoculation). The decrease in capacitance shows that biofilm growth has a negative effect on electrode capacitance, as it could possibly impede or slow down the transport of protons and other ions needed for EDL formation in the granule micro-/mesopores (Korth et al., 2015; Savéant, 1986). This phenomenon needs, however, further study.

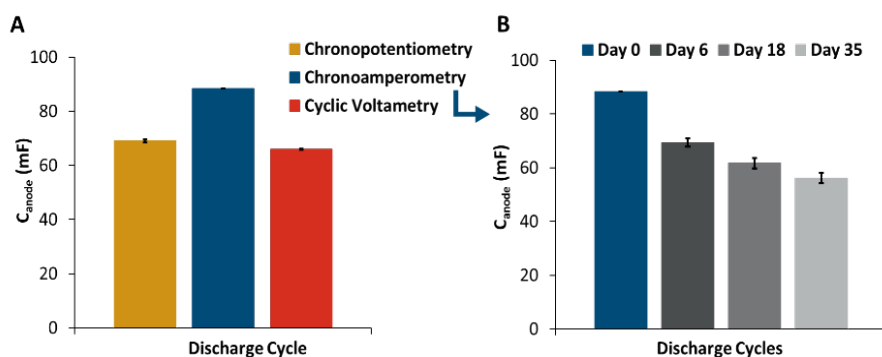


Figure 6. A) Capacitance (mF) of a single AC granule calculated from the average of 3 charge/discharge cycles with three different electrochemical techniques. B) Capacitance (mF) of a single AC granule calculated with chronoamperometry under abiotic (day 0) and biotic (days 6, 18 and 35) conditions.

All above-mentioned measurements to determine the capacitance are based on direct current (DC), which are widely used and studied. However, increasingly often an alternating current (AC) technique, known as electrochemical impedance spectroscopy (EIS), is used. With EIS not only capacitance but also different processes (e.g. charge transfer, diffusion) can be distinguished that occur at the electrode/biofilm/solution interfaces (Dominguez-Benetton et al., 2012; Orazem et al., 2006; Orazem & Tribollet, 2008). There are several parameters to consider when performing EIS measurements, such as the electrode potential, amplitude or range of frequencies (Yoho et al., 2015). Additionally, an equivalent circuit that fits the electrode material needs to be developed in order to obtain absolute values of capacitance and resistances. EIS is a powerful technique that permits to unravel

the different contributes to the ohmic resistance and C_{cell} of the electrochemical cell as described in details in (Orazem & Tribollet, 2008).

Using EIS, it has been found that biofilms can store charge, which has been related to the c-type cytochromes that can accumulate charge (Malvankar, Mester, et al., 2012). Ter Heijne and collaborators (Heijne et al., 2018) also calculated biofilm capacitance with EIS tests, with an increase value (up to $450 \mu\text{F cm}^{-2}$) during the biofilm growth period and a direct relation to current production (A m^{-2}). In this study, biofilm capacitance was determined using flat electrodes (Fluorinated Tin Oxide) with low surface area and thus capacitance (calculated as $25 \mu\text{F cm}^{-2}$). However, when biofilms are grown on capacitive electrodes, differentiating between biofilm and electrode capacitances will again be very difficult with AC techniques.

4. Integrated use of capacitors in MFCs

In this section, we will give an overview of the use of internal capacitors in MFCs by addressing the main research conducted in anodes and cathodes (separately) that use capacitive electrodes.

4.1. Integration of capacitive electrodes as anodes

The use of porous, three-dimensional electrodes for bioanodes is common, as these electrodes have, per volume, a high surface area for biofilm growth increasing the bacteria/electrode interface. Electrode materials, ranging from carbonaceous materials (e.g. graphite fibers or plates, activated carbon granules, graphene, carbon cloth, carbon paper, carbon veil, carbon nanotubes) to metals like titanium, copper or stainless steel, have been a topic of extensive research with the aim of increasing bioanode performance (J. Wei et al., 2011). Generally speaking, the available surface area for bioanode formation is a dominant factor in current production if substrate and internal resistance of the system are not limiting (Blanchet et al., 2016; Chong et al., 2018; Oliot et al., 2017; J. Wei et al., 2011). Providing sufficient area for microorganisms to have access to substrate and allow for adequate mixing to remove the produced protons is of utmost importance. Optimization of other electrode properties, e.g. surface chemistry (Guo et al., 2013; Teravest & Angenent, 2014), biocompatibility (Guo et al., 2015), improved cell configuration (H. Liu et al., 2005; Rodenas Motos et al., 2015) or enhanced electron transfer to and from the electrode (Ishii et al., 2018), are also well-known approaches to increase power densities by reducing internal resistances of BESs.

Operation of a capacitive anode with an electroactive biofilm in intermittent mode was first reported by Deeke and co-workers (Deeke et al., 2012). They made use of a layer of activated carbon that was casted on the surface of a current collector. The biofilm was grown on this capacitive electrode making up a capacitive bioanode. The relative charge recovery, charge transferred by the intermittent operation of the capacitive bioanode as

compared to the continuous operation of a non-capacitive bioanode, was as high as 140% for a 0.2 mm capacitive layer. Thicker layers produced only 104% for a 0.5 mm layer and even decreased to 20% for 1.5 mm (Deeke et al., 2013). The differences in surface roughness and internal surface area confounded the results somewhat, however it was clear the intermittent operation of this capacitive bioanode produced more overall charge compared to continuous operation of a non-capacitive graphite electrode.

4.1.1. Activated carbon granules as bioanodes

Often, activated carbon (AC) is used as capacitive electrode material because it has a high specific surface area (up to 3000 m² g⁻¹). It can be used in granular form, which enables the separation of the charging and discharging process in a fluidized capacitive reactor (Deeke et al., 2015). In a fluidized capacitive reactor, the granules are charged in one part of the reactor through oxidation of organic matter, and discharged at certain times by contacting the charged granules with a discharge electrode to recover electricity (Borsje et al., 2016; Deeke et al., 2015; J. Li et al., 2014; Jia Liu, Zhang, He, Yang, et al., 2014; Jia Liu, Zhang, He, Zhang, et al., 2014; Tejedor-Sanz, Ortiz, et al., 2017; X. Wang et al., 2014). In the following table (Table 1) examples of reactor performances using AC granules as electrode material in bioanodes are shown, with reactors ranging from mL to L scale. These reactors have been operated in intermittent mode either through control or through intermittent contact of the AC granules with the current collector.

Table 1. Performance overview of capacitive MFCs with activated carbon (AC) granules.

Reactor type	V _{total} (mL)	V _{granules} (mL)	Control mode	I _{max} (A m ⁻³ _{reactor}) (I at P _{max})	I _{max} (A m ⁻³ _{granules}) (I at P _{max})	Reference
Single granule fixed with wire current collector with intermittent control	1	0.01	-0.3 V vs Ag/AgCl	757	76765	(Borsje et al., 2016)
Granules with intermittent contact to anode mesh via stirring	7	1.14	external resistor; air cathode	460 (260)	2837 (1603)	(Jia Liu, Zhang, He, Zhang, et al., 2014)
Granules with intermittent contact to anode rod via fluidization through liquid pumping	40	2.27	-0.2 V vs Ag/AgCl	5	89	(Jia Liu, Zhang, He, Yang, et al., 2014)

Granules with intermittent contact to immersed anode plate via fluidization through liquid pumping	680	80	+0.2 V vs Ag/AgCl	25	214	(Tejedor-Sanz, Ortiz, et al., 2017)
Granules with intermittent contact to tubular anode cloth via fluidization through liquid pumping	1000	300	48Ω; air cathode	23 (11)	78 (37)	(J. Li et al., 2014)
Granules with intermittent contact to anode rod via fluidization through liquid pumping	1000	177	external resistor; air cathode	0.8 (0.4)	4.2 (2.3)	(X. Wang et al., 2014)
Granules with intermittent contact to anode plate in external cell via transport using gas lift	2102	392	-0.3 V vs Ag/AgCl	0.7	3.6	(Deeke et al., 2015)

The highest current, both based on reactor and granule volume, has been achieved with a single granule fixed to the current collector (Pt wire); it produced a current of 77 kA m⁻³ granule, several orders of magnitude higher than larger scale systems with intermittent contact with the current collector (Borsje et al., 2016). Both when reactors increase in size and when the granule volume increases, the volumetric current decreases. This indicates that there is room for further improvement in the design of scaled-up systems. Proper contact between granules and current collector seems the most important design criterion for scaling up these reactors, as the current produced by a single granule which is contacted via a wire is several times higher than the current produced by granules that are in contact with the current collector via fluidization.

Many of the studies are fluidized bed systems using different fluidization methods, liquid or gas based, that cause the granules to be contacted with the current collector. The granules can be either charged and discharged in the same reactor (J. Li et al., 2014; Jia Liu, Zhang, He, Yang, et al., 2014; Jia Liu, Zhang, He, Zhang, et al., 2014; Tejedor-Sanz, Ortiz, et al., 2017; X. Wang et al., 2014), or can be charged in one reactor and discharged in another reactor (Deeke et al., 2015). The granules are transported between both reactors through fluidization. Tejedor-Sanz and collaborators (Tejedor-Sanz, Ortiz, et al., 2017) showed that the system with one reactor, where the current collector was immersed in the fluidized bed, increased the performance compared to charging and discharging in two separate reactors, as used by the gas lift reactor developed by (Deeke et al., 2015). The gas flow caused a circulation of the liquid flow that transported the granules past the

current collector. The highest current density of a fluidized system was achieved by Liu and co-workers (Jia Liu, Zhang, He, Zhang, et al., 2014) where the AC granules were fluidized and brought in contact with the current collector through stirring of the anolyte and granules. The authors identify that stirring requires energy and that a larger scale system needs a different fluidization method (Jia Liu, Zhang, He, Zhang, et al., 2014). Further studies are needed to investigate which mode of fluidization is preferred to ensure the best contact between AC granules and current collector.

4.1.2. Other materials for capacitive bioanodes

Besides activated carbon, other materials have been tested as capacitive anode material. For example, transition metal oxides (e.g. based on Fe, Co, Ni, Mn, Cu) show pseudocapacitive behavior, although most have yet to be shown as capacitive bioanodes (Patake et al., 2009; Salunkhe et al., 2017). Wang and co-workers (Y. Wang et al., 2016) successfully applied carbon felt coated with MnO_2 as a capacitive bioanode. The specific capacitance of the coated felt was increased fivefold compared to the carbon felt. This led to an increase in both peak (30-40 times higher) and continuous current production (8.5-8.9 times higher) and showed the possibility to store charge (8.8-9.3 times higher). Liang and co-workers (Liang et al., 2017) investigated charge and discharge ratios of a reduced graphene oxide anode with MnO_2 modification, produced 16% higher current density when operated intermittently. However, after 11 hours of operation, this was reduced to 10% higher current in intermittent mode. Further study showed that a MnO_2 /felt bioanode lost 88% of its capacitance without protection by a conductive polymer layer (polymer/ MnO_2 /felt). The polymer/ MnO_2 /felt bioanode showed a higher electron transfer coefficient than the carbon felt or MnO_2 /felt bioanodes (P. Liu et al., 2018). This could be beneficial for high average current density while under intermittent operation (fast discharge of stored charge). Future studies still will have to show the benefits of this electrode in long term intermittent operation.

Also, other transition metal oxides have been tested in capacitive MFCs. Ruthenium oxide (RuO_2) has a high specific capacitance of over 800 F g^{-1} (Hong et al., 2014a). A carbon cloth anode, modified with Ruthenium oxide, was tested in an MFC and showed an improved current density of 17 times for a mixed community bioanode (4.2 A m^{-2}) compared to an uncoated anode (0.2 A m^{-2}) (Lv et al., 2012). Further study showed that similar to the MnO_2 bioanodes described above, there was a 40% loss of capacitance over 6 months of intermittent operation (Lv et al., 2014). However, application of Ruthenium oxide and other noble metals involves high costs. Therefore, although these materials have been shown applicable as capacitive bioanodes, their use in larger scale systems is expected to be limited.

4.2. Integration of capacitive materials as cathodes

Besides being used as anode, capacitive electrodes can also be used as cathode material with the aim to increase current and power densities of MFCs. Oxygen is the most used oxidant at the cathode due to its natural availability and high redox potential. Two types of cathodes are generally used in MFCs: i) fully submerged cathode and ii) gas-diffusion cathode. In the first case, the cathode is fully submerged in the catholyte liquid and operated with dissolved oxygen. The second case consists of a hydrophobic-type cathode structure that uses oxygen in the gas phase as electron acceptor.

Carbonaceous electrodes are attractive materials for cathodes (Santoro, Kodali, et al., 2017; Z. Wang et al., 2014; Yuan et al., 2016), as they are conductive, have low costs, and possess a high specific surface area. This high specific surface area has two advantages: (i) it can result in lower overpotentials for the oxygen reduction reaction, and (ii) it has capacitive properties that can offer advantages when the system is operated in intermittent mode. The cathode is then positively charged due to reduction reactions (biological or chemical) occurring at the electrode, and balanced out by ions (anions) naturally occurring in the wastewater. For the two types of cathodes used for oxygen reduction in MFCs, the gas-diffusion cathodes have a lower overpotential compared to submerged cathodes because of the higher oxygen concentration at the electrode surface. Whereas submerged cathodes have a large surface area exposed to the electrolyte solution, which is available for EDL formation, gas-diffusion electrodes are less exposed to the electrolyte and therefore, capacitive properties are limited.

When capacitive materials are used as cathode, under open circuit conditions (charge), the cathode potential will increase to a maximum value (see Figure 4). A high cathode potential gives a high cell voltage and results in high power density during capacitive discharge. The intermittent operation of a capacitive cathode can therefore be used to improve the energy and power output during discharges of a capacitive MFC. Activated carbon-based cathodes can be used in combination with catalysts, for example Fe-based materials (Fe-aminoantipyrine, Fe-AAPyr) (Kodali et al., 2017), and enzymes (bilirubin oxidase, BOx) (Santoro, Babanova, et al., 2016). It was been shown, using air-breathing cathodes, that the cathode open cell potential (OCP) increased from +105 mV (AC) to +175 mV with Fe-AAPyr and up to +315 with BOx catalyst. Without catalyst, the maximum power was 0.67 mW. Use of an Fe-AAPyr catalyst increased the power to 0.90 mW (4 W m^{-2}), and the BOx catalyst increased the power to 1.47 mW (6.53 W m^{-2}) (Santoro et al., 2015).

Another effect on integrating the advantages of capacitive materials and an improved ORR was addressed by Santoro and co-workers (Santoro et al., 2015). A gas diffusion electrode was integrated with an additional electrode with high surface area (capacitance) in the electrolyte solution and short-circuited with the cathode electrode. The use of this additional electrode allowed the decrease of internal resistances by one order of magnitude and increased maximum power output with a factor of 10. The maximum power achieved with the additional capacitive electrode increased the maximum power of the air

breathing cathodes to 6 mW (26.7 Wm^{-2}) for the AC cathode, 14 mW (62.2 Wm^{-2}) for Fe-AAPyr cathode and 19 mW (84.4 Wm^{-2}) for BOx cathode.

5. Applications of external capacitors for MFCs

As an alternative to the integrated use of capacitors in MFCs, capacitors can also be connected to MFCs through an external circuit. An external capacitor (of known capacitance) has the advantage of wider potential ranges at which charge/discharge cycles can occur compared to internal capacitors, as there is no living microorganism involved in the charge storage process. Therefore, they can be connected to series of MFCs (to achieve higher voltages) and adjusted to meet the desired power level and so match with the specific requirements of electronic devices (A Dewan et al., 2009).

Dewan and co-workers (A Dewan et al., 2009) described the behavior of an (10-F) external capacitor connected to and MFC, which gradually increased its potential up to 0.5 V (vs SHE) during charge and decreased it drastically to 0 V during discharge. On the contrary, the anode potential gradually decreased down to -0.381 V (vs SHE) during charge, as explained for internal capacitive bioanodes, while it increased drastically to -0.090 V during discharge. The increase in potential of the capacitor during charge caused an increase of the internal resistance in time, which similarly caused a decrease of the current transferred from the MFC to the capacitor. This made the charging process of the capacitor become longer and led to lower power densities in time. Unlike in capacitors, this potential change would not happen with a direct current (DC) power supply, where the potential would keep constant. This study also compared intermittent and continuous energy harvesting modes. Overall, the charge harvested was higher with intermittent mode, although the higher the operating potential the more similar performance was obtained for both modes. The maximum power generated under intermittent mode (at 0.35 V) was 152 μW while the maximum value obtained under continuous mode was 72 μW (at 0.38 V). Another study (Alim Dewan et al., 2010) assessed the effect of different values of capacitance and charge/discharge potentials in order to optimize the performance of two (laboratory-scale and sediment) MFCs. A higher capacitor value decreased the frequency of charge/discharge cycles, which may be adjusted according to the needs of the device to power. While the same capacitance value (3-F) delivered the maximum power output in both MFCs, the potential at which maximum power was achieved varied from one cell to the other. They thereby concluded that the environmental conditions (e.g. pH, temperature) and MFC design (resistances, reaction rates) will determine the electron transfer process and mechanisms and so the optimum capacitance and potential values to use in each system.

Kim and co-workers (Younggy et al., 2011) described how the usage of external capacitors, connected in parallel to MFCs but discharged in series, could avoid voltage reversal of MFC arrays. The study also showed that, when more capacitors were connected

to a single MFC, both the open cell and working voltages increased while the current decreased and the maximum power output kept constant. Similarly, longer charge/discharge times (4 minutes) could increase the peak power from 0.78 mW to 1.95 mW compared to shorter cycle times (1 minute). This research served as prove that external capacitors can be an easy way to manage the power of MFCs, i.e. modifying voltages and currents, making them available for different applications. In fact, key electronic components such as capacitors, but also batteries, boost converters, inductors, transformers, diodes and other devices have been employed into different power management systems (PMS). Energy-harvesting is the first stage of any power management system, designed to harvest (collect) energy from a source and store it in a tank (typically a capacitor) before it can be further distributed. The energy harvesting systems mainly used for MFCs with external capacitors are discussed below (H. Wang et al., 2015).

Successful examples of energy harvesting systems for MFCs based on intermittent energy harvesting have already been achieved, showing that the energy stored by external capacitors was greatly affected by the charge and discharge frequency or duty cycle (S. Ren et al., 2013). Charge-pump systems is another example for voltage boosting that uses capacitors as energy storage devices. These systems, also (called voltage multipliers or even dividers) exploit the flow of current in a closed circuit to charge one capacitor and then discharge it into a second capacitor connected to the DC supply rail, which results in twice the voltage 'seen' at the load stage.⁹⁹ Multiple capacitors can be used as accumulation stages to multiply the amount of source voltage to the desired amount. Pump-charge topologies are better suited for low current levels (<500mA), due to the leakage characteristics of capacitors.

Boost converter-based solutions as energy harvesting systems for MFCs are another method reported in the literature (H. Wang et al., 2015). The key component is the DC/DC converter that is capable of boosting voltage to a higher value for powering real devices. In fact, this configuration is mainly used in sediment (or benthic) MFCs in which individual MFCs can only be connected in parallel, boosting the current at the same voltage, which would be insufficient for powering off-the-shelf sensors. This is due to the fact that MFCs are sharing the same electrolyte and therefore their connection in series is not possible. Sensors require higher voltages to be powered and the currently available literature presents a range of diverse and successful examples of the utilization of this technique (Arias-Thode et al., 2017; Babauta et al., 2018; Donovan et al., 2008, 2013, 2011; Karra et al., 2014; Shantaram et al., 2005; Tender et al., 2008).

Maximum power point tracking (MPPT) systems have also been applied to MFCs as a method for energy harvesting (Alaraj et al., 2014; Degrenne et al., 2012; Park & Ren, 2012b, 2012a). MPPT is dynamic and adapts to the changing MFC output and internal resistance due to environmental or physico-chemical perturbations (e.g. temperature, pH, substrate availability). The advantage of this system is the real-time tracking of the maximum power point and the energy harvesting at that specific point. Given that MFCs

are dynamic, continuous optimization through this technique enables better overall MFC performance.

The first examples of systems in which external capacitors or batteries were used as energy accumulators of MFCs have been Gastrobot (Wilkinson, 2000), the family of EcoBots (I. Ieropoulos et al., 2003; Ioannis Ieropoulos et al., 2010; Melhuish et al., 2006) and more recently, Row-bot (Philamore et al., 2015). The implementation of MFCs within robots led to a more compact and energetically autonomous system that does not require an external supply. In the example of Gastrobot, sugar was fed into a “stomach” populated with *E. coli*, whose (chemically) reduced digestate was fed into chemical fuel cells that extracted energy as electricity and used it to charge the batteries that were powering the robot (Wilkinson, 2000). The EcoBot-I and -II examples demonstrated that electrical energy could be recovered directly inside MFCs (i.e. the MFC stack was the digestive stage) and this energy was transiently stored in electrolytic capacitors that were facilitating a charge/discharge duty cycle, which kept the phototactic robot moving towards the light in a pulsated manner (I. A. Ieropoulos et al., 2012). This was in order to demonstrate a “sleep/wake-up” pattern as part of an on-board energy management system, akin to animals in nature. EcoBot-III went beyond this level of operation since it incorporated a liquid circulatory system and was designed to move towards feeding and watering stations, in order to collect its own food and water; by ingesting (fresh food), digesting (collected food) and egesting (waste), it demonstrated autonomy through the completion of the thermodynamic cycle within a constrained environment. As for Row-bot, it was designed with a compliant lightweight embodiment so that it could operate on water. Inspired by the water boatman, and by rowing itself forward in a nutrient-rich water environment (akin to a polluted lake), whilst at the same time opening a “mouth”, Row-bot demonstrated the potential of ‘living’ in a polluted environment and utilizing the contaminated water as the feedstock for its on-board MFCs (Philamore et al., 2015).

In all three generations of EcoBot as well as Row-bot, external capacitors have been used for temporary storage of the harvested energy, which was only spent (capacitor discharge) when a pre-determined voltage threshold level was reached. From an energy management perspective, the use of capacitors allows the implementation of MFCs in applications where the level of power demanded by a system is greater than the instantaneous level of power produced. From a behavioral point of view, the use of capacitors allows the artificial agent to mimic life-forms, with periods of activity and dormancy that enable a more sustainable management of energy resources and reserves (I. A. Ieropoulos et al., 2012). This interaction between the living entities inside MFCs and the capacitors/electronic circuit artefacts, has given rise to the notion of *artificial symbiosis* that forms part of Artificial Life and Living Machines.

6. Future perspectives

To date, the power output of MFCs is limited. Therefore, the possibility of directly using the power output from MFCs for some practical applications remains a challenge, primarily due to the power requirements of state-of-the-art electronic devices. It is therefore prudent to continue optimizing MFCs for higher levels of performance, whilst at the same time invest in designing and developing electronic commercial products such as devices, motors and actuators that consume less instantaneous power. In this way, the gap that currently exists between off-the-shelf products' power requirements and MFC power output levels, can be met from both directions. As described, capacitors can be used to shorten this gap when used in combination with MFCs, both internally and externally. The combination of MFCs and capacitors can: i) increase power production, ii) bring flexibility in the operation of the system, and iii) allow for scale-up of the system. Capacitive MFCs especially offer the advantage of increased power production when they are operated in intermittent mode, as a capacitor is only beneficial when the power requirement is short.

The cell voltage produced by a single MFC is typically lower than 1 V, which is the thermodynamic limit of the technology when operating with wastewater and using oxygen as electron acceptor. This means that, in order to meet the input requirements of electronic applications, either MFCs need to produce a high current (have a large surface area) so that they can be connected to amplifying/boosting electronics (Alim Dewan et al., 2014, 2010; Donovan et al., 2008, 2011; Ewing et al., 2014; Shantaram et al., 2005) or multiple MFCs are connected as a stack in series, which may be sufficient to run the application directly, depending on input parameters (Ioannis Ieropoulos et al., 2008). Additionally, for practical application of MFCs, storage of energy can be useful, in order to reach a certain level of power output, or to be used when power is required (pulsated or intermittent operation). By using inexpensive activated carbon granules, a new scaled-up reactor was developed, in which the charging and discharging process are separated (Deeke et al., 2015). This allows for a reduction of expensive materials like catalysts, as the discharge process takes place in a small part of the reactor.

Several challenges remain before capacitive MFCs can be applied. The first challenge is to develop fluidized reactors in which good contact between the capacitive electrode and the current collector is ensured, in order to minimize resistances and maximize current density. A second challenge is the competition between electrogens and other microorganisms, like methanogens, especially when real wastewater is used. Strategies to control the anode potential and substrate loading should be further investigated to achieve high Coulombic efficiencies (Sleutels et al., 2016). The duration of charge/discharge cycles is a third challenge that requires further investigation. On one hand, longer cycles result in higher cell voltages and more harvested charge. On the other hand, shorter cycles allow for a better use of the capacitive charge of the system (compared to the faradaic charge). In addition, the ratio between charging and discharging times need further study. Short

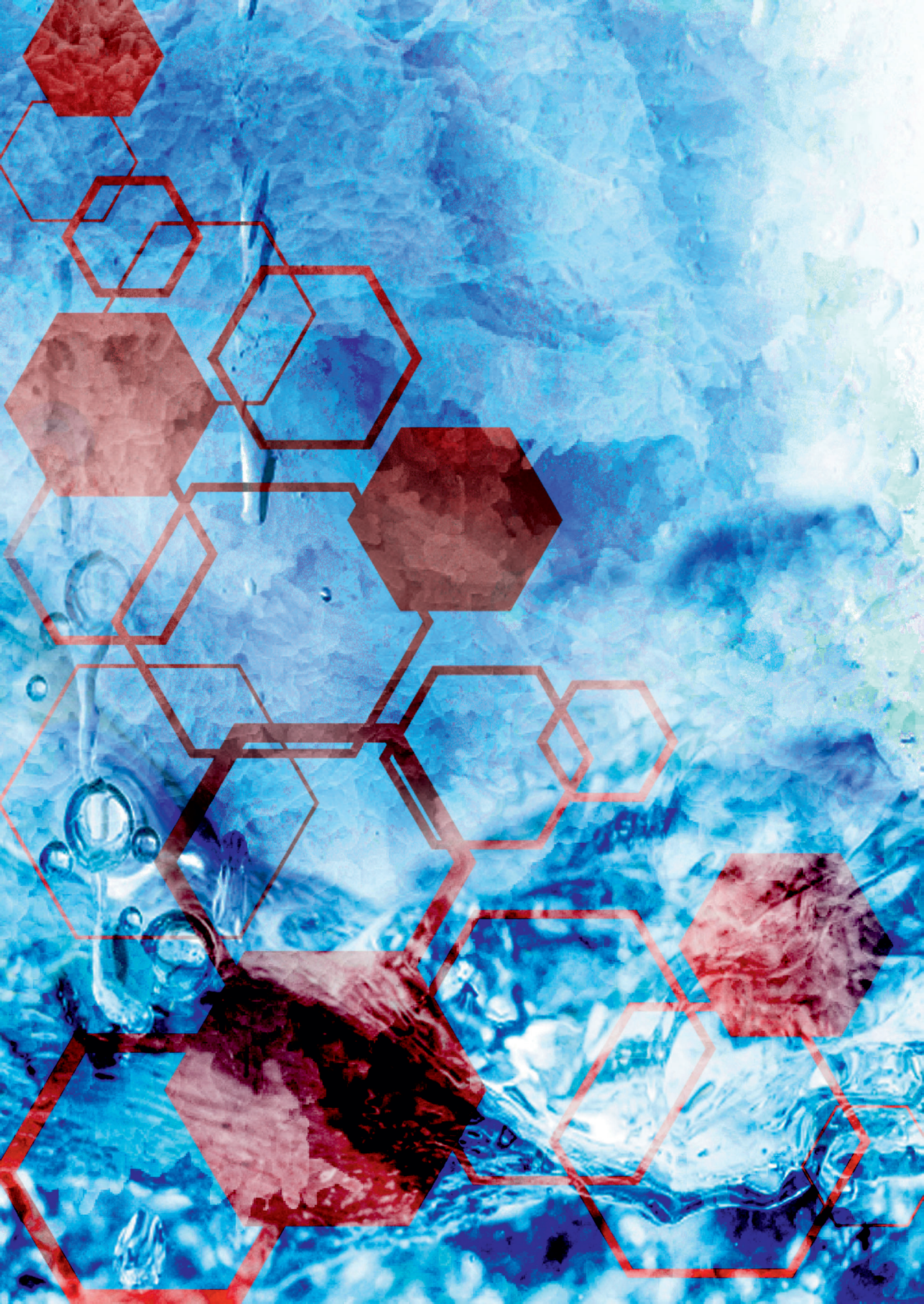
charging times are attractive, as the time that the system is in open circuit conditions (not producing electric power) is limited, which will translate into a more efficient use of the capacitive material and eventually in smaller reactors.

Finding a niche application or market for MFCs is of utmost importance. A clear example of this is sensing technology and robotics. Robotics has integrated this technology to reach self-sustained devices that could not have the same operation features otherwise. A large research field is foreseen on power management strategies, where a lot of research has been done in the past decades but their standardization and more importantly, their commercialization is still a weak spot.

Finally, this review focused on the integration of capacitive electrodes in MFCs, but more generally the use of capacitive electrodes could also offer advantages for other types of BESs. Whether capacitive features, both integrated in the electrodes but also external, can be used to also boost other promising applications, like the CO₂ reduction into valuable products in the cathode of MECs, remains an open research field.

Acknowledgments

This research is supported by the Dutch Technology Foundation STW, which is part of the Netherlands Organization for Scientific Research (NWO), and which is partly funded by the Ministry of Economic Affairs (VENI grant no 13631). The research was performed in cooperation with Wetsus, the European Centre of Excellence for Sustainable Water Technology. Wetsus is co-funded by the Dutch Ministry of Economic Affairs and Ministry of Infrastructure and Environment, the European Union Regional Development Fund, the Province of Fryslân, and the Northern Netherlands Provinces. The authors would like to thank the participants of the research theme “Resource Recovery” for the fruitful discussions and their financial support. FS acknowledges the Italian Minister of Foreign Affairs and the Ministry of the Environment, Land and Sea of the Republic of Italy under the Italian South Africa Research Project 2018 -2020 – Progetto di Grande Rilevanza. It would like to thank the Bill & Melinda Gates Foundation for their support under the grant no. OPP1149065.



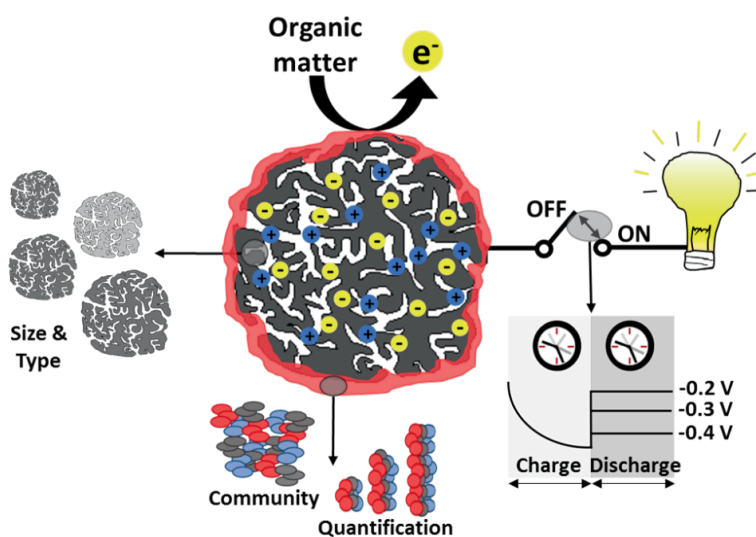
Chapter 3

Electrochemical and microbiological characterization of single carbon granules in a multi-anode Microbial Fuel Cell

Leire Caizán-Juanarena, Ivonne Servin-Balderas, Xuan Chen, Cees J. N. Buisman, Annemiek ter Heijne

Abstract

Capacitive Microbial Fuel Cells (MFCs) use bacteria on a capacitive anode to oxidize organics in wastewater and simultaneously charge the anode material. This study aims to gain knowledge on the performance of single activated carbon (AC) granules, which are used as capacitive bioanode. To this end, a multi-anode MFC that allows the testing of up to 29 granules under the same experimental conditions is used. 2 types of AC granules (PK and GAC) and 3 different size-ranges ($n=8$ each) are studied in terms of current production, biomass quantification, microbial community and charge storage. Additionally, charge storage of PK granules ($n=24$) is determined for different charging/discharging times. Results show that total produced charge directly relates to biomass amount, which has a linear relation towards granule outer surface area. Small AC granules have higher volumetric current densities, which could be of interest for their application in up-scaled reactors. PK granules show slightly higher biomass and current production than GAC granules, while these latter ones show larger volumetric charge storage capacity. Similarly, it is shown that short charging/discharging times are needed to obtain maximum charge storage and current output. These findings are of importance to design and operate MFCs with capacitive properties.



Keywords: capacitive bioanodes; granular activated carbon; total nitrogen; microbial community; charge/discharge cycles; charge storage.

1. Introduction

A Microbial fuel cell (MFC) is a bio-electrochemical system that allows for simultaneous degradation of organic matter in wastewater and production of electricity by the use of microorganisms, also known as electrochemically active bacteria (EAB) (Logan et al., 2006; Logan & Regan, 2006). Compared to the conventional wastewater treatment process, MFCs can recover chemical energy from wastewater that has low concentration of organics (Pham et al., 2006), without demanding energy for aeration (Rabaey & Verstraete, 2005) and reducing sludge production (Pham et al., 2009). Thus, it can be considered a promising and cost-efficient technology for wastewater treatment (H. Liu et al., 2004; Rabaey & Rozendal, 2010; Rozendal et al., 2008). However, the recently reported power production by most MFCs can only reach up to 2-3 W m⁻² (Deeke et al., 2015), which is still relatively low compared to anaerobic digestion. How to increase the power output is still a remaining challenge and so there are many research studies focused on that domain (Borole et al., 2009; Shuiliang Chen et al., 2019; Logan et al., 2015; H. Wang et al., 2012). One possibility is to combine MFCs with capacitors, which act as an energy storage system to improve the power output (Houghton et al., 2016; Santoro et al., 2015). Dewan and co-workers (A Dewan et al., 2009) used an external capacitor to collect the generated power by a MFC and dispended it intermittently, which showed an advantage in providing energy for high-power-consuming devices. It is also possible to integrate a capacitor within the MFC by the use of capacitive materials as electrode (Feng et al., 2014; Santoro, Kodali, et al., 2017). Deeke and co-workers. (Deeke et al., 2012) tested an internal capacitor by using a graphite plate coated with activated carbon powder and a polymer solution, which outperformed a non-capacitive electrode in terms of current density and charge recovery.

The electrode material on the anode plays a vital role in MFCs, as it is the place where the biofilm attaches and electron transfer takes place (F. Li et al., 2010; Pham et al., 2009). By optimizing anode properties such as surface area or roughness, among others, electron transfer can be enhanced and thus the overall MFC performance can be improved (Hou et al., 2013). Carbonaceous materials are the most widely used materials for bioanodes as they have good biocompatibility, good chemical stability, high electrical conductivity and relatively low cost (Santoro, Arbizzani, et al., 2017; J. Wei et al., 2011). Carbon materials with three-dimensional structure and high surface-area-to-volume ratio are of special interest as they can increase volumetric power outputs (Peter Aelterman et al., 2008; H. Ren et al., 2015). Activated carbon (AC) granules have a very porous structure that provides them with a large specific surface area (SSA >1000 m² g⁻¹) (Qu & Shi, 1998), which does not only benefit electron transfer but also allows charge storage (J. Wang & Kaskel, 2012). This feature is particularly important in MFCs with an internal capacitor, where charge storage occurs in the form of electrical double layer (EDL) (Frackowiak & Béguin, 2001; Kastening et al., 1994; Müllier & Kastening, 1994). This is a known charging mechanism of the so-called electrical double layer capacitors (EDLCs) (Sharma & Bhatti, 2010; L. Wei & Yushin, 2011). In the case of MFCs, AC granules will store the electrons produced by

EAB, known as the faradaic current, which can be further released together with the capacitive (stored) current.

Capacitive MFCs also allow intermittent (On-Off) operation of the technology, which similarly can lead to new reactor designs that use AC granules, such as a fluidized bed reactors (Deeke et al., 2015; J. Li et al., 2014; Jia Liu, Zhang, He, Zhang, et al., 2014). Fluidized bed reactors have several advantages compared to classical MFCs, such as the reduction of clogging and ohmic losses, the use of less electrode and membrane materials and a better competition of electrogens over methanogens (Sleutels et al., 2016). To reach reasonable current densities in such reactors, it is crucial to improve the biofilm growth on granules but also the contact between granules and current collector. To assess the maximum performance of AC granules in such a system, Borsje and co-workers (Borsje et al., 2016) studied the electrochemical performance of single AC granules as bioanodes. The produced current density reached up to 76 (PK granules) and 63 (GAC granules) mA cm⁻³ at -0.3 V, which is several orders of magnitude higher than the currents obtained in fluidized reactor systems (Deeke et al., 2015). The potential of single AC granules was thus demonstrated, as well as the possibility of providing valuable information for optimizing up-scaled systems that use this material. However, it is needed to build further on these findings by the study of e.g. more granules that can show reproducibility, important engineering parameters such as granule size, biofilm growth or charge storage at different intermittent operation conditions, among others.

In this study, a multi-anode MFC was built, which allowed for the growth and monitoring of 24 single AC granules under same conditions. The aim was to test several variables of interest for the use of AC granules in MFCs in a reproducible way, looking into outputs such as current production, charge storage, biofilm growth and microbial community of AC granules. The challenges were to: i) determine the performance of different types and sizes of AC granules; and ii) determine the influence of anode discharging potential and optimum charging/discharging times on charge storage.

2. Materials and Methods

2.1. Setup of the multi-anode MFC

The custom-made MFC reactor (Figure 1A) consisted of two compartments: a 2.3 L container as the anode chamber and a glass tube attached to a funnel as the cathode chamber. The anolyte (10 mM NaCH₃COO·3H₂O; 1 mL L⁻¹ Wolfe's Vitamin solution; 1 mL L⁻¹ Wolfe's modified mineral solution; 3.7 mM NH₄Cl, 1.6 mM KCl; 30 mM Na₂HPO₄·2H₂O; 19 mM KH₂PO₄) consisted of 2 L of which 0.2L was inoculum from another active MFC run on acetate, leaving a headspace of 0.3L. The cathode chamber had approximately a volume of 0.13 L (100 mM K₃FeCN₆; 30 mM Na₂HPO₄·2H₂O; 19 mM KH₂PO₄) and was placed in the center of the anode chamber. 24 cm² of graphite felt attached to a titanium wire (1 mm diameter, 36 cm long) was used as current collector in the cathode. To connect

both chambers, a 1.76 cm^2 cation exchange membrane (Fumasep FKB, FuMa-Tech GmbH, St. Ingbert, Germany) was placed on the bottom of the cathode chamber. The lid of the container had one hole for the inflow of substrate, one hole for the reference electrode (Saturated KCl Ag/AgCl) and 29 holes for the working electrodes. Additionally, a hole was made on the side of the container for the outflow. The effect of the distance between working and the reference electrodes on current production was neglected as the latter one was placed outside of the electric field. All potential values in this paper are reported versus Ag/AgCl reference (+0.199 V vs NHE).

Single granules were held up separately with custom-made hook-shaped clamps (Figure 1B). The core of the clamps was titanium (Ti) wire (1 mm diameter) covered by a heat shrink tube (RS Pro 389-634) to prevent its oxidation and the growth of biofilm on its conductive surface. The clamp was passed through a PTFE tube (Polyfluor Plastics BV) surrounded by Tygon® tube (Saint-Gobain Performance Plastics) on the tip. PTFE tape was placed between the PTFE tube and the Ti wire in order to create resistance and ensure a proper and enduring contact with the granule. On the tip of the clamp, a layer of conductive glue (EMS, Pennsylvania, USA) was added and its contact area with the granule was minimized with non-conductive resin (Revlon® Colorstay™) to limit bacterial growth on the clamp. The other side of the titanium wire was passed through a rubber that fitted on the holes made for the working electrodes. The average resistance of the clamps was 0.8 to 1 ohm between the two ends. Each clamp was connected to a channel from the MultiWE32 module (Ivium Technologies, Eindhoven, The Netherlands). This module can operate up to 32 working electrodes that share a common reference electrode and counter electrode. All channels can be simultaneously controlled and sampled with restricted operation modes. Figure 1C is an example of a granule in a clamp with the biofilm in red.

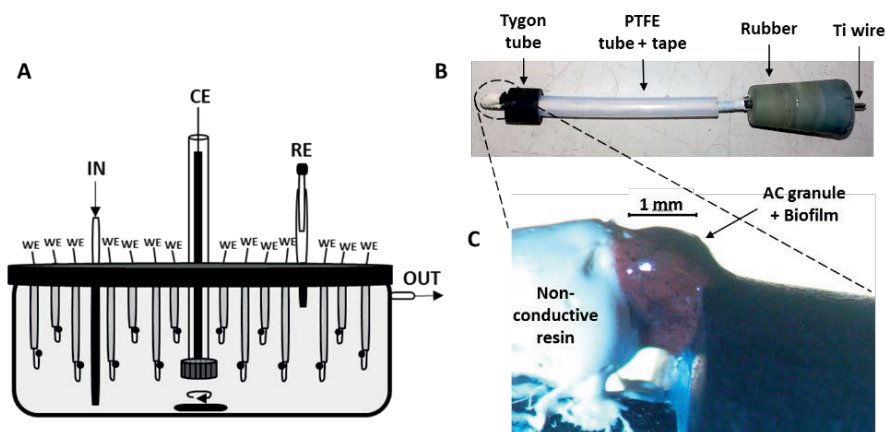


Figure 1. A) A representation of the custom-made multi-anode MFC. B) Picture of a custom-made clamp to hold a single AC granule. C) Biofilm growth on a single AC granule placed on the tip of a clamp.

2.2. Carbon granules

All the granules were first sieved (aperture sizes 2, 2.8 and 4 mm, Retsch®, Germany) and then individually selected for an approximate spherical shape and weighted (Mettler Toledo, $d = 0.001$ mg). Table 1 contains the exact size range and weight information about each of the granules used in this study. After selection, granules were treated with 22% hydrochloric acid (HCl) for 24 hours and washed 3 times with demi water (Wu et al., 2015). This is a common practice to remove surface organic contamination and metal impurities and thus standardize the electrode material under study for comparative purposes.

To analyze the influence of the electrode material and size, two types of activated carbon (PK1-3 and GAC 830W, Cabot Norit Nederland B.V., Amersfoort, the Netherlands) and three ranges of sizes for PK granules (large, 2.8-4.0 mm; medium, 2.0-2.8 mm; small, 1.0-2.0 mm) were tested in the same reactor. Altogether, 24 granules were tested: 6 GAC small granules, 6 PK small granules, 6 PK medium granules and 6 PK large granules. Same granules for the small size-range were used to analyze the influence of the discharging anode potential on charge storage. A new reactor was built with 24 PK granules of three size ranges, 8 granules each. Only the small granules were used to study the effect of different charging/discharging times. As control, three glass beads (B Braun biotech international, Schwarzenberg, Germany) of 2mm diameter covered with PTFE tape were clamped and placed in each reactor. For SEM and NGS experiments, graphite granules (GG), i.e. non-activated carbon granules, were placed in the reactor.

Table 1. Weight and size distribution of the granules selected for the study of: i) granule size, type and potential ii) SEM images, iii) NGS analysis and iv) charging/discharging times.

	Carbon granule	Small (1.0-2.0mm)	Medium (2.0-2.8 mm)	Large (2.8-4.0 mm)
Size & Type & Potential	PK 1-3	1.5 - 2.0 mg	3.2 - 3.9 mg	7.5 - 9.7 mg
	GAC 830W	1.8 - 2.3 mg	-	-
SEM images	PK 1-3	-	4.2 - 6.0 mg	8.1 - 10.3 mg
	GAC 830W	-	7.6 - 9.4 mg	11.2 - 29.8 mg
	GG	-	18.2 - 22.1 mg	46.2 - 50.8 mg
NGS analysis	PK 1-3	-	3.9 - 6.1 mg	-
	GAC 830W	-	4.5 - 7.0 mg	-
	GG	-	8.6 - 14.2 mg	-
Charging / Discharging times	PK 1-3	1.8 - 3.0 mg	5.0 - 8.9 mg	10.0 - 23.3 mg

The weight of granules was the only parameter that was measured, while size was ensured within certain ranges. Therefore, the volume of the granules was estimated by using the apparent density values from the manufacturer: 0.3 g mL^{-1} for PK granules and 0.5 g mL^{-1} for GAC. These are different densities from those used in a previous study for the same type of granules (Borsje et al., 2016). As for the surface area, the radius was approximated from the volume by assuming a spherical granule. The outer surface area (SA) of a sphere was then calculated, without considering the possible roughness or pores where bacteria could have access to. Finally, to calculate the (average) SSA of granules, values determined in a previous study (Borsje et al., 2016) were used for a pore width range of 0.3-50 nm: $764 \text{ m}^2 \text{ g}^{-1}$ for PK and $885 \text{ m}^2 \text{ g}^{-1}$ for GAC. These values are the result from applying a model (2D-NLDFT) to N_2 adsorption measurement data.

2.3. MFC operation

Right after granules were placed in the reactor, cyclic voltammetry (CV) scans (3 cycles, -0.3 V to -0.48 V, at a scan rate of 0.3 mV s^{-1}) were performed to verify if the cables of the MultiWE32 module worked well and if the contact between granule and clamp was good (see Supporting Information, S1). After, granules started to be controlled at a constant anode potential of -0.350 V. Batch mode was maintained for approximately 3 days after inoculation in order to prevent wash out of inoculum. Continuous mode was then started by pumping anolyte at a rate of $200 \text{ } \mu\text{L min}^{-1}$, which translated in an HRT of 7 days. 3 solutions (acetate, PBS with mineral and vitamins, and demi-water) were placed in separate bottles in the fridge (at 4°C) and were continuously flushed with N_2 gas to keep them anaerobic. The pump (Gynkotek M480 CS HPLC Pump - High Precision Pump) was able to mix the solutions, at a ratio of 1:1:2, to have the desired final concentration. The catholyte was replaced once its color faded (pointing out complete reduction of $\text{K}_3\text{Fe}(\text{CN})_6$). In addition, an oxygen sensor spot (PreSens- Precision Sensing GmbH, Regensburg, Germany) was used to monitor the oxygen level in the anolyte, which was kept below 0.1%. A magnetic stirrer at 100 rpm was used to minimize mass transfer limitations and temperature was controlled at 30°C . 2 ml samples were taken daily from the anolyte to measure pH, and stored after at -80°C for further acetate analysis. Current was recorded every 600 seconds.

In the type, size and potential experiment, around 7 days after inoculation clamps were disconnected and granules were collected. Just before that, 3 charge/discharge cycles of 600 seconds each were done. Charge was done at open circuit (OC) and discharge at a constant potential of -0.2 V, -0.3 V or -0.4 V. Only because granules were placed in the same reactor we were able to compare between them. Same was done for SEM images, where 8 granules (4 medium and 4 large) of activated (PK and GAC) and non-activated carbon granules (GG) were placed in the same reactor and controlled at -0.35 V for 9 days (see Supporting Information for cumulative charge, S2). For NGS analysis, same procedure was followed but for 5 granules of each type and for 15 days to ensure enough bacterial

growth (see Supporting Information for cumulative charge, S3). As for the study of charging/discharging times, growth was maintained up to 3 weeks in which charge/discharge cycles were done regularly (every 2-3 days) as previously explained. Before collecting the granules, different charge and discharging time combinations were applied with 2, 5, 10 and 15 minutes at -0.2 V and -0.3 V as discharging potentials. Combinations between 2 and 15 minutes were not addressed, and the discharging potential of -0.4 V was not contemplated as little charge could be measured.

A previous study (Deeke et al., 2012) reported that capacitive electrodes could cope with measurements in intermittent mode during repeated cycles, therefore the dataset obtained from the different charge/discharge cycles in this study are considered valid. The faradaic current, i.e. the current produced from acetate oxidation, was recorded after 600 seconds of stabilization period during discharge. This current was used to calculate the capacitive current, i.e. the current released from the EDL formation, according to Eq. 1.

$$Q_{\text{Stored}} = \int_0^t I_C dt = \int_0^t (I_T - I_F) dt \quad (1)$$

where Q_{Stored} is the stored/capacitive charge (C), I_C is the capacitive current (A), I_F is the faradaic current (A) and I_T is the total current (A) as result of the sum up of capacitive and faradaic currents. More information on current and potential behavior of capacitive electrodes can be found in previous research (Borsje et al., 2016; Deeke et al., 2012).

2.4. Total Nitrogen (TN) analysis

Total nitrogen (organically and inorganically bounded) was determined as indication of the amount of biomass attached to AC granules. After harvest, granules were washed in a buffer solution without NH_4Cl to avoid measuring nitrogen from the anolyte. After, granules were processed according to the protocol of Laton Total Nitrogen cuvette test 20-100 mg L^{-1} TN_b (LCK 338, HACH®, Dusseldorf, Germany). Note that the kit works in terms of volume, therefore 0.2 mL of miliQ water was added in the reaction vessel together with each AC granule. After other chemicals were added, the digestion step consisted of 30 minutes at 120 °C. 0.5 mL of the final sample was transferred from the reaction vessel to the LCK cuvette, from which the nitrogen concentration was read. Some (PK) granules were again checked for nitrogen content after the first TN analysis to verify if any biomass was left behind. Nitrogen content of those granules was $1.9 \pm 0.4 \mu\text{g N}$ (average of 3). Similarly, clean (PK) granules without biomass but with the same acid treatment were also measured for TN as control. Nitrogen content of those granules was $1.3 \pm 0.1 \mu\text{g N}$ (average of 3). These TN contents are more than 5-fold lower than those measured for the smallest PK granules (see Figure 2B).

2.5. Acetate quantification

Before the measurement, liquid samples taken from the reactor were centrifuged for 10 min at 10000 rpm to remove the biomass. Part of the supernatant was mixed with formic

acid (15%) in a 9:1 ratio and added to the GC vessels that were well closed with rubber lids. Acetate concentration was analyzed with the gas chromatograph (Agilent 7890B). Split injection (1:25, 1 μ L volume) was done at constant temperature (250 °C) in a HP-FFAP column (25 m \times 0.32 mm \times 0.50 μ m) with helium as the carrier gas (grade 5.0, at 2 mL min⁻¹ column flow). A flame ionization detector (FID, 240 °C) was used and data were recorded with Chromeleon™ CDS software (6.80 SR13).

2.6. Scanning electron microscopy (SEM)

Granules were individually collected from the reactor and fixated with 2.5% glutaraldehyde for 2 h at room temperature. Afterwards, they were rinsed 3 times with a phosphate buffer solution (30.5 mM Na₂HPO₄ and 19.5 mM KH₂PO₄) and dehydrated with a sequence of ethanol solutions (30%, 50%, 70%, 90% and 100%) for 30 min each. Finally, granules were dried at 105 °C for 1 h. For the imaging, single granules were placed in a specimen holder of the scanning electron microscope (SEM) JEOL JSM-6480 LV (JEOL Technics Ltd., Tokyo, Japan). With a magnification of 30-100,000x, SEM was operated at an acceleration voltage of 3-10 kV and an electron beam diameter of 20-30%. Images were analyzed with the software JEOL SEM Control User Interface version 7.07.

2.7. Next-generation sequencing (NGS) analysis

Five granules of each carbon type were harvested, cleaned individually with phosphate buffer and placed in the same Eppendorf for storage at -80 °C. Genomic DNA was extracted with the Powersoil® DNA isolation kit (MO BIO Laboratories, Carlsbad, CA, USA) and used to amplify the V3-V4 region of 16S rRNA according to the standard illumine library preparation method described by Takahashi and co-workers (Takahashi et al., 2014). The same primer sets were used to analyze bacteria and archaea. Taxonomic analysis was performed by using the QIIME software (package version 1.9.1) and OTU picking was done by the SILVA 128, 16S reference database and the uclust tool (Quast et al., 2013). The same SILVA reference database was subsequently trained by the RDP classifier to perform OTU classification (Q. Wang et al., 2007).

2.8. Statistical analysis

Differences in current production, total produced charge, nitrogen and charge storage were analyzed with one-Way ANOVA at $p < 0.05$ with IBM SPSS Statistics 20, using the following factors: type of activated carbon (PK or GAC), size of activated carbon (small, medium or large) and discharging anode potential (-0.4 V, -0.3 V or -0.2 V). All granules compared with this method were grown under same environmental conditions. The assumption of normality was tested with Shapiro-Wilk statistics and homogeneity of variance was assessed with Levene's test. In case the variance between groups was high or the number of samples between groups was unequal, Welch's *t* test was performed.

3. Results and Discussion

3.1. Current production by different types and sizes of single AC granules under continuous growth conditions

Performance of different granule types and sizes placed in the same reactor was compared. Their current was monitored during one week at -0.35 V anode potential and, after this period, they were collected from the reactor and biofilm growth was quantified (as total nitrogen). Figure 2A shows the current produced by each type of granule (with standard deviations) as a result of average values of 6 granules for PK and GAC, and 3 glass beads for controls. Generally, all granules followed the same growth pattern, with a maximum current around 3 days after inoculation and a steady-state current of 65-71% of the maximum current after 1 week of growth. This shape seems to be typical for potential controlled bioanodes as previously reported in literature (Molenaar et al., 2018), which could relate to an increased ionic diffusion resistance due to the formation of a thicker biofilm (Sun et al., 2016). Nevertheless, nutrients and substrate were continuously supplied (acetate concentration was maintained >5mM) and the solution was continuously stirred.

Average currents, after the maximum was reached (around 3 days after inoculation), were from high to low: 0.3 ± 0.05 mA for large PK, 0.1 ± 0.03 mA for medium PK, 0.1 ± 0.01 mA for small PK and 0.05 ± 0.02 mA for small GAC granules. However, when normalized to granule weight, small PK granules had the highest current densities, 43.3 mA g^{-1} , followed by medium PK (34.2 mA g^{-1}), large PK (31.7 mA g^{-1}) and small GAC (24.6 mA g^{-1}). These values are in the same range to those previously found for single PK and GAC granules at -0.3 V anode potential, i.e. 58 mA g^{-1} and 24 mA g^{-1} , respectively (Borsje et al., 2016). The current measured for controls was more than 10 times lower than the current produced by granules, i.e. 0.003 ± 0.001 mA, showing that the contribution of the current collector (clamp) to the current production by single AC granules was negligible.

Total produced charge was calculated as a result of the current produced throughout the whole growth period. Average values were 107 ± 20.4 C for large PK, 51.2 ± 12.2 C for medium PK, 31.4 ± 4.8 C for small PK, and 20.5 ± 7.6 C for small GAC. Figure 2B shows a positive relation between the produced charge and total nitrogen content of each granule, which is expected as both parameters are meant to increase with bacterial growth. The relation found was $2340.3 \text{ C mg}^{-1} \text{ N}$ ($R^2 = 0.98$), which is half of that recently found for bioanodes in flat (FTO) electrodes, i.e. $4982.2 \text{ C mg}^{-1} \text{ N}$ (Molenaar et al., 2018). The lower value obtained in this study could relate to a lower microbial activity of the biofilm or to a higher nitrogen content of the same, although it is difficult to say since the bioanodes measured in that latter study were grown between 1 to 24 days. Similarly, the graph shows an increased nitrogen content with increased granule size. This was found to be related to the estimated outer SA of granules, which had a linear relation ($R^2 = 0.9$) towards the amount of biomass. In fact, large PK granules had most biomass (0.05 ± 0.005 mg)

followed by medium PK (0.03 ± 0.007 mg), small PK (0.02 ± 0.003 mg) and small GAC (0.01 ± 0.004 mg) granules. Differences in current were significant between all PK sizes among each other ($p < 0.05$), meaning that higher currents were related to more biomass on larger granules. Differences between small PK and GAC granules were non-significant in terms of produced charge and total nitrogen ($p = 0.47$ and $p = 0.37$, respectively), probably due to their similar estimated outer SA (0.16 ± 0.01 cm² and 0.12 ± 0.01 cm² in average, respectively).

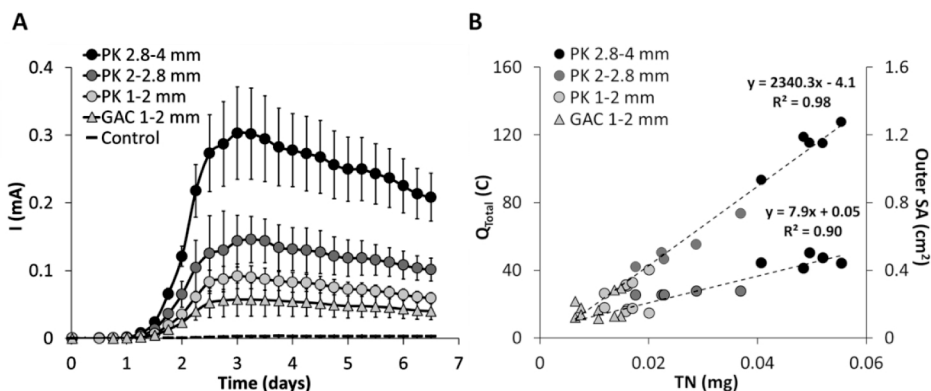


Figure 2. A) Current production (mA) of three sizes of PK and small GAC granules controlled at a constant potential (-0.35 V vs Ag/AgCl). Each data point represents the average current value of every 0.25 days. B) Total produced charge (C; primary axis) by each granule during the whole growth period and estimated granule outer surface area (cm²; secondary axis) as a function of total nitrogen (mg).

3.2. Biofilm visualization and microbial community determination in activated and non-activated carbon granules

Biofilm growth was also assessed by means of SEM images and genetic sequencing for activated (PK and GAC) and non-activated (GG) carbon granules, which were grown in the same reactor and under the same conditions. Figure 3 shows the surface of granules (see Table 1) at different magnifications after 9.4 days of growth. They were all covered by biofilm with no apparent differences among each other, which could mean that: i) the activation process of carbon granules did not have an influence on bacterial growth; ii) the available surface area where bacteria can grow (> 0.5 μ m, bacterial size (Bond & Lovley, 2003)) is similar in every granule type; iii) the surface roughness of all granules is high enough for the attachment of bacteria or, instead, has no influence after the first layer of bacterial growth; or iv) the operation conditions (e.g. a continuous growth, potential control, good contact of the electrode with the current collector and little shearing forces) led to a well-developed biofilm no matter the electrode material. The average produced charge by each granule type (4 medium and 4 large granules) in the reactor was 161.9 ± 45.1 C for GG, 108.7 ± 32.8 C for GAC and 102.1 ± 12.4 C for PK granules (see Supporting

Information, S2). Based on these data we can conclude that, under continuous growth, activated carbon granules did not provide any advantage in terms of biofilm growth and current production compared to non-activated carbon granules, which have in contrast very few pores and therefore have low charge storage capacity. These results contradict what was found in a previous study (Deeke et al., 2012), where the increased current densities of flat capacitive electrodes over non-capacitive ones under continuous growth (at -0.4 V vs Ag/AgCl) were attributed to the increased roughness of the former.

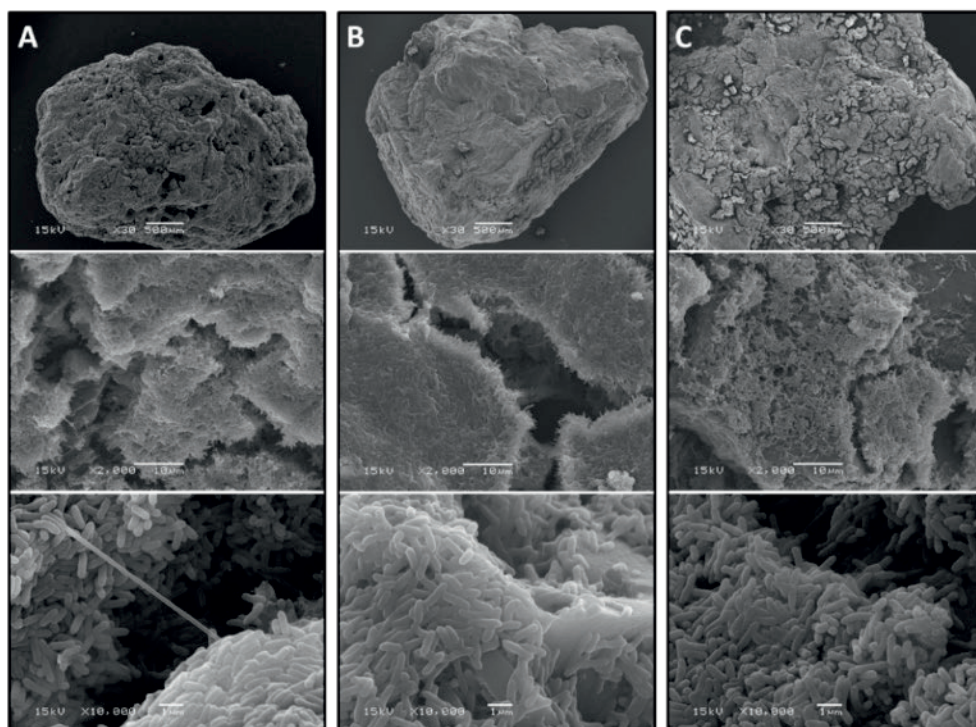


Figure 3. SEM images of PK (A), GAC (B) and GG (C) granules at different magnifications: x30 (up), x2000 (middle) and x10000 (bottom). For this figure, a medium and a large granule were used for PK (4.4 and 8.1 mg), GAC (9.4 and 29.8 mg) and GG (22.1 and 50.8 mg). They were controlled at -0.35 V vs Ag/AgCl in the same reactor for 9.4 days.

Microbial community of the biofilm was characterized for the same type of carbon granules (see Table 1) but in another run that lasted a bit more than 15 days (see Supporting Information, S3). Figure 4 shows the composition of the microbial community, which was similar among the three types of granules. *Geobacter* spp. accounted for 50% of the microbial community in PK granules, 31% in GAC granules and 43% in GG granules. The next most abundant microorganisms were within the family of *Rhodocyclaceae*, which accounted for 11-14.3% of the total microorganisms, and the genus *Acetobacteroides* with relative abundances of 6.4-12.1%. Other bacteria (with > 1% of relative abundance) belonging to the phyla of *proteobacteria*, *bacteroidetes*, *firmicutes* or *synergistetes* could

also be found in the biofilm. This is a similar microbial community composition to what was determined in other studies for bioanodes (Guo et al., 2013). Some studies have searched for changes in microbial composition and biofilm morphology for different electrode materials (surface functional groups) (Guo et al., 2013) and operation modes (periodic polarization over constant control) (X. Zhang et al., 2018). However, in this study, the similar composition and relative abundance of microorganisms as well as current production indicate that the above-mentioned granule properties did not affect biofilm growth or, instead, those properties were overruled by e.g. the continuous and potential controlled operation mode.

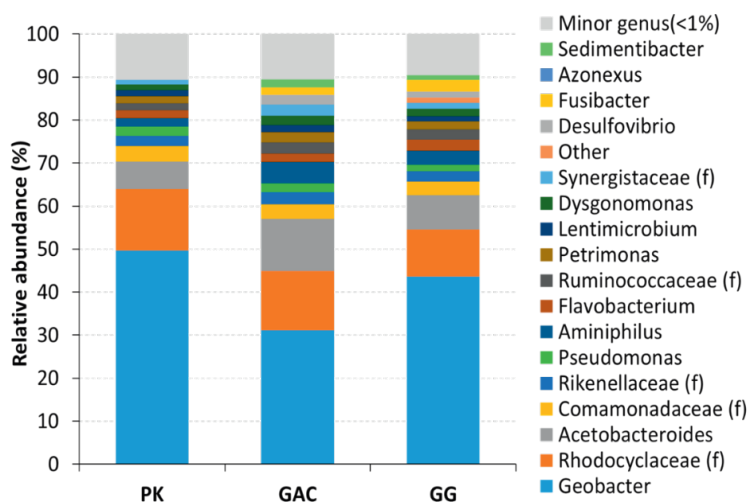


Figure 4. Microbial community at the genus level of three types of carbon granules: GG, GAC and PK. In case the genus was unknown, other taxonomic levels were specified: (f)= family level. Granules were controlled at -0.35 V vs Ag/AgCl in the same reactor for 15 days.

3.3. Influence of the anode discharging potential and charging/discharging times on charge storage of PK and GAC granules

Experiments were performed at OC (charge) and potential control (discharge) to study charge storage in PK and GAC granules. Here, we report on the results for small granules. Overall, more positive discharging potentials increased charge storage of PK and GAC granules, as shown in Figure 5. This is expected as, when the potential difference between charge and discharge cycles increases, the driving force to harvest electrons also increases, leading to a larger charge storage value. Nevertheless, only -0.2 V obtained significantly different values compared to the other two potentials ($p < 0.01$). PK granules had an average stored charge of 1.4 ± 0.5 mC, 4.5 ± 1.8 mC and 15 ± 4.4 mC at discharging potentials of -0.4 V, -0.3 V and -0.2 V, respectively, while GAC had an average stored charge of 1.8 ± 0.7 mC, 5.5 ± 2.7 mC and 16.2 ± 6.8 mC at same potentials. Even

though GAC obtained overall higher values than PK granules (Figure 5A), when normalized to the calculated specific surface area, PK granules showed higher values (Figure 5B) meaning their surface area is used more efficiently for charge storage. This could relate to the increased mesoporosity (2-50 nm pore size) of PK granules (40%) compared to that of GAC granules (20%) (Borsje et al., 2016), which has been related in literature to increased double layer capacitance (Gryglewicz et al., 2005; Han et al., 2014). The pore size distribution could also be the reason for differences in the discharge behavior of each granule type; PK granules had 80% of charge recovery (of the total stored charge released in 10 minutes) after 2 minutes of discharge, while GAC granules reached the 80% charge recovery after 3 minutes of discharge (see Supporting Information, S4). This delay in GAC granules could relate to their increased microporosity (< 2nm pore size) contribution (80%) compared to that of PK granules (60%), which could limit the ion transport (Borsje et al., 2016). Nevertheless, differences in charge storage between materials were non-significant at every potential with and without normalization ($p = 0.22-0.82$). It is important to highlight that charge storage and discharge behavior were highly variable at different stages of biofilm growth (data not shown). Therefore, it is very important to always compare the performance of bioanodes that have strictly grown under the same conditions and for the same amount of time, as done here.

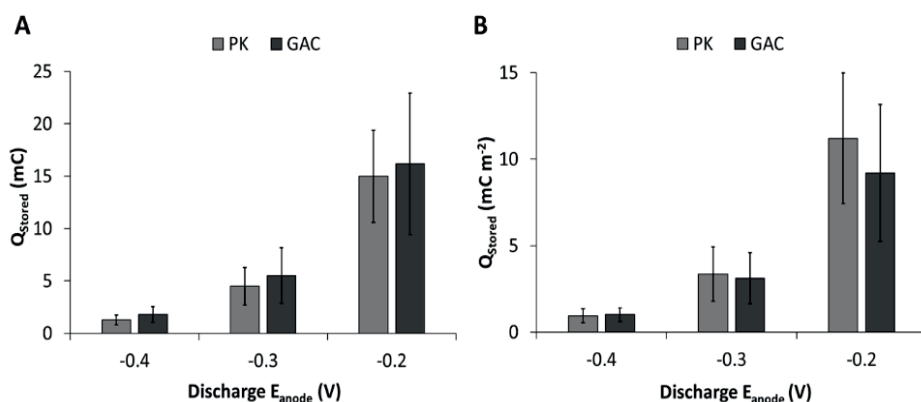


Figure 5. A) Absolute values of stored charge (mC) and B) stored charge normalized to SSA (mC m⁻²), both as a function of anode discharging potential (-0.4 V, -0.3 V and -0.2 V vs Ag/AgCl) for small PK and GAC granules 7 days after inoculation.

As the measurement of charge storage depends on the discharging time (t) used to determine it (see Eq. 1) and the charging time used by bacteria to produce electrons, we studied the effect of combining different time intervals (2, 5, 10 and 15 minutes) for OC periods (charge) and constant potentials (discharge) on charge storage. Figure 6A shows the absolute values of stored charge by small PK granules (see Table 1) for every measured combination at -0.3 V discharging potential. In general, and based on statistical analyses, 2 minutes of charge was significantly lower than 10 and 15 minutes of charge ($p < 0.01$).

This was not the case at the shortest discharging time, where 2 minutes of charge had non-significant differences compared to the rest of charging times. Similarly, no significant differences could be found between 5, 10 and 15 minutes of charge ($p = 0.3-1.5$). As for discharging times, no significant differences were found among them ($p = 0.1-1$). However, if we look at the total duration of the cycle, shorter charge/discharge cycles might be beneficial not only to increase overall charge storage compared to longer cycles but also to reduce the number (mass) of granules needed in the system. As an example, a cycle of 5-2 minutes can store 8.7 mC, while in that same time 1.75 cycles of 2-2 minutes can store 14.5 mC.

If we calculate the total produced charge (faradaic + capacitive), it increased linearly with longer discharging times due to longer faradaic currents (data not shown). Deeke and co-workers (Deeke et al., 2012) studied the effect of different charging/discharging times on the total produced charge and indeed found that longer discharging times favored total produced charge. However, longer discharging times might not be preferable as it limits the contribution of capacitive current. To get more insight about faradaic and capacitive currents, contribution (%) of stored charge to the total produced charge was calculated (Figure 6B). If we consider charging times, similar statistical results to those explained for absolute charge storage values were found. On the contrary, shorter discharging times led in general to significantly larger contribution of the capacitive charge to the total charge ($p < 0.02$). Therefore, from the results we conclude that 2 minutes of discharge should be combined with 2 minutes of charge for the highest contribution of stored charge to the total produced charge, same as for the highest absolute values previously presented. Similar trends were found for PK granules at -0.2 V, with overall higher absolute values and contributions of charge storage due to a larger driving force (see Supporting Information, S5).

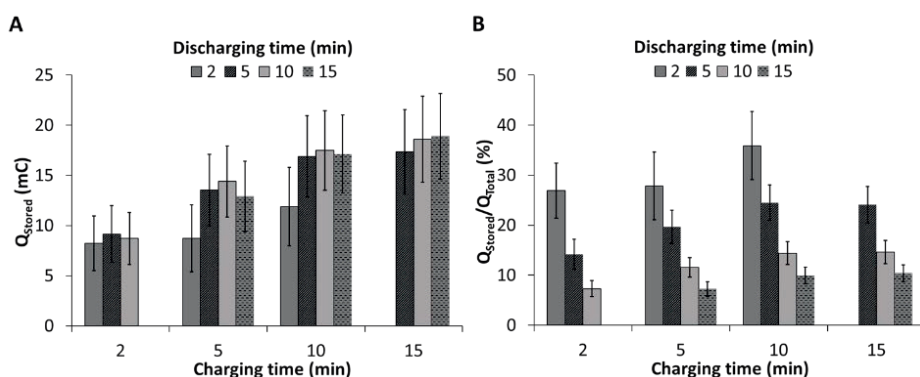


Figure 6. A) Stored charge in absolute values (mC) for PK at -0.3 V vs Ag/AgCl. B) Stored charge contribution (%) to total produced charge for PK at -0.3 V vs Ag/AgCl. Combination of charging/discharging times were 2, 5, 10 and 15 minutes.

3.4. Outlook

As shown in the results section, the outer SA of granules plays an important role in current production, with larger granules providing larger SA for bacterial growth. However, from an engineering point of view, volumetric current densities are most important, as the amount of granular electrode material needed for a system will be generally evaluated per volume. The highest volumetric current densities (average values after the maximum was reached) were achieved by small PK and GAC granules, $12.4 \pm 1.7 \text{ mA mL}^{-1}$ and $12.2 \pm 1.4 \text{ mA mL}^{-1}$, respectively, followed by medium ($9.9 \pm 1.1 \text{ mA mL}^{-1}$) and large ($9.1 \pm 1.0 \text{ mA mL}^{-1}$) PK granules. However, no significant differences were found between them ($p= 1.4\text{-}1.5$). Additionally, the surface-area-to-volume ratio (SA:V) of granules needs to be maximized, as it means larger surface area for bacterial growth will be available per unit of volume. The calculated SA:V ratio of the granules used in this study showed that larger granules have a lower ratio, which again indicated the preference towards the use of small AC granules.

If we look at charge storage normalized to granule volume, small GAC granules showed higher volumetric charge storage ($1.3 \pm 0.6 \text{ mC L}^{-1}$) than small PK granules ($0.74 \pm 0.3 \text{ mC L}^{-1}$) at -0.3 V discharging potential, even though the latter ones could store more charge per SSA. Once again, differences between the two type of granules were non-significant ($p= 0.1$). If we look at granule (PK) size, no linear relation could be found between charge storage and granule weight ($R^2= 0.3$), current ($R^2= 0.5$) or SSA ($R^2= 0.3$). This could relate to an increased variability of charge storage with an increased granule size, as shown in the Supporting Information (S6) as a function of SSA. Therefore, it is possible that other factors affect charge storage at increased granule size, such as larger potential drops, larger internal resistances due to ionic transport or lower actual SSA values, as previously measured on thick electrodes (Deeke et al., 2013).

The studied charging/discharging time combinations are of importance when the capacitive properties of AC granules want to be optimally used. From the results we conclude that short charging and discharging times (2 minutes or less) are needed to achieve higher absolute values and larger contributions of stored charge compared to faradaic charge. Similarly, in terms of current output, short discharging times are preferred as the capacitive current is at highest. This is advantageous when using AC granules in fluidized MFC reactors, where often short discharging times are achieved.

Conclusion

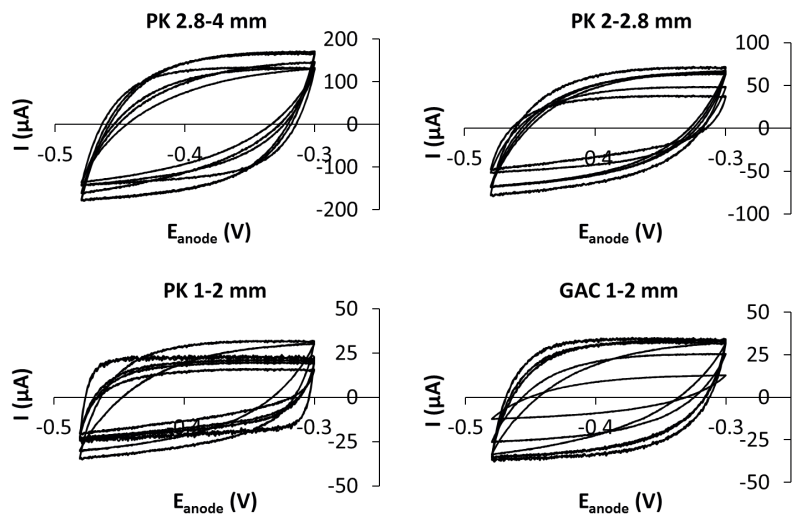
The study of single AC granules can lead to an optimized implementation of this kind of electrode material in up-scaled MFCs. The present study gives insight into the characterization of capacitive AC granules by means of electrochemical and microbiological analyses. Having a reactor with many granules is crucial for simultaneous and reproducible characterization of different types of granule properties, which similarly enables statistical analysis of results.

Acknowledgments

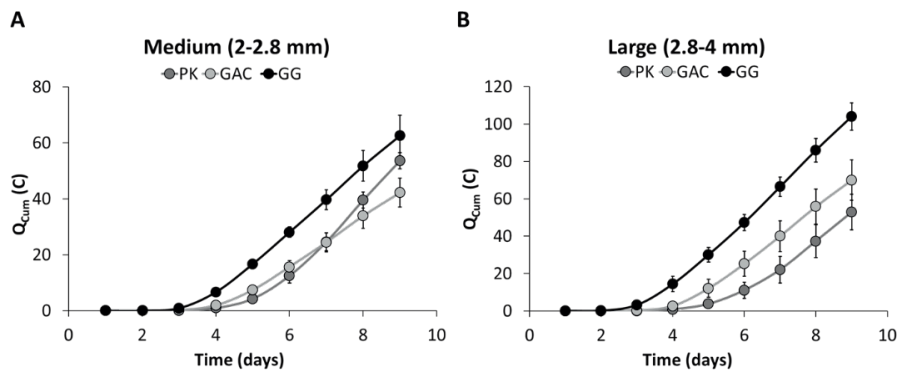
This research is supported by the Dutch Technology Foundation STW, which is part of the Netherlands Organization for Scientific Research (NWO), and which is partly funded by the Ministry of Economic Affairs (VENI grant no 13631). The research was performed in cooperation with Wetsus, the European Centre of Excellence for Sustainable Water Technology. Wetsus is co-funded by the Dutch Ministry of Economic Affairs and Ministry of Infrastructure and Environment, the European Union Regional Development Fund, the Province of Fryslân, and the Northern Netherlands Provinces. The authors would like to thank the participants of the research theme “Resource Recovery” for the fruitful discussions and their financial support. Furthermore, the authors would like to thank Agnieszka Tomaszewska for helping with the SEM images.

Supporting Information

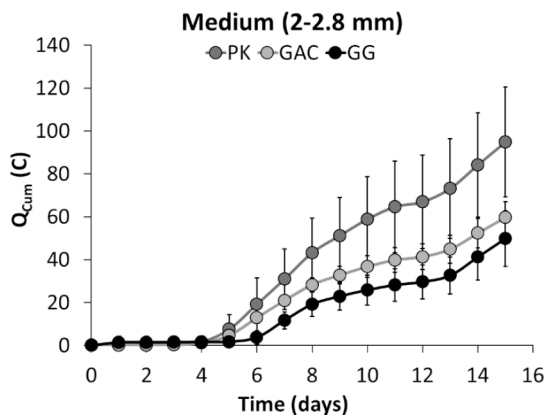
S1. Cyclic Voltammetry scans of single activated carbon granules (PK and GAC) of different sizes before bacterial inoculation.



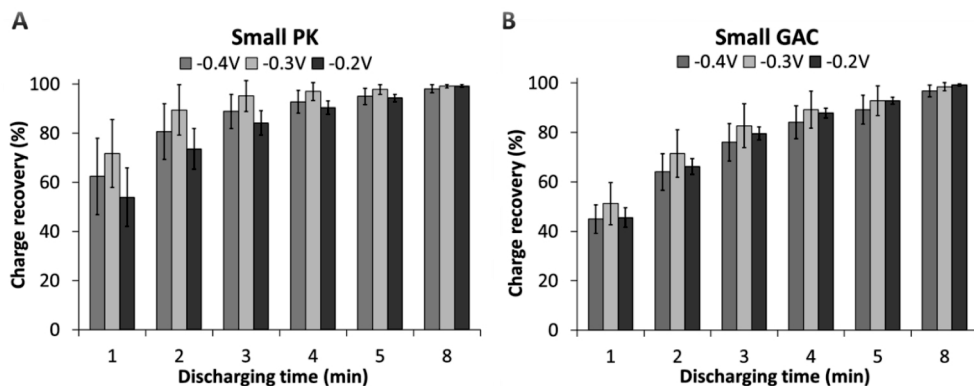
S2. Cumulative charge (Q_{Cum}) of medium (A) and large (B) PK, GAC and GG granules during growth for SEM images.



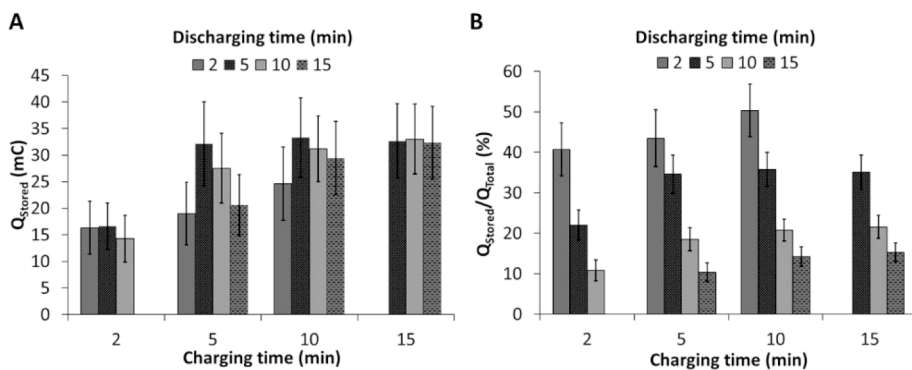
S3. Cumulative charge (QC) of PK, GAC and GG granules during growth for next-generation sequencing (NGS) analysis.



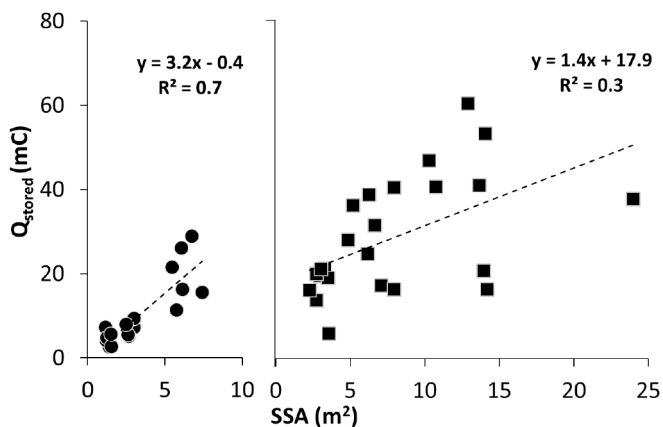
S4. Charge recovery (QR) during different discharge times (1, 2, 3, 4, 5 and 8 minutes) for small PK (A) and GAC (B) granules. The equation used to calculate is the following: $QR (\%) = Q_{Stored,t}/Q_{Stored,t=10} * 100$; where t (min) is the discharging time and 10 (min) is the total duration of the discharging process.

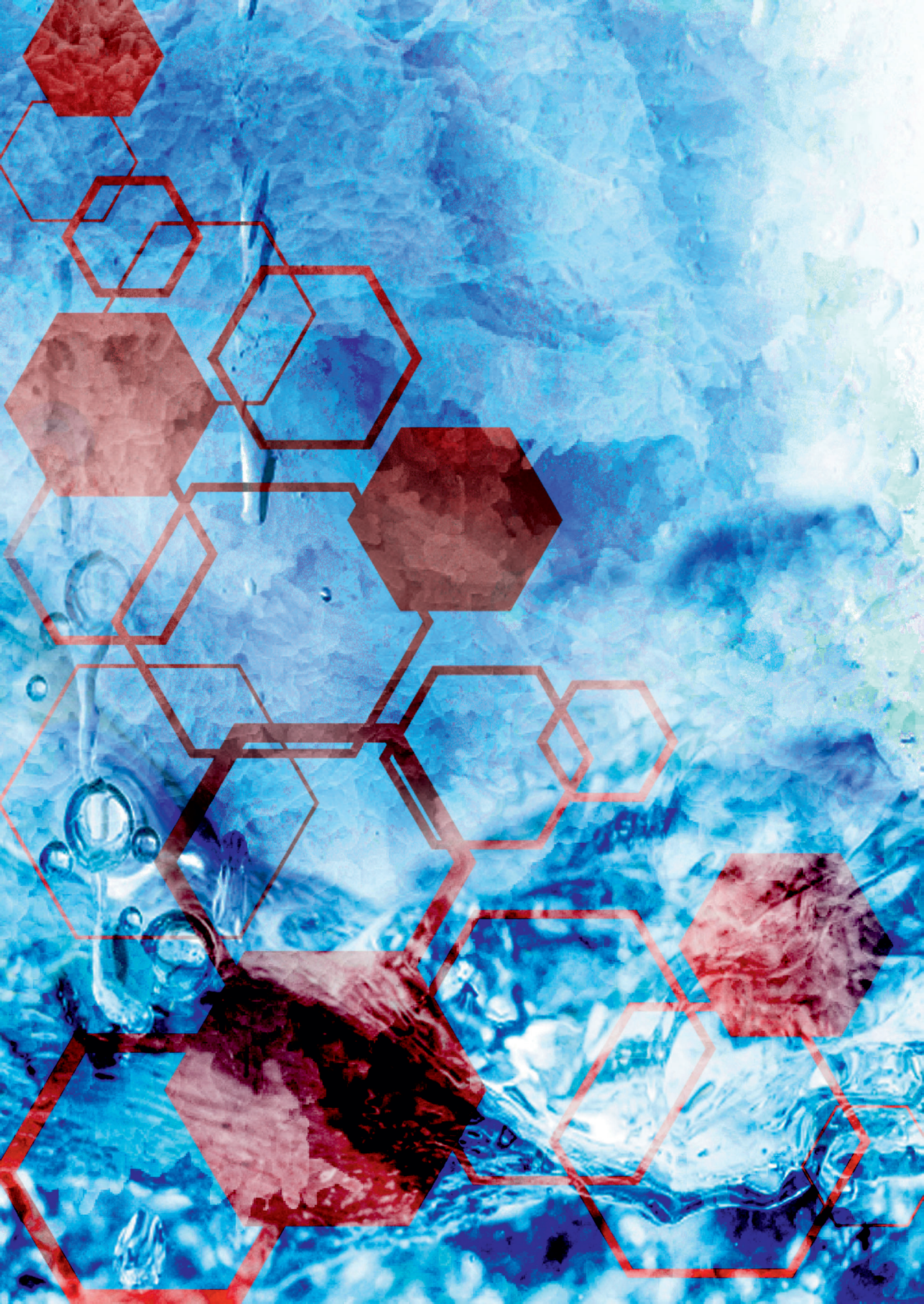


S5. Stored charge (A) and contribution of the same to the total produced charge (B) of small PK granules at -0.2V discharge potential.



S6. Relation between the stored charge and calculated specific surface area (SSA) of PK granules.





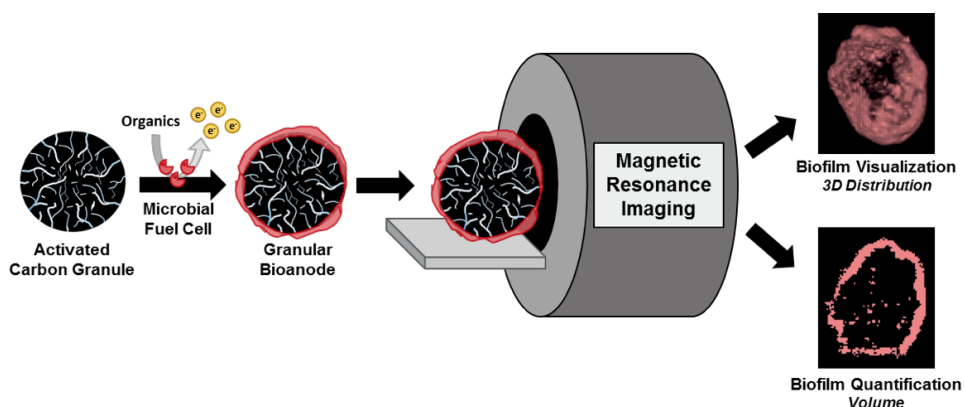
Chapter 4

3D biofilm visualization and quantification on granular bioanodes with Magnetic Resonance Imaging

Leire Caizán-Juanarena, Julia R. Krug, Frank J. Vergeldt, J. Mieke Kleijn, Aldrik H. Velders, Henk van As, Annemiek ter Heijne

Abstract

The use of Microbial fuel cells (MFCs) for wastewater treatment fits in a circular economy as they can produce electricity from the removal of organics. Activated carbon (AC) granules are an attractive electrode material for bioanodes in MFCs, as they are cheap and provide electroactive bacteria with a large surface area for attachment. The characterization of biofilm growth on AC granules, however, is challenging due to their high roughness and three-dimensional structure. In this research, we show that Magnetic Resonance Imaging (MRI) can be used to visualize biofilm distribution and determine its volume on AC granules in a non-destructive way. AC granules with electroactive biofilm were collected at different growth stages (3 to 21 days after microbial inoculation) from the reactor and T_1 -weighted 3D-MRI experiments were performed for three-dimensional visualization. With time, a more homogeneous biofilm distribution and an increased biofilm thickness could be observed in the 3D-MRI images. Biofilm volumes varied from 0.4 μL at day 4 to 2 μL at day 21 and were correlated to the total produced charge of the bioanodes and their total nitrogen content. A linear relation ($R^2 = 0.9$) was found between biofilm volume and each of the parameters, with values of 66.4 $\text{C } \mu\text{L}^{-1}$ and 17 $\mu\text{g } \mu\text{L}^{-1}$ for charge and nitrogen content, respectively. In future, *in situ* MRI measurements could be used to monitor biofilm growth and distribution on electrodes.



Keywords: Microbial Fuel Cells; Activated Carbon Granules; Capacitive Electrodes; Magnetic Resonance Imaging; Biofilm Distribution; Biofilm Volume .

1. Introduction

Recovery of resources from waste streams is necessary to transit towards renewable forms of energy and a circular economy. Wastewater streams from industries, agriculture and households are known to be a valuable source of organics and nutrients that can be recovered and used for energy production (Mo & Zhang, 2013; Nir et al., 2018; Zeeman & Kujawa-Roeleveld, 2011). The Microbial Fuel Cell (MFC) is a technology that uses bacteria to clean wastewater by oxidizing the organics while simultaneously producing electricity (Heilmann & Logan, 2006; Rozendal et al., 2008; Shimoyama et al., 2008). This oxidation reaction occurs at the anode, where bacteria grow by forming a biofilm on the surface of the electrode, known as bioanode. Currently, one of the main bottlenecks regarding the application of MFCs is the low power density that can be achieved (Deeke et al., 2015; Logan et al., 2015). This hinders their ability to compete with other wastewater treatment technologies, such as anaerobic digestion (Arends & Verstraete, 2012). Electrode material properties (e.g. biocompatibility, electrical conductivity and surface area) are of importance for the performance of MFCs and hence the power density (J. Wei et al., 2011; Zhou et al., 2011). Carbonaceous materials are widely used, as they are cheap and hold most of the desired properties. Among them, activated carbon (AC) granules have a three-dimensional structure and a large specific surface area (more than $1000 \text{ m}^2 \text{ g}^{-1}$) (Qu & Shi, 1998) that allows good biofilm attachment, hence leading to high volumetric power density. In this research, we use AC granules as previously described by Borsje and co-workers (Borsje et al., 2016).

Many studies focus on electrochemical (Borsje et al., 2016; Deeke et al., 2012; Rodrigo-Quejigo et al., 2018) and physical properties (Frackowiak & Béguin, 2001; Kastening et al., 1997; Pastor-Villegas & Durán-Valle, 2002) of activated carbon, while quantification and distribution of biofilm on such electrodes are less extensively addressed. Nevertheless, a wide variety of techniques is available for biofilm characterization (Beyenal et al., 2004; Neu et al., 2010; Valladares Linares et al., 2016). Biofilm quantification can be done by using well-established methods, such as protein analysis (Mieke C. A. A. Van Eerten-Jansen et al., 2013) and Total Nitrogen (TN) (Molenaar et al., 2018) content, which relate to the total amount of biomass. The spatial distribution of a biofilm is commonly obtained by microscopy techniques such as scanning electron microscopy (SEM) (Marzorati et al., 2018; Saba et al., 2017; Zakaria et al., 2018) or confocal laser scanning microscopy (CLSM) (Saba et al., 2017; Sun et al., 2016). However, they are destructive (e.g. SEM), need the addition of chemicals (e.g. CLSM) and can only scan small areas of the electrode. Recently, optical coherence tomography (OCT) was introduced to determine biofilm volume and thickness of a bioanode *in situ* and non-invasively (Molenaar et al., 2018). However, the three-dimensional nature of AC granules impedes the application of OCT on these specific electrodes, unlike reported by other studies that use more or less flat surfaces (Fortunato & Leiknes, 2017; Haisch & Niessner, 2007; Xi et al., 2006). Therefore, other

techniques need to be used to visualize and quantify biofilm growth on bioanodes in this study.

Magnetic Resonance Imaging (MRI), a technique well-known from medical diagnostic, is suitable for visualization and characterization of biofilms (Gonzalez-Gil et al., 2001; Neu et al., 2010; Phoenix & Holmes, 2008; Ramanan et al., 2013; Ranzinger et al., 2016). Existing research studies have mainly focused on biofilm structure, transport of water (i.e. diffusion and flow) and transport of metal ions in and around biofilms structures (Bartacek et al., 2016; Herrling et al., 2017; Manz et al., 2005; Phoenix & Holmes, 2008; Ramanan et al., 2010; Seymour et al., 2004; Van As & Lens, 2001; Wieland et al., 2001), and grown on carriers, even with complex geometry (Graf von der Schulenburg et al., 2008; Herrling et al., 2015, 2017). Specifically, MRI research on biofilm growth on electrodes has revealed information about diffusion coefficients (Renslow, Babauta, Majors, et al., 2013) and metabolic activity (i.e. electron transfer) (Renslow, Babauta, Dohnalkova, et al., 2013) within the biofilm growing on flat electrodes. However, to the best of our knowledge, to this date MRI on biofilm growth on electrodes has only been used on flat electrodes and not yet for 3D biofilm visualization and quantification on granular electrodes with such an irregular shape as is the case for AC granules. Because of the irregular shape of AC granules and the thin biofilm layer, high-resolution 3D images are needed, at sub-hundred micrometer resolution. These resolutions are quite exotic in MRI research due to the low sensitivity of the technique and would require long experimental times of days to weeks. To shorten experimental times to obtain these high-resolution images, high magnetic field strengths are needed. This study was therefore conducted at a high magnetic field strength of 14.1 T, which is much stronger than the 1.5 and 3 T MRI scanners used for conventional medical imaging. Magnetic field strengths used in biofilm MRI research are commonly ranging between 4.7 T (e.g. (Herrling et al., 2017)) and 11.7 T (e.g. (Renslow, Babauta, Majors, et al., 2013)) to achieve higher spatial resolutions due to the smaller dimensions of biofilms, but biofilm studies have also been performed at very low field strengths of 0.7 T (e.g. (Bartacek et al., 2016)).

MRI is an imaging modality based on the detection of the signal coming from the magnetic moment (spin) of hydrogen nuclei in a magnetic field after excitation with an appropriate pulse sequence (Westbrook & Talbot, 2018). It allows us to visualize the distribution of hydrogen nuclei in e.g. biological samples. As water is the most abundant component containing hydrogen in biological samples, the main application is to image water distribution. To distinguish different tissues within a biological sample, we can make use of the differences in Magnetic Resonance (MR) signal lifetimes of water in those tissues compared to the surrounding bulk water, called relaxation times (T_1 and/or T_2). As the bulk water signal has a different relaxation time than the biofilm water signal (Hoskins et al., 1999), MRI signal acquisition timings can be selected to maximize the contrast between biofilm and bulk water, which will lead to different signal intensities. Based on this image contrast, the biofilm region can be selected, and the distribution can be visualized.

The aim of this research was to develop an MRI-protocol to non-destructively visualize and quantify the three-dimensional biofilm distribution in AC granules. To this end, we investigated whether biofilm water could be distinguished from bulk water by T_1 -relaxation time at a high magnetic field strength (14.1 T). 3D-MRI images of AC granules, grown as bioanodes in a multi-anode MFC, were collected at different growth stages and image processing techniques were used to determine biofilm volume. Biofilm quantification with MRI was complemented with measurements of total nitrogen and total produced charge by the same bioanodes.

2. Experimental Section

2.1. Preparation of the AC granules

The type of AC granules used were PK1-3 (Cabot Norit Nederland B.V., Amersfoort, the Netherlands). They were first sieved using an aperture size between 1 and 2 mm (Retsch®, Germany), then individually selected for an approximate spherical shape, and finally weighted. The volume was estimated by using the apparent density values from the manufacturer: 0.3 g mL^{-1} . The radius was approximated from the volume by assuming a spherical shape of the granule. The surface area of a sphere was then calculated, without considering the possible roughness or pores where bacteria could have access to. Table 1 in the Supporting Information (S1) contains the exact information about each granule used in this study.

After selection, granules were treated with hydrochloric acid (HCl) 22% for 24 hours to remove surface organic contamination and metal impurities and washed three times with demi water (Wu et al., 2015). This is a common practice to clean electrodes and useful for comparative experiments. Additionally, for MRI experiments it is crucial that the electrode material contains as little concentration of iron ions as possible in order to avoid image artefacts. In the Supporting Information (S2) the composition of AC granules before and after the acid pre-treatment can be seen, measured with Inductive-Coupled Plasma Mass Spectrometry (ICP-MS).

2.2. Preparation and operation of the MFC

A custom-made MFC reactor was built, consisting of two compartments: a 2.3 L container as the anode chamber and a glass tube as the cathode chamber. The anolyte (10 mM $\text{NaCH}_3\text{COO} \cdot 3\text{H}_2\text{O}$; 1 mL L^{-1} Wolfe's Vitamin solution; 1 mL L^{-1} Wolfe's modified mineral solution; 3.7 mM NH_4Cl , 1.6 mM KCl ; 30 mM $\text{Na}_2\text{HPO}_4 \cdot 2\text{H}_2\text{O}$; 19 mM KH_2PO_4) consisted of 2 L of which 0.2 L was an inoculum from another active MFC run on acetate, leaving a headspace of 0.3 L. The cathode chamber had approximately a volume of 0.13 L (100 mM K_3FeCN_6 ; 30 mM $\text{Na}_2\text{HPO}_4 \cdot 2\text{H}_2\text{O}$; 19 mM KH_2PO_4) and was placed in the center of the anode chamber. 24 cm^2 of graphite felt attached to a titanium wire (1 mm diameter, 36

cm long) was used as current collector in the cathode. To connect both chambers, a 1.76 cm² cation exchange membrane (Fumasep FKB, FuMa-Tech GmbH, St. Ingbert, Germany) was placed on the bottom of the cathode chamber. The lid of the container had one hole for the inflow of substrate, one hole for the reference electrode (Saturated KCl Ag/AgCl, +0.199V vs NHE) and 29 holes in total for the working electrodes. Additionally, a hole on the side of the container was made for the outflow. The effect of the distance between working and the reference electrodes on current production was neglected as the latter one was placed outside of the electric field.

Single granules were held separately with clamps made of titanium wire (1 mm diameter), which were covered by a heat shrink tube (RS Pro 389-634) to prevent its oxidation and the growth of biofilm on its conductive surface. One side of the clamp had the shape of a hook, where the granule could be fixated. This side was covered with a layer of conductive glue (EMS, Pennsylvania, USA) and its contact area with the granule was minimized using non-conductive resin (Revlon® Colorstay™) that served to limit bacterial growth on the clamp. The other side of the titanium wire was passed through a rubber that fitted on the holes of the lid for the working electrodes. The average resistance of the clamps was 0.8 to 1 Ω between the two ends. Each clamp was connected to a channel from the MultiWE32 module (Ivium Technologies, Eindhoven, The Netherlands), which can operate up to 32 working electrodes that share a common reference electrode and counter electrode.

AC granules were all operated at -0.35 V vs Ag/AgCl with continuous anolyte inflow. Acetate concentration was maintained above 5 mM. Anaerobic conditions were ensured with N₂ flushing and the stirring velocity was fixed at 100 rpm. Electric current was monitored, with a sampling time of 600 seconds, until granular bioanodes were collected from the reactor (see Table 1 in Supporting Information, S1, for the exact days). Total produced charge by each bioanode was calculated according to Eq. 1:

$$Q_T = \int_0^t I dt \quad (1)$$

where Q_T is the total produced charge (C), I the current (A) and t is the time during which current was measured (s).

After collecting a granule, the rubber stopper was replaced with a new stopper to avoid oxygen leakage into the reactor. Prior to MRI measurements, clamped granules were submerged 2 to 3 times in a buffer solution without nitrogen (1.6 mM KCl; 30 mM Na₂HPO₄·2H₂O; 19 mM KH₂PO₄) to avoid the accounting of additional nitrogen from the buffer in the total nitrogen analysis. Each granule was then transferred to a 3 mm MR-tube (Hilgenberg, Malsfeld, Germany) containing the same buffer solution and an agar block (2% w/w) of approximately 8 mm placed at the bottom.

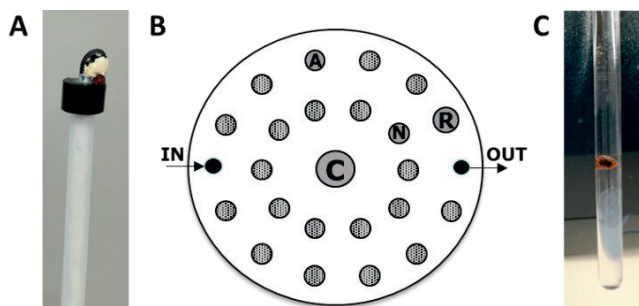


Figure 1. A) A clamped granule with biofilm collected from the reactor; B) Schematic top view of the reactor, where C stands for cathode, R for reference electrode, N for nitrogen inflow and A for abiotic granule. The rest of circles with no name indicate the clamps; C) A granule with biofilm inside a 3mm diameter MRI tube, filled with buffer solution and with an agar block at the bottom.

2.3. MRI measurements

MRI measurements were performed on a 14.1 T Bruker Avance-III-600 spectrometer (Bruker, Karlsruhe, Germany) controlled by ParaVision 5 or 6. The Micro5 imaging probe was equipped with a Micro5 gradient set and Great60 amplifiers, located at MAGNEFY (MAGNEtic resonance research FacilitY, Wageningen, The Netherlands). The RF-coil used was ^1H saddle coil with a diameter of 5 mm. All MRI measurements were performed at room temperature ($\sim 293\text{K}$) with no extra temperature control.

T₁ map

A 2D spin-echo RAREVTR sequence (Echo Time = 2.93 ms, 5 different TR steps (TR= 100 ms, 385 ms, 785 ms, 1464 ms, 5000 ms), 64 averages, receiver bandwidth 50 kHz, Field-of-View $3 \times 3 \text{ mm}^2$, slice thickness 0.2 mm) was used for T_1 measurements. The raw data was Fourier-transformed and phase-corrected. Per pixel the signal intensity as a function of TR was mono-exponentially fitted with in-house developed IDL scripts using IDL Version 6.4 (ITT, Visual Information Solutions, Boulder, CO, USA) to obtain quantitative T_1 -maps according to the function:

$$I(\text{TR}) = I_0 \left(1 - e^{-\frac{\text{TR}}{T_1}} \right) \quad (2)$$

where $I(\text{TR})$ is the image intensity as function of repetition time TR , I_0 the proton density, and the T_1 relaxation time.

3D-RARE

A 3D turbo spin-echo (RARE) sequence (Echo Time= 2.92 ms, turbo factor 4 with centric encoding, isotropic voxel resolution $(28 \mu\text{m})^3$, acquisition time 19 h 42 min, Field-of-View $3.6 \times 2.7 \times 2.7 \text{ mm}^3$, receiver bandwidth 100 kHz) was recorded. TR was chosen to be 700 ms to obtain a T_1 -weighted image with about optimal contrast. Before and after this scan a

control localizer scan was performed to confirm that the sample did not move during the experiment.

2.4. Image processing for 3D reconstruction

To process the 3D-dataset, a script was written in IDL Version 6.4 (ITT, Visual Information Solutions, Boulder, CO, USA). A threshold was set above the noise intensity level to mask areas with no signal intensity. Furthermore, we corrected for inhomogeneous intensity of the bulk water signal due to the inhomogeneity of the B_1 -field, which is caused by the geometry of the detection coil, namely the saddle geometry. After this correction, a threshold was set above the image intensity corresponding to bulk water to distinguish volume elements (voxels) containing biofilm from voxels containing bulk water. Volume elements with a signal intensity higher than the threshold attributed to biofilm were summed and multiplied by the volume of a single volume element ($28 \mu\text{m}^3$). The dataset containing the threshold images was then loaded with ImageJ/FIJI (Schindelin et al., 2012) and a 3D-volume reconstruction was done using the Image J 3D viewer (Schmid et al., 2010) applying a resampling factor of 2.

2.5. Total nitrogen (TN) analysis

After the MRI measurements, granules were processed with the Laton Total Nitrogen (LCK) cuvette test with a concentration range of 20-100 mg L^{-1} TNb (HACH®, Manchester, United Kingdom). This method measures organic and inorganic bound nitrogen, excluding elemental nitrogen (N_2). 0.2 mL of miliQ water was added to the reaction vessel together with the AC granule. The AC granule was directly transferred from the MRI tube (refilled with phosphate buffer) to the miliQ water in the reaction vessel. Direct contact between the two liquids ensured that the granule could move with little interference. The digestion step in the reaction vessel consisted of 30 minutes at 120 °C. The final sample (0.5 mL) was transferred from the reaction vessel to the LCK cuvette, from which the nitrogen concentration (mg L^{-1}) was read after 15 minutes. This concentration was converted to mg by correcting for the initial added volume of miliQ water (i.e. 0.2 mL).

The nitrogen content of abiotic granules, pre-treated similarly, was found to be around 1 mg L^{-1} , which is more than 10 times lower than for granules with biofilm. This residual nitrogen in abiotic granules could originate from the activated carbon that contains some nitrogen. However, the exact value is difficult to specify as it will depend on the exact dry weight of each granule.

3. Results and Discussion

In this section, we present and discuss i) the MRI method used to visualize the biofilm, ii) the 3D-MRI images obtained at different biofilm growth stages of different granular bioanodes, iii) the image processing and determination of biofilm volume, and iv) the

correlation with total charge produced by single AC granular bioanodes and total nitrogen analysis as a measure of biofilm quantification.

3.1. Distinguishing biofilm water from bulk water using MRI

Differences in T_1 -relaxation times provide means to control contrast in MRI experiments. Therefore, it is important to quantify this parameter for both biofilm and bulk water. To determine T_1 -relaxation times of biofilm and bulk water, a 2D spin-echo MRI experiment was performed by varying the (saturation) recovery time, i.e. the repetition time (TR) of the experiment. Figure 2A shows the resulting 2D images for TR varying from 0.1 s (left) to 5 s (right). The absolute image intensity increases with increasing TR as the signal is given more time to recover. The signal intensity of each image element (voxel) was fitted as a function of TR with a mono-exponential recovery curve (Figure 2B). In Figure 2B we plotted the signal intensity as function of TR and the corresponding fit of two voxels (marked in Figure 2A as example), corresponding to biofilm water (red) and bulk water (blue). With this fit, a proton density map (known as signal amplitude map; Figure 2C, left) and a T_1 -parameter map (Figure 2C, right) were obtained. While in the amplitude map the color-coded image corresponds to a certain amount of spins, in the T_1 -map the color-code of the image corresponds to a certain T_1 -value. The amplitude map shows that the proton density is lower inside the biofilm than in the bulk water, while the activated carbon granule has a very low intensity either due to absence of mobile protons in the material or pore water having a too short signal relaxation time (T_2) to be observable in MRI. The T_1 -map shows that T_1 -values of biofilm water (~ 700 ms) and bulk water (~ 2.5 s) can indeed be distinguished, a trend which has also been seen by Hoskin and co-workers (Hoskins et al., 1999). The T_1 -value of the biofilm water is lower than the bulk water as the T_1 -relaxation time of water spins is affected by the different local (physical and chemical) environment in the biofilm (Belton & Ratcliffe, 1985). A T_1 -value of the granule material cannot be established due to the low intensity of the signal in the granule. Having established that biofilm and bulk water signal can be distinguished by their difference in T_1 -relaxation time, the TR for maximum image contrast is determined. Using the recovery curves (Figure 1B), we read the value of TR at which the difference in signal intensity between bulk water and biofilm is the largest. In this case, we chose to use a TR of 700 ms as indicated by the black dotted line (Figure 1B) for all subsequent 3D-MRI experiments on the bioanodes.

As an alternative method to generate image contrast, we proved that T_2 -contrast could be used as well to distinguish biofilm water ($T_{2, \text{apparent}} = \sim 20$ ms) from bulk water ($T_{2, \text{apparent}} = \sim 44$ ms). The reported (apparent) T_2 values are specific for the resolution ($47 \times 47 \times 200 \mu\text{m}^3$) and magnetic field strength (14.1 T) used in this T_2 -experiment (Edzes et al., 1998). However, the low contrast we found between biofilm and activated carbon granule with T_2 -contrast images (Supporting Information, S3) would impede the distinction and subsequent quantification of biofilm. The contrast between biofilm water and bulk water in

T_2 -experiments is also lower than in T_1 -experiments due to the smaller difference in T_2 -relaxation times at the required high resolutions (Edzes et al., 1998). Additionally, full T_2 -contrasted 3D experiments would take longer experimental time than T_1 -contrast experiments as T_2 -contrast experiments would require a TR of $5 \cdot T_1$. Therefore, we proceeded with T_1 -contrast MRI images.

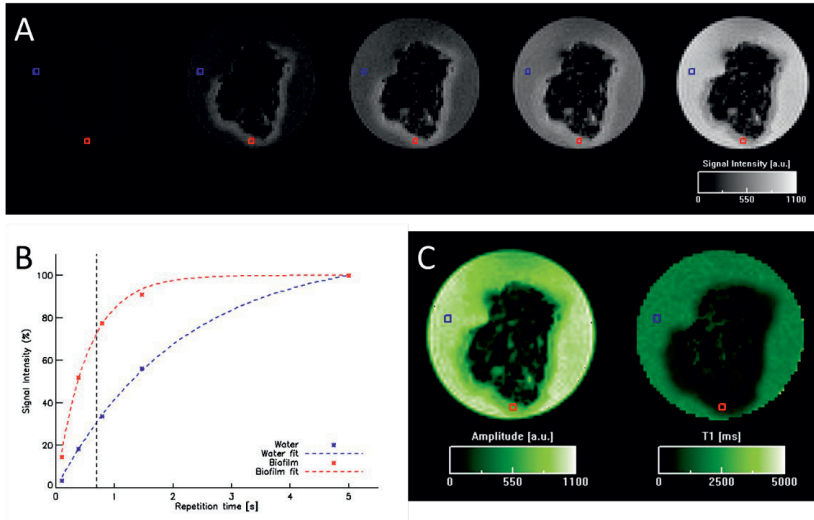


Figure 2. Results for an AC granule with biofilm collected after a growth period of 15 days. A) 2D spin-echo MRI images with different relaxation times TR of 0.10 s, 0.39 s, 0.79 s, 1.46 s and 5 s from left to right. B) Signal intensity values of Figure A of one biofilm voxel (red) and bulk water voxel (blue) plotted against the repetition times. The respective fits are shown by the dotted lines. The black dotted line indicates the recovery time for maximum contrast. C) Amplitude map and T_1 map from a mono-exponential fit of the image intensities in A) are depicted.

3.2. Biofilm distribution using 3D-MRI

To image the biofilm distribution on single AC granules, 3D T_1 -weighted turbo spin-echo (RARE) experiments with a resolution of $28 \mu\text{m} \times 28 \mu\text{m} \times 28 \mu\text{m}$ were performed for every collected granular bioanode. Figure 3A shows a cross-section of the 3D dataset of a granule where the biofilm has grown for 11 days. Here, the signal intensity of biofilm is higher than both the AC granule and the bulk water. However, a cross-section is not representative for the biofilm distribution on the whole granule. Therefore, a 3D reconstruction is needed to visualize the distribution of the biofilm on the granule surface. To this end, the volume elements (voxels) containing biofilm were selected by applying a threshold on the signal intensity using a custom-written script. From the resulting threshold images (Figure 3B), a 3D reconstruction of the biofilm that shows the biofilm distribution and coverage was made (Figure 3C). Cross-sections, threshold images and pictures of the 3D volume reconstruction of every granular bioanode can be found in the Supporting Information (S4). Note that the

area with no biofilm in Figure 3C corresponds to the position of the clamp used as current collector. This partly covered the surface of the AC granules, hence preventing biofilm growth on this area. Therefore, this served as an internal control within the 3D-measurement indicating that no bulk water at the granular surface was falsely attributed to biofilm volume, which is the case when a surface acts as a relaxation sink (Godefroy et al., 2001). This internal control served thus as proof that MRI image artefacts were not interfering in our study. The rest of the AC granule surface at day 11 was covered.

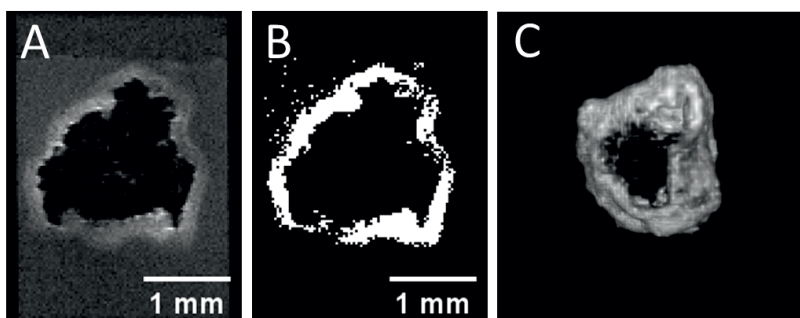


Figure 3. A) One cross-sectional plane through the T_1 -weighted 3D dataset of an 11-day-old granule. B) The same plane is depicted after thresholding analysis. C) 3D volume reconstruction based on the threshold image stack.

Using the 3D visualizations of all different granules (see Supporting Information, S4), we can assess the different granules at different growth stages. In the early stages (days 3 and 4), there were large surface areas of the AC granules that were not covered, and the distribution was not homogeneous over the surface. At later stages (days 6 and 7), the biofilm was more equally distributed over the granule surface but the biofilm was still not very thick. More mature granules, grown for 11 days or more, had thicker biofilms that allowed for a clearer view of the biofilm distribution. It is important to notice that the area of the clamp was visible in every granular bioanode, and so all of them had an internal control as previously explained. At the early biofilm growth stages, this clamp area was not as distinct as for more mature bioanodes, since biofilm was not fully developed. However, when compared to abiotic granules (see Supporting Information, S4), these latter ones did not have any hole and all the surface was covered by an equidistant signal originating from the granule surface acting as a relaxation sink (Godefroy et al., 2001).

3.3. Biofilm volume determination using 3D-MRI

Figure 4A shows the biofilm volume of ten AC granules, each with different weight, collected at different time points. Biofilm volume was determined from 3D-MRI images by summing up all voxels selected during the thresholding analysis (Figure 3B and Supporting Information, S4) and multiplying with the volume of one voxel. Values ranged from 0.4 μL on day 4 to 2 μL on day 21. An increased biofilm volume is observed with longer growth periods for the time range here studied. Biofilm thickness is known to be a crucial

parameter for the electrochemical activity of bioanodes (Sun et al., 2016). Therefore, based on these biofilm volumes and an estimation of the outer surface area of granules (calculated as described in the experimental section), the average biofilm thickness was calculated, assuming that the whole surface was completely covered by biofilm (see Supporting Information, S1). The lowest average thickness obtained was at day 4 with a value of 27.8 μm , while the highest value was 165.9 μm for the granule collected at day 21. This biofilm thickness is in the same range as reported for electro-active biofilms on anodes.(Jana et al., 2014; Molenaar et al., 2018) As volume increases with longer growth periods, biofilm thickness tends to increase as well. This could relate to the decrease of electric current production by bioanodes over time, as shown in Figure 4B. In fact, some studies (Korth et al., 2015; Savéant, 1986) have revealed that diffusion limitations increase with thicker biofilms, which may hinder current production of the system.

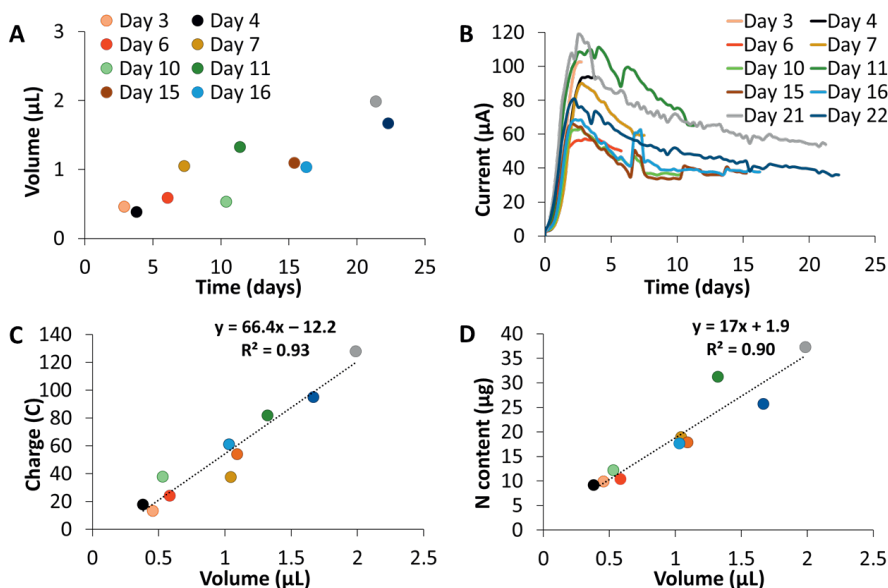


Figure 4. A) Biofilm volume obtained with MRI at different growth stages, B) Current production of bioanodes at the same growth stages, C) Total produced charge by bioanodes as a function of their biofilm volume, and D) Total nitrogen content of bioanodes as a function of their biofilm volume .

3.4. Comparison with electric current production and total nitrogen analysis

Electric current production was recorded for each granule during the biofilm growth period (see Figure 4B). Most of the granules reached the maximum current (ranging from 57 to 119 μA) approximately 3-4 days after inoculation. After those days, the current decreased to values between 87% (in day 6) and 44% (in day 22) of the maximum current value. In fact, three weeks after inoculation current values already approached a steady-state. This

current curve seems to be characteristic for bioanodes that are continuously fed and controlled at a certain potential (Molenaar et al., 2018). We expect current production to be related to biofilm volume, as electroactive bacteria gain energy from transporting electrons from the substrate to the electrode. To prove this, we correlated the biofilm volume with its total produced charge (i.e. current integrated over time, see Materials and Methods). Figure 4C revealed a linear relation of $66.4 \text{ C } \mu\text{L}^{-1}$ ($R^2 = 0.9$). This value is in the same order of magnitude, but 1.6-fold higher than the linear relation found for a bioanode by OCT measurements (Molenaar et al., 2018).

Similarly, total nitrogen content is plotted against biofilm volume (Figure 4D). Nitrogen content of the biofilm consisting of bacteria and extracellular polymeric substances (EPS) can be used as an indication for biofilm amount. The biofilm volume determined from NMR was linearly related to total nitrogen; the relation found was $17 \text{ } \mu\text{g N } \mu\text{L}^{-1}$ of biofilm ($R^2 = 0.9$).

Biofilm stability may be a point of concern for long MRI experimental times. Having no substrate available for approximately one day potentially leads to changes in biofilm morphology. To test if the biofilm is negatively affected by MRI measurement, additional nitrogen measurements were done with fresh granules, directly collected from the reactor without prior MRI measurements. The relation between nitrogen and total charge was similar (see Supporting Information, S5), indicating that sample handling and MRI measurement time had little effect on the amount of biofilm.

4. Challenges and Outlook

Regarding the resolution used to visualize the biofilm distribution on AC granules, MRI images with a resolution of $(28 \text{ } \mu\text{m})^3$ were sufficient to elucidate biofilm distribution but not to discriminate individual bacterial cells ($\sim 1 \text{ } \mu\text{m}$) (Bond & Lovley, 2003) or clusters below $28 \text{ } \mu\text{m}$ potentially present in surface cavities or inner pores. In fact, using SEM on the cross section of AC granules, we found that bacterial growth occurred in their inner pores (see Supporting information, S6). Therefore, this might have caused an underestimation of biofilm growth on AC granules. However, $(28 \text{ } \mu\text{m})^3$ was the optimum resolution with acceptable measurement times ($< 24\text{h}$). Higher resolutions would allow to image the biofilm distribution more accurately, but would require longer measurement times which might damage the integrity of the biofilm. To achieve higher resolutions, more sensitive detection coils or accelerated measurement techniques (Tsao & Kozerke, 2012) are recommended for the future.

The determination of biofilm volume depends on several steps that can introduce errors, which are not exactly quantifiable. The choice of the threshold value in the image processing step is crucial. If this value is too high, biofilm is not counted, if the threshold is too low, voxels containing bulk water are attributed to biofilm. In fact, in the threshold images (Figure 2B and Supporting Information, S4), several voxels in the bulk water region

and in the pore water of granules are accounted as biofilm, while in the biofilm region certain areas are instead underestimated. The signal intensity encountered within AC granules could mean that some water was present in the internal pore structure of the AC granule. This is difficult to resolve using MRI, due to the small sizes of these pore structures ($\sim 0.3\text{-}300\text{ nm}$) (Borsje et al., 2016) and the presence of e.g. iron ions (SI) which can cause MRI image artefacts inside the granule. Furthermore, even though we corrected for image intensity differences caused by an inhomogeneity in the detector of the MRI-equipment (see experimental section), small differences in image intensity remain and can cause local over- or underestimation of the biofilm. Another inaccuracy results from partial volume effects. (González Ballester et al., 2002) This means that if the voxel of $(28\text{ }\mu\text{m})^3$ is partly filled with biofilm and partly filled with bulk water, it might not be accounted to the biofilm volume. The estimation of the partial volume effect has not been done in this study. Next, to obtain a more accurate biofilm thickness from the 3D-MRI volume data, determining the exact interfacial area between the biofilm and the AC granule is needed. However, this requires more sophisticated image processing procedures. Furthermore, the resolution of $(28\text{ }\mu\text{m})^3$ in the MRI experiment of this study is still too low to resolve the surface of the granule due to its irregular microstructure.

A next step in biofilm characterization with MRI would be to perform *in situ* measurements (Renslow et al., 2014) so that biofilm development can be followed in time. In that case, efforts to reduce acquisition time (i.e. more sensitive detector, accelerated techniques) in 3D-MRI measurements would be highly recommended. MRI image artefacts should always be carefully considered for biofilm visualization purposes, as the signal identified as biofilm could originate from different source (e.g. relaxation sinks at the surface of the AC granule).

Conclusion

In this study, we have shown that high-field MRI can be used for high-resolution imaging of thin biofilms on granular electrodes in MFCs. By using 3D MRI, we could visualize the biofilm on single AC granule surfaces with good contrast between biofilm and bulk water, and subsequently determine the biofilm volume. This would have not been possible to obtain with electrochemical, chemical or (other) microscopy techniques. Additionally, as it is a non-destructive technique, it can be combined with other analytical techniques to yield complementary information. In the future, *in situ* experiments can be used to monitor biofilm growth and distribution on AC granules over time.

Acknowledgements

This research is supported by the Dutch Technology Foundation STW, which is part of the Netherlands Organization for Scientific Research (NWO), and which is partly funded by the

Ministry of Economic Affairs (VENI grant no 13631). This research was performed in the cooperation framework of Wetsus, the European Centre of Excellence for Sustainable Water Technology (www.wetsus.eu). Wetsus is co-funded by the Dutch Ministry of Economic Affairs and Ministry of Infrastructure and Environment, the Province of Fryslân, and the Northern Netherlands Provinces. J.R.K. received funding from the NWO-funded graduate school Netherlands Magnetic Resonance Research School [022.005.029]. The authors would like to thank the participants of the Resource Recovery research theme of Wetsus for the fruitful discussions and their financial support. Furthermore, the authors would like to thank Agnieszka Tomaszewska for the SEM images and Roos Goedhart for her help with preliminary experiments. We also thank John Philippi and Pieter de Waard for their technical assistance at the MAGnetic resonance research Facility (MAGNEFY) at Wageningen University & Research.

Supporting Information

S1. Information about each of the AC granules used in this study: harvest day, weight and estimated volume and surface area.

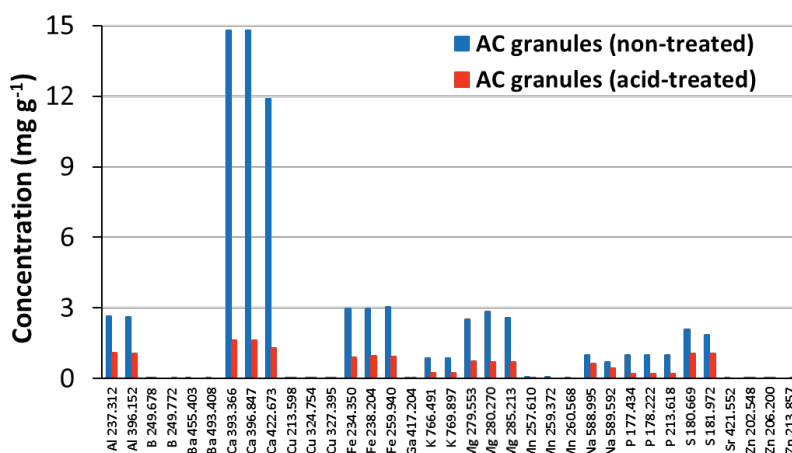
Harvest day	Weight (mg)	Estimated volume (μL)	Estimated surface area (mm ²)	Estimated biofilm thickness (μm)
3	1.02	3.52	11.18	40.9
4	1.39	4.79	13.75	27.8
6	1.46	5.03	14.20	41.2
7	1.16	4.00	12.19	85.8
10	0.97	3.34	10.82	49.2
11	1.75	6.03	16.03	82.6
15	0.80	2.76	9.51	115.0
16	1.05	3.62	11.40	90.5
21	1.13	3.90	11.97	166.0
22	1.16	4.00	12.19	136.9

Density of PK granules used: 1.03 g mL⁻¹

Volume of a sphere: $V = \frac{4}{3} \pi r^3$

Surface area of a sphere: $A = 4 \pi r^2$

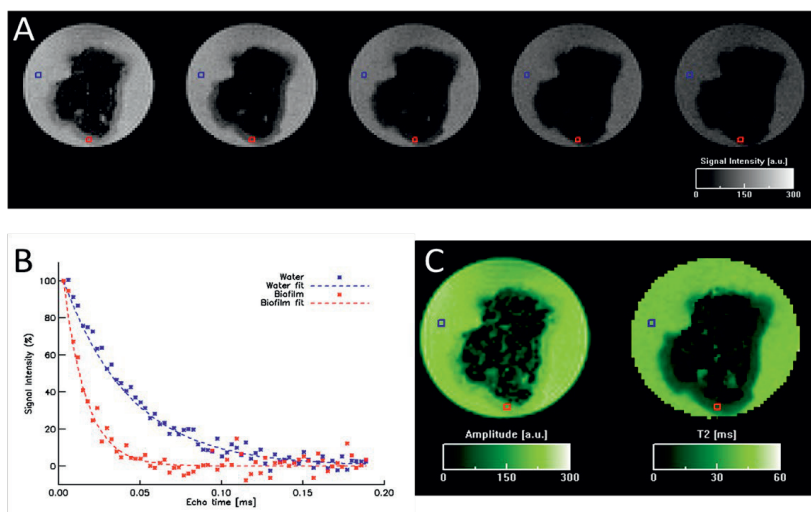
S2. Elemental composition of AC granules (PK 1-3) with no treatment (in blue) and with 22% HCl acid-treatment (in red). Results were obtained with ICP-MS.



The elemental composition of AC granules was analyzed with an inductively coupled plasma analyzer (ICP-OES, Varian Vista MPX). 0.209 g of PK granules with no treatment and 0.203 g of PK granules with acid treatment (22% HCl for 24h) were used for the analysis. Multi- and single-element standard solutions were prepared (with aqua regia as dissolvent) to cover a concentration range from 0.2 to 5 mgL⁻¹. These standards contained the following elements: Ag, Al, B, Ba, Bi, Ca, Cd, Co, Cr, Cu, Fe, Ga, In, K, Li, Mg, Mn, Na Ni, P, Pb, S, Sr, Ti and Zn.

Prior to measurements, granules were mixed with 4 mL HNO₃, 1mL HClO₄, 1 mL H₂O₂ and 1 mL H₂O in a vessel with vent-and-reseal technology, and digested in a microwave (ETHOS 1, Milestone S.r.l.). The overall digestion program took 1 hour with a maximum temperature of 220 °C. After samples were cooled down, the resulting liquid was diluted in a 100 mL volumetric flask with milli-Q water. Results were normalized to the initial weight of the samples.

S3. T2 measurements of an AC granule with biofilm that was collected after a growth period of 15 days. A) 2D spin echo MRI images of the echo times $t = 2.9, 11.8, 20.6, 29.5, 38.3$ ms are shown. B.) Signal intensity values of all recorded echo images of one biofilm voxel (red) and bulk water voxel (blue) (positions indicated in Figure S3A) are plotted against the echo time. C) Amplitude map and T2 map from the mono-exponential fit of the image intensities in A.) are depicted.



T₂ map – Methods

A 2D spin-echo MSME sequence (Echo time (TE) = 2.9 ms, 64 echoes, Repetition time= 12500 ms), 24 averages, receiver bandwidth 100 kHz, Field-of-View 3x3 mm², slice thickness 0.2 mm) was used. The raw data was phase-corrected, Fourier-transformed. The signal intensity within a pixel as a function of actual echo time (t = n*TE) was mono-exponentially fitted with a home-written IDL script using IDL Version 6.4 (ITT, Visual Information Solutions, Boulder, CO, USA) to obtain quantitative T₂-Maps according to the function:

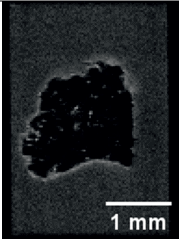

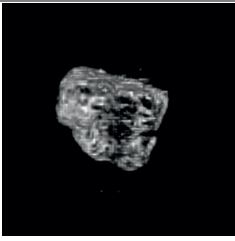
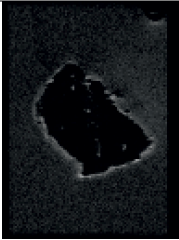

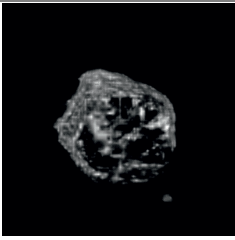
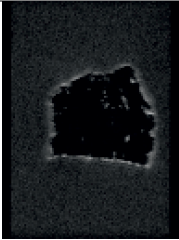
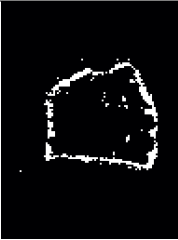
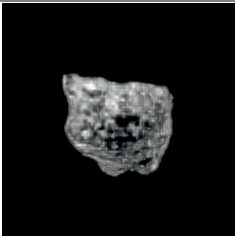
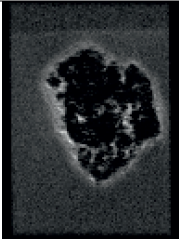

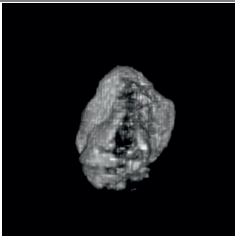
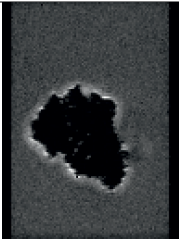

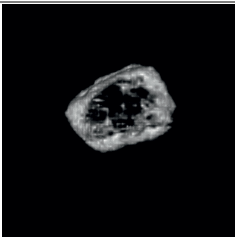
$$I(t) = I_0 e^{-\frac{t}{T_2}}$$

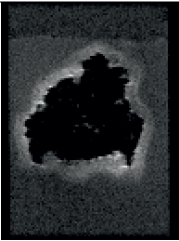

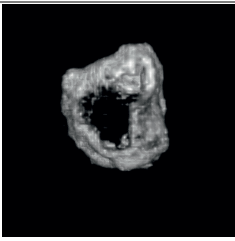
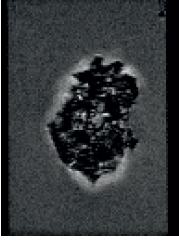

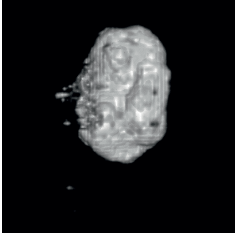
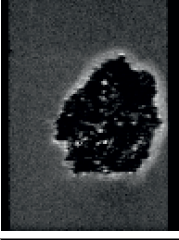

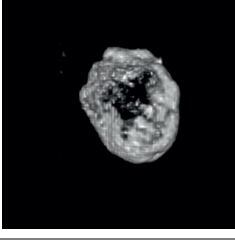
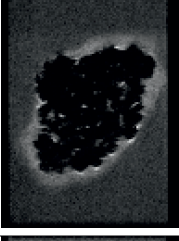

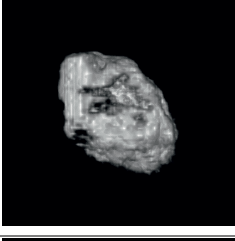
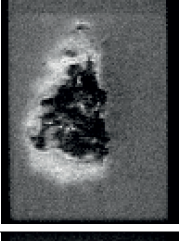

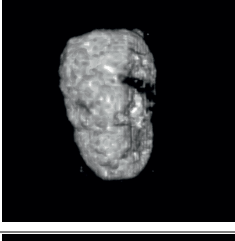


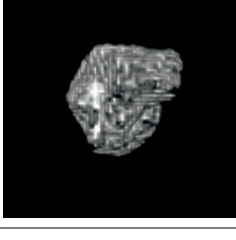
where $I(t)$ is the image intensity as function of echo time $t = n \cdot TE$, I_0 the proton density, and the T₂ relaxation time.

T₂ map – Results

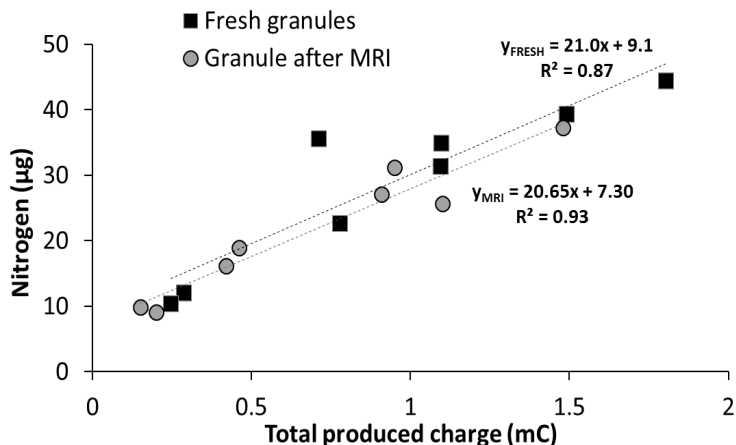
The spin-echo images at different echo times show that biofilm and bulk water can be distinguished based on T₂- contrast (Figure S1A). However, the contrast of biofilm to AC granule is lower than in the T₁-weighted images. Therefore, the distinction between these two regions is easier based on T₁-contrast than on T₂-contrast.

S4. This table shows one cross-section of the MRI-data (left), the corresponding image after the threshold procedure has been applied (middle) and the 3D-volume reconstruction (right). The scale bars shown in the picture of day 3 can be used for the rest of figures as well, which have the exact same dimensions.

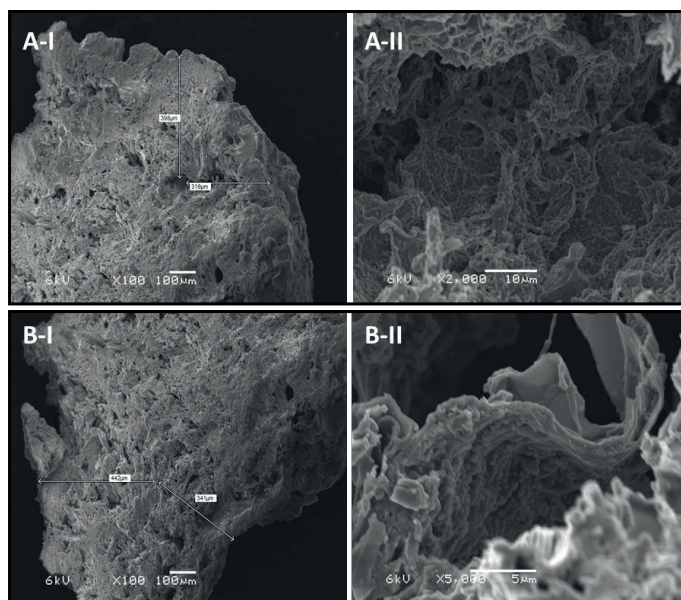
Biofilm growth period [d]	MRI data	Thesholded image	3D- reconstruction
3			
4			
6			
7			
10			

11			
15			
16			
22			
23			
Abiotic			

S5. Nitrogen content of granular bioanodes that were i) previously used for MRI images (in grey); and ii) fresh, directly taken from the MFC reactor (in black). The correlation of the nitrogen content and the total produced charge was as linear in both cases, meaning that no damage was caused to the biofilm during MRI measurements.

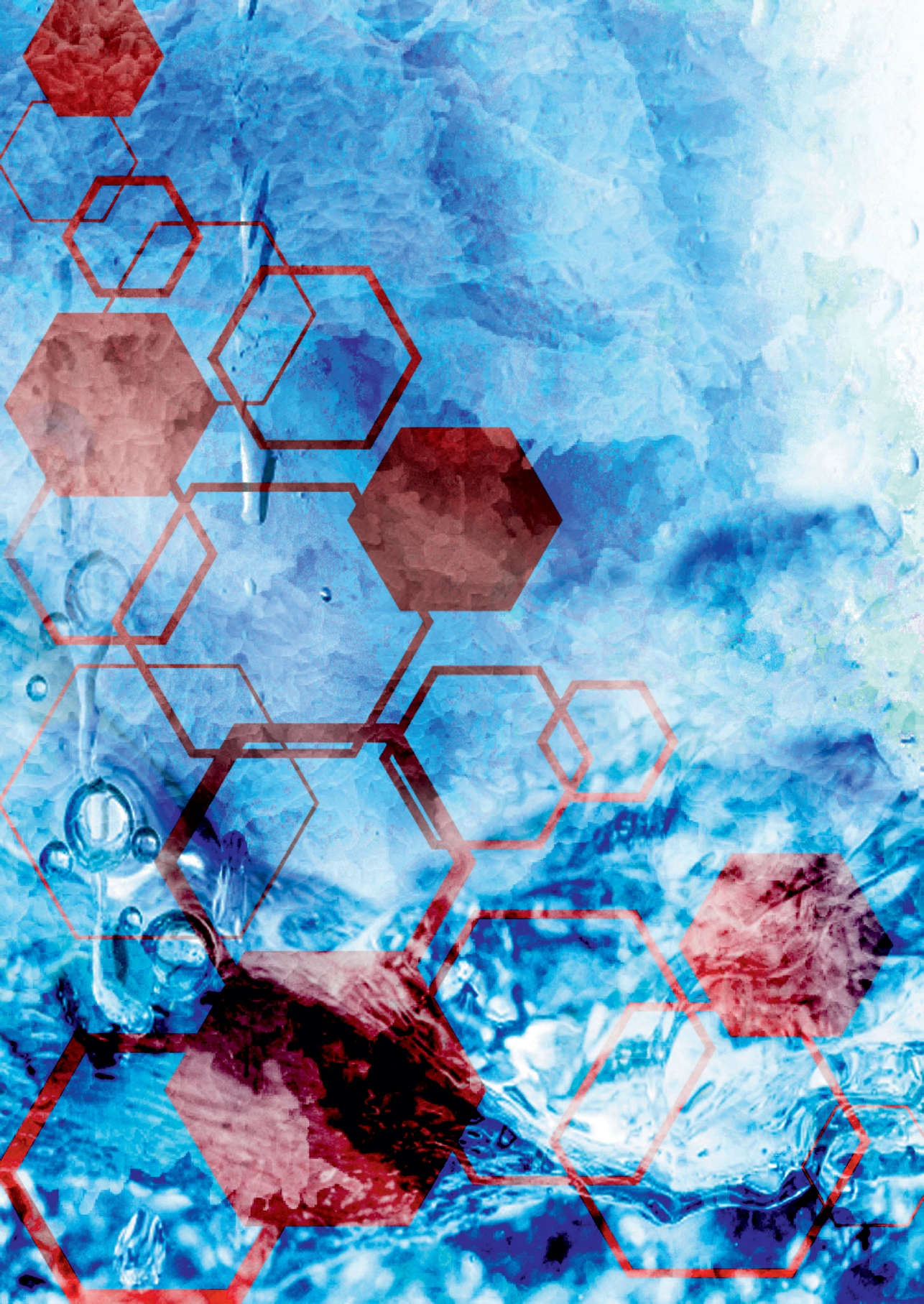


S6. Two cross-section images of AC granules taken with SEM. In the left (A-I and B-I), the granule inner surface can be seen (100x), and the cavities that were further checked for bacterial growth are marked with arrows, at a distance of about 300 to 400 µm from the granule surface. In the right (A-II and B-II), a closer view of the cavities can be seen (2000x and 5000x), where bacterial growth is visible.



Granules were individually collected from the reactor and fixated with 2.5% glutaraldehyde for 2 h at room temperature. Afterwards, they were rinsed 3 times with a phosphate buffer solution (30.5 mM Na_2HPO_4 and 19.5 mM KH_2PO_4) and dehydrated with a sequence of ethanol solutions (30%, 50%, 70%, 90% and 100%) for 30 min each. Finally, granules were dried at 105 °C for 1 h.

Prior to imaging, granules were embedded in optimal cutting temperature (OCT) compound to do the frozen sectioning on a microtome-cryostat. Usually, this process is done to create very thin slides of a sample. However, AC granules were too brittle and the slides broke. Therefore, several cuts were done until the middle of the granule (~0.7 mm) was approximately reached. The remaining sample was then left at room temperature until the OCT melted, washed with PBS and dried for 1h. For the imaging, single granules were placed in a specimen holder of the scanning electron microscope (SEM) JEOL JSM-6480 LV (JEOL Technics Ltd., Tokyo, Japan). With a magnification of 100x, SEM was operated at an acceleration voltage of 6 kV and an electron beam diameter of 20-30%. Images were analyzed with the software JEOL SEM Control User Interface version 7.07.



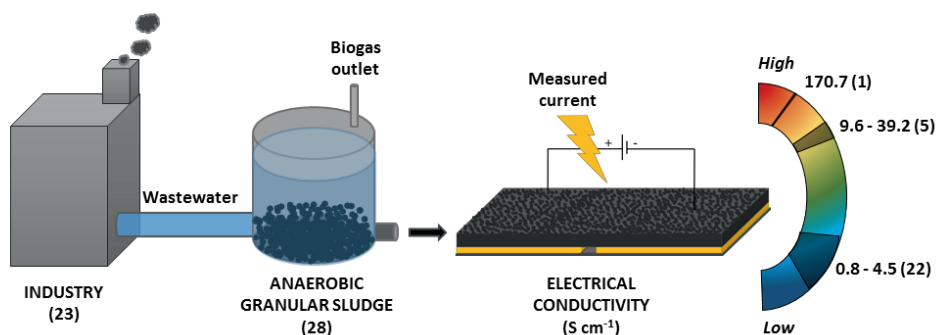
Chapter 5

Screening for electrical conductivity in anaerobic granular sludge from full-scale wastewater treatment plants

Leire Caizán-Juanarena, Annemiek ter Heijne, Jan Weijma, Doekle Yntema, Diego A. Suárez-Zuluaga, Cees J. N. Buisman

Abstract

The application of granulation bioreactors for treatment of industrial wastewater is widespread. Anaerobic granular sludge treating brewery wastewater has been shown to have electrical conductivity, however, it is not known if electrical conductivity also occurs in granular sludge of other industries. Therefore, we determined electrical conductivity of anaerobic granular sludges from 28 full-scale reactors treating a wide variety of wastewaters. Conductivity was studied in relation to physical, chemical and biological granule properties. Electrical conductivity was a highly variable characteristic among sludges. One sludge had a high conductivity of $171\ \mu\text{S cm}^{-1}$, which is 4 times higher than the maximum reported for industrial anaerobic granules. Conductivity of 5 other anaerobic sludges was intermediate, ranging between 9.6 and $39\ \mu\text{S cm}^{-1}$, while 22 anaerobic sludges had a low electrical conductivity below $4.5\ \mu\text{S cm}^{-1}$. A positive correlation between electrical conductivity and iron and sulfur contents of granules was found. No other correlation between granule properties and electrical conductivity was found. Electrical conductivity is a scarce rather than a widespread characteristic of anaerobic granular sludge. Although a relation to iron and sulfur content was observed, the origin and role of electric conductivity is not yet well understood.



Keywords: anaerobic granules; extracellular electron transfer; elemental composition, microbial community; direct interspecies electron transfer.

1. Introduction

Granular biofilms are common in anaerobic wastewater treatment reactors (Angenent, Sung, et al., 2004; Lettinga et al., 1980). In anaerobic granules, distances between microbial species involved in sequential degradation of organic matter are small (micron scale), which facilitates substrate degradation (Schmidt & Ahring, 1996; Stams et al., 2012). Interspecies hydrogen transfer (IHT) is a key mechanism in anaerobic degradation, as hydrogen is formed from the oxidation of organic intermediates by fermentative microorganisms. The hydrogen is transferred to hydrogen-consuming microorganisms, in particular methanogens and sulfate reducing bacteria (Stams & Plugge, 2009). Hydrogen consumption is crucial to keep its concentration below the critical thermodynamic limit for the fermentative microorganisms (Müller et al., 2010). In addition to hydrogen, formate has also been reported as an electron carrier in anaerobic communities (Schink & Stams, 2006; Stams et al., 2006).

Alternatively to interspecies H_2 /formate transfer, it has been shown that electrons can be transferred directly between microbial species by redox-mediating proteins (e.g. c-cytochromes) or conductive appendages (pili) (Malvankar & Lovley, 2014; Reguera et al., 2005). Most research on direct interspecies electron transfer (DIET) has focused on defined co-cultures of *Geobacter* spp. (Shrestha et al., 2013; Summers et al., 2010) or *Geobacter* spp. with methanogenic archaea (Rotaru, Shrestha, Liu, Markovaite, et al., 2014). This mechanism of DIET has also been proposed for granules in anaerobic digesters, especially those treating brewery wastewater (Dubé & Guiot, 2015). For example, Rotaru and co-workers (Rotaru, Shrestha, Liu, Shrestha, et al., 2014) suggested DIET between *Geobacter* and *Methanosaeta* spp. in aggregates from a brewery wastewater digester, and further demonstrated that DIET could have a metabolic advantage by not only producing methane from acetate but also from the electrons released during the conversion of ethanol to acetate.

Electrical conductivity is the characteristic of a material to conduct electric current, i.e. to transport electrons along a certain distance, which can happen by different mechanisms (Cheng Li et al., 2017; Malvankar & Lovley, 2015). Electrical conductivity has been measured for living structures in short distances, such as molecules (Reguera et al., 2005), cells (Summers et al., 2010), or biofilms (Malvankar, Lau, et al., 2012), but also in marine sediments where electrons were transported over centimeter distances (Malvankar et al., 2015; Pfeffer et al., 2012). Electric conductivity measurements can thus be performed to study the ability of microorganisms to transport electrons, which can, for example, also be valuable to increase current densities from the oxidation of organics in microbial fuel cells (MFCs) (Malvankar, Tuominen, et al., 2012). Measurement of electric conductivity in anaerobic granular sludge has been proposed (Morita et al., 2011) and related to the occurrence of DIET (Rotaru, Shrestha, Liu, Shrestha, et al., 2014; Zisheng Zhao et al., 2016). For example, Morita and co-workers (Morita et al., 2011) measured an electrical conductivity of $6.1 \mu S \text{ cm}^{-1}$ in anaerobic granules obtained from a brewery UASB reactor,

while Shrestha et al. (2014)(Shrestha et al., 2014) reported electrical conductivities between 0.8 and 36.7 $\mu\text{S cm}^{-1}$ in fourteen samples of granules obtained from four brewery UASB reactors. Furthermore, many studies at laboratory scale have observed an enhanced methanogenesis rate of anaerobic digesters when including conductive materials (e.g. carbon felt/cloth, graphite), which was proposed to be the result of direct electron transfer. This higher rate usually comes along with a shift of the microbial community and an increased sludge conductivity (Lei et al., 2016; Zhiqiang Zhao et al., 2015; Zisheng Zhao et al., 2016).

So far, electrical conductivity has only been studied and reported for anaerobic granular sludge treating brewery wastewater due to presence of ethanol (Morita et al., 2011; Shrestha et al., 2014). It is not known how widespread this characteristic for other anaerobic granular sludges in other industries. In this study, we measured electrical conductivity of anaerobic granular sludge obtained from a wide variety of industries: food and beverage, brewery, alcohol production, paper and textile, petrochemical and chemical. All these sludges were predominantly methanogenic except one which was predominantly sulfidogenic. Granules were examined to relate differences in electrical conductivity to microbial community composition, and chemical and physical factors.

2. Material and Methods

2.1. Characteristics and origin of anaerobic granular sludge

Anaerobic granules were collected from 28 anaerobic reactors located at 23 different industrial sites. They were stored in airtight plastic bottles at 4 °C to ensure anaerobic conditions and limit metabolic activity. Bottles were placed at room temperature approximately one hour before conductance measurements were done.

Table 1 classifies the samples into 6 groups according to the type of industry they originated from: 1) food and beverage; 2) brewery; 3) alcohol production; 4) paper and textile; 5) petrochemical; and 6) chemical.

Table 1: Classification of granular sludges according to their origin. 'R' stands for 'Reactor' and the number that follows refers to the reactor number within the same wastewater treatment plant.

Sludge	Industry	Process
1	Food and beverage	Fruit canning and juice production*
2	Food and beverage	Soft drinks and juice production*
3	Food and beverage	Food-ingredient production
4	Food and beverage	Inuline production
5	Food and beverage	Lactic acid fermentation*
6	Food and beverage	Production of frozen potato products

7	Food and beverage	Food, agricultural and industrial products*
8	Brewery	Brewery 1- R2*
9	Brewery	Brewery 1- R1*
10	Brewery	Brewery 1- R3*
11	Brewery	Brewery 2- R2*
12	Brewery	Brewery 3- R3
13	Brewery	Brewery 3- R1*
14	Brewery	Brewery 2- R1*
15	Brewery	Brewery 3- R2
16	Alcohol production	Alcohol distillery*
17	Alcohol production	Ethanol production
18	Alcohol production	Ethanol production*
19	Alcohol production	Cider production
20	Paper and textile	Paper Industry 1*
21	Paper and textile	Textile industry*
22	Paper and textile	Recycled paper industry 1
23	Paper and textile	Recycled paper industry 2
24	Paper and textile	Paper Industry 2
25	Paper and textile	Recycled paper industry 3
26	Paper and textile	Production of cardboard*
27	Petrochemical	Propylene epoxidation process*
28	Chemical	Sulfate reduction*

* denotes samples analyzed with ICP for elemental composition.

2.2. Electrode slide and sample handling

Electrical conductance was determined with two gold electrodes fixated on a glass slide, separated by a non-conductive gap of 50 μm . The design of the electrode slide was similar to the one reported by Malvankar and co-workers (Malvankar et al., 2011). The gold layer had a thickness of 100 nm and was placed on top of a 10 nm chromium adhesion layer. The gold electrodes were connected to a potentiostat (N-stat, Ivium Technologies) by a clamp with a platinum contact surface area of around 0.1 cm^2 . Figure 1 shows a sketch of the electrode slide with dimensions.

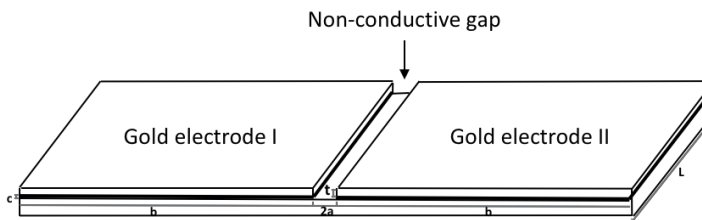


Figure 1. Sketch of the gold electrode slide used for conductivity measurements of anaerobic granular sludge. $L \approx 2$ cm; $b \approx 3.5$ cm; $2a \approx 50$ μ m; $c \approx 10$ nm; $t_g \approx 40$ nm.

Before each test, at room temperature and atmospheric conditions, the electrode slide was cleaned with ethanol (70%) and demi-water. Before conductance measurement, a layer of granules was gently crushed to form an homogeneous and confluent layer (Morita et al., 2011) on top of the electrode slide, covering the whole surface area including the non-conductive gap. Two independent measurements (replicates) were performed for each granular sludge. Media, i.e. the aqueous phase from the bioreactor from which the sludge originated, were also analyzed for electrical conductance and served as controls (one measurement per medium). Media were centrifuged twice (4500 rpm, 20 min) to eliminate suspended sludge particles and about 2.5 mL of supernatant was distributed with a syringe on the electrode slide until the whole surface was evenly covered.

Conductance of several selected granule samples and their media were also measured inside an anaerobic hood (<0.05 mg L^{-1} oxygen) to evaluate the effect of exposure to oxygen.

2.3. Electrochemical test and determination of conductance

Chronoamperometry was used to measure conductance of granular sludge and media. A two-electrode set up was used, where one gold electrode served as working electrode and the other one as counter electrode. Therefore, the potential applied in these measurements corresponded to a cell voltage difference between the working and counter electrode. This cell voltage drives an electron flow from one electrode to another, but only if the sample that crosses the non-conductive gap is electrically conductive. The measured current is related to the applied voltage and this reveals the electrical conductance of the sample. When a sample is not electrically conductive (dissolved salts in media only result in ionic conductance), theoretically, there should be no current.

As in previous studies (Morita et al., 2011; Shrestha et al., 2014), cell voltages from 0.3 V to -0.3 V were applied in steps of 0.05 V (13 in total), and each step was set for 200 s to assure that current reached the steady-state after the decay of current transients due to surface charging effects (Boyd et al., 2015). Additionally, an equilibration time (200 s) was applied prior to each measurement in order to stabilize the initial current. The steady-state current obtained after that time at each voltage was used to plot current as a function of voltage (Figure 2 is an example). The slope corresponding to a linear regression line of

this plot was used to calculate conductance, i.e. the measured current within a certain voltage range. However, it is necessary to normalize conductance (in S) to conductivity (in S cm^{-1}) in order to compare the results with those in the literature. This was done by using the Schwarz-Christoffel transformation (Malvankar et al., 2011) (Eq. 1) that converts the measured conductance to conductivity by correcting for the non-uniformity in current distribution occurring in the sludge that is placed on the gold electrode slide. The applied transformation is valid for the case in which $a < g < b$ (see Figure 1 for the value of b).

$$\vartheta = G \frac{\pi}{L} / \ln \left(\frac{8g}{\pi a} \right) \quad (1)$$

where ϑ is the conductivity (calculated), G is the conductance (measured), L is the electrode length (2 cm), g is the thickness of the sludge/media layer (2 mm), and $2a$ is the width of the non-conductive gap (50 μm).

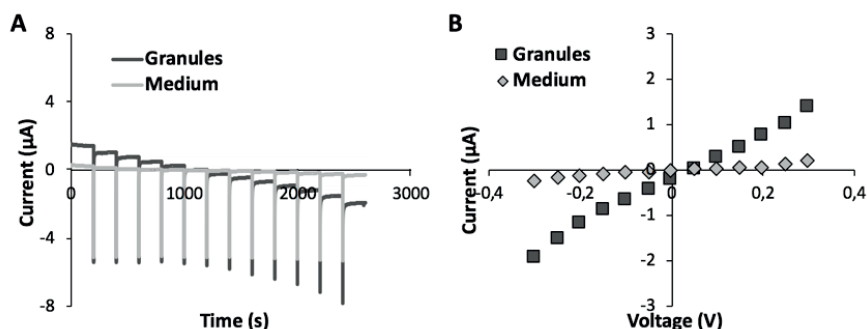


Figure 2. Electrochemical method to determine electrical conductivity of granular sludge and media. Current is first measured at different cell voltages and recorded in time (a). Then, it is plotted as a function of voltage (b). The slope of the Voltage-Current line represents the electrical conductance.

2.4. Elemental composition of granular sludge

The composition of granular sludge, including metallic and non-metallic elements, was analyzed with an inductively coupled plasma analyzer (ICP-OES, Varian Vista MPX). Samples analyzed were: 1, 2, 5 and 7 from food and beverage industries; 8-11, 13 and 14 from breweries; 16 and 18 from alcohol production industries; 20, 21 and 26 from paper and textile industries; 27 from a petrochemical industry; and 28 from a chemical industry. Multi- and single-element standard solutions were prepared (with aqua regia as dissolvent) to cover a concentration range from 0.2 to 5 mg L^{-1} . These standards contained the following elements: Ag, Al, B, Ba, Bi, Ca, Cd, Co, Cr, Cu, Fe, Ga, In, K, Li, Mg, Mn, Na, Ni, P, Pb, S, Sr, Ti and Zn.

Prior to measurements, granules were dried overnight at 100 °C. Dried samples (0.3 to 0.5 g of dry weight) were mixed with 10 mL aqua regia in a vessel with vent-and-reseal technology, and digested in a microwave (ETHOS 1, Milestone S.r.l.). The overall digestion

program took 30 min, with 12 min at maximum temperature of 175 °C. After samples were cooled down, the resulting liquid was diluted in a 100 mL volumetric flask with milli-Q water. Results were normalized to the initial dry weight of sample.

2.5. Microbial community analysis

Each anaerobic granular sludge was collected in separate 2mL Eppendorf tubes and kept at -80 °C until DNA extraction. Genomic DNA was extracted with the Powersoil ® DNA isolation kit (MO BIO Laboratories, Carlsbad, CA, USA) and used to amplify the V3-V4 region of 16S rRNA according to the standard illumine library preparation method described by Takahashi and co-workers (Takahashi et al., 2014). The same primer sets were used to analyze bacteria and archaea. Taxonomic analysis was performed by using the QIIME software (package version 1.9.1) and OTU picking was done by the SILVA 128, 16S reference database and the uclust tool (Quast et al., 2013). The same SILVA reference database was subsequently trained by the RDP classifier to perform OTU classification (Q. Wang et al., 2007).

2.6. SEM-imaging of granular sludge

To prepare for SEM analysis, granules were fixated with 2.5% glutaraldehyde for 2 h at room temperature. Afterwards, they were rinsed 3 times with a phosphate buffer solution (30.5 mM Na₂HPO₄ and 19.5 mM KH₂PO₄) and dehydrated with a sequence of ethanol solutions (30%, 50%, 70%, 90% and 100%) for 30 min each. Finally, granules were dried at 105 °C for 1 h. For the imaging, single granules were placed in a specimen holder of the scanning electron microscope (SEM) JEOL JSM-6480 LV (JEOL Technics Ltd., Tokyo, Japan). With a magnification of 30-100,000x, SEM was operated at an acceleration voltage of 3-10 kV and an electron beam diameter of 20-30%. Images were analyzed with the software JEOL SEM Control User Interface version 7.07. Samples analyzed with SEM were number 1, 2, 8, 11 and 27.

2.7. Statistical analysis

All data were analyzed using IBM SPSS Statistics 20. A paired-samples t-test was conducted to evaluate the differences in electrical conductivity between duplicates. Additionally, the correlation between electrical conductivity and concentration of elements was investigated by using Pearson product-moment correlation coefficient.

3. Results and Discussion

3.1. Electrical conductivity varies strongly among anaerobic granular sludges

Figure 3 shows the measured conductance values (in μS) of anaerobic granules from 28 full-scale reactors, ordered from high to low and classified in 6 groups according to the type of industry. Conductance of media is also included.

Of the 28 granular sludges, 22 had a conductance below $15.2 \mu\text{S}$. This corresponds to a conductivity range from 0.8 to $4.5 \mu\text{S cm}^{-1}$ (Eq. 1). These numbers are within the low range of electrical conductivities of anaerobic granules reported in literature (Y. Li et al., 2017; Shrestha et al., 2014; Zhiqiang Zhao, Zhang, Yu, et al., 2016). Five granular sludges had higher electrical conductance between 32.5 and $132.8 \mu\text{S}$, which corresponds to conductivities of 9.6 to $39.2 \mu\text{S cm}^{-1}$. The latter value is similar to the maximum conductivity reported in the literature for anaerobic granules from reactors treating brewery wastewater, which is $36.7 \mu\text{S cm}^{-1}$ (Shrestha et al., 2014). Of these 5 granular sludges, 3 originated from separate reactors of the same brewery (samples 8, 9 and 10). The other 2 sludges originated from an alcohol distillery (sample 16) and an industry carrying out a propylene epoxidation process (sample 27). Finally, one granular sludge (sample 1) was highly conductive with a conductance of $578 \mu\text{S}$, corresponding to a conductivity of $171 \mu\text{S cm}^{-1}$, which is more than 4 times higher than the maximum reported in the literature among industrial samples (Shrestha et al., 2014). This latter conductivity is in the range of that for conductive materials such as magnetite, i.e. $160 \mu\text{S cm}^{-1}$, but lower than stainless steel ($667 \mu\text{S cm}^{-1}$) or granular activated carbon ($3000 \mu\text{S cm}^{-1}$) (Y. Li et al., 2017). No significant differences ($p > 0.39$, two-tailed) were found for the replicates, i.e. between the first group of samples ($M_1 = 40.0$, $SD_1 = 111.4$) and the second one ($M_2 = 38.6$, $SD_2 = 106.8$) (see Supporting Information, S1).

No direct relation was found between electrical conductivity of granules and the type of industry they originated from. The granular sludge with highest conductivity, sample 1, was fed with wastewater from a fruit canning and juice production industry. The second most conductive sludge, sample 27, was taken from a bioreactor fed with wastewater consisting primarily of benzoate and acetate, generated by a propylene epoxidation process. Granular sludge from only 4 out of 13 ethanol-related industries showed high electrical conductivity, revealing that wastewater from such industries does not by default result in electrical conductivity. High variety in electrical conductivity of brewery granules has been reported before (Shrestha et al., 2014), and conductivity may thus not be a generic characteristic. Our results show that electrical conductivity is not solely a characteristic of granular sludge from reactors treating brewery wastewater, as was thought until now, but it is also found in other industries.

For the 6 most conductive granules, conductance values were more than an order of magnitude higher than that of their medium, confirming that these granular sludges were

indeed electrically conductive (see Figure 3). In general, the conductance values of media were surprisingly high (0.7 - 7.1 μS) compared to near-zero values reported in the literature at the same voltage range (Morita et al., 2011). Several of the studies on sludge conductivity even do not report the values for such control measurements on media (Shrestha et al., 2014; Zhiqiang Zhao et al., 2015; Zisheng Zhao et al., 2016). A potential cause for conductivity at such low voltage would be reaction of oxygen on the electrode (coupled to oxygen evolution on the other). To exclude any effects of oxygen, media from samples 19 and 25 were measured once more inside an anaerobic chamber and showed similar electrical conductance to that measured at atmospheric conditions (data not shown). Another cause for current could be the short-term polarization effects of ions present in the media. This is also unlikely, as each potential step was sustained for a long time period (200s). Therefore, for granules that had a conductance in the same range as their medium (see Figure 3), it is unclear if the conductance was due to the medium or due to granule.

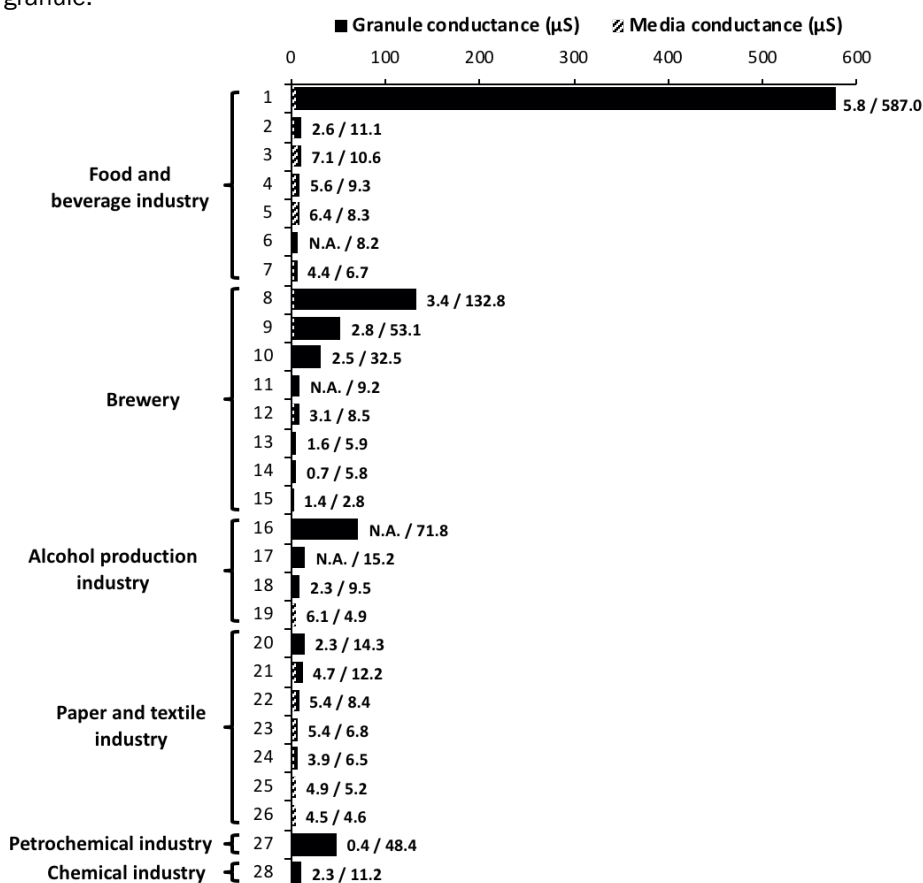


Figure 3. Conductance (μS) of 28 granular sludge (black) and their media (black and white stripes) from different wastewater treatment plants classified in 6 groups according to the type of industry. Next to the bars, the exact values for media (left) and granules (right). N.A. is written for non-available data.

3.2. Electrical conductivity in relation to microbial community composition

Many studies have analyzed the microbial community of anaerobic granular sludge to screen for microorganisms involved in DIET, such as *Geobacter* spp. or *Methanosaeta* spp. (Baek et al., 2016; Rotaru, Shrestha, Liu, Shrestha, et al., 2014; Shrestha et al., 2014; Yin et al., 2017; Zhiqiang Zhao, Zhang, Holmes, et al., 2016). Here, we studied the microbial community of 3 sludges with conductivities above $14.3 \mu\text{S cm}^{-1}$ (samples 1, 8, and 27) and compared them to 3 sludges with conductivities below $3.3 \mu\text{S cm}^{-1}$ (samples 2, 11 and 19). Results at the genus level are shown in Figure 4. These were not very conclusive, as some of the granules with low conductivity (samples 11 and 19) contained *Geobacter* spp., known to carry out DIET (Morita et al., 2011), while this genus was present below 5% in granules with higher conductivity (samples 8 and 27). Therefore, no relation was found between electrical conductance and the relative abundance of *Geobacter* spp. ($R^2 < 0.1$). The same lack of correlation was found for *Methanosaeta* spp., which are also known to carry out DIET (Rotaru, Shrestha, Liu, Markovaite, et al., 2014; Rotaru, Shrestha, Liu, Shrestha, et al., 2014). On the contrary, a strong positive correlation was found between electrical conductance and *Sulfurimonas* spp. ($R^2 = 0.95$) (see Supporting Information, S2), which had a relative abundance of 10% in the most conductive sludge (number 1). However, no conclusion could be derived from this relation, as most of the sludges had a relative abundance below 5% (i.e. within the minor phyla) and the sample size for NGS analysis was small ($n=6$).

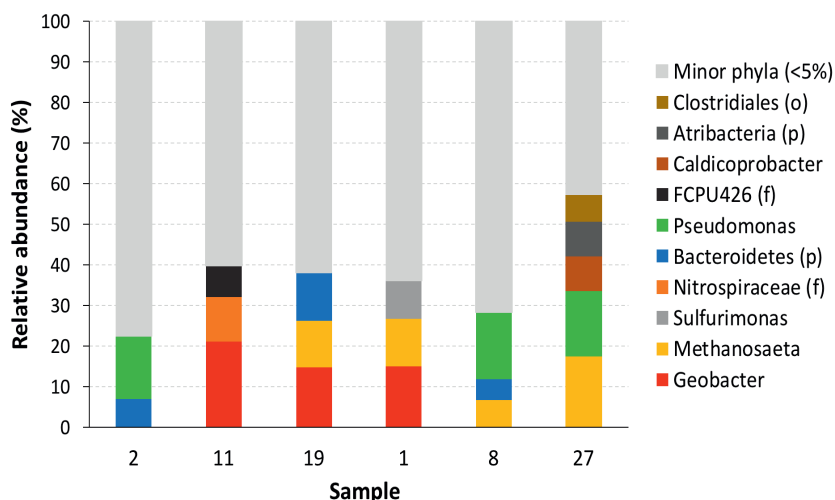


Figure 4. Microbial community of six granular sludges at genus level expressed in relative abundance (%). Samples 2, 11 and 19 had a conductivity below $3.3 \mu\text{S/cm}$ while samples 1, 8 and 27 had a conductivity above $14.3 \mu\text{S/cm}$. In case the genus was unknown, other taxonomic levels were specified: (p)= phylum; (o)= order; (f)= family.

3.3. Iron and sulfur contents in granular sludge follow a positive trend with increased electrical conductance

Microbial community composition alone does not explain why some granular sludges are conductive and others are not. Therefore, physical and chemical granular sludge properties were studied. Firstly, 17 granular sludges (marked with '*' in Table 1) with varying conductivity were analyzed for a wide range of elements, including metals.

Most abundant elements in the granular sludges were iron (4 to 123 mg g⁻¹), sulfur (10 to 98 mg g⁻¹), sodium (1 to 59 mg g⁻¹), calcium (5 to 24 mg g⁻¹), phosphorous (6 to 18 mg g⁻¹) and potassium (1 to 18 mg g⁻¹). Of these, two element concentrations showed positive correlation with electrical conductance (Figure 5): iron ($r = 0.45$) and sulfur ($r = 0.27$). Clear exceptions were sample 27, with a high conductance (48.4 μ S) but low sulfur and iron content, and sample 28, with a fairly low conductance (11.2 μ S) but high sulfur concentration. Fe:S ratio was calculated and found to be below 1 in every sample (0.6 ± 0.2) except for the most conductive one, which had a Fe:S ratio of 1. All other most abundant elements did not show a positive correlation with electrical conductance.

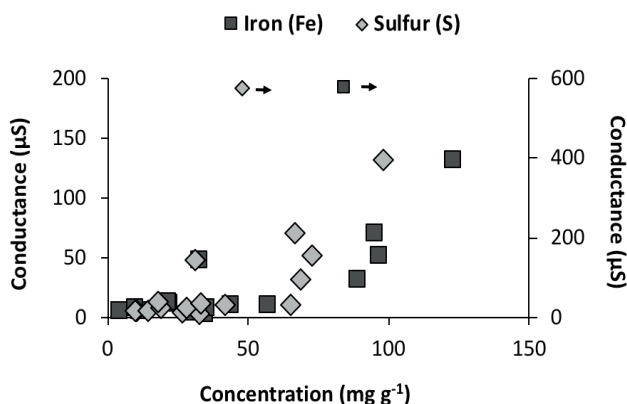


Figure 5. Electrical conductance (μ S) as function of iron (Fe) and sulfur (S) concentrations (mg g⁻¹) of 17 granular sludges. Data points for the sludge with the highest conductance are shown on the secondary y-axis.

Iron is likely present in the sludge mainly as Fe(II) precipitates, such as ferrous sulfide (FeS) and ferrous phosphate (vivianite, $\text{Fe}_3(\text{PO}_4)_2 \cdot 8\text{H}_2\text{O}$), although the presence of (partially) oxidized minerals like magnetite (Fe_3O_4) cannot be excluded (Behrends & Cappellen, 2007). Iron and sulfur is also a constituent of methanogenic biomass, but measured values were much higher than would be measured in case it was only present in biomass (3 mg g⁻¹ for iron and 6-12 mg g⁻¹ for sulfur (Takashima et al., 1990)) Identification of iron minerals in dried sludge samples with XRD was attempted but not successful, presumably because

the individual minerals were too small and too finely dispersed, as revealed with SEM-EDX (See Supporting Information, S3). Recently, the fact that conductive materials can enhance electron transfer in anaerobic granules has received much attention. These conductive materials can act in a similar way (or as substitute) to the biological connections during DIET (Rotaru, Shrestha, Liu, Shrestha, et al., 2014; Zisheng Zhao et al., 2016). Conductive minerals (Kato et al., 2012), in particular iron oxides (Zhiqiang Zhao et al., 2017), are examples of such conductive materials. It has been shown, for example, that magnetite (Fe_3O_4) particles stimulated DIET in microbial biofilms grown in an anaerobic reactor fed with dairy industry effluent, which led to increased biofilm stability and methanogenic activity (Baek et al., 2016). In addition, the presence of iron oxides has been shown to increase the degradation rate of benzoate (Sieber et al., 2012; Stams et al., 2012), and could be related to DIET driven methanogenesis (Zhuang et al., 2015). The presence of iron could therefore play a role in electric conductivity for the anaerobic granular sludge fed with benzoate (sample 27).

3.4. Other factors could not be related to electrical conductance of anaerobic granules

Other factors were analyzed for a possible relation with electrical conductance, i.e. pH and ionic conductivity of the bioreactor medium, type of bioreactor, size of granules, visual surface roughness and ash content. No correlation (r close to zero) was found between electrical conductivity of granular sludges and media pH (ranging from 7.2 to 8.3) or ionic conductivities (ranging from 2.3 to 32.3 mS cm^{-1}) (see Supporting Information, S4). Granular sludges originating from reactors with different designs, namely upflow anaerobic sludge blanket (UASB), expanded granular sludge bed (EGSB) or internal circulation (IC) reactors, did not reveal any apparent relation with the occurrence of electrical conductance. The size of granules was also considered, as diffusion limitations may play a more important role in larger granules, and these could benefit from conductivity via enhanced DIET (Satoh et al., 2007). However, no apparent relation between conductance and granular size could be found. Regarding the roughness of granules, some study (Baek et al., 2016) has related the high roughness of granules to the presence of metal particles, that led to an enhanced direct electron transfer compared to granules with a clean and smooth surface. Based on the apparent roughness of granules observed on SEM images (Figure 6), sample 8 (B), a conductive sample from a brewery, had a rougher surface compared to sample 11 (C), a non-conductive sample from another brewery, which had more smooth and mature granules. Even though this could go in line to literature findings, the most conductive granules (Figure 6, A) did not have a rough surface like samples 8 (B) and 27 (D), which were less conductive. Finally, the ash content (% dry basis) of granules with high conductance (average 27.5% for samples 1, 8 and 27) did not differ substantially from granules with a low conductance (29.8% average for samples 5, 13 and 26).

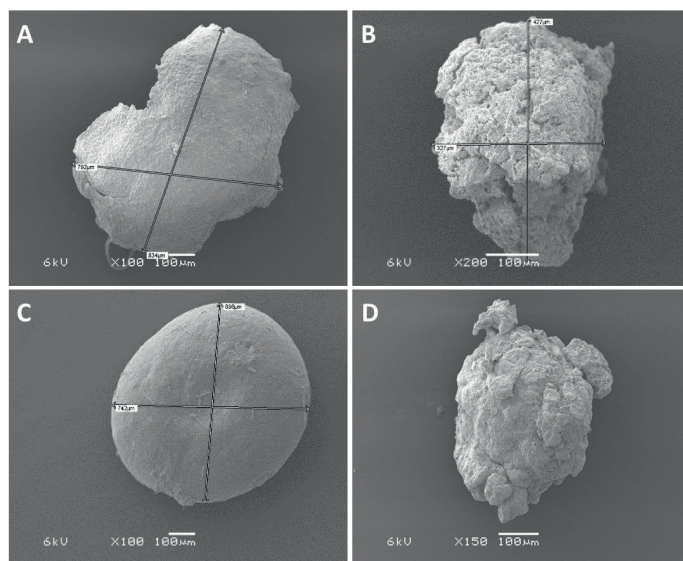


Figure 6. SEM images of anaerobic granules with different surface roughness. A) Sample 1, 587.0 μS ; B) Sample 8, 132.8 μS ; C) Sample 11, 9.2 μS ; and D) Sample 27.

Outlook

Electrical conductivity is a highly variable characteristic among anaerobic granular sludges in industrial wastewater treatment reactors. Several studies have related anaerobic ethanol degradation to the development of DIET as the primary electron transfer mechanism between syntrophic microorganisms, both in UASB reactors treating brewery wastes (Morita et al., 2011; Shrestha et al., 2014) as well as in defined co-cultures (Summers et al., 2010). A positive effect of ethanol addition on the electrical conductivity and methanogenic activity of granular sludge grown on butyrate and propionate was also reported by Zhao and co-workers (Zhiqiang Zhao, Zhang, Yu, et al., 2016), suggesting that DIET is stimulated by the addition of ethanol. We show here that electric conductivity is not always present in granular sludge from breweries, and can also be observed in industry that have no relation to ethanol. The fact that conductivity is highly variable among granular sludges could mean that i) factors or conditions needed for granular sludge to be electrically conductive are not always present; ii) there is not always sufficient ‘driving force’ or selection pressure for microbial aggregates to conduct electrons.

The microbial community composition did not explain the occurrence of electrical conductivity, while the elemental analysis pointed out a positive correlation between conductance and iron and sulfur content.

A challenge in determining the origin and mechanism of electrical conductivity relates to the complexity and variability of factors in full-scale wastewater treatment plant reactors (e.g. operation conditions, wastewater composition). Laboratory experiments under

controlled conditions could reduce complexity and help to understand electrical conductivity in anaerobic granules, also considering the relation between electrical conductivity and the metabolic activity and electron transfer mechanisms of microorganisms.

Acknowledgments

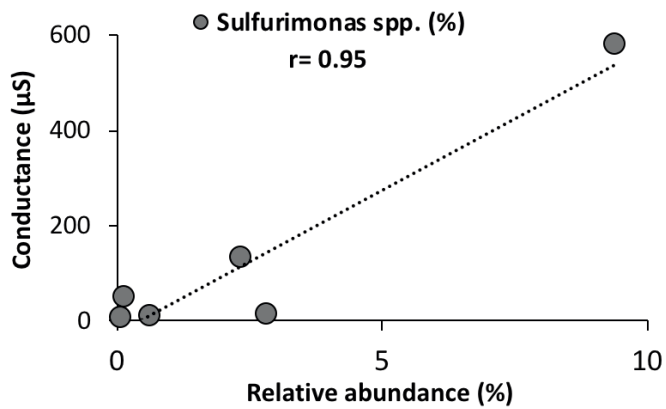
This work was performed in the cooperation framework of Wetsus, European Centre of Excellence for Sustainable Water Technology (www.wetsus.eu). Wetsus is co-funded by the Dutch Ministry of Economic Affairs and Ministry of Infrastructure and Environment, the European Union Regional Development Fund, the Province of Fryslân, and the Northern Netherlands Provinces. The authors would like to thank the participants of the research theme “Resource Recovery” for the fruitful discussions and their financial support. Furthermore, the authors would like to thank Agnieszka Tomaszewska from Wetsus for helping with the SEM images, and Ilse Gerrits from Wageningen University for the support with ICP tests.

Supporting Information

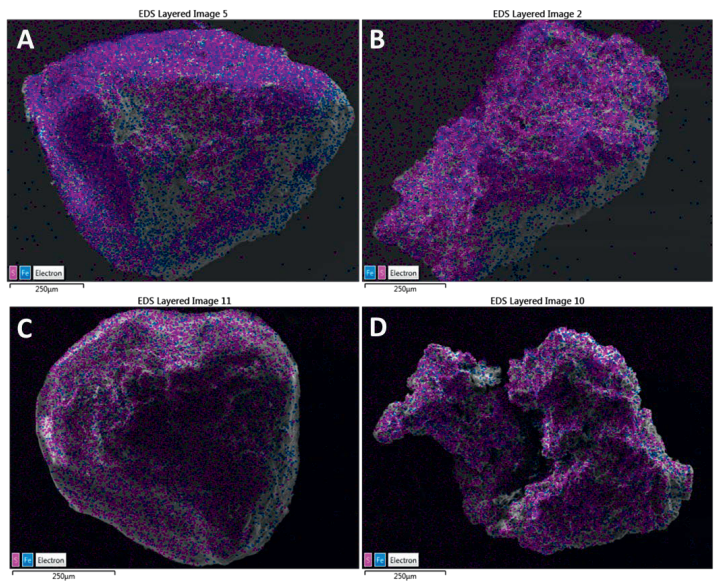
S1. Electrical conductance (μS) from two independent measurements of 28 anaerobic granular sludge, classified according to the type of industry.

Sludge	Industry	Conductance 1 (μS)	Conductance 2 (μS)
1	Food and beverage	589.3	566.7
2	Food and beverage	11.2	11.1
3	Food and beverage	14.1	7.1
4	Food and beverage	8.9	9.8
5	Food and beverage	9.4	7.3
6	Food and beverage	6.3	10.0
7	Food and beverage	6.8	6.7
8	Brewery	138.8	126.8
9	Brewery	47.1	59.0
10	Brewery	31.6	33.4
11	Brewery	5.2	6.4
12	Brewery	9.8	7.3
13	Brewery	5.4	6.5
14	Brewery	6.4	11.9
15	Brewery	2.6	3.0
16	Alcohol production	70.8	72.8
17	Alcohol production	11.4	19.1
18	Alcohol production	9.9	9.1
19	Alcohol production	6.1	3.8
20	Paper and textile	15.9	12.8
21	Paper and textile	10.3	14.3
22	Paper and textile	5.7	11.2
23	Paper and textile	5.4	8.3
24	Paper and textile	7.8	5.3
25	Paper and textile	4.9	5.6
26	Paper and textile	3.9	5.3
27	Petrochemical	63.2	33.5
28	Chemical	13.2	9.3

S2. Correlation between electrical conductance and relative abundance of *Sulfurimonas* in 6 granular sludges.

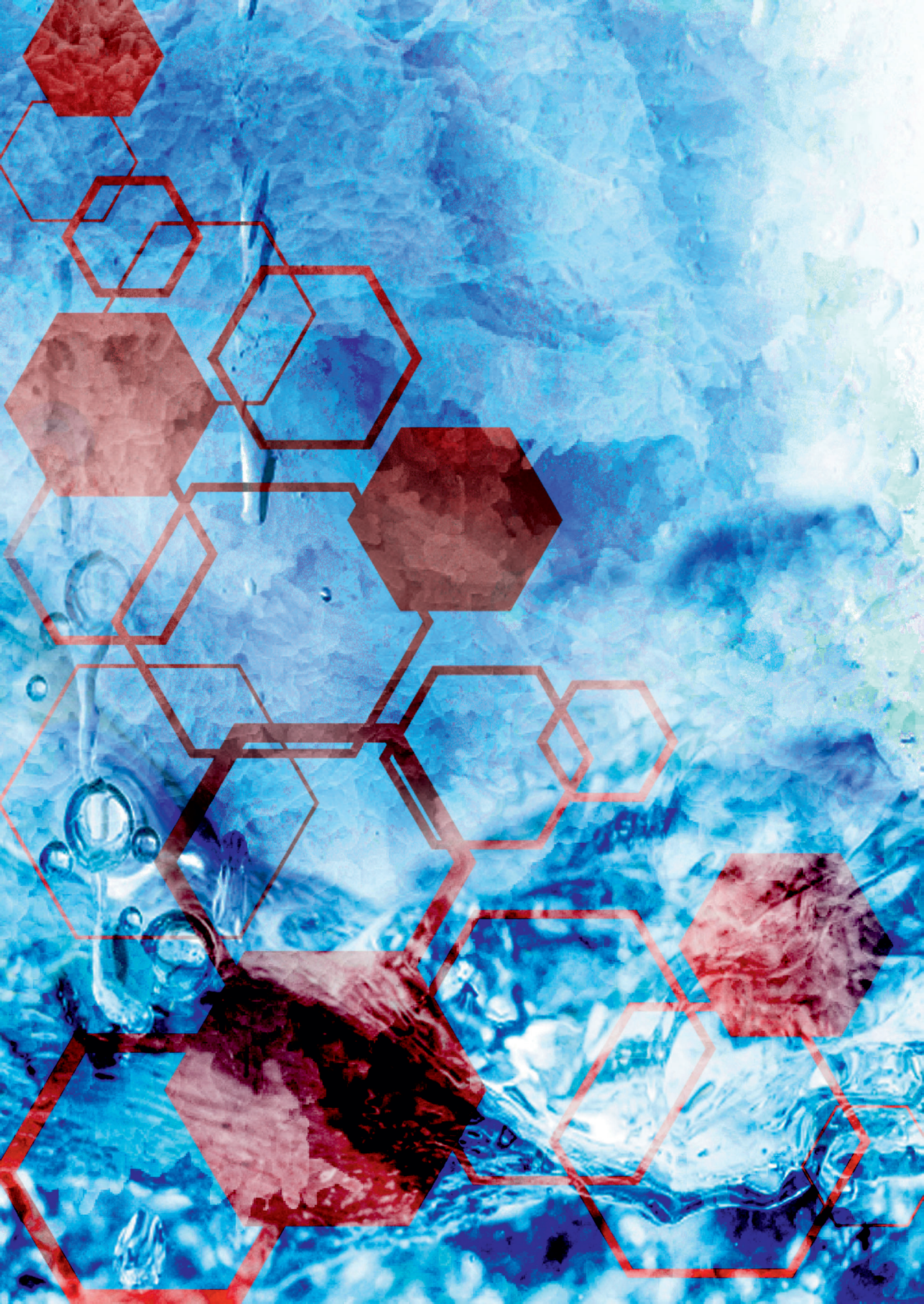


S3. SEM-EDX imaging SEM-EDX images of anaerobic granules with the elemental distribution of Fe (blue) and S (pink) on their surface. A) Sample 1, 587.0 μS ; B) Sample 8, 132.8 μS ; C) Sample 11, 9.2 μS ; and D) Sample 2, 11.1 μS .



S4. Average electrical conductance (μS), ordered from high to low, together with pH and ionic conductivities of 28 anaerobic granular sludge.

Sample	Conductance (μS)	pH	Ionic conductivity ($\text{mS}/\text{cm cm}^{-1}$)
1	578.0	7.6	8.2
8	132.8	7.6	13.8
16	71.8	7.8	11.5
9	53.1	7.3	9.0
27	48.4	8.1	25.5
10	32.5	7.4	10.0
12	32.5	7.4	10.0
4	15.2	7.5	13.9
17	15.2	7.5	13.9
20	14.3	7.7	2.3
21	12.3	7.6	7.8
28	11.2	7.4	6.4
2	11.1	7.6	10.9
3	10.6	7.9	19.5
18	9.5	7.6	6.0
11	9.2	7.5	5.1
22	8.4	7.3	6.6
5	8.3	7.7	9.7
6	8.2	7.7	8.8
23	6.8	7.5	7.7
7	6.7	7.2	11.6
24	6.5	7.5	6.7
13	5.9	8.3	32.3
14	5.8	7.4	5.4
25	5.2	7.2	4.5
19	4.9	7.5	5.2
26	4.6	7.3	6.4
15	2.8	8.1	21.6



Chapter 6

General Discussion



1. Capacitive bioanodes

The use of capacitive electrodes in MFCs is a new field as there are few studies that use porous electrodes (W. Chen et al., 2018; Deeke et al., 2012; Santoro et al., 2015) or modified electrodes with capacitive properties (Feng et al., 2014; Y. Wang et al., 2018, 2016) for electricity harvest and storage. This thesis addresses the combination of capacitive electrodes and electroactive biofilms as bioanodes in microbial fuel cells (MFCs), with focus on activated carbon (AC) granular electrodes. AC granules have a very complex structure that makes the charge storage process difficult to understand and the interaction with biofilm difficult to determine. Additionally, bioanodes are very sensitive towards operational conditions of MFCs, such as the availability of substrate, electrolyte composition, internal resistances or cell design, among others. Therefore, it is important to undergo a systematic approach to characterize capacitive bioanodes, by maintaining all these factors constant and ensuring sufficient replicates to prove the reproducibility of results. To this end, the study of single AC granules was performed with a multi-channel potentiostat in Chapter 3, where all bioanodes (up to 24) were placed in the same electrolyte and controlled in a simultaneous way. The focus was to learn more about the effect of granule type and size, not only in charge storage but also in biofilm growth. The same approach was followed in Chapter 4, where the focus was to visualize the 3D distribution of biofilm and quantify its volume on AC granules with magnetic resonance imaging (MRI). The study of single AC granules allows for a closer look into: i) granule properties and ii) interaction between biofilm and granule. These two aspects are discussed more in depth in the following sub-sections.

1.1. AC granule properties

1.1.1. Volume

AC granules are brittle, very porous, and have a rough surface with a three-dimensional structure. This makes the determination of granule volume and surface area challenging. In this study granule weight was individually measured for each of the granules, so their weight was taken as the standard property.

To calculate granule volume, different kind of densities can be used, as shown in Figure 1 (Webb, 2001b). Bulk volume refers to a group of particles, in which case an additional space is included, i.e. the inter-particle volume. This volume will largely depend on the size and shape of the individual particles and how well they are packed. When regarding a single particle, bulk volume refers to the dimensional measurements of such particle (i.e. length x width x depth), also known as geometric volume. The roughness of a particle refers to the space in between the open pores (penetrating in the interior of the particle) and the bulk solution, while the open pores cover three different sizes: macropores (> 50 nm), mesopores (2- 50 nm) and micropores (< 2 nm) (J. Lee et al., 2006). Together with the carbon structure, these volumes account for the envelope density. When the volume of

carbon structure and closed pores is considered, the skeletal density is defined, while if only the carbon volume is considered, the true density of the material is determined. The true density is therefore the highest density, while the bulk density is the lowest one. When reporting current densities then, it should be clear which volume of the carbon particle we are referring to. In this study, we used the bulk density (also referred to as the apparent density) provided by the manufacturer, which is 0.3 g mL^{-1} for PK granules and 0.5 g mL^{-1} for GAC granules. On the contrary, in a previous single granule study the envelope density was used, which was calculated from N_2 adsorption as 1.03 g mL^{-1} for PK and 1.06 g mL^{-1} for GAC (Borsje et al., 2016). However, the maximum pore size included in this calculation was 245.9 nm for PK and 339.3 nm for GAC. Therefore, from an application point of view, it would be more accurate to use the bulk density or instead an envelope density that includes both roughness and bigger pore sizes.

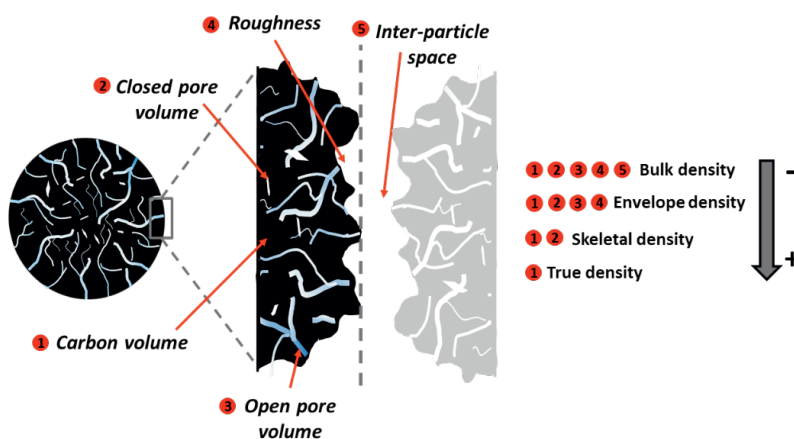


Figure 1. Illustration of the complex structure of AC granule(s) and the possible volumes to consider (1 to 5) in order to calculate their density (Webb, 2001b).

1.1.2. Surface area

Considering which surface area is relevant for assessing the performance of AC granules is also important. As current production relates to microbial activity and bacteria can only colonize the carbon surface (roughness) and pores bigger than their size ($0.5\text{--}1 \mu\text{m}$, as shown in SEM images in Chapter 4), relating it to the outer surface area seemed the most reasonable. The outer surface area (SA) was calculated from the volume by assuming the granules were spherical. Even though a spherical shape seldom corresponds to the real shape of AC granules, in Chapter 3 a linear relation ($R^2 = 0.9$) between the outer SA and the amount of quantified biomass (as total nitrogen) was found. Therefore, as larger surface area benefits bacterial growth, AC granules with high surface-area-to-volume (SA:V) ratio would be beneficial from an application point of view. In this sense, small granules

would be preferable as they have a larger SA:V ratio (as shown in Figure 2) and showed higher volumetric current densities.

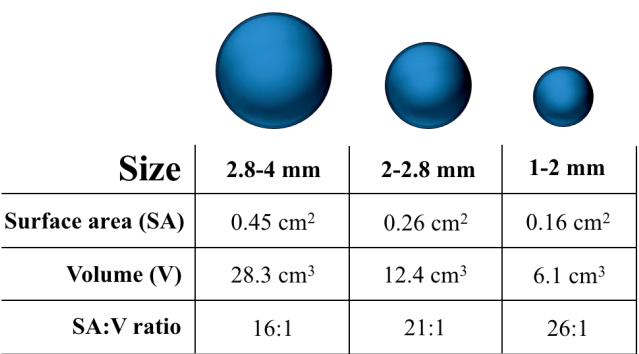


Figure 2. Size range of PK granules used in Chapter 3, with their approximated outer surface area, volume, and surface-area-to-volume ratio values. The smallest the (spherical) granule, the higher the SA:V ratio.

Unlike current production, charge storage should be related to the specific surface area (SSA) of AC granules, as it represents the available internal area for ion adsorption and hence the support for EDL formation. In a previous study, the SSA of PK and GAC granules was determined as 764 m² g⁻¹ and 885 m² g⁻¹, respectively (Borsje et al., 2016). This means GAC granules have 16% more area per granule mass and 20% more area per granule volume than PK granules. The proportion of micropores (< 2 nm) and mesopores (2-50 nm), which are the pores contributing most to the EDL formation (Pandolfo & Hollenkamp, 2006), is 60-40% for PK granules and 80-20% for GAC granules, respectively. Based on granule size, a large variability of charge storage was found mostly on bigger (> 6 mg) granules (see Chapter 3), and no linear correlation was found between charge storage and granule weight (R²=0.3). The reason why bigger granules did not lead to an increased charge storage could relate to that proposed in a previous study (Deeke et al., 2013) for a thick capacitive electrode, i.e. that SSA decreased and internal resistances (due to ion transport) increased compared to a thin capacitive electrode. These results suggest that small granules are thus preferable also for increased volumetric charge storage purposes. Alternatively, the electrochemical performance of a thin capacitive layer (e.g. activated carbon powder) coated on a non-capacitive (granular) carrier could also be studied in the future.

Based on granule types, GAC granules reached higher volumetric charge storage than PK granules due to their higher SSA. However, when normalized to the SSA itself, charge storage was slightly higher for PK granules. This could relate to an increased mesopore proportion, which has proven to facilitate ion transport towards narrower pores and thus enhance EDL formation. Nevertheless, the differences were non-significant between granule types in terms of charge storage, bacterial growth and current production in the multi-anode study performed in Chapter 3, suggesting that granule type (with different

porosity and kind of precursor) were not determinant on the performance of capacitive bioanodes. Materials with more reproducible properties and more uniform pore size and distribution (PSD) (W. Gu & Yushin, 2014; J. Lee et al., 2006) could help in the future to better relate the micro/mesoporosity, total pore volume or SSA to the charge storage or charge/discharge behavior of capacitive electrodes.

1.1.3. Importance of porosity

Non-porous granular carbon, i.e. non-activated graphite granules (GG), was also tested for biofilm growth and current production. The output (Chapter 3) was similar to that found for AC granules in terms of: i) current production; ii) biofilm growth, determined by SEM images (nitrogen analysis was not done); and microbial community, determined by next-generation sequencing (NGS). This means that the porosity of carbon granules did not determine their microbial activity, which probably relates to the fact that biofilm growth occurred under continuous potential control (at -0.35 V vs Ag/AgCl). This means the intermittent operation mode by repetitive charge/discharge cycles was not applied or, in other words, that the storage capacity of granules was not used. The reason for this was that the potentiostat used in this study, i.e. the MultiWE 32 (Ivium Technologies), was only able to control the potential of all bioanodes simultaneously, and not the current. Therefore, charge/discharge cycles could only be applied sequentially one bioanode after the other.

In the introduction (Figure 6), it was shown how the potential behavior of a non-capacitive material differed from that of a capacitive material during charge, which had a larger potential drop within the same time period. Here, Figure 3 illustrates how the charging of PK (capacitive granule) and GG (non-capacitive granule) would occur under open circuit conditions, when electroactive bacteria (EAB) charge the electrode at a certain current. In the case of GG granules, the surface area is relatively small and so there is a small storage capacity, which leads to a large decrease in potential. On the contrary, PK granules have a large surface area that facilitates the distribution of charges and allows for large storage capacity, leading to a lower potential drop than GG granules. Therefore, the charge process depends both on the bacterial activity (current production) and the time. If the time is not limiting or the bacterial activity is high, the use of materials with high capacitance is recommended, as the potential will eventually drop to the equilibrium open cell potential (OCP) and the recovered charge higher. When this time is more limited or the bacterial activity is low, the use of a material with lower capacitance is instead recommended, so the equilibrium potential is reached faster and the driving force is larger when the discharge potential is applied.

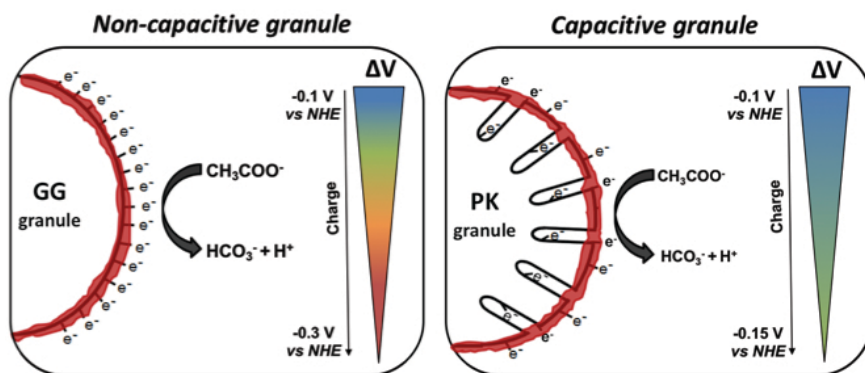


Figure 3. Schematic representation of the surface area in non-capacitive (GG) and capacitive (PK) granules and the respective electron distribution.

Even though electrode porosity did not influence microbial activity under continuous controlled conditions, it is known that capacitive bioanodes perform better than non-capacitive ones under intermittent conditions. In terms of charge storage, a previous study (Borsje et al., 2016) showed a factor 18-times lower charge storage by GG granules compared to AC granules, during a period of 40 charge/discharge cycles. Another study on MFCs with capacitive bioanodes (layer) showed that their increased charge production (53%) over non-capacitive bioanodes was, not only related to the increase in charge storage (35%), but also to the enhanced current production (18%) by the electroactive biofilm. This latter did not occur in this study, which suggests the importance of operation mode when working with capacitive but also with non-capacitive anodes. In line with this, a recent study (X. Zhang et al., 2018) showed that intermittent operation of flat electrodes (glassy carbon) led to an increased current density due to the presence of (3.6 times) more charge carriers within the biofilm. These charge carriers increased the charge storage capacity of the biofilm (pseudocapacitance) and allowed for a faster electron discharge from the biofilm to the electrode. Similarly, the morphology of the biofilm changed and had a mushroom-like structure compared to a flat structure under continuous operation mode. Therefore, for future research the growth of capacitive bioanodes under intermittent conditions is strongly recommended, where the study of current production, biomass quantification, and microbial community determination should be done. Biofilm visualization might also be interesting to study, as it can give information on its distribution and morphology around the AC granules like done in Chapter 4 with MRI. It would also be interesting to see if the (pseudo)capacitance of biofilm increases, since the capacitive would already confer a large surface area and hence a higher number of catalytic sites for electron transfer that do not exist with non-capacitive electrodes.

Apart from porosity, this study showed that other material properties of carbon granules, like electrical conductivity or surface roughness, also did not affect the microbial activity of the different type of bioanodes. In fact, it is known that graphite is a more conductive material than activated carbon (see next section), and the AFM results showed

lower surface roughness for GG granules compared to PK granules. The little differences between carbon granule types is again more likely related to the control of operation mode rather than the similar environmental conditions, i.e. same reactor or same inoculum.

1.1.4. Other material properties and possible electrode modifications

The research direction of carbon-based electrochemical capacitors focuses on materials with high SSA and a rational pore distribution, but also with smaller internal resistances and surface modification (Yong Zhang et al., 2009). Regarding internal resistances, using highly electrically conductive (S m^{-1}) carbon materials is crucial to achieve high power output supercapacitors (Pandolfo & Hollenkamp, 2006). The electrical conductivity will depend on the chemical and structural morphology of the carbon, i.e. the degree of crystallographic orientation. In general, carbon precursors have very high resistivity ($>10^{12} \Omega \text{ cm}$), hence low electrical conductivity, but when they are heat treated (up to 600-700 °C) this resistivity decreases as electrons delocalize and become available as charge carriers. Active carbon has an approximate electrical resistivity of $\sim 0.2 \Omega \text{ cm}$ (calculated at a compaction pressure of 2000 kgf cm^{-2}) (Pandolfo & Hollenkamp, 2006), while graphite has a resistivity of $1.3 \cdot 10^{-3} \Omega \text{ cm}$ and titanium of $42 \cdot 10^{-6} \Omega \text{ cm}$ (J. Wei et al., 2011). As suggested in the previous section, a thin capacitive layer could be coated on a (spherical) carrier, which could actually be a material more conductive than AC, such as graphite or a metallic particle. In this way, the combined effect of a capacitive material (in the outer layer) and a conductive material (in the inner layer) could be investigated, which might benefit both a high charge storage and roughness but also a high electron transfer rate. It is important to realize that, during electrode formation with AC powder, for example, a binder (often polytetrafluoroethylene, PTFE) is also needed, which will add extra electrical resistivity and might also block some pores of the carbon (W. Gu & Yushin, 2014). While resistivity is an intrinsic material property, electrical resistance is linearly related to the path length of electron flow. Therefore, special attention should be paid to the electrode configuration in order to minimize travel distances and so decrease electrode ohmic losses (J. Wei et al., 2011). This can be the case on a granular bed reactor consisting of several layers of carbon particles, where the resistivity might not be dependent of the carbon properties but instead relate to the contact between particles or the particles and the current collector (Pandolfo & Hollenkamp, 2006).

Regarding surface properties, these can modify the electrochemical interfacial state of carbon and its double-layer properties, such as wettability, point of zero charge, adsorption of ions (capacitance) and self-discharge characteristics. Carbon-oxygen complexes are by far the most important surface groups on carbon. If the functional groups are electrochemically inert, they can enhance surface wettability and lead to larger specific capacitance of the carbon due to the improved pore accessibility. However, when they react, they can contribute to self-discharge of the capacitive carbon, as it is the case for

oxygen functional groups that serve as active sites. Therefore, the removal of oxygen from the carbon (e.g. by high temperature treatment) generally improves the stability of capacitive electrodes (Pandolfo & Hollenkamp, 2006). A lot of research has been done on electrode surface modifications not only to increase MFC power output but also to explore on the effect of functional groups on capacitance and on biofilm colonization of the electrode surface (Frackowiak & Béguin, 2001). Generally, the addition of pseudocapacitive materials that undergo quick faradaic reactions increase the energy density of electrochemical supercapacitors. This can be done by adding heteroatoms on the carbon surface (e.g. oxygen, nitrogen), modifying carbon materials with conductive polymers (e.g. aniline, pyrrole) or inserting electroactive particles of transition metal oxides (e.g. RuO_2 , TiO_2 , MnO_2) (Frackowiak & Béguin, 2001; Lota et al., 2009; Yong Zhang et al., 2009). Regarding the interface between biofilms and electrodes, recent research has focused on the treatment or modification of carbon-based materials to increase MFC performance in terms of current density and power output (Chang et al., 2016; J. Wei et al., 2011). For example, it was found that negatively charged groups at the surface (carboxylate) decrease MFC power output while the introduction of positively charged groups (e.g. aryl-amine groups) doubled the power output due to an enhanced biofilm growth (Picot et al., 2011). Biofilm attachment and hence MFC current density and power output were also increased by adding surface functionalities like boronic acids that have high affinity to compounds (lipopolysaccharides) present in the external membrane of known electroactive bacteria (Lapinonnière et al., 2013).

1.2. Interaction between biofilm and AC granules

1.2.1. Techniques to visualize the biofilm

As the electrochemical performance of capacitive electrodes is related to biofilm growth, quantifying the biofilm and determining its distribution can give us valuable information to better understand electrode responses like charge storage or discharge curves. Bacterial growth occurs on the granule surface and within pores that are bigger than their size ($0.5\text{--}1\text{ }\mu\text{m}$) (Bond & Lovley, 2003). Therefore, measurement techniques that focus on the determination of pore sizes similar or bigger than the bacterial cells are recommended to better assess the area available for biofilm growth. Under abiotic conditions, Atomic Force Microscopy (AFM) was used to determine the roughness of the granule surface. However, we did not achieve representative data as only small areas of the granules could be scanned and the measurement probe often broke due to the high roughness of (non-straight) granules. For these reasons, AFM is a challenging technique to use with AC granules, but has been used to characterize flat capacitive electrodes (Deeke et al., 2013). Alternatively, mercury porosimetry (Webb, 2001a) can give information about a big range of pores (diameters from $0.003\text{ }\mu\text{m}$ to $360\text{ }\mu\text{m}$), covering those where bacteria can grow. Therefore, the use of this technique is recommended to get more accurate values of the volume of mesopores and macropores (Pastor-Villegas & Durán-Valle, 2002), as well as

the envelope density of AC granules, although there is still the risk of measuring inter-particle volume. Some research studies have also used SEM together with digital image processing to determine specific morphology parameters (e.g. roughness and porosity, in the meso-/macropore regime) of electrocatalysts (Artyushkova et al., 2012) and carbon electrodes (Santoro et al., 2014).

In this study, more attention was put on techniques that could show the biofilm growth on the electrode, i.e. with biotic samples. To this end, biofilm distribution on AC granules was visualized with magnetic resonance imaging (MRI), which allowed for three-dimensional images of $(28\ \mu\text{m})^3$ resolution. Chapter 4 explains in detail how these measurements were performed and shows the biofilm distribution on the outer surface area of AC granules at different growth stages. MRI was thus proven to successfully determine the biofilm distribution and its volume with the biggest advantage of not destroying the sample. In fact, even though the granular bioanodes were taken outside of the reactor, MRI analyses were done within 24 hours while the biofilm was kept in phosphate saline buffer (PBS). The biofilm could also be quantified by means of nitrogen content after MRI, which shows the advantage of using non-destructive techniques, i.e. that can be complementary to others. Nitrogen content was also quantified for granules that did not undergo MRI measurements, and they obtained a similar value proving that no damage was caused to the biofilm during sample preparation and measurements (see Chapter 4). Potentially, *in situ* measurements could also be done, which have already proven to work on electroactive biofilms (Renslow et al., 2014, 2010). However, there were some aspects that needed further improvement. For example, the resolution used was not high enough to determine the roughness of AC granules and to visualize bacterial growth in the inner macropores. The complex porous structure of AC granules was the main impediment to have voxels of $(28\ \mu\text{m})^3$ completely full of biofilm that could be detected under the settings and image processing here used. For the future, higher resolutions should be foreseen in order to define the exact growth interface of the biofilm and the AC granule, and thus determine the biofilm thickness. Visualizing bacteria inside the pores, up to $1\ \mu\text{m}$ scale, might be a more difficult task, but other techniques like SEM could be used instead to complement the information. *In situ* experiments could also be very useful to, for example, examine the microbial growth on AC granules over time in a fluidized bed reactor.

Table 1 gives an overview of some techniques used to visualize biofilms on electrode surfaces, including MRI, based on the information they could provide on AC granular bioanodes at different levels: visualization, quantification, 3D distribution and invasion level to the sample. Some of them were explored in this project, like scanning electron microscopy (SEM) or confocal laser electron microscopy (CLSM), while others were not, like optical-coherence tomography (OCT) or X-ray tomography (XRT). SEM was used to visualize the biofilm on AC granules in Chapter 3, but the information was qualitative and could not be used to determine the biofilm volume or thickness. To this end, cross-sections were made by cutting frozen granules with the microtome. However, thin slices could not be

done as the carbon was too brittle and broke, so the several slices were removed (~ 0.7 mm) until reaching approximately half-way the granule. SEM images of cross-sections showed that bacteria were also growing on pores located more towards the inside of the granules and not only in the outer layers (see images in Chapter 4). However, the distribution and thickness of the biofilm on the surface of the granule could not be observed as the manipulation of the sample during the cutting process caused significant damage. CLSM was also explored to determine live/dead cells distribution along the biofilm and determine the biofilm thickness of the whole and cross-sectioned AC granules. The main challenge was to deal with the three-dimensional structure and high roughness of AC granules, which made difficult to obtain good quality images. However, it is proven in literature that CLSM works to determine biofilm thickness (Tejedor-Sanz, Ortiz, et al., 2017) and 3D distribution ($\sim 100 \times 150 \mu\text{m}$) of microbial species on granular activated carbon electrodes (particle size: 0.6-1 mm) similar to those used in this study. The main drawback of SEM and CLSM is that they are destructive techniques (e.g. drying or staining is needed) and that only small areas (in the micrometer scale) can be visualized. Some techniques that can overcome these drawbacks, similar to MRI, are OCT and XRT. OCT can be used to scan extended sample areas, in the millimeter scale range, and does not need the addition of any substance. Reconstruction of 3D biofilm distribution has been done on flat surfaces such as electrodes (22.3 cm^2), (Molenaar et al., 2018) carriers (48 mm^2) (Chunyan Li et al., 2016) and glass capillaries (1 mm^2). (Xi et al., 2006) As for XRT, it enables 3D reconstruction of biofilms growing on electrodes, e.g. cathodes (150 mm^2) inserted in a rotating tube (transparent to XRT) (Santini et al., 2015). For the future, these techniques could also show potential to determine the biofilm thickness and give valuable information on the biofilm-AC granule interface. However, they provide less possibilities than MRI; nuclear magnetic resonance (NMR) spectroscopy, with the same working principle as MRI, can also be used to determine useful information on bioanodes such as biofilm composition and molecular mobility (Garny et al., 2010), diffusion coefficients (Yan Zhang et al., 2016) or pore size distribution of mesoporous materials (Aksnes & Kimtysb, 2001).

Table 1. Summary of the techniques that can possibly use to visualize and quantify biofilm growing on AC granules, including on the granule-biofilm interfacial area (i.e. roughness) and macropores (bigger than $1 \mu\text{m}$). In green (✓), the aspects that are possible to investigate and in red (x), the ones that are not.

	Visualize	Quantify	3D distribution	Non-destructive	Roughness	Macropores
SEM	✓	x	x	x	x	✓
CLSM	✓	✓	x	x	x	✓
MRI	✓	✓	✓	✓	✓	x
XRT	✓	✓	✓	✓	✓	x
OCT	✓	✓	✓	✓	✓	x

1.2.2. Biofilm influences capacitance measurements

For electricity storage purposes, the electrode must be operated intermittently, meaning that it should experience a charge process where the electrochemical double layer (EDL) (Jayalakshmi & Balasubramanian, 2008; Kötzt & Carlen, 2000) is formed in the electrode/electrolyte interface, and a discharge process where the stored charge is being released. In the case of a bioanode, the EDL formation (charge) in the porous electrode is a result of the electrons released during a faradaic reaction, i.e. the chemical oxidation of substrate by electroactive biofilms. During discharge under continuous operation mode, the current released by the bioanode will only belong to the faradaic reaction, while under intermittent operation mode the current released will be a combination of faradaic (I_{MFC}) and capacitive (I_{EDL}) currents. Figure 4 illustrates the electron flow (current) during charge/discharge processes on a single AC granule without (abiotic) and with (biotic) biofilm. Under abiotic conditions, with no faradaic current, charge/discharge processes occur by an applied external current. This current (I_{EDL}) only belongs to the stored charge, so it can be directly related to the capacitance of AC granules. Oppositely, under biotic conditions, the faradaic reaction continuously charges the granule, which means during discharge it will be measured together with the stored charge ($I_{MFC} + I_{EDL}$). This current cannot be directly related to the capacitance of AC granules, but instead the apparent capacitance, which will always be higher than the electrode capacitance as explained in Chapter 2.

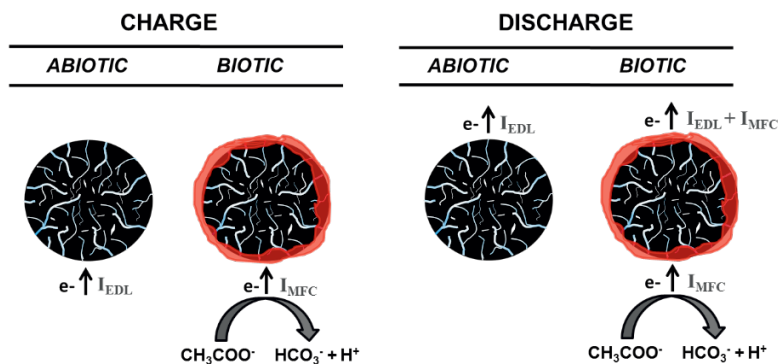


Figure 4. Charge (left) and discharge (right) processes on single AC granules without (abiotic) and with (biotic) biofilm growth. The arrows show the direction of electron flow. Under abiotic conditions, the granule is charged and discharged by an applied external current, while under biotic conditions, the oxidation of acetate charges the granule and a current also needs to be externally applied for discharge.

It is important to understand these electron flows for any electrochemical measurement technique used during charge/discharge cycles, mostly when an electroactive biofilm is present. In Chapter 2, three techniques were presented for the capacitance measurements of single AC granules under abiotic conditions. Here, the same techniques are shown when

biofilm is present at different growth stages: day 0, which serves as a control before bacterial inoculation and days 6, 18 and 35 after bacterial inoculation. The potential values are written vs Ag/AgCl (3M, +205 mV vs NHE), and were set between -0.48V and -0.3V. Figure 5A shows the results for chronopotentiometry (galvanostatic) measurements. The current applied during charge was the same as in abiotic conditions, but was higher during discharge as the I_{MFC} (calculated from the polarization curve of bioanodes at -0.3 V) was also applied. The potential varied faster than under biotic conditions, i.e. 3.7, 3.5 and 2.6 minutes for days 6, 18 and 35. Figure 5B shows the results for chronoamperometry (potentiostatic) measurements. During charge, the current response is similar to that under abiotic conditions, as no I_{MFC} is produced at -0.48 V (the open cell potential, OCP). However, during discharge the current did not decrease to zero as in abiotic conditions but instead reached a steady-state, which was considered to be the I_{MFC} at -0.3 V. Figure 5C shows the results for cyclic voltammetry (CV) measurements. As the same potential range and scan rate (0.3 mV s⁻¹) were applied, the potential response was the same as for abiotic tests. However, the current response was not symmetric as in abiotic conditions, but had a quasi linear response reaching negative values only at the most negative (closer to the OCP) potentials.

Regarding the (apparent) capacitance, it was higher under biotic conditions than under abiotic conditions, as already expected. However, there is a decrease over time of the apparent capacitance, which could be due to the decrease of the I_{MFC} , which was actually measured as 67, 62 and 53 μ A on days 6, 18 and 35, respectively, or due to a decrease of the I_{EDL} itself. This is more likely since, in the chronoamperometry measurements, the decrease of peak-currents was determined as 139 μ A between 0-6 days, 117 μ A between 6-18 days, and 88 μ A between 18-35 days. In Chapter 2 the electrode capacitance showed the largest decrease already at day 6, indicating that bacterial colonization of the carbon surface rather than an increase of biofilm thickness influences it. Two possible reasons are that i) bacterial growth block the pores of the granule, thus decreasing the available surface area for EDL formation (and the storage capacity); and ii) the surface for EDL formation is the same way but the rate at which is formed is limited by an increased ion transport resistance. On the one hand, bacterial growth cannot affect the pores involved on charge storage (< 50 nm) as they are too little for the cells to access, but they could grow on larger pores that are the path for ion transport during EDL formation. On the other hand, electroactive biofilms have shown to be limited in some processes, such as the transport of nutrients, the transport of electron equivalents or the movement of protons and pH-buffering compounds.(Renslow, Babauta, Majors, et al., 2013) In the case of EDL formation, the transport of electron and protons, together with other counterions (Korth et al., 2015; Savéant, 1986), might influence charge storage capacity of the electrode when biofilm is present, even though these effects seem to be more important in on mature biofilms (as consequence of thickness, dead cells) rather than in thin biofilms (Beyenal & Babauta, 2015; Sun et al., 2016). Nevertheless, transport limitations could already be considerable after 6 days of biofilm growth when compared to abiotic conditions. Further

study of the microscopic effects of these processes during EDL formation is recommended. Nuclear magnetic resonance (NMR) has been used to calculate effective diffusion coefficients (D_e) in electroactive biofilms (Renslow, Babauta, Majors, et al., 2013; Renslow et al., 2010), which could be useful to do during *in situ* charge/discharge experiments.

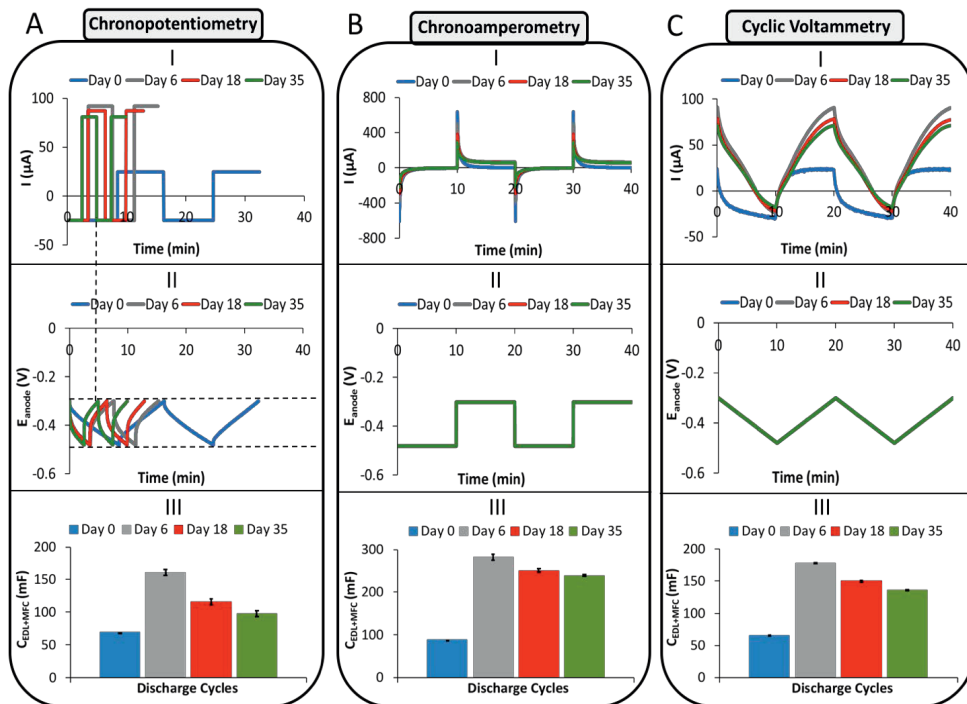


Figure 5. Current (I) and potential (II) responses of a capacitive anode (single AC granule) with biofilm during 2 charge/discharge cycles with different electrochemical techniques: A) Chronopotentiometry; B) Chronoamperometry and C) Cyclic Voltammetry. The horizontal dotted lines mark the potential range at which the measurements were set, while the vertical dotted line points the end of a charge/discharge cycle in both current and potential graphs. The average apparent capacitance (III) of 3 discharge cycles was also calculated.

Regarding the techniques used, the highest capacitance values were achieved with chronoamperometry (potentiostatic) measurements, which applies sudden potential changes and causes current peaks that are several orders higher than the current with the other two techniques. However, chronoamperometry was chosen to determine the charge storage of capacitive bioanodes in this study, since the fixed potential (-0.3 V) during discharge allows the determination of I_{MFC} (faradaic current) as the steady-state current (see Figure 6 in the introduction). In this way, it can be subtracted to the total current and determine the I_{EDL} (capacitive current), as shown in Chapter 2. Whether this is correctly calculated is still not clear. On the one hand, the values of faradaic current are difficult to determine as they depend on the anode potential and even at a constant potential

discharge it could have fluctuated. Therefore, reporting the apparent capacitance could be a safer option than calculating the electrode capacitance under biotic conditions. On the one hand, the values for potential range cannot always be correctly taken. For example, in Chapter 3 the open cell potential (OCP) could not be recorded in the multi-anode MFC. Therefore, charge storage instead of capacitance was reported, which describes the actual charge release by the capacitive bioanodes at a certain potential. Of course, the OCP will largely vary according to bacterial activity and so it is important to keep bacterial growth similar between the capacitive anodes in order to make a more reasonable comparison between them. In fact, it was found that lower charge storage was found for the same type and size of granules that have a lower current production during discharge, although not specific differences could be found on the discharge rate or curve. For the future, impedance electrode microscopy (EIS) could be used to determine not only the capacitance value of AC granules but also information about charge transfer resistance, diffusion resistance and potentially also biofilm/electrode resistances in the capacitive bioanodes. It is a powerful technique that has proven to give valuable information of capacitance in bioanodes, for porous graphite plates (1 mF cm^{-2} at OCP) (Ter Heijne et al., 2015), biofilms ($450 \text{ } \mu\text{F cm}^{-2}$ at -0.35 vs Ag/AgCl), and also the separation between carbon veil (porous) electrode capacitance (0.1 mF cm^{-2} at OCP) and biofilm ($8.2 \text{ } \mu\text{F}$ at -0.30 vs Ag/AgCl) (Fradler et al., 2014). However, the right interpretation of data requires a very good understanding of the electrode-biofilm system.

3. Electrical conductivity of anaerobic granular sludge

3.1. Electron transfer mechanisms

In the introduction, the possible extracellular electrons transfer (EET) mechanisms between microorganisms and an electrode were presented. These EET mechanisms can be direct with cytochromes or nanowires, or can be indirect with a mediator, usually a soluble molecule. another microbial species that can accept those electrons and carry a reduction reaction, instead of the anode or current collector. The formation of aggregates makes the exchange of molecules (i.e. substrate/products) and also electrons between microorganisms feasible (Morita et al., 2011). This way of electron transfer, denominated as interspecies electron transfer (IET), allows for syntrophic interactions between microorganisms and are essential in many processes, in engineered and also natural systems, that require this joint metabolic activity (Cheng Li et al., 2017). The different transfer mechanisms between microorganisms are illustrated in Figure 6. When transfer is indirect, it occurs via soluble molecules like hydrogen, formate or electron shuttles like flavins or humic substances (e.g. quinone moieties). When the transfer is direct, electrons are being transferred in the form of electrical current between donors and acceptors, both on micro but also on centimeter scale, via cytochromes, nanowires or conductive insoluble

materials such as AC granules or iron oxide minerals (e.g. magnetite, hematite) (Holmes & Smith, 2016).

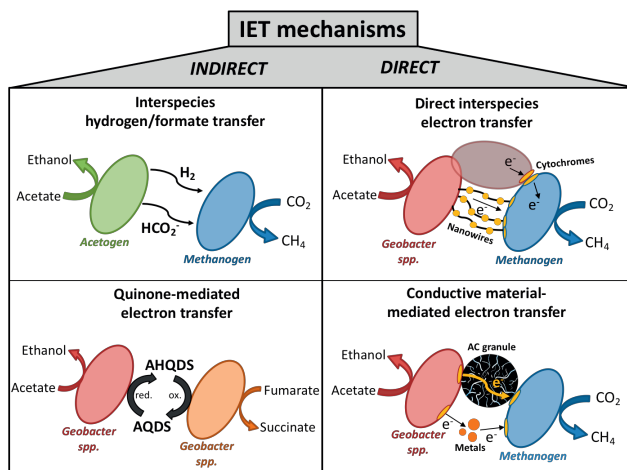


Figure 6. Interspecies electron transfer (IET) mechanisms that are possible on syntrophic partnerships between bacteria and methanogens. Indirect electron transfer (left) is possible via soluble molecules like hydrogen (H_2) or formate (HCO_2^-) and other electron shuttle such as AQDS (AHQDS is its reduced form), a humic acid analogue that stands for anthraquinone-2,6-disulfonate. Direct electron transfer (right) is possible via outer membrane cytochromes, bacterial pili/nanowires (that also have cytochromes) and conductive insoluble materials such as metals or AC granules. Modified from (Holmes & Smith, 2016).

In anaerobic granules, interspecies hydrogen transfer (IHT) is a key process that is essential for the degradation of many compounds (e.g. chlorinated compounds) under anaerobic conditions (Stams et al., 2006). However, the fact that hydrogen concentration was too low to explain certain growth rates of syntrophic partners, opened up the search for other electron transfer mechanisms (Cheng Li et al., 2017). Other indications of direct electron transfer were found in a study of consortia of methane-oxidizing archaea and sulphate reducing bacteria, where the cellular activity was independent of the distance to the bulk solution or of the distance between the electron acceptors and donors. Moreover, diffusivity values were closer to that of electrons rather than intermediates, and a large number of cytochromes were detected on the genomes of methanotrophic archaea (McGlynn et al., 2015). *Geobacter spp.* are commonly known for exchanging electrons with metals and electrodes, but they are also known for syntrophic growth as, for example, in anaerobic treatment of brewery wastewater where most likely they oxidize the ethanol and organic acids (Morita et al., 2011). In fact, the addition of ethanol as electron donor led to higher methane production rates than other electron donors, such as formate and acetate combined, which indicated that IHT or FHT were not the only electron transfer mechanism. The presence of *Methanosaeta spp.* in anaerobic granules can also give an indication of

direct electron transfer as these methanogens can only use acetate as electron donor, and cannot use hydrogen, in which case IHT would be expected. It is not completely clear yet how methanogens can directly accept electrons, but it has been shown that the formation of conductive pili is crucial for electron transfer between a co-culture of *Geobacter metallireducens* and *Methanosaeta barkeri* (Rotaru, Shrestha, Liu, Markovaite, et al., 2014). Similarly, it has been shown that *Methanosaeta harundinacea* was able to accept electrons via DIET for the reduction of CO₂ to CH₄ (Rotaru, Shrestha, Liu, Shrestha, et al., 2014).

The question remains whether direct interspecies electron transfer (DIET) can enhance methanogenic rates over other electron transfer mechanisms. On the one hand, some studies have proven an enhanced DIET in co-cultures with the use of conductive materials, such as carbon cloth (Shanshan Chen, Rotaru, Liu, et al., 2014), biochar (Shanshan Chen, Rotaru, Shrestha, et al., 2014), or activated carbon (F. Liu et al., 2012). On the other hand, the use of conductive materials like magnetite (J. Zhang & Lu, 2016; Zhuang et al., 2015) or activated carbon (J.-Y. Lee et al., 2016; Xu et al., 2015) have shown an enhanced methanogenic activity, which has been linked to the enrichment of microorganisms involved in DIET. Therefore, from these experiments, there is a strong indication that DIET benefits methanogenic rates in anaerobic digesters. Depending on the size and properties of the conductive materials, methanogenesis could be enhanced with different mechanisms; for example, magnetite nanoparticle approach more the role of an outer-membrane cytochrome, while larger carbon material might directly confer electronic connection between syntrophic partners (Cheng Li et al., 2017).

3.2. Measurement of electrical conductivity

3.2.1. Biofilms vs Anaerobic granules

Electrical conductivity of biological samples is a measure of the electron transfer that can potentially occur along that sample. It is a quite a new practice to measure biological conductivity and the methods and conductive mechanisms of microbial samples are still under development and debated (Cheng Li et al., 2017). The measurement of electrical conductivity has been reported in many studies, mostly *in situ* on electroactive biofilms growing on a conductive surface (probe) but also *ex situ* on microbial aggregates like anaerobic granules. When having *in situ* biofilm growth on a probe with conductive surface, the attachment of the biological sample is stronger than when *ex situ* placing and pressing the anaerobic granules against the probe. Additionally, the use of a reference electrode is easier during *in situ* measurements, as there is a better contact with the electrolyte, than when measured *ex situ*. A reference electrode is useful to measure the potential of each electrode on the probe when e.g. cell voltage is being controlled. Nevertheless, *ex situ* measurements of the electrical conductivity of anaerobic granules has proven to be valid and is used in many literature studies (Morita et al., 2011; Summers et al., 2010) and also done in this thesis, as explain in Chapter 5.

Biofilms grown in MFC are known to perform direct electron transfer from the electrolyte to the electrode, and also between microbial cells. Electrical conductivity of biofilms growing in bioanodes have been found to range from $250\ \mu\text{S cm}^{-1}$ to $2.44\ \text{mS cm}^{-1}$. The increase in electrical conductivity of these biofilms, either by enhancing the expression of conductive pili or by adding conductive nanoparticles, has been proven to decrease internal resistances of MFCs and boost their power output, but also to increase the release of protons into the biofilm and thus lower its pH. For anaerobic granular sludge, conductivities between $0.8\ \mu\text{S cm}^{-1}$ to $36.7\ \mu\text{S cm}^{-1}$ have been reported. Differences in conductivity between biofilm and granules might be due to the fact that, biofilms need to make an actual connection to the electrode in order to grow, while this does not happen in anaerobic granules. Even though the presence of *Geobacter* spp. is thought to increase the conductive networks within anaerobic granules (Morita et al., 2011; Shrestha et al., 2014), when the electrical conductivity of sludge is higher than the conductivity measured for pure *Geobacter* aggregates (Summers et al., 2010), it means that other microorganisms are likely to be also involved in DIET. Nevertheless, in Chapter 5, no correlation could be found between microbial species in anaerobic granules and their electrical conductivity. This means that other factors in the full-scale reactors, which we did not analyze, could have triggered the electron transfer in these aggregates.

3.2.2. Probe types and characteristics

A main discussion regarding conductivity measurements is the probe configuration and electrochemical technique. Figure 7 shows the four setups that are most commonly used. The 2-electrode probe, i.e. 2 electrodes separated by one non-conductive gap, is the one used in this thesis. By applying a voltage difference between the two electrodes, the current is measured and from the I-V relation, the conductivity value can be determined. Only when the non-conductive gap is covered by a conductive sample (e.g. granular sludge), the connection between the two electrodes can be made and the electron transfer occurs from one electrode to the other. The 4-electrode probe consists of 4 electrodes with a total of 3 non-conductive gaps. The potential difference (V) is measured between the two-inner electrodes while the potential (V) or current (I) is applied on the outer two electrodes. This configuration is meant to avoid the polarization effect on the electrode, which is the potential change that occurs on the probe-electrolyte interface when a current is applied (Malvankar & Lovley, 2015). These two probe configurations usually have a non-conductive gap of 50-1000 μm and contain a large electrode surface ($\sim 6\text{-}7\ \text{cm}^2$). On the contrary, another type of electrode configuration called interdigitated arrays (IDA), have smaller electrodes (2 mm long, 10 μm wide and 90 nm thick), intercalated one after the other, with non-conductive gaps of 5 μm wide. On the one hand, IDA configuration is reported to cause less signal-to-noise ratios, while on the other hand, biofilm growth is more limited due to a lower ratio between electrode surface and non-conductive gaps. Moreover, the thin non-conductive gap brings to question if the scale is suitable to analyze long-distance electron transfer in biofilms (Malvankar et al., 2016). However, when working with anaerobic

granules this might not be a problem as their size is in the order of hundred micrometers (see SEM images in Chapter 5). Finally, the use of nanoelectrodes is also possible, with even smaller dimensions (10 μm long, 2 μm wide and 30 nm thick), to measure conductivity of smaller microbial aggregates or appendages, such as individual pili. As an example of the importance of the electrode configuration, the conductivity measured for *G. sulfurreducens* biofilms varied from 5 mS cm^{-1} using the 2-electrode probe to 5 $\mu\text{S cm}^{-1}$ using an IDA (Cheng Li et al., 2017). However, no clear explanation for this is available in literature. From our experience with anaerobic granules, when using very small probes (about the size of one granule), the current signal was 1000 times lower than that found with the 2-electrode setup. Therefore, we concluded that more electrode surface is needed to decrease the ambient noise and be able to determine the conductivity of the sample. Nevertheless, for future research it is crucial to better understand the differences between measurement probes and how they influence electrical conductivity values, both for biofilms but also for anaerobic granule sludge, in order to conclude on the principle and applicability of conductive biological samples.

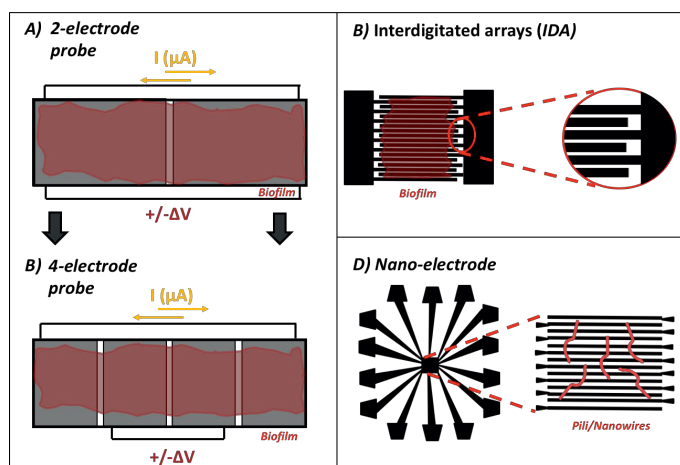


Figure 7. Different probe designs available and tested so far for biofilm, granular aggregates and nanowire conductivity determination. Modified from (Malvankar & Lovley, 2015) and (Cheng Li et al., 2017).

3.2.3. Factors to consider for conductivity measurements

Biological aggregates are very sensitive to external changes (e.g. moisture, temperature) (Phan et al., 2016) and, in order to lower uncertainties on the measurement current, it is important to maintain samples under optimum and constant conditions. In this thesis, all the granules were treated in a similar manner, the probe used was always the same and the thickness of the aggregates' layer was kept similar. Moreover, the ohmic resistance between the gold electrode and the current collector was always measured prior to I-V tests and maintained lower than 1.5 Ω . Granules were always placed fresh on the probe,

meaning they were in contact with their media during conductivity measurements. In addition to the results presented in Chapter 5, we investigated the effect of biological activity on conductivity. Two types of anaerobic granular sludge were sterilized via exposure to elevated temperature and pressure in an autoclave. This process caused a 10-fold decrease of their electrical conductivity, which indicates that conductivity is related to biological components (e.g. proteins) or inorganic matter (e.g. recrystallization of precipitates (Demopoulos, 2009)). Similarly, it was found that, disintegrating the physical structure of sludge by vigorously pressing the granules, led to a considerable decrease (60 to 80%) of their electrical conductivity. This means that physical structure should be maintained, for example to not disturb the interaction between closely placed redox-active proteins or nanowires that may play a role in electric conductivity.

Another important matter to consider is the possible interfering currents that might affect (overestimate) electrical conductivity measurements. These currents could relate to pseudocapacitive charging processes, redox reactions or the diffusion of counterions. The use of inert materials as the electrode, such as platinum or gold, is therefore recommended to prevent oxidation or reduction reactions related to the electrode. In addition, it is important to measure conductivity under steady-state conditions and not under transient conditions (e.g. cyclic voltammetry). That is why the use of long potential steps (in our case, 100 seconds) is necessary, as done in this thesis. The use of EIS, which applies alternating current (AC) instead of direct current (DC) like chronoamperometry, could give more insight on the intrinsic electrical conductivity of biological samples, as it can be used to determine interfering currents like capacitive currents of the electrode (EDL formation) or currents from ionic diffusion. The effect of ion diffusion was not identified completely in this study, as media also showed a current under the influence of an electric field (potential difference). Ionic conductivity relates to the diffusivity of ions, which can translate into a time-dependent current (polarization) that, after a certain time, reaches equilibrium. By applying long enough voltage levels, as done in Chapter 5, this transient signal should disappear and the measured conductivity should be only electronic (Malvankar & Lovley, 2015). However, even after 100 s of duration for each voltage step, there was still some current measured for medium alone, without conductive granules. This led to calculated electrical conductivity values of media in the same range as some anaerobic granules, although this was not the case for the most conductive ones. Figure 8 (left) shows ionic conductivity values typically found on wastewater, a 50 mM phosphate buffer prepared in the lab, and three samples of combined media and granules used in this thesis. Values ranged from 1.3 to 13.8 mS cm⁻¹. On the right hand, electrical conductivity values of the same media and granules separately can be seen, ranging from 1 to 171 μS cm⁻¹ as measured with the conductivity probe. These are somewhat lower than typical values of electrical conductivity for anodic biofilms (600 μS cm⁻¹) and redox polymers (1000 μS cm⁻¹), but the reason for their electric conductivity needs to be better understood.

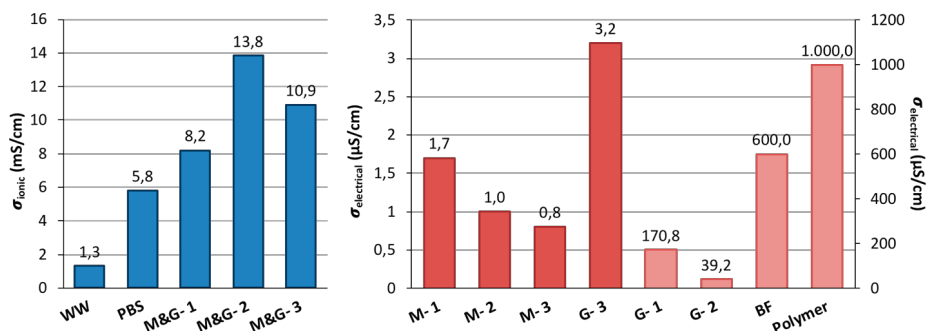


Figure 8. Ionic conductivity (left, in mS cm^{-1}) and electrical conductivity (right, in $\mu\text{S cm}^{-1}$) of some of the samples in this study and some other from literature, like wastewater and polymer.

3.2.4. Other aspects of electrical conductivity

In MFCs special attention has been put to *strong* electroactive microorganisms (electricigens), which can efficiently convert organic matter into electricity. However, there are many other microorganisms (e.g. *Pseudomonas aeruginosa*, *Bacillus*, other gram-positives) that are not as efficient in electron transport, known in literature as *weak* electricigens, that preferably respire with soluble electron acceptors but can adapt their metabolism and use insoluble (or solid) electron acceptors instead under stressful situations – whereas non-electricigens cannot respire without a soluble electron acceptor. As an example, while *Geobacter* is a strict anaerobe, *Shewanella* is a facultative anaerobe and that is why it generally has a 10-fold lower current production (Doyle & Marsili, 2018). It is important to consider this kind of metabolic differences when interpreting electrical conductivity values on e.g. anaerobic granular sludge. The role of weak electricigens in mixed microbial communities can be important and they have different roles such as being oxygen scavengers, degrading complex substrates so strong electricigens can oxidize them further, or performing reactions for bioelectrosynthesis on the cathode. Therefore, investigating electron transfer mechanisms of weak electricigens can be as important to gain knowledge on the possible triggering factors for electroactivity, which rather than an energy generation mode, it can serve as a microbial selection advantage under certain environmental conditions (Koch & Harnisch, 2016).

Nevertheless, elucidating the nature of electrical conductivity is still a challenge, as the microbial aggregates include a mixture of cells, biopolymers, redox proteins and other components in the extracellular matrix. (Phan et al., 2016) For example, there is a big debate on the direct electron transfer mechanisms along biofilms, with two main types been discussed in literature: redox conductivity (similar to redox polymers) and metallic-like conductivity (similar to semiconductors). (Lovley, 2012a) The former one relates to redox-active proteins like cytochromes that undergo an electron transfer mechanism denominated electron-hopping or tunneling, (Lovley, 2012b) while the latter one is based on the delocalization of electrons that are typical in biological nanowires. (Malvankar &

Lovley, 2012) Each of them has a different response towards external conditions such as the pH, temperature or redox potential, as shown in several studies (Malvankar & Lovley, 2012; Yates et al., 2016). Understanding the conductivity of microbial aggregates can help to improve engineered systems, such as anaerobic digestors, and to discover new forms of microbial interactions that might serve as inspiration for the manufacturing of conductive materials. However, further research is still needed in order to use the full potential of electron transfer by biological aggregates.

4. Outlook

With an increased use of renewable and sustainable energy sources, an urgent need for power storage devices have arisen due to their non-constant power generation. Storage devices are already available for large-scale applications, among which double-layer capacitors (EDLCs) have shown special potential for powering portable electronics and the electrification of the transportation sector (Jilei Liu et al., 2018). EDLCs confer features intermediate between batteries and conventional capacitors; they can provide 10-100 times higher energy density (Wh kg^{-1}) than conventional capacitors, and >10 times higher power density (W kg^{-1}) and longer lifetime of charge-discharge cycles ($> 10^6$ cycles) than batteries (Emmenegger et al., 2003; Yong Zhang et al., 2009). In the case of MFCs, the use of EDLCs allow for energy storage, which can be delivered intermittently at a higher power density. Chapter 2 shows an overview of the approximate number of research studies that use MFCs in combination with external capacitors (~ 136) and internal capacitors (~ 66). In the latter case, capacitive materials can be integrated within the MFC and similarly serve as electrode for bacterial growth. The increased capacitance of electrodes has shown to boost the overall performance of MFCs in terms of microbial attachment to the electrode, total produced charge and the increase of current and power densities (W. Chen et al., 2018; Houghton et al., 2016; Peng et al., 2012). The commercially available EDLCs usually have a capacitance in the order of Farads (50-7000 F) (Yassine & Fabris, 2017) that would require recharging times in the order of several minutes to hours at the low current regimes of MFCs (order of μA). These long open circuit periods might not always be desirable by MFCs, thus deciding upon the size of the capacitor is a crucial design point (Santoro et al., 2015). Table 2 shows some values of capacitance and BET surface area for carbon materials used in MFC studies, together with some others from the field of EDLCs and capacitive deionization (CDI). The reported capacitance values are several orders of magnitude different among each other, even though the BET area is in the same order of magnitude, which shows the variability found in literature. This can be caused by the complex carbon properties other than the BET surface area (e.g. porosity, surface functional groups), the electrolyte composition (in this case all aqueous) or the electrochemical technique used to determine it, as previously mentioned in this thesis. Capacitance values of electrodes are normally obtained under static conditions, i.e. with constant contact to the current collector, and without the presence of biofilm. In MFCs,

there are some studies reporting the apparent capacitance of capacitive electrodes (Santoro et al., 2019) or not reporting it at all (Deeke et al., 2012; Liang et al., 2017; Tejedor-Sanz, Quejigo, et al., 2017).

Table 2. Capacitance values of different carbon-based materials with certain Brunauer–Emmett–Teller (BET) surface area under aqueous electrolytes.

Electrode material	Capacitance ($\mu\text{F cm}^{-2}$)	BET surface area ($\text{m}^2 \text{g}^{-1}$)	Electrolyte	Application field	Source
Activated carbon granule	9.2	764	50 mM PBS	MFC	This study
Plain activated carbon	$1.6 \cdot 10^6$	542	50 mM PBS	MFC	(Peng et al., 2013)
Carbon black	$0.5 \cdot 10^6$	213	50 mM PBS	MFC	(Peng et al., 2013)
Carbon brush	$46 \cdot 10^3^*$	-	50% buffer solution [†]	MFC	(Houghton et al., 2016)
Graphite plate	$1 \cdot 10^3^*$	-	20 mM PBS	MFC	(Ter Heijne et al., 2015)
3D-graphene nanosheets	$13 \cdot 10^{-3}$	300-400	Buffer solution [†]	MFC	(Santoro, Kodali, et al., 2017)
Activated carbon	12.6	1072	1 M H_2SO_4	EDLC	(Gryglewicz et al., 2005)
Graphite cloth	10.7	630	10% NaCl	EDLC	(Pandolfo & Hollenkamp, 2006)
Activated carbon cloth	12.2	778	0.1 M [‡]	CDI	(Han et al., 2014)

*Electrode projected surface area

[†]Mixture of stock solutions (0.1M) of LiCl, NaCl, KCl, NaBr and NaNO_3

[‡]0.1 M Potassium phosphate buffer and 0.1M KCl

PBS= Phosphate Buffered Saline

The use of electrode capacitance in MFCs is only possible under intermittent operation mode, as the faradaic current charges the electrode at open circuit, while discharging it when connected to an external circuit. A crucial aspect to consider and studied in Chapter 3 is the duration of charge/discharge cycles. Figure 9 is an illustration of current production over time at continuous operation mode, i.e. when the faradaic current is continuously released, and at intermittent mode (with two different charge/discharge cycle duration), i.e. when no current is released during charge and both the capacitive (I_{EDL}) and faradaic (I_{MFC}) currents are released during discharge. We found that longer charging and discharging times benefitted the value of stored charge (resulting from I_{EDL}), even though only longer discharging times benefitted the value of total produced charge ($I_{\text{EDL}} + I_{\text{MFC}}$). As for the contribution of stored charge to the total produced charge, this was only benefitted by shorter discharging times, which is expected due to a decreased contribution of the I_{MFC} .

These results suggest that: i) the contribution of I_{EDL} is only valuable at short discharging times (2 minutes); and ii) I_{MFC} is more determinant than I_{EDL} for the overall performance of capacitive bioanodes, as even at the shortest discharging times it accounted for 70% of the total produced charge. Nevertheless, I_{EDL} could become more determinant for even shorter discharging times, where the contribution of I_{MFC} further decreases, or for a less well-developed biofilm, where bacterial activity (I_{MFC}) is more limited. A previous study (Deeke et al., 2012) compared the total cumulative charge (result of 15 cycles) for different charging (5-60 minutes) and discharging (10-120 minutes) times. It was concluded that the discharging process was more limiting than the charging process, as longer discharging times increased the cumulative charge produced while longer charging times did not. These results are similar to those found in this study; if we would calculate the cumulative charge of 15 cycles for 5-10 minutes and 5-15 minutes charging/discharging times, respectively, the charge would increase from 1023 mC to 1857 mC. Here, this increase is not attributed to a limited release of the stored charge, but to a larger contribution of the I_{MFC} , as already explained. Nevertheless, the electrode properties (e.g. volume, conductivity, capacitance) should be always considered when concluding on the effect of charge/discharge times, as for example, a thicker or a less conductive electrode might need more time to release the stored charge (Deeke et al., 2013; Hong et al., 2014b).

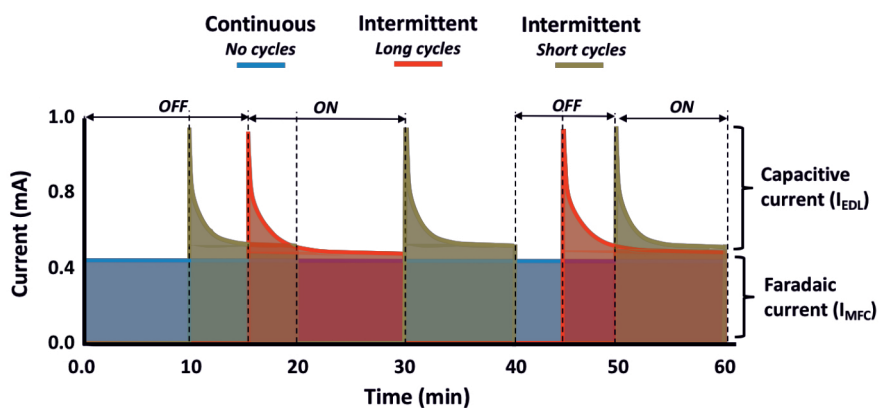


Figure 9. Current production at continuous operation mode (blue), related to the faradaic current (I_{MFC}) and at intermittent operation mode, which short (yellow) and long (red) cycles, related to the sum of faradaic current (I_{MFC}) and capacitive current (I_{EDL}).

The increased charge release during intermittent operation mode is undeniable, as the current is released at a higher rate (for short periods) compared to a continuous energy harvest (Deeke et al., 2015; A Dewan et al., 2009). However, the intermittent operation mode needs open circuit periods where there is no current production, so its overall performance should be compared to that under continuous operation mode (with no “off” period). There is a concept defined in literature that helps on this comparison, called charge recovery (η_{rec}). As shown in Eq. 1, this is the charge produced by a capacitive electrode

under intermittent operation mode (Q_{int}), with n charge/discharge cycles, normalized to the charge produced by a non-capacitive electrode under continuous conditions operation mode (Q_{cont}). When $\eta_{rec} > 1$, the intermittent mode performs better, while when $\eta_{rec} < 1$, the continuous mode is preferable.

$$\eta_{rec} = \frac{\sum Q_{int}}{n Q_{cont}} \quad (1)$$

Previous single granule study showed that AC granules accumulated 20-100% more charge under intermittent conditions than non-activated (GG) granules under continuous conditions, unlike the GG granules themselves under the two different conditions (Borsje et al., 2016). This suggests that, the lack of current production during open circuit conditions, is compensated with the high-peak current production during discharge in the case of AC granules, but not in GG granules. The same results were achieved by another study with capacitive and non-capacitive electrodes, which calculated the cumulative produced charge for 15 charge/discharge cycles (Deeke et al., 2012). The increase of cumulative charge by capacitive electrodes was not only related to an increased charge storage (35%), but also to an increased faradaic current (18%) compared to non-capacitive electrodes. In this thesis, we also calculated the total cumulative charge of PK granules for 15 cycles based on the study of different charge/discharge times. Q_{int} was the total produced charge at each discharge time, while Q_{cont} was the charge produced by the same PK granules at continuous operation mode, considering the steady-state current after 15 minutes of discharge. Therefore, we did not use non-capacitive granules from another reactor for normalization, but assumed to be a fair comparison as no effect of electrode porosity was seen in current production (section 1.1.3.). The values of η_{rec} can be seen in Table 3, for only the discharge process (left) and for the full charge/discharge cycle (right). From these values we conclude that only in the former case is better to operate the granules intermittently, as the cumulative charge increases 15 to 58% over continuous operation mode.

Table 3. η_{rec} of small PK granules for the discharge (left) and full charge/discharge (right) cycles.

η_{rec} [Discharge]		Discharge time (min)				η_{rec} [Full Cycle]		Discharge time (min)			
Charge time (min)		2	5	10	15	Charge time (min)		2	5	10	15
	2	1.47	1.25	1.15			2	0.73	0.89		
	5	1.49	1.33	1.21	1.15		5	0.43	0.67	0.81	0.86
	10	1.58	1.34	1.18	1.12		10	0.26	0.45	0.59	0.67
	15		1.39	1.24	1.18		15		0.35	0.49	0.59

In terms of current production, in Chapter 2 the performance of some fluidized bed reactors was shown under intermittent operation mode, which achieved maximum current densities ranging from 0.0036 mA cm³ at -0.3 vs Ag/AgCl (Deeke et al., 2015), to 0.2 at

+0.2 vs Ag/AgCl (Tejedor-Sanz, Ortiz, et al., 2017). These current densities are 100 to 10000 times lower than those achieved in this study under continuous mode (26.8 – 44 mA cm³) and intermittent mode (84.1 – 173.1 mA cm³) at -0.3 vs Ag/AgCl. These increased current densities, also shown in previous single granule study (Borsje et al., 2016), are attributed to an optimum contact to the current collector, better flow (hydrodynamic) conditions and less biofilm damage than in up-scaled reactors. Figure 10 gives an overview of the different reactor types described in literature that use carbon granules, from left to right: 1) fixed or packed bed reactor, where (graphite) granules are immobilized and filling the whole anode compartment (Rabaey et al., 2005; Tran et al., 2010); 2) a cell where AC granules are mobilized (optional) by stirring and intermittently contacting the current collector (Jia Liu, Zhang, He, Zhang, et al., 2014); 3) a fluidized bed reactor where AC granules are being fluidized with gas and intermittently contacting the current collector (J. Li et al., 2014; Jia Liu, Zhang, He, Yang, et al., 2014; Tejedor-Sanz, Ortiz, et al., 2017; Tejedor-Sanz, Quejigo, et al., 2017; X. Wang et al., 2014); and 4) a fluidized bed reactor with AC granules that are recirculated to a smaller cell where they get in contact with the anode electrode (Deeke et al., 2015). In the case of fixed beds, the contact with the current collector is constant, although not ideal due to the resistances between granules. The operation mode here is optional, unlike in the other examples where the contact of AC granules to the current collector is intermittent. Nevertheless, it is important to realize that, even at intermittent energy harvest, the current production can result stable as different AC granules might be always contacting the current collector. The granule mass and flow rate to use will be crucial parameters to consider, which have shown to increase the current density in previous studies (Deeke et al., 2015; Jia Liu, Zhang, He, Yang, et al., 2014; Jia Liu, Zhang, He, Zhang, et al., 2014). An optimized use of capacitive bioanodes, i.e. at their maximum (peak) current density, will lead to higher volumetric current outputs that can eventually translate into less electrode mass needed, hence a more economically feasible reactor. In Chapter 3, we concluded that the shortest charge and discharge times (2 minutes) should be combined to use the maximum potential of charge storage in AC granules. This information could be used to decide upon operational conditions such fluidization or recirculation velocities in up-scaled reactors. However, it is important to point out that, because of the constant movement of AC granules, electroactive biofilm might undergo a selective pressure in terms of e.g. biofilm thickness, microbial population and activity, that do not suffer under static conditions (this study). Particularly when the granules are in contact with each other and touch the current collector, the biofilm might get damaged and detached. Due to these shear forces, granules could erode and have a smoother surface, and bacteria might only grow in the inner mesopores in order to get protected from the outside, or could use more substrate for growth instead of for electricity production. Even though it is difficult to translate single granule performance to up-scaled reactors, this study can give valuable information about the potential of AC granules in MFCs: it shows the maximum performance such systems could achieve when conditions are ideal.

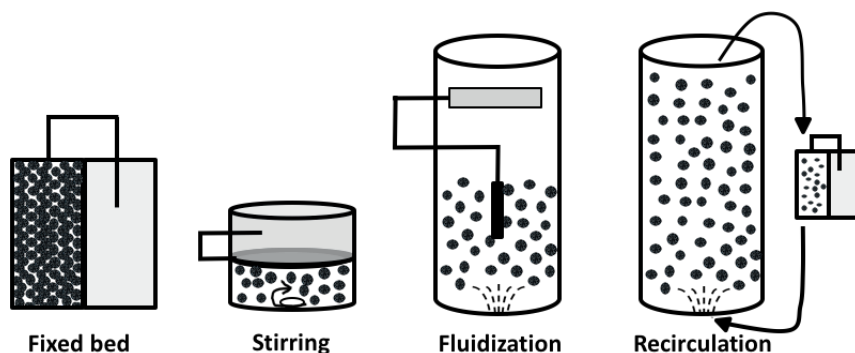
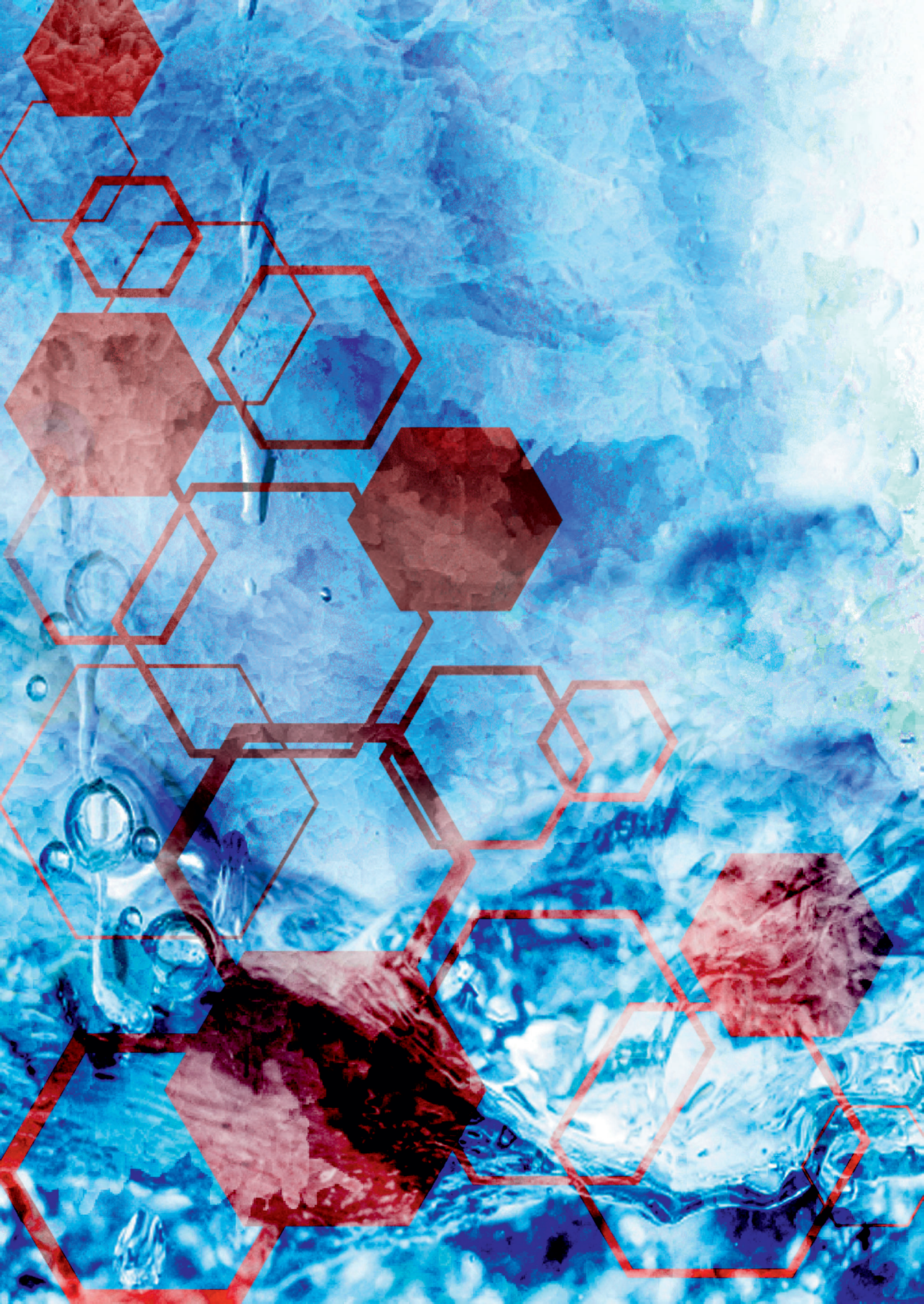


Figure 10. Different set-up configurations of reactors using AC granules as bioanodes. From left to right: fixed or static reactors (Rabaey et al., 2005; Tran et al., 2010), stirring reactors (Jia Liu, Zhang, He, Zhang, et al., 2014), fluidized reactors without (J. Li et al., 2014; Jia Liu, Zhang, He, Yang, et al., 2014; Tejedor-Sanz, Ortiz, et al., 2017; Tejedor-Sanz, Quejigo, et al., 2017; X. Wang et al., 2014) and with recirculation (Deeke et al., 2015).

In order to make MFCs a competitive technology for wastewater treatment, together with high current densities and power output, a high removal efficiency of organics is needed. To this end, understanding the growth kinetics and electron transfer mechanisms among microorganisms and their competitive metabolisms is of importance. However, an engineering approach of the system might be even more valuable in order to bring MFCs to application, such as investigating reactor designs or electrode materials. For example, the use of three-dimensional electrode has shown to be crucial to increase bacterial growth and activity. Moreover, the use of fluidized bed reactors has shown to decrease internal resistances of the system when scaling up, compared to fixed bed reactors. In this context, granular activated carbon can play an important role on new MFC designs for wastewater treatment. For the future, expanding the research on bioelectrochemical systems beyond electricity production is needed to find smart niches where this technology can provide added value and be situated within a sustainable concept.



References



A

- Aelterman, P., Rabaey, K., Clauwaert, P., & Verstraete, W. (2006). Microbial fuel cells for wastewater treatment. *Water Science & Technology*, 54(8), 9.
<https://doi.org/10.2166/wst.2006.702>
- Aelterman, Peter, Rabaey, K., Pham, H. T., Boon, N., & Verstraete, W. (2006). Continuous electricity generation at high voltages and currents using stacked microbial fuel cells. *Environmental Science and Technology*, 40(10), 3388–3394.
<https://doi.org/10.1021/es0525511>
- Aelterman, Peter, Versichele, M., Marzorati, M., Boon, N., & Verstraete, W. (2008). Loading rate and external resistance control the electricity generation of microbial fuel cells with different three-dimensional anodes. *Bioresource Technology*, 99(18), 8895–8902. <https://doi.org/10.1016/j.biortech.2008.04.061>
- Agnès, C., Holzinger, M., Le Goff, A., Reuillard, B., Elouarzaki, K., Tingry, S., & Cosnier, S. (2014). Supercapacitor/biofuel cell hybrids based on wired enzymes on carbon nanotube matrices: autonomous reloading after high power pulses in neutral buffered glucose solutions. *Energy Environ. Sci.*, 7(6), 1884–1888.
<https://doi.org/10.1039/C3EE43986K>
- Aksnes, D. W., & Kintysb, L. (2001). Pore size distribution in mesoporous materials as studied by 1H NMR, 3203–3207. <https://doi.org/10.1039/b103228n>
- Alaraj, M., Ren, Z. J., & Park, J. Do. (2014). Microbial fuel cell energy harvesting using synchronous flyback converter. *Journal of Power Sources*, 247, 636–642.
<https://doi.org/10.1016/j.jpowsour.2013.09.017>
- Almuktar, S. A. A. N., Abed, S. N., & Scholz, M. (2018). Wetlands for wastewater treatment and subsequent recycling of treated effluent: a review. *Environmental Science and Pollution Research*, 25, 23595–23623.
<https://doi.org/10.1007/s11356-018-2629-3>
- Andoni, M., Robu, V., Flynn, D., Abram, S., Geach, D., Jenkins, D., ... Peacock, A. (2019). Blockchain technology in the energy sector: A systematic review of challenges and opportunities. *Renewable and Sustainable Energy Reviews*, 100, 143–174.
<https://doi.org/10.1016/J.RSER.2018.10.014>
- Angenent, L. T., Karim, K., Al-Dahhan, M. H., Wrenn, B. A., & Domínguez-Espinosa, R. (2004). Production of bioenergy and biochemicals from industrial and agricultural wastewater. *Trends in Biotechnology*, 22(9), 477–485.
<https://doi.org/10.1016/j.tibtech.2004.07.001>
- Angenent, L. T., Sung, S., & Raskin, L. (2004). Formation of granules and Methanosaeta fibres in an anaerobic migrating blanket reactor (AMBR). *Environmental Microbiology*, 6(4), 315–322. <https://doi.org/10.1111/j.1462-2920.2004.00597.x>
- Ansari, S. A., Parveen, N., Han, T. H., Ansari, M. O., & Cho, M. H. (2016). Fibrous polyaniline@manganese oxide nanocomposites as supercapacitor electrode materials and cathode catalysts for improved power production in microbial fuel

- cells. *Phys. Chem. Chem. Phys.*, 18, 9053. <https://doi.org/10.1039/c6cp00159a>
- Arends, J. B. A., & Verstraete, W. (2012). 100 years of microbial electricity production: Three concepts for the future. *Microbial Biotechnology*, 5(3), 333–346. <https://doi.org/10.1111/j.1751-7915.2011.00302.x>
- Arias-Thode, Y. M., Hsu, L., Anderson, G., Babauta, J., Fransham, R., Obratsova, A., ... Chadwick, D. B. (2017). Demonstration of the SeptiStrand benthic microbial fuel cell powering a magnetometer for ship detection. *Journal of Power Sources*, 356, 419–429. <https://doi.org/10.1016/j.jpowsour.2017.03.045>
- Artyushkova, K., Pylypenko, S., Dowlapalli, M., & Atanassov, P. (2012). Use of digital image processing of microscopic images and multivariate analysis for quantitative correlation of morphology, activity and durability of electrocatalysts. *RSC Advances*, 2(10), 4304. <https://doi.org/10.1039/c2ra00574c>

B

- Babauta, J. T., Kerber, M., Hsu, L., Phipps, A., Chadwick, D. B., & Arias-Thode, Y. M. (2018). Scaling up benthic microbial fuel cells using flyback converters. *Journal of Power Sources*, 395(November 2017), 98–105. <https://doi.org/10.1016/j.jpowsour.2018.05.042>
- Baek, G., Kim, J., & Lee, C. (2016). A long-term study on the effect of magnetite supplementation in continuous anaerobic digestion of dairy effluent - Enhancement in process performance and stability. *Bioresource Technology*, 222, 344–354. <https://doi.org/10.1016/j.biortech.2016.10.019>
- Bard, A. J., & Faulkner, L. R. (2001). *Fundamentals and Applications. Electrochemical methods* (Vol. 2). John Wiley & Sons.
- Bartacek, J., Vergeldt, F. J., Maca, J., Gerkema, E., Van As, H., & Lens, P. N. L. (2016). Iron, Cobalt, and Gadolinium Transport in Methanogenic Granules Measured by 3D Magnetic Resonance Imaging. *Frontiers in Environmental Science*, 4(March), 13. <https://doi.org/10.3389/fenvs.2016.00013>
- Béguin, F., Presser, V., Balducci, A., & Frackowiak, E. (2014). Carbons and Electrolytes for Advanced Supercapacitors. *Advanced Materials*, 26(14), 2219–2251. <https://doi.org/10.1002/adma.201304137>
- Behrends, T., & Cappellen, van P. (2007). Transformation of hematite into magnetite during dissimilatory iron reduction - Conditions and mechanisms. *Geomicrobiology Journal*, 24(5), 403–416. <https://doi.org/10.1080/01490450701436497>
- Belton, P. S., & Ratcliffe, R. G. (1985). NMR and compartmentation in biological tissues. *Progress in Nuclear Magnetic Resonance Spectroscopy*, 17(C), 241–279. [https://doi.org/10.1016/0079-6565\(85\)80010-8](https://doi.org/10.1016/0079-6565(85)80010-8)
- Beyenal, H., & Babauta, J. T. (2015). *Biofilms in bioelectrochemical systems: From Laboratory Practice to Data Interpretation*.
- Beyenal, H., Lewandowski, Z., & Harkin, G. (2004). Quantifying Biofilm Structure: Facts and Fiction. *Biofouling*, 20(1), 1–23.

<https://doi.org/10.1080/0892701042000191628>

- Blanchet, E., Erable, B., De Solan, M. L., & Bergel, A. (2016). Two-dimensional carbon cloth and three-dimensional carbon felt perform similarly to form bioanode fed with food waste. *Electrochemistry Communications*, 66, 38–41.
<https://doi.org/10.1016/j.elecom.2016.02.017>
- Bond, D. R., & Lovley, D. R. (2003). Electricity Production by *Geobacter sulfurreducens* Attached to Electrodes. *Applied and Environmental Microbiology*, 69(3), 1548–1555. <https://doi.org/10.1128/AEM.69.3.1548>
- Borole, A. P., Hamilton, C. Y., Vishnivetskaya, T., Leak, D., & Andras, C. (2009). Improving power production in acetate-fed microbial fuel cells via enrichment of exoelectrogenic organisms in flow-through systems. *Biochemical Engineering Journal*, 48(1), 71–80. <https://doi.org/10.1016/j.bej.2009.08.008>
- Borsje, C., Liu, D., Buisman, C. J. N., & Heijne, A. (2016). Supporting Information: Performance of Single Carbon Granules As Perspective for Larger Scale Capacitive Bioanodes. *Journal of Power Sources*, 325, 690–696.
<https://doi.org/10.1016/j.jpowsour.2016.06.092>
- Boyd, D. A., Snider, R. M., Erickson, J. S., Roy, J. N., Strycharz-Glaven, S. M., & Tender, L. M. (2015). Theory of Redox Conduction and the Measurement of Electron Transport Rates Through Electrochemically Active Biofilms. *Biofilms in Bioelectrochemical Systems: From Laboratory Practice to Data Interpretation*, 177–210.
<https://doi.org/10.1002/9781119097426.ch6>
- Brousse, T., Bélanger, D., & Long, J. W. (2015). To Be or Not To Be Pseudocapacitive? *Journal of The Electrochemical Society*, 162(5), A5185–A5189.
<https://doi.org/10.1149/2.0201505jes>
- Busalmen, J. P., Esteve-Núñez, A., Berná, A., & Feliu, J. M. (2008). C-Type Cytochromes Wire Electricity-Producing Bacteria to Electrodes. *Angewandte Chemie*, 120(26), 4952–4955. <https://doi.org/10.1002/ange.200801310>

C

- Call, D., & Logan, B. E. (2008). Hydrogen Production in a Single Chamber Microbial Electrolysis Cell Lacking a Membrane. *Environmental Science and Technology*, 42(9), 3401–3406. <https://doi.org/10.1021/es8001822>
- Candelaria, S. L., Shao, Y., Zhou, W., Li, X., Xiao, J., Zhang, J. G., ... Cao, G. (2012). Nanostructured carbon for energy storage and conversion. *Nano Energy*, 1(2), 195–220. <https://doi.org/10.1016/j.nanoen.2011.11.006>
- Chang, S.-H., Liou, J.-S., Liu, J.-L., Chiu, Y.-F., Xu, C.-H., Chen, B.-Y., & Chen, J.-Z. (2016). Feasibility study of surface-modified carbon cloth electrodes using atmospheric pressure plasma jets for microbial fuel cells.
<https://doi.org/10.1016/j.jpowsour.2016.10.058>
- Chen, Shanshan, Rotaru, A.-E., Liu, F., Philips, J., Woodard, T. L., Nevin, K. P., & Lovley, D. R. (2014). Carbon cloth stimulates direct interspecies electron transfer in syntrophic

- co-cultures. *Bioresource Technology*, 173, 82–86.
<https://doi.org/10.1016/j.biortech.2014.09.009>
- Chen, Shanshan, Rotaru, A.-E., Shrestha, P. M., Malvankar, N. S., Liu, F., Fan, W., ... Lovley, D. R. (2014). Promoting interspecies electron transfer with biochar. *Scientific Reports*, 4(1), 5019. <https://doi.org/10.1038/srep05019>
- Chen, Shuiliang, Patil, S. A., Brown, R. K., & Schröder, U. (2019). Strategies for optimizing the power output of microbial fuel cells: Transitioning from fundamental studies to practical implementation. *Applied Energy*, 233–234, 15–28.
<https://doi.org/10.1016/j.apenergy.2018.10.015>
- Chen, W., Liu, Z., Hou, J., Zhou, Y., Lou, X., & Li, Y. (2018). Enhancing performance of microbial fuel cells by using novel double-layer-capacitor-materials modified anodes. *International Journal of Hydrogen Energy*, 43(3), 1816–1823.
<https://doi.org/10.1016/j.ijhydene.2017.11.034>
- Chernicharo, C. A. L., van Lier, J. B., Noyola, A., & Bressani Ribeiro, T. (2015). Anaerobic sewage treatment: state of the art, constraints and challenges. *Reviews in Environmental Science and Biotechnology*, 14, 649–679.
<https://doi.org/10.1007/s11157-015-9377-3>
- Chong, P., Erable, B., & Bergel, A. (2018). Microbial anodes: What actually occurs inside pores? *International Journal of Hydrogen Energy*, 44(9), 4484–4495.
<https://doi.org/10.1016/j.ijhydene.2018.09.075>
- Conway, B. E. (1999). *Electrochemical Supercapacitors : Scientific Fundamentals and Technological Applications*. Springer US.

D

- Deeke, A., Sleutels, T. H. J. A., Donkers, T. F. W., Hamelers, H. V. M., Buisman, C. J. N., & Ter Heijne, A. (2015). Fluidized Capacitive Bioanode As a Novel Reactor Concept for the Microbial Fuel Cell. *Environmental Science & Technology*, 49(3), 1929–1935.
<https://doi.org/10.1021/es503063n>
- Deeke, A., Sleutels, T. H. J. A., Hamelers, H. V. M., & Buisman, C. J. N. (2012). Capacitive bioanodes enable renewable energy storage in microbial fuel cells. *Environmental Science and Technology*, 46, 3554–3560. <https://doi.org/10.1021/es204126r>
- Deeke, A., Sleutels, T. H. J. A., Heijne, A. Ter, Hamelers, H. V. M., & Buisman, C. J. N. (2013). Influence of the thickness of the capacitive layer on the performance of bioanodes in Microbial Fuel Cells. *Journal of Power Sources*, 243, 611–616.
<https://doi.org/10.1016/j.jpowsour.2013.05.195>
- Degrenne, N., Allard, B., Buret, F., Adami, S.-E., Labrousse, D., Vollaïre, C., & Morel, F. (2012). A 140 mV Self-Starting 10 mW DC/DC Converter for Powering Low-Power Electronic Devices from Low-Voltage Microbial Fuel Cells. *Journal of Low Power Electronics*, 8(4), 485–497. <https://doi.org/10.1166/jolpe.2012.1209>
- Dekker, A., Ter Heijne, A., Saakes, M., Hamelers, H. V. M., & Buisman, C. J. N. (2009). Analysis and improvement of a scaled-up and stacked microbial fuel cell.

- Environmental Science and Technology*, 43(23), 9038–9042.
<https://doi.org/10.1021/es901939r>
- Demopoulos, G. P. (2009). Aqueous precipitation and crystallization for the production of particulate solids with desired properties. *Hydrometallurgy*, 96(3), 199–214.
<https://doi.org/10.1016/j.hydromet.2008.10.004>
- Dewan, A, Beyenal, H., & Lewandowski, Z. (2009). Intermittent energy harvesting improves the performance of microbial fuel cells. *Environ. Sci. Technol.*, 43(12), 4600–4605. <https://doi.org/10.1021/es8037092>
- Dewan, Alim, Ay, S. U., Karim, M. N., & Beyenal, H. (2014). Alternative power sources for remote sensors: A review. *Journal of Power Sources*, 245, 129–143.
<https://doi.org/10.1016/j.jpowsour.2013.06.081>
- Dewan, Alim, Donovan, C., Heo, D., & Beyenal, H. (2010). Evaluating the performance of microbial fuel cells powering electronic devices. *Journal of Power Sources*, 195, 90–96. <https://doi.org/10.1016/j.jpowsour.2009.07.001>
- Di Lorenzo, M., Scott, K., Curtis, T. P., & Head, I. M. (2010). Effect of increasing anode surface area on the performance of a single chamber microbial fuel cell. *Chemical Engineering Journal*, 156(1), 40–48. <https://doi.org/10.1016/j.cej.2009.09.031>
- Dominguez-Benetton, X., Sevda, S., Vanbroekhoven, K., & Pant, D. (2012). The accurate use of impedance analysis for the study of microbial electrochemical systems. *Chemical Society Reviews*, 41, 7228–7246. <https://doi.org/10.1039/c2cs35026b>
- Donovan, C., Dewan, A., Heo, D., & Beyenal, H. (2008). Batteryless, wireless sensor powered by a sediment microbial fuel cell. *Environmental Science and Technology*, 42(22), 8591–8596. <https://doi.org/10.1021/es801763g>
- Donovan, C., Dewan, A., Heo, D., Lewandowski, Z., & Beyenal, H. (2013). Sediment microbial fuel cell powering a submersible ultrasonic receiver: New approach to remote monitoring. *Journal of Power Sources*, 233, 79–85.
<https://doi.org/10.1016/j.jpowsour.2012.12.112>
- Donovan, C., Dewan, A., Peng, H., Heo, D., & Beyenal, H. (2011). Power management system for a 2.5 W remote sensor powered by a sediment microbial fuel cell. *Journal of Power Sources*, 196(3), 1171–1177.
<https://doi.org/10.1016/j.jpowsour.2010.08.099>
- Doyle, L. E., & Marsili, E. (2018). Weak electricigens: A new avenue for bioelectrochemical research. *Bioresource Technology*, 258(December 2017), 354–364.
<https://doi.org/10.1016/j.biortech.2018.02.073>
- Du, Z., Li, H., & Gu, T. (2007). A state of the art review on microbial fuel cells: A promising technology for wastewater treatment and bioenergy. *Biotechnology Advances*, 25, 464–482. <https://doi.org/10.1016/j.biotechadv.2007.05.004>
- Dubé, C.-D., & Guiot, S. R. (2015). Direct Interspecies Electron Transfer in Anaerobic Digestion: A Review. *Advances in Biochemical Engineering/Biotechnology*, 151, 101–115. https://doi.org/10.1007/978-3-319-21993-6_4

E

- Edzes, H. T., Van Dusschoten, D., & Van As, H. (1998). Quantitative T2 imaging of plant tissues by means of multi-echo MRI microscopy. *Magnetic Resonance Imaging*, 16(2), 185–196.
- Ellabban, O., Abu-Rub, H., & Blaabjerg, F. (2014). Renewable energy resources: Current status, future prospects and their enabling technology. *Renewable and Sustainable Energy Reviews*, 39, 748–764. <https://doi.org/10.1016/j.rser.2014.07.113>
- Emmenegger, C., Mauron, P., Sudan, P., Wenger, P., Hermann, V., Gallay, R., & Züttel, A. (2003). Investigation of electrochemical double-layer (ECDL) capacitors electrodes based on carbon nanotubes and activated carbon materials. *Journal of Power Sources*, 124, 321–329. [https://doi.org/10.1016/S0378-7753\(03\)00590-1](https://doi.org/10.1016/S0378-7753(03)00590-1)
- Erbay, C., Carreon-Bautista, S., Sanchez-Sinencio, E., & Han, A. (2014). High Performance Monolithic Power Management System with Dynamic Maximum Power Point Tracking for Microbial Fuel Cells. *Environmental Science & Technology*, 48, 13992–13999. <https://doi.org/10.1021/es501426j>
- European Commission. (2019). The Sustainable Development Goals | International Cooperation and Development. Retrieved January 18, 2019, from https://ec.europa.eu/europeaid/policies/sustainable-development-goals_en
- Ewing, T., Babauta, J. T., Atci, E., Tang, N., Orellana, J., Heo, D., & Beyenal, H. (2014). Self-powered wastewater treatment for the enhanced operation of a facultative lagoon. *Journal of Power Sources*, 269, 284–292. <https://doi.org/10.1016/j.jpowsour.2014.06.114>

F

- Fan, Y., Hu, H., & Liu, H. (2007). Enhanced Coulombic efficiency and power density of air-cathode microbial fuel cells with an improved cell configuration. *Journal of Power Sources*, 171(2), 348–354. <https://doi.org/10.1016/j.jpowsour.2007.06.220>
- Fan, Y., Sharbrough, E., & Liu, H. (2008). Quantification of the Internal Resistance Distribution of Microbial Fuel Cells. *Environmental Science & Technology*, 42(21), 8101–8107. <https://doi.org/10.1021/es801229j>
- Feng, C., Lv, Z., Yang, X., & Wei, C. (2014). Anode modification with capacitive materials for a microbial fuel cell: an increase in transient power or stationary power. *Physical Chemistry Chemical Physics: PCCP*, 16(22), 10464–10472. <https://doi.org/10.1039/c4cp00923a>
- Fortunato, L., & Leiknes, T. (2017). In-situ biofouling assessment in spacer filled channels using optical coherence tomography (OCT): 3D biofilm thickness mapping. *Bioresource Technology*, 229, 231–235. <https://doi.org/10.1016/j.biortech.2017.01.021>
- Frackowiak, E., & Béguin, F. (2001). Carbon materials for the electrochemical storage of energy in capacitors. *Carbon*, 39(6), 937–950. <https://doi.org/10.1016/S0008->

- Fradler, K. R., Kim, J. R., Boghani, H. C., Dinsdale, R. M., Guwy, A. J., & Premier, G. C. (2014). The effect of internal capacitance on power quality and energy efficiency in a tubular microbial fuel cell. *Process Biochemistry*, 49(6), 973–980. <https://doi.org/10.1016/j.procbio.2014.02.021>
- Franks, A. E., Malvankar, N., & Nevin, K. P. (2010). Bacterial biofilms: the powerhouse of a microbial fuel cell. *Biofuels*, 1(4), 589–604. <https://doi.org/10.4155/bfs.10.25>

G

- Garny, K., Neu, T. R., Horn, H., Volke, F., & Manz, B. (2010). Combined application of ¹³C NMR spectroscopy and confocal laser scanning microscopy-Investigation on biofilm structure and physico-chemical properties. *Chemical Engineering Science*, 65(16), 4691–4700. <https://doi.org/10.1016/j.ces.2010.05.013>
- Gasparatos, A., Stromberg, P., & Takeuchi, K. (2013). Sustainability impact of first-generation biofuels. *Animal Frontiers*, 3(2), 12–26. <https://doi.org/10.2527/af.2013-0011>
- Godefroy, S., Korb, J.-P., Fleury, M., & Bryant, R. G. (2001). Surface nuclear magnetic relaxation and dynamics of water and oil in macroporous media. *Physical Review E*, 64(2), 021605. <https://doi.org/10.1103/PhysRevE.64.021605>
- Gonzalez-Gil, G., Lens, P. N., Van Aelst, A., Van As, H., Versprille, a I., & Lettinga, G. (2001). Cluster structure of anaerobic aggregates of an expanded granular sludge bed reactor. *Applied and Environmental Microbiology*, 67(8), 3683–3692. <https://doi.org/10.1128/AEM.67.8.3683-3692.2001>
- González Ballester, M. Á., Zisserman, A. P., & Brady, M. (2002). Estimation of the partial volume effect in MRI. *Medical Image Analysis*, 6(4), 389–405. [https://doi.org/10.1016/S1361-8415\(02\)00061-0](https://doi.org/10.1016/S1361-8415(02)00061-0)
- Graf von der Schulenburg, D. A., Vrouwenvelder, J. S., Creber, S. A., van Loosdrecht, M. C. M., & Johns, M. L. (2008). Nuclear magnetic resonance microscopy studies of membrane biofouling. *Journal of Membrane Science*, 323(1), 37–44. <https://doi.org/10.1016/j.memsci.2008.06.012>
- Gryglewicz, G., Machnikowski, J., Lorenc-Grabowska, E., Lota, G., & Frackowiak, E. (2005). Effect of pore size distribution of coal-based activated carbons on double layer capacitance. *Electrochimica Acta*, 50(5), 1197–1206. <https://doi.org/10.1016/j.electacta.2004.07.045>
- Gu, W., & Yushin, G. (2014). Review of nanostructured carbon materials for electrochemical capacitor applications: advantages and limitations of activated carbon, carbide-derived carbon, zeolite-templated carbon, carbon aerogels, carbon nanotubes, onion-like carbon, and graphene. *Wiley Interdisciplinary Reviews: Energy and Environment*, 3(5), 424–473. <https://doi.org/10.1002/wene.102>
- Gu, Y., Li, Y., Li, X., Luo, P., Wang, H., Wang, X., ... Li, F. (2017). Energy self-sufficient wastewater treatment plants: feasibilities and challenges. *Energy Procedia*, 105,

- 3741–3751. <https://doi.org/10.1016/j.egypro.2017.03.868>
- Guo, K., Freguia, S., Dennis, P. G., Chen, X., Donose, B. C., Keller, J., ... Rabaey, K. (2013). Effects of surface charge and hydrophobicity on anodic biofilm formation, community composition, and current generation in bioelectrochemical systems. *Environmental Science and Technology*, 47(13), 7563–7570. <https://doi.org/10.1021/es400901u>
- Guo, K., PrévotEAU, A., Patil, S. A., & Rabaey, K. (2015). Engineering electrodes for microbial electrocatalysis. *Current Opinion in Biotechnology*, 33(October 2016), 149–156. <https://doi.org/10.1016/j.copbio.2015.02.014>

H

- Haisch, C., & Niessner, R. (2007). Visualisation of transient processes in biofilms by optical coherence tomography. *Water Research*, 41, 2467–2472. <https://doi.org/10.1016/j.watres.2007.03.017>
- Han, L., Karthikeyan, K. G., Anderson, M. A., & Gregory, K. B. (2014). Exploring the impact of pore size distribution on the performance of carbon electrodes for capacitive deionization. *Journal of Colloid and Interface Science*, 430, 93–99. <https://doi.org/10.1016/j.jcis.2014.05.015>
- Heidrich, E. S., Dolfing, J., Scott, K., Edwards, S. R., Jones, C., & Curtis, T. P. (2013). Production of hydrogen from domestic wastewater in a pilot-scale microbial electrolysis cell. *Applied Microbiology and Biotechnology*, 97, 6979–6989. <https://doi.org/10.1007/s00253-012-4456-7>
- Heijne, A. ter, Liu, D., Sulonen, M., Sleutels, T. H. J. A., & Fabregat-Santiago, F. (2018). Quantification of bio-anode capacitance in bioelectrochemical systems using Electrochemical Impedance Spectroscopy. *Journal of Power Sources*, 400, 533–538. <https://doi.org/10.1016/j.jpowsour.2018.08.003>
- Heilmann, J., & Logan, B. E. (2006). Production of Electricity from Proteins Using a Microbial Fuel Cell. *Water Environment Research*, 78(5), 531–537. <https://doi.org/10.2175/106143005X73046>
- Herrling, M. P., Guthausen, G., Wagner, M., Lackner, S., & Horn, H. (2015). Determining the flow regime in a biofilm carrier by means of magnetic resonance imaging. *Biotechnology and Bioengineering*, 112(5), 1023–1032. <https://doi.org/10.1002/bit.25510>
- Herrling, M. P., Weisbrodt, J., Kirkland, C. M., Williamson, N. H., Lackner, S., Codd, S. L., ... Horn, H. (2017). NMR investigation of water diffusion in different biofilm structures. *Biotechnology and Bioengineering*, 114(12), 2857–2867. <https://doi.org/10.1002/bit.26392>
- Holmes, D. E., & Smith, J. A. (2016). Biologically Produced Methane as a Renewable Energy Source. *Advances in Applied Microbiology*, 97, 1–61. <https://doi.org/10.1016/bs.aambs.2016.09.001>
- Hong, S.-C., Kim, S., Jang, W.-J., Han, T.-H., Hong, J.-P., Oh, J.-S., ... Lee, J.-H. (2014a).

- Supercapacitor characteristics of pressurized RuO₂/carbon powder as binder-free electrodes. <https://doi.org/10.1039/c4ra06370h>
- Hong, S.-C., Kim, S., Jang, W.-J., Han, T.-H., Hong, J.-P., Oh, J.-S., ... Lee, J.-H. (2014b). Supercapacitor characteristics of pressurized RuO₂/carbon powder as binder-free electrodes. *RSC Advances*, 4, 48276–48284. <https://doi.org/10.1039/c4ra06370h>
- Hoskins, B. C., Majors, P. D., Sharma, M. M., & Georgiou, G. (1999). Non-Invasive Imaging of Biofilms in Porous Media Using NMR Methods. *Exploration and Production Environmental Conference*, 73, 67–73.
- Hou, J., Liu, Z., & Zhang, P. (2013). A new method for fabrication of graphene/polyaniline nanocomplex modified microbial fuel cell anodes. *Journal of Power Sources*, 224, 139–144. <https://doi.org/10.1016/J.JPOWSOUR.2012.09.091>
- Houghton, J., Santoro, C., Soavi, F., Serov, A., Ieropoulos, I., Arbizzani, C., & Atanassov, P. (2016). Supercapacitive microbial fuel cell: Characterization and analysis for improved charge storage/delivery performance. *Bioresource Technology*, 218, 552–560. <https://doi.org/10.1016/j.biortech.2016.06.105>

I

- Ieropoulos, I. A., Greenman, J., & Melhuish, C. (2013). Miniature microbial fuel cells and stacks for urine utilisation. *International Journal of Hydrogen Energy*, 38, 492–496. <https://doi.org/10.1016/j.ijhydene.2012.09.062>
- Ieropoulos, I. A., Greenman, J., Melhuish, C., & Horsfield, I. (2012). Microbial fuel cells for robotics: Energy autonomy through artificial symbiosis. *ChemSusChem*, 5(6), 1020–1026. <https://doi.org/10.1002/cssc.201200283>
- Ieropoulos, I., Melhuish, C., & Greenman, J. (2003). Artificial metabolism: towards true energetic autonomy in artificial life. *Advances in Artificial Life*, (January 2003), 792–799. <https://doi.org/10.1007/978-3-540-39432-7>
- Ieropoulos, Ioannis, Greenman, J., & Melhuish, C. (2008). Microbial fuel cells based on carbon veil electrodes: Stack configuration and scalability. *International Journal of Energy Research*, 32(13), 1228–1240. <https://doi.org/10.1002/er.1419>
- Ieropoulos, Ioannis, Greenman, J., Melhuish, C., & Horsfield, I. (2010). EcoBot-III: a robot with guts. *The 12th International Conference on the Synthesis and Simulation of Living Systems*, 733–740.
- Intermite, S., Arbizzani, C., Soavi, F., Gholipour, S., Turren-Cruz, S.-H., Correa-Baena, J. P., ... Grätzel, M. (2017). Perovskite solar cell – electrochemical double layer capacitor interplay. *Electrochimica Acta*, 258, 825–833. <https://doi.org/10.1016/j.electacta.2017.11.132>
- International Energy Agency. (2017). *Key World Energy Statistics*. Retrieved from <https://www.iea.org/publications/freepublications/publication/KeyWorld2017.pdf>
- International Energy Agency. (2018). *Renewables 2018*. Retrieved January 18, 2019, from <https://www.iea.org/renewables2018/>

Ishii, S., Suzuki, S., Tenney, A., Nealson, K. H., & Bretschger, O. (2018). Comparative metatranscriptomics reveals extracellular electron transfer pathways conferring microbial adaptivity to surface redox potential changes. *The ISME Journal*, 12, 2844–2863. <https://doi.org/10.1038/s41396-018-0238-2>

J

Jana, P. S., Katuri, K., Kavanagh, P., Kumar, A., & Leech, D. (2014). Charge transport in films of *Geobacter sulfurreducens* on graphite electrodes as a function of film thickness. *Phys. Chem. Chem. Phys.*, 16(19), 9039–9046. <https://doi.org/10.1039/C4CP01023J>

Jayalakshmi, M., & Balasubramanian, K. (2008). Simple capacitors to supercapacitors-An overview. *Int. J. Electrochem. Sci*, 3, 1196–1217.

Jeremiasse, A. W., Hamelers, H. V. M., Kleijn, J. M., & Buisman, C. J. N. (2009). Use of Biocompatible Buffers to Reduce the Concentration Overpotential for Hydrogen Evolution. *Environmental Science & Technology*, 43(17), 6882–6887. <https://doi.org/10.1021/es9008823>

Jha, S. K., Bilalovic, J., Jha, A., Patel, N., & Zhang, H. (2017). Renewable energy: Present research and future scope of Artificial Intelligence. *Renewable and Sustainable Energy Reviews*, 77, 297–317. <https://doi.org/10.1016/j.rser.2017.04.018>

Jiang, Y., Van Der Werf, E., Van Ierland, E. C., & Keesman, K. J. (2017). The potential role of waste biomass in the future urban electricity system. *Biomass and Bioenergy*. <https://doi.org/10.1016/j.biombioe.2017.10.001>

K

Karra, U., Muto, E., Umaz, R., Kölln, M., Santoro, C., Wang, L., & Li, B. (2014). Performance evaluation of activated carbon-based electrodes with novel power management system for long-term benthic microbial fuel cells. *International Journal of Hydrogen Energy*, 39(36), 21847–21856. <https://doi.org/10.1016/j.ijhydene.2014.06.095>

Kastening, B., Hahn, M., & Kremeskötter, J. (1994). The double layer of activated carbon electrodes: Part 1- The contribution of ions in the pores. *Journal of Electroanalytical Chemistry*, 374(1–2), 159–166. [https://doi.org/10.1016/0022-0728\(94\)03373-0](https://doi.org/10.1016/0022-0728(94)03373-0)

Kastening, B., Hahn, M., Rabanus, B., Heins, M., & zum Felde, U. (1997). Electronic properties and double layer of activated carbon. *Electrochimica Acta*, 42(18), 2789–2799. [https://doi.org/10.1016/S0013-4686\(97\)00082-0](https://doi.org/10.1016/S0013-4686(97)00082-0)

Kato, S., Hashimoto, K., & Watanabe, K. (2012). Microbial interspecies electron transfer via electric currents through conductive minerals. *Proceedings of the National Academy of Sciences of the United States of America*, 109(25), 10042–10046. <https://doi.org/10.1073/pnas.1117592109>

Kelly, P. T., & He, Z. (2014). Nutrients removal and recovery in bioelectrochemical systems: A review. *Bioresource Technology*, 153, 351–360.

<https://doi.org/10.1016/j.biortech.2013.12.046>

- Khan, M. R., Baranitharan, E., Prasad, D. M. R., & Cheng, C. K. (2016). Fast Biofilm Formation and Its Role on Power Generation in Palm Oil Mill Effluent Fed Microbial Fuel Cell. *MATEC Web of Conferences*, 62, 1–6. <https://doi.org/10.1051/04002>
- Kim, J. R., Premier, G. C., Hawkes, F. R., Rodríguez, J., Dinsdale, R. M., & Guwy, A. J. (2010). Modular tubular microbial fuel cells for energy recovery during sucrose wastewater treatment at low organic loading rate. *Bioresource Technology*, 101(4), 1190–1198. <https://doi.org/10.1016/j.biortech.2009.09.023>
- Kinoshita, K. (1992). *Electrochemical oxygen technology*. Wiley.
- Koch, C., & Harnisch, F. (2016). What Is the Essence of Microbial Electroactivity? *Frontiers in Microbiology*, 7, 1–5. <https://doi.org/10.3389/fmicb.2016.01890>
- Kodali, M., Santoro, C., Serov, A., Kabir, S., Artyushkova, K., Matanovic, I., & Atanassov, P. (2017). Air Breathing Cathodes for Microbial Fuel Cell using Mn-, Fe-, Co- and Ni-containing Platinum Group Metal-free Catalysts. *Electrochimica Acta*, 231, 115–124. <https://doi.org/10.1016/J.ELECTACTA.2017.02.033>
- Korth, B., Rosa, L. F. M., Harnisch, F., & Picioreanu, C. (2015). A framework for modeling electroactive microbial biofilms performing direct electron transfer. *Bioelectrochemistry*, 106, 194–206. <https://doi.org/10.1016/j.bioelechem.2015.03.010>
- Kötz, R., & Carlen, M. (2000). Principles and applications of electrochemical capacitors. *Electrochimica Acta*, 45, 2483–2498.
- Kracke, F., Vassilev, I., & Krömer, J. O. (2015). Microbial electron transport and energy conservation - The foundation for optimizing bioelectrochemical systems. *Frontiers in Microbiology*, 6(JUN), 1–18. <https://doi.org/10.3389/fmicb.2015.00575>
- Kujawa-Roeleveld, K., & Zeeman, G. (2006). Anaerobic treatment in decentralised and source-separation-based sanitation concepts. *Reviews in Environmental Science and Bio/Technology*, 5, 115–139. <https://doi.org/10.1007/s11157-005-5789-9>
- Kumar, A., Hsu, L. H.-H., Kavanagh, P., Barrière, F., Lens, P. N. L., Lapinonnière, L., ... Leech, D. (2017). The ins and outs of microorganism–electrode electron transfer reactions. *Nature Reviews Chemistry*, 1(3), 0024. <https://doi.org/10.1038/s41570-017-0024>

L

- Lapinonnière, L., Picot, M., Poriel, C., & Barrière, F. (2013). Phenylboronic Acid Modified Anodes Promote Faster Biofilm Adhesion and Increase Microbial Fuel Cell Performances. *Electroanalysis*, 25(3), 601–605. <https://doi.org/10.1002/elan.201200351>
- Lee, J.-Y., Lee, S.-H., & Park, H.-D. (2016). Enrichment of specific electro-active microorganisms and enhancement of methane production by adding granular activated carbon in anaerobic reactors. *Bioresource Technology*, 205, 205–212. <https://doi.org/10.1016/j.biortech.2016.01.054>

- Lee, J., Kim, J., & Hyeon, T. (2006). Recent progress in the synthesis of porous carbon materials. *Advanced Materials*, 18(16), 2073–2094. <https://doi.org/10.1002/adma.200501576>
- Lei, Y., Sun, D., Dang, Y., Chen, H., Zhao, Z., Zhang, Y., & Holmes, D. E. (2016). Stimulation of methanogenesis in anaerobic digesters treating leachate from a municipal solid waste incineration plant with carbon cloth. *Bioresource Technology*, 222, 270–276. <https://doi.org/10.1016/j.biortech.2016.10.007>
- Lettinga, G., van Velsen, A. F. M., Hobma, S. W., de Zeeuw, W., & Klapwijk, A. (1980). Use of the upflow sludge blanket (USB) reactor concept for biological wastewater treatment, especially for anaerobic treatment. *Biotechnology and Bioengineering*, 22(4), 699–734. <https://doi.org/10.1002/bit.260220402>
- Li, Cheng, Lesnik, K. L., & Liu, H. (2017). Stay connected: Electrical conductivity of microbial aggregates. *Biotechnology Advances*, 35(6), 669–680. <https://doi.org/10.1016/j.biotechadv.2017.07.010>
- Li, Chunyan, Felz, S., Wagner, M., Lackner, S., & Horn, H. (2016). Investigating biofilm structure developing on carriers from lab-scale moving bed biofilm reactors based on light microscopy and optical coherence tomography. *Bioresource Technology*, 200, 128–136. <https://doi.org/10.1016/j.biortech.2015.10.013>
- Li, F., Sharma, Y., Lei, Y., Li, B., & Zhou, Q. (2010). Microbial Fuel Cells: The Effects of Configurations, Electrolyte Solutions, and Electrode Materials on Power Generation. *Applied Biochemistry and Biotechnology*, 160(1), 168–181. <https://doi.org/10.1007/s12010-008-8516-5>
- Li, J., Ge, Z., & He, Z. (2014). A fluidized bed membrane bioelectrochemical reactor for energy-efficient wastewater treatment. *Bioresource Technology*, 167, 310–315. <https://doi.org/10.1016/j.biortech.2014.06.034>
- Li, Y., Zhang, Y., Yang, Y., Quan, X., & Zhao, Z. (2017). Potentially direct interspecies electron transfer of methanogenesis for syntrophic metabolism under sulfate reducing conditions with stainless steel. *Bioresource Technology*, 234, 303–309. <https://doi.org/10.1016/j.biortech.2017.03.054>
- Liang, P., Zhang, C., Jiang, Y., Bian, Y., Zhang, H., Sun, X., ... Huang, X. (2017). Performance enhancement of microbial fuel cell by applying transient-state regulation. *Applied Energy*, 185, 582–588. <https://doi.org/10.1016/j.apenergy.2016.10.130>
- Liu, B., Weinstein, A., Kolln, M., Garrett, C., Wang, L., Bagtzoglou, A., ... Li, B. (2015). Distributed multiple-anodes benthic microbial fuel cell as reliable power source for subsea sensors. *Journal of Power Sources*, 286, 210–216. <https://doi.org/10.1016/j.jpowsour.2015.03.161>
- Liu, F., Rotaru, A.-E., Shrestha, P. M., Malvankar, N. S., Nevin, K. P., & Lovley, D. R. (2012). Promoting direct interspecies electron transfer with activated carbon. *Energy & Environmental Science*, 5, 8982–8989. <https://doi.org/10.1039/c2ee22459c>
- Liu, H., Cheng, S., & Logan, B. E. (2005). Power generation in fed-batch microbial fuel

- cells as a function of ionic strength, temperature, and reactor configuration. *Environmental Science and Technology*, 39(14), 5488–5493.
<https://doi.org/10.1021/es050316c>
- Liu, H., Ramnarayanan, R., & Logan, B. E. (2004). Production of electricity during wastewater treatment using a single chamber microbial fuel cell. *Environmental Science & Technology*, 38(7), 2281–2285. <https://doi.org/10.1021/es034923g>
- Liu, Jia, Zhang, F., He, W., Yang, W., Feng, Y., & Logan, B. E. (2014). A microbial fluidized electrode electrolysis cell (MFEEC) for enhanced hydrogen production. *Journal of Power Sources*, 271, 530–533. <https://doi.org/10.1016/j.jpowsour.2014.08.042>
- Liu, Jia, Zhang, F., He, W., Zhang, X., Feng, Y., & Logan, B. E. (2014). Intermittent contact of fluidized anode particles containing exoelectrogenic biofilms for continuous power generation in microbial fuel cells. *Journal of Power Sources*, 261, 278–284.
<https://doi.org/10.1016/j.jpowsour.2014.03.071>
- Liu, Jilei, Wang, J., Xu, C., Jiang, H., Li, C., Zhang, L., ... Shen, Z. X. (2018). Advanced Energy Storage Devices: Basic Principles, Analytical Methods, and Rational Materials Design. *Advanced Science*, 5, 1–19. <https://doi.org/10.1002/advs.201700322>
- Liu, P., Zhang, C., Liang, P., Jiang, Y., Zhang, X., & Huang, X. (2018). Enhancing extracellular electron transfer efficiency and bioelectricity production by vapor polymerization Poly (3,4-ethylenedioxythiophene)/ MnO₂ hybrid anode. *Bioelectrochemistry*, 126, 72–78.
<https://doi.org/10.1016/j.bioelechem.2018.07.011>
- Liu, Z., Liu, J., Zhang, S., & Su, Z. (2008). A novel configuration of microbial fuel cell stack bridged internally through an extra cation exchange membrane. *Biotechnology Letters*, 30(6), 1017–1023. <https://doi.org/10.1007/s10529-008-9658-9>
- Logan, B. E., Hamelers, B., Rozendal, R., Schoder, U., Keller, J., Freguia, S., ... Rabaey, K. (2006). Microbial Fuel Cells: Methodology and Technology. *Environmental Science & Technology*, 40(17), 5181–5192. <https://doi.org/10.1021/es0605016>
- Logan, B. E., & Regan, J. M. (2006). Electricity-producing bacterial communities in microbial fuel cells. *Trends in Microbiology*, 14(12), 512–518.
<https://doi.org/10.1016/j.tim.2006.10.003>
- Logan, B. E., Wallack, M. J., Kim, K. Y., He, W., Feng, Y., & Saikaly, P. E. (2015). Assessment of Microbial Fuel Cell Configurations and Power Densities. *Environmental Science and Technology Letters*, 2(8), 206–214.
<https://doi.org/10.1021/acs.estlett.5b00180>
- Lota, G., Tyczkowski, J., Kapica, R., Lota, K., & Frackowiak, E. (2009). Carbon materials modified by plasma treatment as electrodes for supercapacitors. *Journal of Power Sources*, 195, 7535–7539. <https://doi.org/10.1016/j.jpowsour.2009.12.019>
- Lovley, D. R. (2006). Bug juice: harvesting electricity with microorganisms. *Nature Reviews. Microbiology*, 4(7), 497–508. <https://doi.org/10.1038/nrmicro1442>
- Lovley, D. R. (2008). The microbe electric: conversion of organic matter to electricity. *Current Opinion in Biotechnology*, 19(6), 564–571.

- <https://doi.org/10.1016/j.copbio.2008.10.005>
- Lovley, D. R. (2012a). Electromicrobiology. *Annual Review of Microbiology*, 66(1), 391–409. <https://doi.org/10.1146/annurev-micro-092611-150104>
- Lovley, D. R. (2012b). Long-range electron transport to Fe(III) oxide via pili with metallic-like conductivity. *Biochemical Society Transactions*, 40(6), 1186–1190. <https://doi.org/10.1042/BST20120131>
- Lv, Z., Xie, D., Li, F., Hu, Y., Wei, C., & Feng, C. (2014). Microbial fuel cell as a biocapacitor by using pseudo-capacitive anode materials. *Journal of Power Sources*, 246, 642–649. <https://doi.org/10.1016/j.jpowsour.2013.08.014>
- Lv, Z., Xie, D., Yue, X., Feng, C., & Wei, C. (2012). Ruthenium oxide-coated carbon felt electrode: A highly active anode for microbial fuel cell applications. *Journal of Power Sources*, 210, 26–31. <https://doi.org/10.1016/j.jpowsour.2012.02.109>

M

- Malvankar, N. S., King, G. M., & Lovley, D. R. (2015). Centimeter-long electron transport in marine sediments via conductive minerals. *The ISME Journal*, 9(2), 527–531. <https://doi.org/10.1038/ismej.2014.131>
- Malvankar, N. S., Lau, J., Nevin, K. P., Franks, A. E., Tuominen, M. T., & Lovley, D. R. (2012). Electrical conductivity in a mixed-species biofilm. *Applied and Environmental Microbiology*, 78(16), 5967–5971. <https://doi.org/10.1128/AEM.01803-12>
- Malvankar, N. S., & Lovley, D. R. (2012). Microbial nanowires: A new paradigm for biological electron transfer and bioelectronics. *ChemSusChem*, 5(6), 1039–1046. <https://doi.org/10.1002/cssc.201100733>
- Malvankar, N. S., & Lovley, D. R. (2014). Microbial nanowires for bioenergy applications. *Current Opinion in Biotechnology*, 27, 88–95. <https://doi.org/10.1016/j.copbio.2013.12.003>
- Malvankar, N. S., & Lovley, D. R. (2015). Electronic conductivity in living biofilms: physical meaning, mechanisms and measurement methods. In *Biofilms in Bioelectrochemical Systems: From Laboratory Practice to Data Interpretation* (pp. 211–247). John Wiley & Sons, Inc.
- Malvankar, N. S., Mester, T., Tuominen, M. T., & Lovley, D. R. (2012). Supercapacitors based on c-type cytochromes using conductive nanostructured networks of living bacteria. *ChemPhysChem*, 13(2), 463–468. <https://doi.org/10.1002/cphc.201100865>
- Malvankar, N. S., Rotello, V. M., Tuominen, M. T., & Lovley, D. R. (2016). Reply to Yates by Lovley on the paper: “Measuring conductivity of living *Geobacter sulfurreducens* biofilms.” *Nature Nanotechnology*, 11(11), 913–914.
- Malvankar, N. S., Tuominen, M. T., & Lovley, D. R. (2012). Biofilm conductivity is a decisive variable for high-current-density *Geobacter sulfurreducens* microbial fuel cells. *Energy & Environmental Science*, 5(2), 5790. <https://doi.org/10.1039/c2ee03388g>

- Malvankar, N. S., Vargas, M., Nevin, K. P., Franks, A. E., Leang, C., Kim, B.-C., ... Lovley, D. R. (2011). Tunable metallic-like conductivity in microbial nanowire networks. *Nature Nanotechnology*, 6(9), 573–579. <https://doi.org/10.1038/nnano.2011.119>
- Manz, B., Volke, F., Goll, D., & Horn, H. (2005). Investigation of biofilm structure, flow patterns and detachment with magnetic resonance imaging. *Water Science and Technology*, 52(7), 1–6.
- Marzorati, S., Goglio, A., Fest-Santini, S., Mombelli, D., Villa, F., Cristiani, P., & Schievano, A. (2018). Air-breathing bio-cathodes based on electro-active biochar from pyrolysis of Giant Cane stalks. *International Journal of Hydrogen Energy*, 1–12. <https://doi.org/10.1016/J.IJHYDENE.2018.07.167>
- Mccarty, P. L., Bae, J., & Kim, J. (2011). Domestic Wastewater Treatment as a Net Energy Producer- Can This be Achieved? *Environ. Sci. Technol*, 45, 7100–7106. <https://doi.org/10.1021/es2014264>
- McGlynn, S. E., Chadwick, G. L., Kempes, C. P., & Orphan, V. J. (2015). Single cell activity reveals direct electron transfer in methanotrophic consortia. *Nature*, 526(7574), 531–535. <https://doi.org/10.1038/nature15512>
- Melhuish, C., Ieropoulos, I., Greenman, J., & Horsfield, I. (2006). Energetically autonomous robots: Food for thought. *Autonomous Robots*, 21(3), 187–198. <https://doi.org/10.1007/s10514-006-6574-5>
- Meng, F., Zhao, Q., Na, X., Zheng, Z., Jiang, J., Wei, L., & Zhang, J. (2017). Bioelectricity generation and dewatered sludge degradation in microbial capacitive desalination cell. *Environ Sci Pollut Res*, 24, 5159–5167. <https://doi.org/10.1007/s11356-016-6853-4>
- Mo, W., & Zhang, Q. (2013). Energy-nutrients-water nexus: Integrated resource recovery in municipal wastewater treatment plants. *Journal of Environmental Management*, 127, 255–267. <https://doi.org/10.1016/j.jenvman.2013.05.007>
- Molenaar, S., Sleutels, T. H. J. A., Pereira, J., Lorio, M., Borsje, C., Zamudio, J. A., ... Heijne, A. (2018). In situ biofilm quantification in Bioelectrochemical Systems using Optical Coherence Tomography. *ChemSusChem*, 11, 1–9. <https://doi.org/10.1002/cssc.201800589>
- Morita, M., Malvankar, N. S., Franks, A. E., Interspecies, D., Transfer, E., Wastewater, M., ... Journal, A. S. M. (2011). Potential for direct interspecies electron transfer in methanogenic wastewater digester aggregates. *MBio*, 2(4), 5–7. <https://doi.org/10.1128/mBio.00159-11>
- Müller, N., Worm, P., Schink, B., Stams, A. J. M., & Plugge, C. M. (2010). Syntrophic butyrate and propionate oxidation processes: from genomes to reaction mechanisms. *Environmental Microbiology Reports*, 2(4), 489–499. <https://doi.org/10.1111/j.1758-2229.2010.00147.x>
- Müllier, M., & Kastening, B. (1994). The double layer of activated carbon electrodes. *Journal of Electroanalytical Chemistry*, 374(1–2), 149–158. [https://doi.org/10.1016/0022-0728\(94\)03372-2](https://doi.org/10.1016/0022-0728(94)03372-2)

N

- Nancharaiyah, Y. V., Venkata Mohan, S., & Lens, P. N. L. (2015). Metals removal and recovery in bioelectrochemical systems: A review. *Bioresource Technology*, 195, 102–114. <https://doi.org/10.1016/j.biortech.2015.06.058>
- Neu, T. R., Manz, B., Volke, F., Dynes, J. J., Hitchcock, A. P., & Lawrence, J. R. (2010). Advanced imaging techniques for assessment of structure, composition and function in biofilm systems. *FEMS Microbiology Ecology*, 72(1), 1–21. <https://doi.org/10.1111/j.1574-6941.2010.00837.x>
- Nielsen, M. E., Wu, D. M., Girguis, P. R., & Reimers, C. E. (2009). Influence of substrate on electron transfer mechanisms in chambered benthic microbial fuel cells. *Environmental Science and Technology*, 43(22), 8671–8677. <https://doi.org/10.1021/es9013773>
- Nir, O., Sengpiel, R., & Wessling, M. (2018). Closing the cycle: Phosphorus removal and recovery from diluted effluents using acid resistive membranes. *Chemical Engineering Journal*, 346(March), 640–648. <https://doi.org/10.1016/j.cej.2018.03.181>
- Nixon, S. W. (1995). Coastal marine eutrophication: A definition, social causes, and future concerns. *Ophelia*, 41(1), 199–219. <https://doi.org/10.1080/00785236.1995.10422044>

O

- Oh, S. E., & Logan, B. E. (2007). Voltage reversal during microbial fuel cell stack operation. *Journal of Power Sources*, 167(1), 11–17. <https://doi.org/10.1016/j.jpowsour.2007.02.016>
- Oh, S. T., Kim, J. R., Premier, G. C., Lee, T. H., Kim, C., & Sloan, W. T. (2010). Sustainable wastewater treatment: how might microbial fuel cells contribute. *Biotechnology Advances*, 28(6), 871–881. <https://doi.org/10.1016/j.biotechadv.2010.07.008>
- Oliot, M., Chong, P., Erable, B., & Bergel, A. (2017). Influence of the electrode size on microbial anode performance. *Chemical Engineering Journal*, 327, 218–227. <https://doi.org/10.1016/j.cej.2017.06.044>
- Orazem, M. E., Pébère, N., & Tribollet, B. (2006). Enhanced Graphical Representation of Electrochemical Impedance Data. *Journal of The Electrochemical Society*, 153(4), B129–B136. <https://doi.org/10.1149/1.2168377>
- Orazem, M. E., & Tribollet, B. (2008). *Electrochemical Impedance Spectroscopy*. John Wiley & Sons.

P

- Pandolfo, A. G., & Hollenkamp, A. F. (2006). Carbon properties and their role in supercapacitors. *Journal of Power Sources*, 157(1), 11–27. <https://doi.org/10.1016/j.jpowsour.2006.02.065>

- Pankratov, D., Blum, Z., Suyatin, D. B., Popov, V. O., & Shleev, S. (2014). Self-Charging Electrochemical Biocapacitor. *ChemElectroChem*, 1(2), 343–346. <https://doi.org/10.1002/celc.201300142>
- Pankratov, D., Conzuelo, F., Pinyou, P., Alsaoub, S., Schuhmann, W., & Shleev, S. (2016). A Nernstian Biosupercapacitor. *Angewandte Chemie International Edition*, 55(49), 15434–15438. <https://doi.org/10.1002/anie.201607144>
- Pankratov, D., Falkman, P., Blum, Z., & Shleev, S. (2014). A hybrid electric power device for simultaneous generation and storage of electric energy. *Energy and Environmental Science*, 7, 989–993. <https://doi.org/10.1039/c3ee43413c>
- Pant, D., Singh, A., Van Bogaert, G., Irving Olsen, S., Singh Nigam, P., Diels, L., & Vanbroekhoven, K. (2012). Bioelectrochemical systems (BES) for sustainable energy production and product recovery from organic wastes and industrial wastewaters. *RSC Advances*, 2(4), 1248. <https://doi.org/10.1039/c1ra00839k>
- Pant, D., Van Bogaert, G., Diels, L., & Vanbroekhoven, K. (2010). A review of the substrates used in microbial fuel cells (MFCs) for sustainable energy production. *Bioresource Technology*, 101(6), 1533–1543. <https://doi.org/10.1016/j.biortech.2009.10.017>
- Papachristos, G. (2017). Diversity in technology competition: The link between platforms and sociotechnical transitions. *Renewable and Sustainable Energy Reviews*, 73, 291–306. <https://doi.org/10.1016/j.rser.2017.01.146>
- Papaharalabos, G., Stinchcombe, A., Horsfield, I., Melhuish, C., Greenman, J., & Ieropoulos, I. (2017). Autonomous Energy Harvesting and Prevention of Cell Reversal in MFC Stacks. *Journal of The Electrochemical Society*, 164(3), 3047–3051. <https://doi.org/10.1149/2.0081703jes>
- Park, J. Do, & Ren, Z. (2012a). High efficiency energy harvesting from microbial fuel cells using a synchronous boost converter. *Journal of Power Sources*, 208, 322–327. <https://doi.org/10.1016/j.jpowsour.2012.02.035>
- Park, J. Do, & Ren, Z. (2012b). Hysteresis controller based maximum power point tracking energy harvesting system for microbial fuel cells. *Journal of Power Sources*, 205, 151–156. <https://doi.org/10.1016/j.jpowsour.2012.01.053>
- Pastor-Villegas, J., & Durán-Valle, C. J. (2002). Pore structure of activated carbons prepared by carbon dioxide and steam activation at different temperatures from extracted rockrose. *Carbon*, 40(3), 397–402. [https://doi.org/10.1016/S0008-6223\(01\)00118-X](https://doi.org/10.1016/S0008-6223(01)00118-X)
- Patake, V. D., Joshi, S. S., Lokhande, C. D., & Joo, O. S. (2009). Electrodeposited porous and amorphous copper oxide film for application in supercapacitor. *Materials Chemistry and Physics*, 114(1), 6–9. <https://doi.org/10.1016/j.matchemphys.2008.09.031>
- Patil, S. A., Hägerhäll, C., & Gorton, L. (2012). Electron transfer mechanisms between microorganisms and electrodes in bioelectrochemical systems. *Bioanalytical Reviews*, 4, 159–192. https://doi.org/10.1007/11663_2013_2x

- Peng, X., Yu, H., Wang, X., Zhou, Q., Zhang, S., Geng, L., ... Cai, Z. (2012). Enhanced performance and capacitance behavior of anode by rolling Fe₃O₄ into activated carbon in microbial fuel cells. *Bioresource Technology*, 121, 450–453. <https://doi.org/10.1016/j.biortech.2012.06.021>
- Peng, X., Yu, H., Yu, H., & Wang, X. (2013). Lack of anodic capacitance causes power overshoot in microbial fuel cells. *Bioresource Technology*, 138, 353–358. <https://doi.org/10.1016/j.biortech.2013.03.187>
- Pfeffer, C., Larsen, S., Song, J., Dong, M., Besenbacher, F., Meyer, R. L., ... Nielsen, L. P. (2012). Filamentous bacteria transport electrons over centimetre distances. *Nature*, 491(7423), 218–221. <https://doi.org/10.1038/nature11586>
- Pham, T. H., Aelterman, P., & Verstraete, W. (2009). Bioanode performance in bioelectrochemical systems: recent improvements and prospects. *Trends in Biotechnology*, 27(3), 168–178. <https://doi.org/10.1016/j.tibtech.2008.11.005>
- Pham, T. H., Rabaey, K., Aelterman, P., Clauwaert, P., De Schampelaire, L., Boon, N., & Verstraete, W. (2006). Microbial fuel cells in relation to conventional anaerobic digestion technology. *Engineering in Life Sciences*, 6(3), 285–292. <https://doi.org/10.1002/elsc.200620121>
- Phan, H., Yates, M. D., Kirchhofer, N. D., Bazan, G. C., Tender, L. M., & Nguyen, T.-Q. (2016). Biofilm as a redox conductor: a systematic study of the moisture and temperature dependence of its electrical properties. *Phys. Chem. Chem. Phys*, 18, 17815–17821. <https://doi.org/10.1039/c6cp03583c>
- Philamore, H., Rossiter, J., Stinchcombe, A., & Ieropoulos, I. (2015). Row-bot: An energetically autonomous artificial water boatman. *International Conference on Intelligent Robots and Systems (IROS)*, 3888–3893. <https://doi.org/10.1109/IROS.2015.7353924>
- Phoenix, V. R., & Holmes, W. M. (2008). Magnetic resonance imaging of structure, diffusivity, and copper immobilization in a phototrophic biofilm. *Applied and Environmental Microbiology*, 74(15), 4934–4943. <https://doi.org/10.1128/AEM.02783-07>
- Picot, M., Lapinonnière, L., Rothballer, M., & Barrière, F. (2011). Graphite anode surface modification with controlled reduction of specific aryl diazonium salts for improved microbial fuel cells power output. *Biosensors and Bioelectronics*, 28(1), 181–188. <https://doi.org/10.1016/j.bios.2011.07.017>
- Pinto, R. P., Srinivasan, B., Guiot, S. R., & Tartakovsky, B. (2011). The effect of real-time external resistance optimization on microbial fuel cell performance. *Water Research*, 45, 1571–1578. <https://doi.org/10.1016/j.watres.2010.11.033>
- Potter, M. C. (1911). Electrical Effects Accompanying the Decomposition of Organic Compounds the Decomposition Electrical Effects accompanying of Organic the fermentative activity of yeast and other organisms . Cultures of. *Proceedings of the Royal Society of London*, 84(571), 260–276.

Q

- Qu, D., & Shi, H. (1998). Studies of the activated carbons used in double-layer supercapacitors. *Journal of Power Sources*, 74(1), 99–107.
[https://doi.org/10.1016/S0378-7753\(02\)00108-8](https://doi.org/10.1016/S0378-7753(02)00108-8)
- Quast, C., Pruesse, E., Yilmaz, P., Gerken, J., Schweer, T., Yarza, P., ... Glöckner, F. O. (2013). The SILVA ribosomal RNA gene database project: Improved data processing and web-based tools. *Nucleic Acids Research*, 41(D1), 590–596.
<https://doi.org/10.1093/nar/gks1219>

R

- Rabaey, K. (2009). Bioelectrochemical Systems: From Extracellular Electron Transfer to Biotechnological Application. *Water Intelligence Online*, 8, 1–488.
<https://doi.org/10.2166/9781780401621>
- Rabaey, K., Clauwaert, P., Aelterman, P., & Verstraete, W. (2005). Tubular microbial fuel cells for efficient electricity generation. *Environmental Science and Technology*, 39(20), 8077–8082. <https://doi.org/10.1021/es050986i>
- Rabaey, K., & Rozendal, R. A. (2010). Microbial electrosynthesis - revisiting the electrical route for microbial production. *Nature Reviews. Microbiology*, 8(10), 706–716.
<https://doi.org/10.1038/nrmicro2422>
- Rabaey, K., & Verstraete, W. (2005). Microbial fuel cells: Novel biotechnology for energy generation. *Trends in Biotechnology*, 23(6), 291–298.
<https://doi.org/10.1016/j.tibtech.2005.04.008>
- Ramanan, B., Holmes, W. M., Sloan, W. T., & Phoenix, V. R. (2010). Application of Paramagnetically Tagged Molecules for Magnetic Resonance Imaging of Biofilm Mass Transport Processes □, 76(12), 4027–4036.
<https://doi.org/10.1128/AEM.03016-09>
- Ramanan, B., Holmes, W. M., Sloan, W. T., & Phoenix, V. R. (2013). Magnetic resonance imaging of mass transport and structure inside a phototrophic biofilm. *Current Microbiology*, 66(5), 456–461. <https://doi.org/10.1007/s00284-012-0292-3>
- Ranzinger, F., Herrling, M. P., Lackner, S., Grande, V. W., Baniodeh, A., Powell, A. K., ... Guthausen, G. (2016). Direct surface visualization of biofilms with high spin coordination clusters using Magnetic Resonance Imaging. *Acta Biomaterialia*, 31, 167–177. <https://doi.org/10.1016/j.actbio.2015.12.007>
- Reguera, G., McCarthy, K. D., Mehta, T., Nicoll, J. S., Tuominen, M. T., & Lovley, D. R. (2005). Extracellular electron transfer via microbial nanowires. *Nature*, 435(7045), 1098–1101. <https://doi.org/10.1038/nature03661>
- Reguera, G., Nevin, K. P., Nicoll, J. S., Covalla, S. F., Woodard, T. L., & Lovley, D. R. (2006). Biofilm and nanowire production leads to increased current in *Geobacter sulfurreducens* fuel cells. *Applied and Environmental Microbiology*, 72(11), 7345–7348. <https://doi.org/10.1128/AEM.01444-06>

- Ren, H., Pyo, S., Lee, J.-I. I., Park, T.-J. J., Gittleson, F. S., Leung, F. C. C. C., ... Chae, J. (2015). A high power density miniaturized microbial fuel cell having carbon nanotube anodes. *Journal of Power Sources*, 273, 823–830. Retrieved from <https://www.sciencedirect.com/science/article/pii/S0378775314015845>
- Ren, S., Xia, X., Yuan, L., Liang, P., & Huang, X. (2013). Enhancing charge harvest from microbial fuel cells by controlling the charging and discharging frequency of capacitors. *Bioresource Technology*, 146, 812–815. <https://doi.org/10.1016/j.biortech.2013.08.055>
- Renslow, R. S., Babauta, J. T., Dohnalkova, A., Boyanov, M. I., Kemner, K. M., Majors, P. D., ... Beyenal, H. (2013). Metabolic spatial variability in electrode-respiring *Geobacter sulfurreducens* biofilms. *Energy & Environmental Science*, 6(6), 1827–1836. <https://doi.org/10.1039/C3EE40203G>
- Renslow, R. S., Babauta, J. T., Majors, P. D., & Beyenal, H. (2013). Diffusion in biofilms respiring on electrodes. *Energy & Environmental Science*, 6(2), 595–607. <https://doi.org/10.1039/c2ee23394k>
- Renslow, R. S., Babauta, J. T., Majors, P. D., Mehta, H. S., Ewing, R. J., Ewing, T. W., ... Beyenal, H. (2014). A biofilm microreactor system for simultaneous electrochemical and nuclear magnetic resonance techniques. *Water Science & Technology*, 69(5), 966–973. <https://doi.org/10.2166/wst.2013.802>
- Renslow, R. S., Majors, P. D., McLean, J. S., Fredrickson, J. K., Ahmed, B., & Beyenal, H. (2010). In situ effective diffusion coefficient profiles in live biofilms using pulsed-field gradient nuclear magnetic resonance. *Biotechnology and Bioengineering*, 106(6), 928–937. <https://doi.org/10.1002/bit.22755>
- Rodenas Motos, P., Molina, G., ter Heijne, A., Sleutels, T., Saakes, M., & Buisman, C. (2017). Prototype of a scaled-up microbial fuel cell for copper recovery. *Journal of Chemical Technology and Biotechnology*, 92(11), 2817–2824. <https://doi.org/10.1002/jctb.5353>
- Rodenas Motos, P., ter Heijne, A., van der Weijden, R., Saakes, M., Buisman, C. J. N., & Sleutels, T. H. J. A. (2015). High rate copper and energy recovery in microbial fuel cells. *Frontiers in Microbiology*, 6, 1–8. <https://doi.org/10.3389/fmicb.2015.00527>
- Rodrigo-Quejigo, J., Rosa, L. F. M., & Harnisch, F. (2018). Electrochemical characterization of bed electrodes using voltammetry of single granules. *Electrochemistry Communications*, 90, 78–82. <https://doi.org/10.1016/j.elecom.2018.04.009>
- Rodríguez-Arredondo, M., Kuntke, P., Jeremiasse, A. W., Sleutels, T. H. J. A., Buisman, C. J. N., & ter Heijne, A. (2015). Bioelectrochemical systems for nitrogen removal and recovery from wastewater. *Environ. Sci.: Water Res. Technol.*, 1(1), 22–33. <https://doi.org/10.1039/C4EW00066H>
- Rossi, R., Jones, D., Myung, J., Zikmund, E., Yang, W., Gallego, Y. A., ... Logan, B. E. (2019). Evaluating a multi-panel air cathode through electrochemical and biotic tests. *Water Research*, 148, 51–59. <https://doi.org/10.1016/j.watres.2018.10.022>

- Rotaru, A. E., Shrestha, P. M., Liu, F., Markovaite, B., Chen, S., Nevin, K. P., & Lovley, D. R. (2014). Direct interspecies electron transfer between *Geobacter metallireducens* and *Methanosarcina barkeri*. *Applied and Environmental Microbiology*, 80(15), 4599–4605. <https://doi.org/10.1128/AEM.00895-14>
- Rotaru, A. E., Shrestha, P. M., Liu, F., Shrestha, M., Shrestha, D., Embree, M., ... Lovley, D. R. (2014). A new model for electron flow during anaerobic digestion: direct interspecies electron transfer to *Methanosaeta* for the reduction of carbon dioxide to methane. *Energy and Environmental Science*, 7(1), 408–415. <https://doi.org/10.1039/c3ee42189a>
- Rozendal, R. A., Hamelers, H. V. M., Rabaey, K., Keller, J., & Buisman, C. J. N. (2008). Towards practical implementation of bioelectrochemical wastewater treatment. *Trends in Biotechnology*, 26(8), 450–459. <https://doi.org/10.1016/j.tibtech.2008.04.008>

S

- Saba, B., Christy, A. D., Yu, Z., Co, A. C., Islam, R., & Tuovinen, O. H. (2017). Characterization and performance of anodic mixed culture biofilms in submersed microbial fuel cells. *Bioelectrochemistry*, 113, 79–84. <https://doi.org/10.1016/j.bioelechem.2016.10.003>
- Salunkhe, R. R., Kaneti, Y. V., & Yamauchi, Y. (2017). Metal–Organic Framework-Derived Nanoporous Metal Oxides toward Supercapacitor Applications: Progress and Prospects. *ACS Nano*, 11, 5293–5308. <https://doi.org/10.1021/acsnano.7b02796>
- Santini, M. ;, Guilizzone, M. ;, Lorenzi, M. ;, Atanassov, P. ;, Marsili, E. ;, Fest-Santini, S. ;, ... Santoro, C. (2015). Three-dimensional X-ray microcomputed tomography of carbonates and biofilm on operated cathode in single chamber microbial fuel cell. *Biointerphases*, 10(3), 1–9. <https://doi.org/10.1116/1.4930239>
- Santoro, C., Arbizzani, C., Erable, B., & Ieropoulos, I. (2017). Microbial fuel cells: From fundamentals to applications. A review. *Journal of Power Sources*, 356(March), 225–244. <https://doi.org/10.1016/j.jpowsour.2017.03.109>
- Santoro, C., Babanova, S., Erable, B., Schuler, A., & Atanassov, P. (2016). Bilirubin oxidase based enzymatic air-breathing cathode: Operation under pristine and contaminated conditions. *Bioelectrochemistry*, 108, 1–7. <https://doi.org/10.1016/J.BIOELECTCHEM.2015.10.005>
- Santoro, C., Guilizzone, M., Correa Baena, J. P., Pasaogullari, U., Casalegno, A., Li, B., ... Atanassov, P. (2014). The effects of carbon electrode surface properties on bacteria attachment and start up time of microbial fuel cells. *Carbon*, 67, 128–139. <https://doi.org/10.1016/j.carbon.2013.09.071>
- Santoro, C., Kodali, M., Kabir, S., Soavi, F., Serov, A., & Atanassov, P. (2017). Three-dimensional graphene nanosheets as cathode catalysts in standard and supercapacitive microbial fuel cell. *Journal of Power Sources*, 356, 371–380. <https://doi.org/10.1016/j.jpowsour.2017.03.135>

- Santoro, C., Kodali, M., Shamoan, N., Serov, A., Soavi, F., Merino-Jimenez, I., ... Atanassov, P. (2019). Increased power generation in supercapacitive microbial fuel cell stack using Fe N C cathode catalyst. *Journal of Power Sources*, 412, 416–424. <https://doi.org/10.1016/j.jpowsour.2018.11.069>
- Santoro, C., Serov, A., Stariha, L., Kodali, M., Gordon, J., Babanova, S., ... Atanassov, P. (2016). Iron based catalysts from novel low-cost organic precursors for enhanced oxygen reduction reaction in neutral media microbial fuel cells. *Energy & Environmental Science*, 9(7), 2346–2353. <https://doi.org/10.1039/C6EE01145D>
- Santoro, C., Soavi, F., Serov, A., Arbizzani, C., & Atanassov, P. (2015). Self-powered supercapacitive microbial fuel cell: The ultimate way of boosting and harvesting power. *Biosensors and Bioelectronics*, 78, 229–235. <https://doi.org/10.1016/j.bios.2015.11.026>
- Satoh, H., Miura, Y., Tsushima, I., & Okabe, S. (2007). Layered structure of bacterial and archaeal communities and their in situ activities in anaerobic granules. *Applied and Environmental Microbiology*, 73(22), 7300–7307. <https://doi.org/10.1128/AEM.01426-07>
- Savéant, J. M. (1986). Electron hopping between fixed sites- Equivalent diffusion and migration laws. *J. Electroanal. Chem*, 201, 211–213.
- Schindelin, J., Arganda-Carreras, I., Frise, E., Kaynig, V., Longair, M., Pietzsch, T., ... Schmid, B. (2012). Fiji: An open-source platform for biological-image analysis. *Nature Methods*, 9(7), 676.
- Schink, B., & Stams, A. J. M. (2006). Syntrophism among Prokaryotes. *The Prokaryotes*, 2, 309–335. <https://doi.org/10.1007/0-387-30742-7>
- Schmid, B., Schindelin, J., Cardona, A., Longair, M., & Heisenberg, M. (2010). A high-level 3D visualization API for Java and ImageJ. *BMC Bioinformatics*, 11(1), 274.
- Schmidt, J. E., & Ahring, B. K. (1996). Granular sludge formation in upflow anaerobic sludge blanket (UASB) reactors. *Biotechnology and Bioengineering*, 49(4), 229–246.
- Schröder, U. (2007). Anodic electron transfer mechanisms in microbial fuel cells and their energy efficiency. *Phys. Chem. Chem. Phys.*, 9(21), 2619–2629. <https://doi.org/10.1039/B703627M>
- Seymour, J. D., Codd, S. L., Gjersing, E. L., & Stewart, P. S. (2004). Magnetic resonance microscopy of biofilm structure and impact on transport in a capillary bioreactor. *Journal of Magnetic Resonance*, 167(2), 322–327. <https://doi.org/10.1016/j.jmr.2004.01.009>
- Shantaram, A., Beyenal, H., Veluchamy, R. R. A., & Lewandowski, Z. (2005). Wireless Sensors Powered by Microbial Fuel Cells. *Environmental Science & Technology*, 39(13), 5037–5042. <https://doi.org/10.1021/es0480668>
- Sharma, P., & Bhatti, T. S. (2010). A review on electrochemical double-layer capacitors. *Energy Conversion and Management*, 51(12), 2901–2912. <https://doi.org/10.1016/j.enconman.2010.06.031>
- Shimoyama, T., Komukai, S., Yamazawa, A., Ueno, Y., Logan, B. E., & Watanabe, K.

- (2008). Electricity generation from model organic wastewater in a cassette-electrode microbial fuel cell. *Applied Microbiology and Biotechnology*, 80(2), 325–330. <https://doi.org/10.1007/s00253-008-1516-0>
- Shin, S. H., Choi, Y., Na, S. H., Jung, S., & Kim, S. (2006). Development of bipolar plate stack type microbial fuel cells. *Bulletin of the Korean Chemical Society*, 27(2), 281–285. <https://doi.org/10.5012/bkcs.2006.27.2.281>
- Shrestha, P. M., Malvankar, N. S., Werner, J. J., Franks, A. E., Elena-Rotaru, A., Shrestha, M., ... Lovley, D. R. (2014). Correlation between microbial community and granule conductivity in anaerobic bioreactors for brewery wastewater treatment. *Bioresource Technology*, 174, 306–310. <https://doi.org/10.1016/j.biortech.2014.10.004>
- Shrestha, P. M., Rotaru, A.-E., Aklujkar, M., Liu, F., Shrestha, M., Summers, Z. M., ... Lovley, D. R. (2013). Syntrophic growth with direct interspecies electron transfer as the primary mechanism for energy exchange. *Environmental Microbiology Reports*, 5(6), 904–910. <https://doi.org/10.1111/1758-2229.12093>
- Sieber, J. R., McInerney, M. J., & Gunsalus, R. P. (2012). Genomic insights into syntrophy: the paradigm for anaerobic metabolic cooperation. *Annual Review of Microbiology*, 66(1), 429–452. <https://doi.org/10.1146/annurev-micro-090110-102844>
- Slate, A. J., Whitehead, K. A., Brownson, D. A. C., & Banks, C. E. (2019). Microbial fuel cells: An overview of current technology. *Renewable and Sustainable Energy Reviews*, 101, 60–81. <https://doi.org/10.1016/j.rser.2018.09.044>
- Sleutels, T. H. J. A., Darus, L., Hamelers, H. V. M., & Buisman, C. J. N. (2011). Effect of operational parameters on Coulombic efficiency in bioelectrochemical systems. *Bioresource Technology*, 102(24), 11172–11176. <https://doi.org/10.1016/j.biortech.2011.09.078>
- Sleutels, T. H. J. A., Hamelers, H. V. M., Rozendal, R. A., & Buisman, C. J. N. (2009). Ion transport resistance in Microbial Electrolysis Cells with anion and cation exchange membranes. *International Journal of Hydrogen Energy*, 34(9), 3612–3620. <https://doi.org/10.1016/j.ijhydene.2009.03.004>
- Sleutels, T. H. J. A., Molenaar, S., Heijne, A., & Buisman, C. J. N. (2016). Low Substrate Loading Limits Methanogenesis and Leads to High Coulombic Efficiency in Bioelectrochemical Systems. *Microorganisms*, 4(1), 1–11. <https://doi.org/10.3390/microorganisms4010007>
- Sleutels, T. H. J. A., Ter Heijne, A., Buisman, C. J. N., & Hamelers, H. V. M. (2012). Bioelectrochemical systems: An outlook for practical applications. *ChemSusChem*, 5(6), 1012–1019. <https://doi.org/10.1002/cssc.201100732>
- Soavi, F., Giacomo Bettini, L., Piseri, P., Milani, P., Santoro, C., Atanassov, P., & Arbizzani, C. (2016). Miniaturized supercapacitors: key materials and structures towards autonomous and sustainable devices and systems. *Journal of Power Sources*, 326, 717–725. <https://doi.org/10.1016/j.jpowsour.2016.04.131>
- Stams, A. J. M., de Bok, F. A. M., Plugge, C. M., van Eekert, M. H. A., Dolfig, J., & Schraa, G. (2006). Exocellular electron transfer in anaerobic microbial communities.

- Environmental Microbiology*, 8(3), 371–382. <https://doi.org/10.1111/j.1462-2920.2006.00989.x>
- Stams, A. J. M., & Plugge, C. M. (2009). Electron transfer in syntrophic communities of anaerobic bacteria and archaea. *Nature Reviews Microbiology*, 7(8), 568–577. <https://doi.org/10.1038/nrmicro2166>
- Stams, A. J. M., Sousa, D. Z., Kleerebezem, R., & Plugge, C. M. (2012). Role of syntrophic microbial communities in high-rate methanogenic bioreactors. *Water Science and Technology: A Journal of the International Association on Water Pollution Research*, 66(2), 352–362. <https://doi.org/10.2166/wst.2012.192>
- Stoll, Z. A., Forrestal, C., Jason Ren, Z., & Xu, P. (2015). Shale gas produced water treatment using innovative microbial capacitive desalination cell. *Journal of Hazardous Materials*, 283, 847–855. <https://doi.org/10.1016/j.jhazmat.2014.10.015>
- Summers, Z. M., Fogarty, H. E., Leang, C., Franks, A. E., Malvankar, N. S., & Lovley, D. R. (2010). Direct exchange of electrons within aggregates of an evolved syntrophic coculture of anaerobic bacteria. *Science (New York, N.Y.)*, 330(6009), 1413–1415. <https://doi.org/10.1126/science.1196526>
- Sun, D., Chen, J., Huang, H., Liu, W., Ye, Y., & Cheng, S. (2016). The effect of biofilm thickness on electrochemical activity of *Geobacter sulfurreducens*. *International Journal of Hydrogen Energy*, 41(37), 16523–16528. <https://doi.org/10.1016/j.ijhydene.2016.04.163>

T

- Takahashi, S., Tomita, J., Nishioka, K., Hisada, T., & Nishijima, M. (2014). Development of a Prokaryotic Universal Primer for Simultaneous Analysis of Bacteria and Archaea Using Next-Generation Sequencing. *PLoS ONE*, 9(8), e105592. <https://doi.org/10.1371/journal.pone.0105592>
- Takashima, M., Speece, R. E., & Parkin, G. F. (1990). Mineral requirements for methane fermentation. *Critical Reviews in Environmental Control*, 19(5), 465–479. <https://doi.org/10.1080/10643389009388378>
- Tchobanoglous, G., & Burton, F. L. (1991). *Wastewater engineering : treatment, disposal, and reuse* (3rd ed.). McGraw-Hill International Editions.
- Tejedor-Sanz, S., Ortiz, J. M., & Esteve-Núñez, A. (2017). Merging microbial electrochemical systems with electrocoagulation pretreatment for achieving a complete treatment of brewery wastewater. *Chemical Engineering Journal*, 330, 1068–1074. <https://doi.org/10.1016/j.cej.2017.08.049>
- Tejedor-Sanz, S., Quejigo, J. R., Berná, A., & Esteve-Núñez, A. (2017). The Planktonic Relationship Between Fluid-Like Electrodes and Bacteria: Wiring in Motion. *ChemSusChem*, 10(4), 693–700. <https://doi.org/10.1002/cssc.201601329>
- Tender, L. M., Gray, S. A., Groveman, E., Lowy, D. A., Kauffman, P., Melhado, J., ... Dobarro, J. (2008). The first demonstration of a microbial fuel cell as a viable power

- supply: Powering a meteorological buoy. *Journal of Power Sources*, 179(2), 571–575. <https://doi.org/10.1016/j.jpowsour.2007.12.123>
- Ter Heijne, A., Liu, F., Van Rijnsoever, L. S., Saakes, M., Hamelers, V. M., & Buisman, C. J. N. (2011). Performance of a scaled-up Microbial Fuel Cell with iron reduction as the cathode reaction. *Journal of Power Sources*, 196, 7572–7577. <https://doi.org/10.1016/j.jpowsour.2011.04.034>
- Ter Heijne, A., Schaetzle, O., Gimenez, S., Navarro, L., Hamelers, B., & Fabregat-Santiago, F. (2015). Analysis of bio-anode performance through electrochemical impedance spectroscopy. *Bioelectrochemistry*, 106, 64–72. <https://doi.org/10.1016/j.bioelechem.2015.04.002>
- Teravest, M. A., & Angenent, L. T. (2014). Oxidizing Electrode Potentials Decrease Current Production and Coulombic Efficiency through Cytochrome c Inactivation in *Shewanella oneidensis* MR-1. *ChemElectroChem*, 1(11), 2000–2006. <https://doi.org/10.1002/celec.201402128>
- Tomić, T., & Schneider, D. R. (2018). The role of energy from waste in circular economy and closing the loop concept – Energy analysis approach. *Renewable and Sustainable Energy Reviews*, 98, 268–287. <https://doi.org/10.1016/j.rser.2018.09.029>
- Tran, H. T., Ryu, J. H., Jia, Y. H., Oh, S. J., Choi, J. Y., Park, D. H., & Ahn, D. H. (2010). Continuous bioelectricity production and sustainable wastewater treatment in a microbial fuel cell constructed with non-catalyzed granular graphite electrodes and permeable membrane. *Water Science & Technology*, 1819–1827. <https://doi.org/10.2166/wst.2010.140>
- Tsao, J., & Kozerke, S. (2012). MRI temporal acceleration techniques. *Journal of Magnetic Resonance Imaging*, 36(3), 543–560.

V

- Valladares Linares, R., Fortunato, L., Farhat, N. M., Bucs, S. S., Staal, M., Fridjonsson, E. O., ... Leiknes, T. (2016). Mini-review: novel non-destructive in situ biofilm characterization techniques in membrane systems. *Desalination and Water Treatment*, 57(48–49), 22894–22901. <https://doi.org/10.1080/19443994.2016.1180483>
- Van As, H., & Lens, P. (2001). Use of ¹H NMR to study transport processes in porous biosystems. *Journal of Industrial Microbiology and Biotechnology*, 26(1), 43–52. <https://doi.org/10.1038/sj.jim.7000087>
- Van Eerten-Jansen, M. C. A. A., Ter Heijne, A., Buisman, C. J. N., & Hamelers, H. V. M. (2012). Microbial electrolysis cells for production of methane from CO₂: long-term performance and perspectives. *International Journal of Energy Research*, 36, 809–819. <https://doi.org/10.1002/er>
- Van Eerten-Jansen, M. C. A. A., Veldhoen, A. B., Plugge, C. M., Stams, A. J. M., Buisman, C. J. N., & Ter Heijne, A. (2013). Microbial community analysis of a

- methane-producing biocathode in a bioelectrochemical system. *Archaea*, 2013, 1–12. <https://doi.org/10.1155/2013/481784>
- Van Ginkel, S. W., Oh, S.-E., & Logan, B. E. (2005). Biohydrogen gas production from food processing and domestic wastewaters. *International Journal of Hydrogen Energy*, 30, 1535–1542. <https://doi.org/10.1016/j.ijhydene.2004.09.017>
- Van Lier, J. B. (2008). High-rate anaerobic wastewater treatment: diversifying from end-of-the-pipe treatment to resource-oriented conversion techniques. *Water Science & Technology*, 1137–1147. <https://doi.org/10.2166/wst.2008.040>
- Van Lier, J. B., Mahmoud, N., & Zeeman, G. (2008). Anaerobic Wastewater Treatment. In *Biological wastewater treatment: principles, modelling and design* (pp. 401–442).
- Villano, M., Aulenta, F., Ciucci, C., Ferri, T., Giuliano, A., & Majone, M. (2010). Bioelectrochemical reduction of CO₂ to CH₄ via direct and indirect extracellular electron transfer by a hydrogenophilic methanogenic culture. *Bioresource Technology*, 101, 3085–3090. <https://doi.org/10.1016/j.biortech.2009.12.077>

W

- Walter, X. A., Greenman, J., & Ieropoulos, I. A. (2014). Intermittent load implementation in microbial fuel cells improves power performance. *Bioresource Technology*, 172, 365–372. <https://doi.org/10.1016/j.biortech.2014.09.034>
- Walters, P., Lewis, A., Stinchcombe, A., Stephenson, R., & Ieropoulos, I. (2013). Artificial heartbeat: design and fabrication of a biologically inspired pump. *Bioinspiration & Biomimetics*, 8(4), 046012. <https://doi.org/10.1088/1748-3182/8/4/046012>
- Wang, H., Park, J. Do, & Ren, Z. J. (2012). Active energy harvesting from microbial fuel cells at the maximum power point without using resistors. *Environmental Science and Technology*, 46(9), 5247–5252. <https://doi.org/10.1021/es300313d>
- Wang, H., Park, J. Do, & Ren, Z. J. (2015). Practical Energy Harvesting for Microbial Fuel Cells: A Review. *Environmental Science & Technology*, 49(6), 3267–3277. <https://doi.org/10.1021/es5047765>
- Wang, J., & Kaskel, S. (2012). KOH activation of carbon-based materials for energy storage. *Journal of Materials Chemistry*, 22(45), 23710–23725. <https://doi.org/10.1039/c2jm34066f>
- Wang, Q., Garrity, G. M., Tiedje, J. M., & Cole, J. R. (2007). Naïve Bayesian classifier for rapid assignment of rRNA sequences into the new bacterial taxonomy. *Applied and Environmental Microbiology*, 73(16), 5261–5267. <https://doi.org/10.1128/AEM.00062-07>
- Wang, X., Yue, X., & Guo, Q. (2014). Production of Electricity during Wastewater Treatment Using Fluidized-Bed Microbial Fuel Cells. *Chemical Engineering & Technology*, 37(4), 703–708. <https://doi.org/10.1002/ceat.201300241>
- Wang, Y., Chen, Y., & Wen, Q. (2018). Microbial fuel cells: enhancement with a polyaniline/carbon felt capacitive bioanode and reduction of Cr(VI) using the intermittent operation. *Environmental Chemistry Letters*, 16, 319–326.

- <https://doi.org/10.1007/s10311-017-0678-3>
- Wang, Y., Wen, Q., Chen, Y., Yin, J., & Duan, T. (2016). Enhanced Performance of a Microbial Fuel Cell with a Capacitive Bioanode and Removal of Cr (VI) Using the Intermittent Operation. *Applied Biochemistry and Biotechnology*, 180, 1372–1385. <https://doi.org/10.1007/s12010-016-2173-x>
- Wang, Z., Cao, C., Zheng, Y., Chen, S., & Zhao, F. (2014). Abiotic Oxygen Reduction Reaction Catalysts Used in Microbial Fuel Cells. *ChemElectroChem*, 1(11), 1813–1821. <https://doi.org/10.1002/celec.201402093>
- Webb, P. A. (2001a). *An introduction to the physical characterization of materials by mercury intrusion porosimetry with emphasis on reduction and presentation of experimental data*. Micromeritics Instrument Corp. Retrieved from <https://www.micromeritics.com/>
- Webb, P. A. (2001b). *Volume and Density Determinations for Particle Technologists*. Retrieved from <https://www.micromeritics.com>
- Wegener, G., Krukenberg, V., Riedel, D., Tegetmeyer, H. E., & Boetius, A. (2015). Intercellular wiring enables electron transfer between methanotrophic archaea and bacteria. *Nature*, 526(7574), 587–590. <https://doi.org/10.1038/nature15733>
- Wei, J., Liang, P., & Huang, X. (2011). Recent progress in electrodes for microbial fuel cells. *Bioresource Technology*, 102(20), 9335–9344. <https://doi.org/10.1016/j.biortech.2011.07.019>
- Wei, L., & Yushin, G. (2011). Electrical double layer capacitors with activated sucrose-derived carbon electrodes. *Carbon*, 49(14), 4830–4838. <https://doi.org/10.1016/j.carbon.2011.07.003>
- Westbrook, C., & Talbot, J. (2018). *MRI in Practice*. John Wiley & Sons.
- Wieland, A., de Beer, D., van Dusschoten, D., Damgaard, L. R., Kuehl, M., & van As, H. (2001). Fine-scale measurement of diffusivity in a microbial mat with NMR imaging. *Limnol. Oceanogr.*, 44(3), 248–259.
- Wielemaker, R. C., Weijma, J., & Zeeman, G. (2018). Harvest to harvest: Recovering nutrients with New Sanitation systems for reuse in Urban Agriculture. *Resources, Conservation and Recycling*, 128, 426–437. <https://doi.org/10.1016/J.RESCONREC.2016.09.015>
- Wilkinson, S. (2000). “Gastrobots” - benefits and challenges of microbial fuel cells in food powered robot applications. *Autonomous Robots*, 9(2), 99–111. <https://doi.org/10.1023/A:1008984516499>
- Wu, S., Liang, P., Zhang, C., Li, H., Zuo, K., & Huang, X. (2015). Enhanced performance of microbial fuel cell at low substrate concentrations by adsorptive anode. *Electrochimica Acta*, 161, 245–251. <https://doi.org/10.1016/j.electacta.2015.02.028>

X

- Xi, C., Marks, D., Schlachter, S., Luo, W., & Boppart, S. A. (2006). High-resolution three-

- dimensional imaging of biofilm development using optical coherence tomography. *Journal of Biomedical Optics*, 11(3), 034001. <https://doi.org/10.1117/1.2209962>
- Xu, S., He, C., Luo, L., Lü, F., He, P., & Cui, L. (2015). Comparing activated carbon of different particle sizes on enhancing methane generation in upflow anaerobic digester. *Bioresource Technology*, 196, 606–612. <https://doi.org/10.1016/j.biortech.2015.08.018>

Y

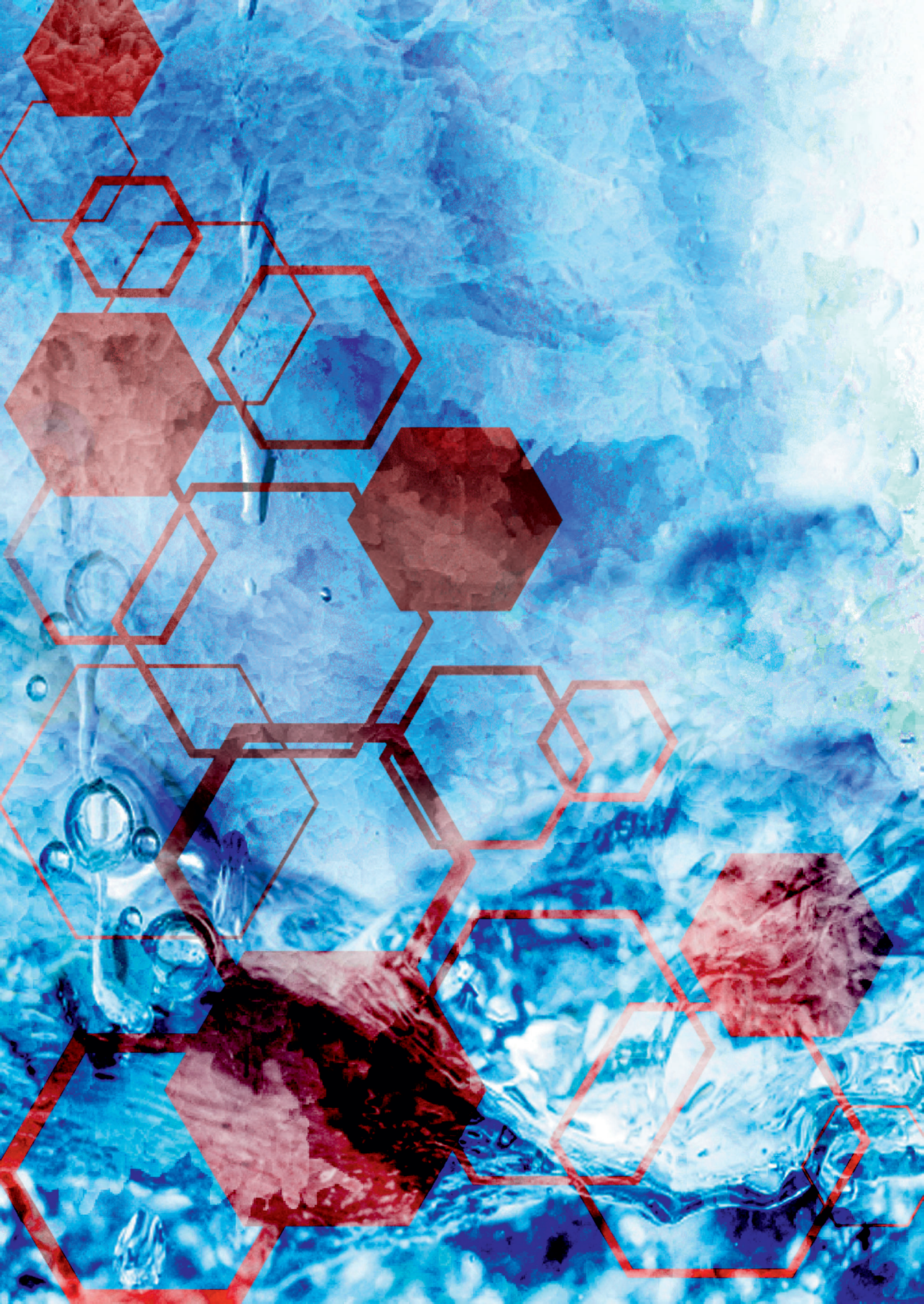
- Yang, W., & Logan, B. E. (2016). Immobilization of a Metal-Nitrogen-Carbon Catalyst on Activated Carbon with Enhanced Cathode Performance in Microbial Fuel Cells. *ChemSusChem*, 9(16), 2226–2232. <https://doi.org/10.1002/cssc.201600573>
- Yassine, M., & Fabris, D. (2017). Performance of commercially available supercapacitors. *Energies*, 10(9). <https://doi.org/10.3390/en10091340>
- Yates, M. D., Eddie, B. J., Kotloski, N. J., Lebedev, N., Malanoski, A. P., Lin, B., ... Tender, L. M. (2016). Toward understanding long-distance extracellular electron transport in an electroautotrophic microbial community. *Energy & Environmental Science*, 9(11), 3544–3558. <https://doi.org/10.1039/C6EE02106A>
- Yin, Q., Miao, J., Li, B., & Wu, G. (2017). Enhancing electron transfer by ferroferric oxide during the anaerobic treatment of synthetic wastewater with mixed organic carbon. *International Biodeterioration and Biodegradation*, 119, 104–110. <https://doi.org/10.1016/j.ibiod.2016.09.023>
- Yoho, R. A., Popat, S. C., Fabregat-Santiago, F., Giménez, S., ter Heijne, A., & Torres, C. I. (2015). Electrochemical impedance spectroscopy as a powerful analytical tool for the study of microbial electrochemical cells. In *Biofilms in Bioelectrochemical Systems: From Laboratory Practice to Data Interpretation* (pp. 249–280). John Wiley & Sons, Inc. Retrieved from <https://onlinelibrary.wiley.com/doi/pdf/10.1002/9781119097426.ch8>
- Younggy, K., Hatzell, M. C., Hutchinson, A. J., & Logan, B. E. (2011). Capturing power at higher voltages from arrays of microbial fuel cells without voltage reversal. *Energy and Environmental Science*, 4(11), 4662–4667. <https://doi.org/10.1039/c1ee02451e>
- Yuan, H., Hou, Y., Abu-Reesh, I. M., Chen, J., & He, Z. (2016). Oxygen reduction reaction catalysts used in microbial fuel cells for energy-efficient wastewater treatment: a review. *Materials Horizons*, 3(5), 382–401. <https://doi.org/10.1039/c6mh00093b>

Z

- Zakaria, B. S., Barua, S., Sharaf, A., Liu, Y., & Dhar, B. R. (2018). Impact of antimicrobial silver nanoparticles on anode respiring bacteria in a microbial electrolysis cell. *Chemosphere*, 213, 259–267. <https://doi.org/10.1016/J.CHEMOSPHERE.2018.09.060>
- Zamora, P., Georgieva, T., Ter Heijne, A., Sleutels, T. H. J. A., Jeremiasse, A. W., Saakes,

- M., ... Kuntke, P. (2017). Ammonia recovery from urine in a scaled-up Microbial Electrolysis Cell. *Journal of Power Sources*, 356, 491–499.
<https://doi.org/10.1016/j.jpowsour.2017.02.089>
- Zeeman, G., & Kujawa-Roeleveld, K. (2011). Resource recovery from source separated domestic waste(water) streams; full scale results. *Water Science & Technology*, 64(10), 1987–1992. <https://doi.org/10.2166/wst.2011.562>
- Zhang, F., Tian, L., & He, Z. (2011). Powering a wireless temperature sensor using sediment microbial fuel cells with vertical arrangement of electrodes. *Journal of Power Sources*, 196, 9568–9573.
<https://doi.org/10.1016/j.jpowsour.2011.07.037>
- Zhang, J., & Lu, Y. (2016). Conductive Fe₃O₄ Nanoparticles Accelerate Syntrophic Methane Production from Butyrate Oxidation in Two Different Lake Sediments. *Frontiers in Microbiology*, 7(AUG), 1316.
<https://doi.org/10.3389/fmicb.2016.01316>
- Zhang, X., Prévosteau, A., Louro, R. O., Paquete, C. M., & Rabaey, K. (2018). Periodic polarization of electroactive biofilms increases current density and charge carriers concentration while modifying biofilm structure. *Biosensors and Bioelectronics*, 121(July), 183–191. <https://doi.org/10.1016/j.bios.2018.08.045>
- Zhang, Yan, Xiao, L., Liao, G., & Song, Y. Q. (2016). Direct correlation of diffusion and pore size distributions with low field NMR. *Journal of Magnetic Resonance*, 269, 196–202. <https://doi.org/10.1016/j.jmr.2016.06.013>
- Zhang, Yong, Feng, H., Wu, X., Wang, L., Zhang, A., Xia, T., ... Zhang, L. (2009). Progress of electrochemical capacitor electrode materials: A review. *International Journal of Hydrogen Energy*, 34, 4889–4899.
<https://doi.org/10.1016/j.ijhydene.2009.04.005>
- Zhao, Zhiqiang, Li, Y., Quan, X., & Zhang, Y. (2017). Towards engineering application: Potential mechanism for enhancing anaerobic digestion of complex organic waste with different types of conductive materials. *Water Research*, 115, 266–277.
- Zhao, Zhiqiang, Zhang, Y., Holmes, D. E., Dang, Y., Woodard, T. L., Nevin, K. P., & Lovley, D. R. (2016). Potential enhancement of direct interspecies electron transfer for syntrophic metabolism of propionate and butyrate with biochar in up-flow anaerobic sludge blanket reactors. *Bioresource Technology*, 209, 148–156.
<https://doi.org/10.1016/j.biortech.2016.03.005>
- Zhao, Zhiqiang, Zhang, Y., Wang, L., & Quan, X. (2015). Potential for direct interspecies electron transfer in an electric-anaerobic system to increase methane production from sludge digestion. *Scientific Reports*, 5(April), 1–12.
<https://doi.org/10.1038/srep11094>
- Zhao, Zhiqiang, Zhang, Y., Yu, Q., Dang, Y., Li, Y., & Quan, X. (2016). Communities stimulated with ethanol to perform direct interspecies electron transfer for syntrophic metabolism of propionate and butyrate. *Water Research*, 102, 475–484.
<https://doi.org/10.1016/j.watres.2016.07.005>

- Zhao, Zisheng, Zhang, Y., Quan, X., & Zhao, H. (2016). Evaluation on direct interspecies electron transfer in anaerobic sludge digestion of microbial electrolysis cell. *Bioresource Technology*, 200, 235–244.
<https://doi.org/10.1016/j.biortech.2015.10.021>
- Zhou, M., Chi, M., Luo, J., He, H., & Jin, T. (2011). An overview of electrode materials in microbial fuel cells. *Journal of Power Sources*, 196(10), 4427–4435.
<https://doi.org/10.1016/j.jpowsour.2011.01.012>
- Zhuang, L., Tang, J., Wang, Y., Hu, M., & Zhou, S. (2015). Conductive iron oxide minerals accelerate syntrophic cooperation in methanogenic benzoate degradation. *Journal of Hazardous Materials*, 293(808), 37–45.
<https://doi.org/10.1016/j.jhazmat.2015.03.039>



Summary

Resumen

Laburpena



Summary

Capacitive Microbial Fuel Cells

Wastewater represents a very suitable source for electricity production, as it contains compounds such as organics and nutrients (nitrogen, phosphate, potassium) that can be recovered or converted into valuable products (e.g. methane, chemicals). Wastewater needs to be treated before releasing it to the environment, as these compounds can cause problems like eutrophication (i.e. excess of algae growth). In this context, microbial fuel cell (MFC) is a carbon dioxide neutral, sustainable and efficient technology to recover electricity from organics in wastewater, thus making profit from a treatment process.

Microbial fuel cells consist of two compartments, an anode and a cathode, separated (optionally) by a membrane. In the anode, microorganisms known as electroactive bacteria oxidize the organics in the wastewater and produce electrons. These bacteria usually grow a biofilm on an electrode (conductive) surface forming the so-called bioanode. The electrons are then transferred from the anode to the cathode by an external circuit, where a reduction reaction occurs. The reduction reaction is usually the conversion of oxygen to water, but it can also occur through hydrogen production. In that latter case, an external load is needed. MFCs confer advantages over other wastewater treatment technologies; firstly, MFCs don't require aeration as in the aerobic treatment process, and secondly, MFCs can directly produce electricity rather than an intermediate product, such as methane in anaerobic digestion. However, currently the efficiencies of organic conversion into electricity are not high enough to make MFCs competitive at large-scale. The main reason for this is the energy losses due to high resistances in the system, which lead to low power outputs, and the high material cost (e.g. membrane, electrodes).

In this study, the concept of capacitive MFCs is presented, which differ from the classical MFCs. The main difference is on the use of capacitive electrodes that are conductive and highly porous. This porosity provides a large surface area for bacterial growth and allows the storage of electrons by forming the so-called electrical double-layer (EDL), i.e. a layer of negative and positive charges in the electrode/electrolyte (wastewater) interface.

The combination of EDL capacitors (EDLCs) and MFCs is thoughtfully addressed in **Chapter 2** of this thesis. EDLCs can be placed outside of the MFC or can be instead integrated by the use of capacitive electrodes, as previously mentioned. Charge storage on capacitive electrodes allows for a subsequent release at a higher current rate and less potential losses, which leads to higher power output. Moreover, it allows the separation of charge and discharge processes (i.e. intermittent operation mode), not only in time but also spatially, which can open new possibilities for reactor designs for wastewater treatment. In this way, the use of capacitive MFCs can bring the technology closer to application. Nevertheless, EDL formation is a complex process that depends on many parameters. Moreover, it is challenging to measure the storage capacity of an electrode, particularly

when this is combined with biofilm growth. Therefore, the study of capacitive electrodes in MFCs needs further research in future, and their application in other bioelectrochemical systems is yet to be discovered.

Granular Activated Carbon

Among capacitive electrodes, granular activated carbon (AC) has shown high potential, as it has a three-dimensional structure, it is biocompatible, it can be easily available and it is cheap. AC granules are already used in many reactor systems, such as fluidized bed reactors where a gas flow is utilized at high enough velocities to maintain the granules in suspension. When used to treat wastewater, AC granules are fluidized in the reactor while being charged by the electroactive bacteria, and they are discharged when touching the current collector. Because the performance of these fluidized bed reactors is still low in terms of current production, a fundamental study of AC granules is needed to better understand the chemical and physical processes occurring during charge/discharge cycles, as well as the interaction of the electrode material with the electroactive biofilm.

With this aim, the present work focuses on the study of single AC granules. In **Chapter 3**, the focus is put on investigating the effect of granule size and type, as we believe these are important design parameters to consider for up-scaled application purposes. In order to perform a comparative study on the effect of granule size and type and perform statistical analyses, it was crucial to design a configuration that allowed for simultaneous measurement and control of several (up to 24) single AC granules under the same operational conditions, in fact a multi-anode MFC. Regarding granule size, we showed that biofilm growth, which is measured as total nitrogen and current production, have a linear relationship to the calculated outer surface area of AC granules. Small AC granules led to higher volumetric current production, which are thus preferable for application over large granules. The granule size did not have much effect on charge storage, which again makes small granules preferable for higher volumetric performances. As for the granule type, two different AC granules were tested, commercially known as: PK, activated from peat, and GAC, activated from coal. Their specific surface area and pore size and distribution were slightly different, however, no significant effect on biofilm growth and charge storage could be seen. The fact that the granular bioanodes were controlled at a continuous potential and under similar conditions, seemed to be more determinant for their overall performance than the physical granule properties themselves.

Biofilm Growth and Electrical Conductivity

The interaction between biofilm and electrode is of utmost importance on the performance of an MFC. As previously mentioned, it has been shown that a larger electrode surface allows for more catalytic sites, which increase the electron transfer and thus current production of the bioanodes. In the case of AC granules, they have a very complex porous

structure that makes very challenging to determine what is the surface area being used by the bacteria. This is important when, for example, normalizing the current production to the electrode surface area or determining the total pore volume that bacteria could use to grow. With the aim of getting a closer look to the biofilm development on AC granules, a multi-anode MFC was also used (only with PK granules), where bioanodes were harvested at 10 different growth stages and visualized with magnetic resonance imaging (MRI), as explained in **Chapter 4**. Magnetic resonance imaging, unlike other microscopy techniques, can deliver high resolution 3D images of biofilm growing on a granular, rough, opaque and brittle electrode, as it is the case of AC granules. The experimental procedure used was optimized in order to differentiate between biofilm and granule phases and perform high resolution ($(28\ \mu\text{m})^3$) measurements in short times ($< 24\text{h}$). Even though MRI was proven to be a useful technique to visualize the biofilm in 3D non-invasively, the images did not allow to determine the biofilm-granule interface and bacterial growth on inner pores of the granule. Nevertheless, the obtained biofilm volume at different growth stages related linearly to the total produced charge (i.e. current) and the nitrogen content (i.e. biomass growth) of the granular bioanodes.

Apart from the biofilm interaction with the electrode, the mechanisms of electron transfer along biofilms has arisen multiple research questions. In electroactive biofilms, direct electron transfer is a well-known mechanism, which bacteria can carry out through conductive structures (pili/nanowires) or redox proteins like cytochromes. However, direct electron transfer has not only been found in electroactive biofilms but also in other biological niches (such as marine sediments) or in microbial aggregates (such as anaerobic granular sludge). By determining the electrical conductivity of these latter aggregates, their ability to transfer electrons can be evaluated. The only granular sludge from full-scale wastewater treatment reactors tested for conductivity in the literature is from breweries. Therefore, we screened the electrical conductivity of 28 anaerobic granular sludges from very varied full-scale wastewater treatment plants, as shown in **Chapter 5**. Results showed a large variability of conductivity, which demonstrated that anaerobic granular sludge from breweries and other alcohol production industries were not consistently conductive. Even though a positive correlation was found between electrical conductivity and the iron and sulphur concentrations measured in the granules, no relation was found with the microbial community, surface structure or other elements. Based on these results, we concluded that the variability and complexity of full-scale reactors made difficult elucidating the drivers for electrical conductivity of anaerobic granular sludge.

Resumen

Celdas de Combustible Microbianas Capacitivas

Las aguas residuales representan una fuente apropiada para la producción de electricidad, ya que contienen materia orgánica y nutrientes (nitrógeno, fosfato, potasio) que se pueden recuperar o convertir en productos valiosos como el metano u otros compuestos químicos de interés. Las aguas residuales deben tratarse antes de ser vertidas al medio ambiente, ya que el exceso de materia orgánica o nutrientes pueden causar problemas medioambientales como es el caso de la eutrofización (i.e. el exceso de crecimiento de algas). En este contexto, las celdas de combustible microbianas (CCMs) son una tecnología eficiente, sostenible y neutral en emisiones de dióxido de carbono, capaz de producir electricidad a partir de la materia orgánica presente en las aguas residuales y así obtener beneficios a través de su tratamiento.

Las CCMs constan de dos compartimentos, un ánodo y un cátodo, separados (opcionalmente) por una membrana. En el ánodo, los microorganismos también conocidos como bacterias electroactivas, oxidan la materia orgánica presente en las aguas residuales y producen electrones. Estas bacterias generalmente crean un biofilm en una superficie conductora (electrodo) que actúa como aceptor de sus electrones, formando lo denominado como un bioánodo. Los electrones se transfieren del ánodo al cátodo mediante un circuito externo. En el cátodo, ocurre una reacción de reducción que suele ser la conversión de oxígeno en agua. En caso de que la reacción de reducción sea la producción de hidrógeno, se necesitaría aplicar una corriente externa adicional. Las CCMs confieren ventajas sobre otras tecnologías de tratamiento de aguas residuales; en primer lugar, no requieren aireación como en el proceso de tratamiento de aguas aeróbico y, en segundo lugar, pueden producir electricidad de una forma directa en lugar de a través de un producto intermediario (como es el caso del metano en la digestión anaerobia). Sin embargo, en la actualidad, la eficiencia de conversión de materia orgánica en electricidad no es lo suficientemente alta como para que las CCMs sean competitivas a gran escala. La razón principal es la pérdida de energía debido a las altas resistencias dentro de las celdas que conducen a una baja potencia eléctrica, y los altos costes de material como puede ser el caso de las membranas o los electrodos.

En este estudio, presentamos el concepto de CCMs capacitivas que difieren de las CCM clásicas principalmente en el uso de electrodos capacitivos, los cuales a parte de ser conductores son altamente porosos. Esta porosidad proporciona una gran área de superficie para el crecimiento bacteriano y permite el almacenamiento de electrones formando la llamada doble capa eléctrica (EDL, por sus siglas en inglés), una capa de cargas negativas y positivas en la interfaz del electrodo y el electrolito (es decir, el agua residual).

La combinación entre CCMs y condensadores de doble capa eléctrica (EDLCs, por sus siglas en inglés) se aborda detalladamente en el **Capítulo 2** de esta tesis. Los

condensadores de doble capa eléctrica pueden colocarse fuera de las CCMs o, por el contrario, pueden integrarse mediante el uso de electrodos capacitivos como se ha mencionado anteriormente. El almacenamiento de carga eléctrica en los electrodos capacitivos permite una liberación posterior de la misma a una tasa de corriente más alta y con menos pérdidas de potencial, lo que conduce a una mayor potencia eléctrica. Además, permite la separación de procesos de carga y descarga (es decir, un modo de operación intermitente) no sólo a nivel temporal sino también a nivel espacial, lo cual puede conducir a nuevos diseños de reactores para el tratamiento de aguas residuales. De esta forma, el uso de CCMs capacitivas puede acercar más la tecnología hacia su aplicación. Sin embargo, la formación de la doble capa eléctrica es un proceso complejo que depende de muchos parámetros. Además, es un desafío medir la capacidad de almacenamiento de un electrodo, sobretodo cuando se combina con el crecimiento de biofilm. Por todo ello, es necesario potenciar el estudio de los electrodos capacitivos en CCMs en el futuro e investigar sobre su posible aplicación en otros sistemas bioelectroquímicos.

Carbón Activado Granular

Entre los electrodos capacitivos, el carbón activado (CA) granular ha mostrado un alto potencial, ya que tiene una estructura tridimensional, es biocompatible, está fácilmente disponible y es barato. Los gránulos de CA se utilizan en muchos sistemas de reactores, como por ejemplo los reactores de lecho fluidizado, donde un flujo de gas a velocidades suficientemente altas mantiene los gránulos en suspensión. Así, los gránulos de CA se fluidizan en el reactor mientras son cargados por las bacterias electroactivas que crecen en ellos y oxidan la materia orgánica, y se descargan al tocar el colector de corriente. Debido a que el rendimiento de los reactores de lecho fluidizado es aún bajo en términos de producción de corriente, se necesita un estudio científico básico sobre los gránulos de CA para comprender mejor, por un lado, los procesos químicos y físicos que ocurren durante su carga y descarga eléctrica y, por otro lado, la interacción entre el electrodo y el biofilm electroactivo.

Con este objetivo, esta tesis se centra en el estudio de gránulos de CA individuales. En el **Capítulo 3** el principal propósito es investigar el efecto del tamaño y tipo de los gránulos, ya que pensamos que son parámetros de diseño importantes a considerar para su aplicación a gran escala. Para realizar un estudio comparativo sobre el efecto del tamaño y tipo de los gránulos, así como realizar análisis estadísticos, fue crucial diseñar una configuración que permitiera la medición y el control simultáneo de varios gránulos de CA individuales (hasta 24) en las mismas condiciones operativas, es decir, una CCM con múltiples ánodos. Los resultados indican que el crecimiento del biofilm, el cual se evaluó en base al contenido total de nitrógeno y la producción de corriente, tiene una relación lineal con la superficie exterior calculada de los gránulos de CA. Los gránulos más pequeños de CA obtuvieron una mayor producción de corriente volumétrica, por lo que son

preferibles su utilización en comparación con los gránulos más grandes. El tamaño de los gránulos, por el contrario, no afectó al almacenamiento de carga eléctrica, lo que nuevamente indica que los gránulos pequeños son preferibles para un rendimiento volumétrico más alto. En cuanto al tipo de gránulo, se analizaron dos tipos de CA comercialmente conocidos como PK, activado a partir de turba y GAC, activado a partir de hulla. A pesar de las diferencias en su superficie específica, así como en su tamaño y distribución de poros, no se encontraron diferencias significativas en el crecimiento del biofilm o el almacenamiento de carga eléctrica. El hecho de que los bioánodos granulares se controlaran continuamente con un determinado potencial y bajo condiciones similares, podría haber sido más determinante en el rendimiento general de los gránulos que sus propias propiedades físicas.

Crecimiento del Biofilm y su Conductividad Eléctrica

La interacción entre el biofilm y el electrodo es de suma importancia en el rendimiento de una CCM. Como ya se ha mencionado anteriormente, una superficie de electrodo más grande permite más sitios catalíticos que aumentan la transferencia de electrones y, por lo tanto, la producción de corriente de los bioánodos. En el caso de los gránulos de CA, éstos tienen una estructura porosa muy compleja que hace que sea muy difícil determinar cuál es exactamente la superficie que utilizan las bacterias. Esto es importante cuando, por ejemplo, se quiere normalizar la producción de corriente en base a la superficie del electrodo o determinar el volumen de poro que las bacterias podrían utilizar para crecer. Con el objetivo de conocer más de cerca el crecimiento del biofilm en los gránulos de CA, se recolectaron gránulos de PK (también de una CCM con múltiples bioánodos) en 10 etapas de crecimiento diferentes para ser visualizados con imágenes por resonancia magnética (IRM), tal y como se explica en el **Capítulo 4**. Las IRM, al contrario que otras técnicas de microscopía, pueden proporcionar imágenes en 3D de alta resolución del biofilm que crece en un electrodo granular, rugoso, opaco y quebradizo, como es el caso de los gránulos de CA. El procedimiento experimental se optimizó para poder diferenciar entre el biofilm y el CA, así como para realizar mediciones de alta resolución ($(28\ \mu\text{m})^3$) en tiempos razonablemente cortos ($< 24\text{h}$). Aunque se demostró que la técnica de IRM es muy útil para visualizar el biofilm en 3D de forma no invasiva, las imágenes no permitieron determinar la interfaz entre el biofilm y el gránulo de CA, ni tampoco el crecimiento bacteriano en los poros internos del gránulo. De todas formas, se pudo determinar una relación lineal entre el volumen del biofilm obtenido en las diferentes etapas de crecimiento y la carga eléctrica total producida (es decir, la corriente eléctrica) así como el contenido de nitrógeno (es decir, el crecimiento de la biomasa) de los bioánodos granulares.

Además de la interacción entre el biofilm y el electrodo, los mecanismos de transferencia de electrones a través del biofilm han sido motivo de muchos estudios de investigación. En los biofilm electroactivos, la transferencia directa de electrones es un

mecanismo bien conocido que realizan las bacterias a través de estructuras conductoras (pili/nanocables) o proteínas redox como los citocromos. Sin embargo, la transferencia directa de electrones no sólo se ha encontrado en biofilms electroactivos, sino también en otros nichos biológicos (como los sedimentos marinos) o en agregados microbianos (como la biomasa granular anaeróbica). Al determinar la conductividad eléctrica de estos últimos agregados, se puede evaluar su capacidad de transferir electrones. La única biomasa granular anaeróbica que se ha sometido a prueba de conductividad eléctrica y que procede de reactores de tratamiento de aguas residuales a gran escala, es la procedente de cervecerías. Por ese motivo, en el **Capítulo 5** evaluamos la conductividad eléctrica de 28 biomasas granulares anaeróbicas de diversas plantas de tratamiento de aguas residuales a gran escala. Los resultados mostraron una gran variabilidad de la conductividad eléctrica, lo que indica que la biomasa granular anaeróbica procedente de cervecerías y otras industrias de producción de alcohol no son consistentemente conductivas. A pesar de que se encontró una correlación positiva entre la conductividad eléctrica y las concentraciones de hierro y azufre medidas en los gránulos, no se observó relación alguna con la comunidad microbiana, estructura de superficie u otros elementos. Con estos resultados, concluimos que la variabilidad y la complejidad de los reactores a gran escala dificultan la dilucidación de los desencadenantes para la conductividad eléctrica en la biomasa granular anaeróbica.

Laburpena

Mikrobio Erregai-Pila Kapazitiboak

Hondakin-ura elektrizitate ekoizpenerako oso iturri egokia da, izan ere, dituen materia organiko eta elikagai inorganikoak (nitrogeno, fosfato eta potasio) berreskuratu edo bestelako produktu baliagarrietan bihurtu ahal dira (adibidez, metanoa edo produktu kimikoak). Hondakin-ura ingurunera bota aurretik garbitzea ezinbestekoa da kutsadura arazoak sortu ez ditzan, besteak beste, eutrofizazioa (algen gehiegizko hazkundera). Testuinguru honetan, mikrobio erregai-pila (MEP) ur kutsatuen tratamendu prozesuari etekina atera ahal dion teknologia da, hondakin-uraren materia organikotik elektrizitatea modu eraginkor eta jasangarri batean sortuz eta karbono dioxidoaren isuria neutrala mantenduz.

Mikrobio erregai-pilek bi konpartimentu dituzte, anodo bat eta katodo bat, bereizten dituen mintza bat erdian izanik (hautazkoa). Anodoan, mikroorganismoek edo, bestela esanda bakteriatik elektroaktiboak, materia organikoa oxidatu eta ondorioz elektroiak sortzen dituzte. Normalean, bakteriatik hauek azal eroale batean (elektrodoan) hazten dira, zein elektroio hartzaile gisa jarduten duen, bioanodo bat osatuz. Elektroiak anodotik katodora zirkuitu elektriko baten bidez transferitzen dira. Modu honetan, katodoan erredukzio-erreakzio bat gertatzen da; ohikoena oxigenoa ur bihurtzea da, baina hidrogenoaren ekoizpena posiblea ere bada korrante elektriko osagarri bat erabiliz gero. Mikrobio erregai-pilek hondakin-uraren beste tratamendu teknologiekiko abantailak dituzte; alde batetik, ez dute aireztapenaren (oxigenoaren) beharrik prozesu aerobikoek bezala eta, bestetik, elektrizitatea zuzenean ekoiztu ahal dute tarteko produktuak ekoiztu ordez (esaterako metanoa, digestio anaerobikoan gertatzen den moduan). Hala ere, gaur egun MEP-en elektrizitate ekoizpena ez da behar bezain altua merkatuan lehiakorrek izateko. Arrazoi nagusien artean, alde batetik, MEP-en barruan gertatzen diren energia-galerak (erresistentziak) daude, zein potentzia elektrikoa murrizten duten eta, beste aldetik, kapital koste handiko materialak, hala nola, mintzak edo zenbait elektrodo mota.

Ikerketa honetan, MEP kapazitiboaren kontzeptua aurkeztzen dugu, hau da, elektrodo kapazitiboaren erabilera oinarritzen dena. Alegia, horretan datza MEP klasikoekiko ezberdintasun handiena. Elektrodo kapazitiboak eroale elektriko onak izateaz gain, oso porotsuak dira. Porositate maila altu horrek, bakteriatik hazteko azalera handia eskaintzen du alde batetik, eta karga elektrikoaren biltegiratzeak aukera ematen du bestetik. Biltegiratzea geruza elektriko bikoitza (ingelesez, EDL) osatzearen ondorioa da, hau da, elektrodoaren eta elektrolitoaren (hondakin-uraren) arteko interfazearen karga positiboz eta negatiboz osatutako geruza sortzearen ondorioa.

MEP eta geruza bikoitzeko kondentsadoreen (ingelesez, EDLCs) arteko konbinazioa tesi honen **2. Kapituluan** xehetasunez azaltzen da. Geruza bikoitzeko kondentsadoreak MEP-aren kanpoan edo, ordez, barruan integraturik jarri daitezke. Karga elektrikoaren biltegiratzeak, elektrodotik karga hori eraginkortasun handiagoarekin eta energia-galera

gutxiagorekin isuri ahal izatea du ondorioztat, era berean, potentzia elektriko handiagoa sortuz. Halaber, elektrodoaren karga/deskarga prozesuak denboran eta espazioan bereiztea posiblea egiten ditu (hau da, aldizkako operazio modua izatea), hondakin-urak garbitzeko errektore-diseinu berriak aurkitzeko aukerak irekiz. Modu honetan, MEP kapazitiboek teknologia hau aplikaziotik gertuago egotea ahalegintzen dute. Hala ere, geruza elektriko bikoitzaren osaera konplexua da eta parametro askoren menpe dago. Beraz, elektrodoen biltegitratze ahalmena neurtzea erronka bat da, are gehiago biofilm hazkundearekin konbinatuta daudenean. Beraz, elektrodo kapazitiboen inguruko ikerkuntza lanak etorkizunean jarraitzea ezinbestekoa da, baita beste sistema bioelektrokimikoetan egon daitezkeen aplikazioak aztertzea ere.

Ikatz Aktibatu Granularra

Ikatz aktibatu (IA) granularrak ahalmen handia erakutsi du elektrodo kapazitibo gisa, hiru dimentsiotako egitura duelako, biobateragarria delako, erraz lortu daitekeelako eta merkea delako. IA-zko granuluak errektore-sistema askotan erabiltzen dira, esaterako, ohe fluidizatuen errektoreetan non abiadura handiko gas-fluxuek granuluak soluzioan esekita mantentzen dituzten. Beraz, alde batetik, bakterio elektroaktiboek granuluak elektrikoki kargatzen dituzte hondakin-ura garbitu bitartean eta, bestetik, karga elektriko hori granuluak elektrodi hartzailearekin kontaktuan jartzerakoan askatzen da. Korrante ekoizpenari dagokionez, ohe fluidizatuen errendimendua oraindik baxua denez, IA-zko granuluen oinarritzko ikerketa beharrezkoa da karga/deskarga elektrikoan gertatzen diren prozesu fisiko eta kimikoak hobeto ulertzeko, baita elektrodoaren eta biofilm elektroaktiboaren arteko interakzioa hobeto ezagutzeko ere.

Helburu horrekin, banakako IA-zko granuluen azterketan oinarritzen da tesi hau. **3. Kapitulu**an, helburu nagusia granuluen tamaina eta motaren eraginak ikertzeko da, eskala handiko aplikazioetan garrantzitsuak diren bi diseinu-parametroak baitira. Lan konparatibo on bat eta estatistika lanak egin ahal izateko, banakako granulu askoren (24) aldi bereko neurketak ahalbidetzen zituen errektore konfigurazio bat erabili zen, anodo anitzen MEP-a alegia, non granulu guztiak baldintza berdinetan zeuden. Granuluen tamainari dagokionez, biofilm hazkundearen (nitrogeno-edukia eta karga elektrikoaren neurketetan oinarritua) eta IA-zko granuluen azaleraren arteko harreman zuzena aurkitu zen. Granulu txikienei, korrante ekoizpen bolumetrikoki handiagoa erakutsi zuten granulu handiagoek baino, beraz, zentzu horretan errektoreetan erabiltzeko hobeagoak izanik. Granuluen tamainak, ordea, ez zuen ondorioz izan granuluen karga biltegitratzeari dagokionez. Honek, granulu txikiak erabilerak errektore batetan etekin bolumetrikoki handiagoa izango duela erakusten du berriz ere. Tamainaz gain, bi granulu mota aztertu egin ziren ere: komertzialki PK (zohikatzetik aktibatuta) eta GAC (harrikatzetik aktibatuta) bezala ezagutuak. Nahiz eta granulu mota ezberdinek azalera espezifiko edota poroen tamaina eta banaketa ezberdinak izan, biofilm hazkundera eta karga biltegitratzea oso antzekoak izan ziren bi kasuetan. Antzeko errendimendu honek granuluak baldintza

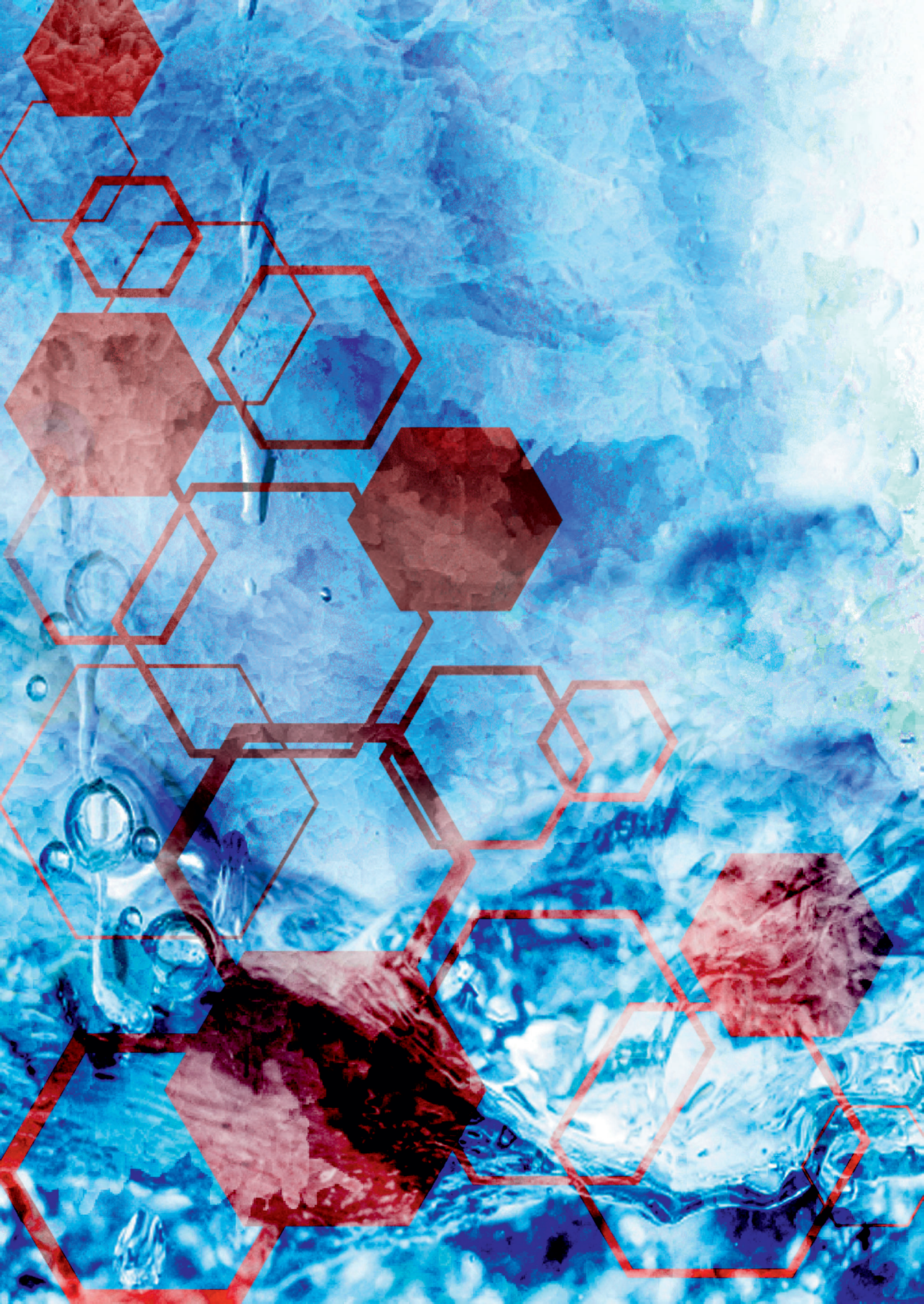
berdinetan eta potentzial jakin batean kontrolatuak izatearen ondorioa direla pentsarazten digu eta ez, ordea, granuluen propietate fisikoekin erlazionatutako zerbait.

Biofilm-aren Hazkundera eta Eroankortasun Elektrikoa

Biofilm-aren eta elektrodoaren arteko harremana ezagutzea funtsezkoa da, MEP-aren errendimendua mugatu ahal baitu. Azalera handiko elektrodo batek gune katalitiko gehiago ahalbidetzen ditu, elektroli transferentzia hobetuz eta, era berean, bioanodo-en elektrizitate ekoizpena handituz. IA-zko granuluen egitura porotsua oso konplexua da. Honek, bakteriek zehatz-mehatz erabiltzen duten edo erabili dezaketen elektrodoaren azalera (poroak kontuan izanda) zehaztea zailtzen du, baita elektrizitate ekoizpena elektrodoaren azalerarekiko estandarizatzea ere. Biofilm-aren hazkundera IA-zko granuluetan hobe ezagutzeko, anodo anitzen MEP-a (PK granuluekin) erabiliz 10 bioanodo erreaktoretik hartu ziren hazkunde momentu ezberdinetan eta erresonantzia magnetiko bidezko irudigintza (ingelesez, MRI) egin zen, tesiaren **4. Kapituluan** azaldu bezala. Beste teknika mikroskopikoak ez bezala, erresonantzia magnetiko bidezko irudigintzak biofilm-aren bereizmen handiko 3D irudiak har ditzake borobil, zimurtsu, opakua eta hauskorra den elektrodo batean. Hau da, alegia, IA-zko granuluen kasua. Erabilitako prozedura esperimentalak optimizatu egin zen, alde batetik biofilm-a eta IA-aren artean behar bezala bereiztu ahal izateko eta, bestetik, bereizmen handiko neurketak ((28 μm)³) ahal bezain denbora laburrean (< 24h) burutzeko. Ikerketa honetan, erresonantzia magnetiko bidezko irudigintza biofilm-aren 3D irudiak modu ez inbaditzaile batean ateratzeko eta biofilm bolumena zehazteko oso teknika baliagarria dela erakusten dugu. 10 hazkunde ezberdinetako biofilm bolumenaren eta ekoiztutako karga elektrikoaren (hau da, korrante elektrikoaren) eta nitrogeno-edukiaren (hau da, biomasa hazkunderaren) arteko erlazio zuzena aurkitu zen. Hala ere, lortutako irudiekin ezin izan zen biofilm eta granuluen arteko interfasea zehazki zehaztu, ezta bakterien hazkundera granuluen barruko poroetan ikusi ere.

Biofilm-a eta elektrodoaren arteko harremanaren antzera, ikerketa askoren gaia izan da biofilm-aren barrena dauden elektroli transferentzia mekanismoak aztertzea. Zuzeneko elektroli transferentzia oso mekanismo ezaguna da biofilm elektroaktiboetan, non bakteriek egitura eroaleen bidez (pili/nano-kableak) edo erredox proteinen bidez (zitokromoak) transferitzen dituzten elektroliak. Hala ere, zuzeneko elektroli transferentzia ez da soilik biofilm elektroaktiboetan aurkitzen, baita beste nitxo biologikoetan (itsas sedimentuetan bezala) edo agregatu mikrobiologikoetan ere (adibidez, biomasa granular anaerobikoetan). Agregatu mikrobiologikoek elektroliak transferitzeko duten gaitasuna zehazteko, bere eroankortasun elektrikoa neurtu daiteke. Momentuz, literaturan neurtu den biomasa granular anaerobiko bakarra, eskala handiko erreaktoretik sortua, garagardo-lantegitik sortutako ur-hondakinak garbitzen dituen biomasa izan da. Horregatik, **5. Kapituluan** eskala handiko oso industria ezberdineko (28) biomasa granular anaerobikoen eroankortasuna balioztatzen dugu. Emaizak oso aldakorrak izan ziren, non

garagardo edo bestelako alkohol-ekoizpen lantegiko biomasa ez zuen beti eroankortasuna erakutsi (literaturan esan bezala). Biomasaren eroankortasun elektrikoa eta bere burdin eta sufre edukiaren arteko harreman positiboa aurkitu egin zen. Ordea, ez zen biomasa eroankortasunaren eta bere mikrobio komunitatearen, azalera egituraren edota beste elementu kimikoen arteko harremanik aurkitu. Orokorrean, eskala handiko erreaktoreen konplexutasunaren eta aldakortasunaren ondorioz, biomasa granular anaerobikoak eroankortasun elektrikoa izatearen arrazoia zehazki aurkitzea oso lan zaila da.



Acknowledgments



My first thanks to my supervisor, Annemiek, who trusted me and gave me the opportunity to be part of her team. It has been a true pleasure to have this ride with you, which I think both of us enjoyed and where we managed to team up and bring the work forward. I appreciate your always positive attitude, kindness, constructive feedback and constant support towards me. I feel very lucky for having had the opportunity of working with you, as you taught me many aspects related to the supervision, scientific career and at a personal level that I will always carry with me in the future.

My thanks also to my promotor, Cees, for supporting me from the very beginning and also challenging me throughout these years of research at ETE. You gave me a different vision of science, from a more industrial and applied point of view, and helped me to communicate in a more clear, practical and simplified way. Thank you as well for the advice on the body language during my last oral presentation, which apparently paid off.

I would like to thank the technical staff at the department for all the support you gave me with my experiments and your contribution on making the labs at ETE a pleasant place to work in. Those in the analytical lab for helping me with the different devices and analyses, and those in the Modutech for your support on the design and construction of reactors. Special thanks to Vinnie and Livio for your patience and flexibility with my late working hours in the lab. I would like to also thank all the technicians I had the pleasure to work with at Wetsus, specially Agnieszka for all the *long-distance* discussions and arrangements and fully-scheduled measurement days. Special mention to Willem, from Ilium Technologies, for his electrochemistry lessons and for providing me with many software updates.

My special thanks to the colleagues who were involved and helped me on the research. Dandan, you have been a very big support since the beginning, mostly with the setting up of experiments but also with your many *senior* advices about the PhD life. Casper, you entered this *capacitive* adventure a bit earlier than me and we have shared our challenging research ever since. It has been a pleasure to share all the meetings, discussions, Wageningen/Leeuwarden journeys and nice trips to China, France, Rome and Newcastle. Ludo, my *Australian* colleague, thanks for all the helpful knowledge you transferred to me and your willingness to do so, mostly when we had a project in common. Tom, thank you for been a big support at Wetsus back in my Master's period and during the writing of the review paper, as well as for being such an approachable person to talk and share opinions with. Julia, I was so lucky to be able to collaborate with you in a project, we worked very hard but had a lot of fun at the same time. Thank you for the many explanations on the *amazing* MRI technique, the enthusiasm for research you have shown me and your persistence with our common project. Also, thanks to all the students I had the opportunity to supervise (Lucia, Vincent, Xuan, Marta, Roos and Ivonne) for their nice contribution to the research and for helping me to become a better supervisor. To my lab-mates, thank you Ivonne, for sharing with me both the funniest and hardest moments; Roxanni, for always offering your help mostly when my reactors needed some extra care; and Annemerel, for cheering up the lab work with music contests. And then thanks to many

others I had discussions with in the daily basis and from whom, at some point, I needed the support with a specific work-related (or Dutch-translating, also quite often) matter.

To all the staff and colleagues of ETE in general, I feel very lucky for having been part of this department and having met you. I think you all contribute to make this place special and boost a nice work atmosphere. I take with me all the nice moments shared in the coffee breaks, lunch times, borrels, all the togetherness activities like the Christmas dinners, department trips, WE-days, birthday celebrations or ice cream times; loved them all! The China trip was also an unforgettable experience for me, where I had the opportunity to get to know some of you better. I would like to make a special mention to the secretary team that keeps all the gears of ETE running; in my case, mostly thanks to Liesbeth and Gea for helping me a lot during the PhD and solve many of my doubts. I would like to particularly thank the Dutch people for making me feel comfortable in the Netherlands and showing me part of your culture and way of living, which I will always carry with me. Also to the spin-off of ETE, the *Stich and Bitch* club, for promoting my motivation for knitting and learning new stuff, but mostly for sharing many fun moments (and gossips) with me. Delaram, thank you for being such an important person for me and nice housemate in the last years and for all the kindness you have shown me. And also, Lucia, for been so generous with me and for even formalizing our relationship by introducing me to your parents.

I would like to emphasize the support of my officemates during my PhD, who I consider my family at ETE. I have felt really comfortable sharing the working place with you, until the very end, as you helped me a lot with maintaining my motivation and general performance at work. I loved all the dinners we had together, as I found them really fun and learnt many culinary tricks. Dandan, already told you what your support meant to me, special thanks for making me feel less lonely during some weekend-working days. Azzie, you were so sweet with me, patient, always willing to help me (mostly with my lack of knowledge in photoshop), sharing all the nice adventures of your trips and bringing me super nice souvenirs from all around the world. Emilius, you are such an easy-going person, always relaxed and with a positive attitude towards any problem. Thank you for sharing with me all the amazing cultural and historical background of your country. Laura, the *center* of the office, we were so lucky you landed in no matter the *little* space. Thanks for all the chats, jokes and the fun moments we had together, for being such an amazing person and for making me feel like I have known you forever. And no, you don't complain *that* much. Rosanne, my most creative friend ever, thank you for your friendship, for sharing with me many of your interesting projects, for being a person who inspires me, for taking care of me (and the plants surrounding me) and for letting me enjoy your handmade jewelry. And please, forgive me for not being such an active person in the gym.

También me gustaría agradecer a la gente con la que he tenido la oportunidad de compartir momentos fuera del departamento. A Karin y a Laura, por preocuparos por mí y ser una vía de escape a la rutina de trabajo en Wageningen. A Ramón, Xabi y Jordi, el trio *lerele* de Droevendaal, que siempre me habéis abierto las puertas de vuestra casa, con

energía infinita y ganas de hacer planes. Y como no a Marko, que nuestro destino se volvió a juntar en tierras holandesas y nos dio la oportunidad de compartir nuevos momentos juntos. Gracias a ti también, Luis, por ser un gran apoyo en mi día a día, ayudarme a entender lo que necesitaba en cada momento, ser tan generoso conmigo, por todo lo que me has enseñado y por dejarme descubrir un mundo nuevo a través de ti. A mis amigas/os de Tuter (Aleio), Iruñea (Hintz) y Auzperri (Kuadrillatxo), porque sin vosotras/os nada tendría sentido. Gracias a todas/os por mantener muy presentes mis raíces, por estar allí siempre que he vuelto a casa y por hacerme sentir querida por todas/os vosotras/os aun estando tantos años fuera. Y darte las gracias especialmente a ti, Rakel, por ser una artista y haber diseñado la portada de este libro. También a mis biotecnólogas favoritas, Cappont, porque el tiempo se para siempre que nos juntamos. Sois lo mejor que me podría haber pasado en Lleida y siempre os llevaré conmigo.

Por último, me gustaría acabar dando las gracias a mi familia, tanto a la tudelana como a la espinalera, por ser un gran apoyo para mí y representar un pilar tan sólido en mi vida. Tengo muchísima suerte de teneros como familia y quiero dar las gracias a cada una/o de vosotras/os por ser tal y como sois conmigo. Especialmente a ti, ama, por estar siempre tan pendiente de mí, cuidarme tanto y ser tan generosa conmigo. Y a ti, aita, por tu energía y tu disposición siempre que he necesitado tu ayuda. Gracias a los dos por confiar en mí, por darme alas y por abrirme las puertas a muchas de las oportunidades que he podido tener en mi vida, porque sin vosotros no hubiera podido llegar a donde hoy estoy. A ti, Urko, por ser siempre tan cariñoso conmigo y echarme tanto de menos todos estos años. Y, finalmente, dar las gracias a mi abuela por ser un referente en mi vida y por haberme transmitido su espíritu luchador, su humildad, su amabilidad infinita y su amor incondicional.

About the author



Leire was born on the 24th of April, 1990, in Tudela (Navarra), a city in the north-east of Spain. After going to the 'Ikastola Argia' school for 12 years, she moved to Pamplona to finish her high school studies in 'San Fermin Ikastola'. After that, she did her Bachelor studies in Biotechnology at the University of Lleida, Spain, where she got the degree in 2012. For her last year, she entered the Erasmus Programme and was able to continue her studies at the University of Helsinki (Viikki campus).

As her interest on green technologies and sustainable processes increased, she got accepted for the master program of Biosystems Engineering at the University of Wageningen, under the specialization of Environmental Engineering. Her Master thesis was about wood degradation for sustainable heat production, which she did at the department of Environmental Technology. She got her degree in 2014. Soon after, she started her PhD research at the same department on the field of Microbial Fuel Cells. Her main focus was the study of granular activated carbon for bioanodes, i.e. the combination of porous electrodes with electroactive bacteria for the production and storage of electricity from wastewater.



*Netherlands Research School for the
Socio-Economic and Natural Sciences of the Environment*

D I P L O M A

For specialised PhD training

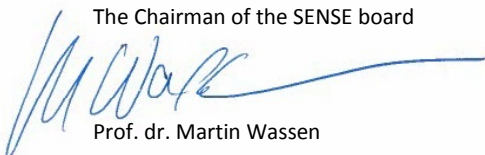
The Netherlands Research School for the
Socio-Economic and Natural Sciences of the Environment
(SENSE) declares that

Leire Caizán Juanarena

born on 24 April 1990 in Tudela, Spain

has successfully fulfilled all requirements of the
Educational Programme of SENSE.

Wageningen, 14 June 2019

The Chairman of the SENSE board

Prof. dr. Martin Wassen

the SENSE Director of Education

Dr. Ad van Dommelen

The SENSE Research School has been accredited by the Royal Netherlands Academy of Arts and Sciences (KNAW)



K O N I N K L I J K E N E D E R L A N D S E
A K A D E M I E V A N W E T E N S C H A P P E N



The SENSE Research School declares that **Leire Caizán Juanarena** has successfully fulfilled all requirements of the Educational PhD Programme of SENSE with a work load of 44.3 EC, including the following activities:

SENSE PhD Courses

- o Environmental research in context (2015)
- o SENSE summer symposium: Make a change! Successful interaction with society in sustainability sciences (2015)
- o Teaching and supervising Thesis students, Wageningen University (2016)
- o Research in context activity: 'Co-organizing and excellent reporting on preparation of: 5th Wageningen PhD Symposium 2018: "Bridging Science & Society: Unifying Knowledge" (Wageningen, 17 May 2018)'

Selection of other PhD and Advanced MSc Courses

- o Coupled processes in chemistry, physics and biology, Wageningen University (2015)
- o European Summer School Electrochemical Engineering, Leeuwarden (2015)
- o Techniques for writing and presenting a scientific paper, Wageningen University (2016)
- o Dynamic models in R, Wageningen University (2017)
- o Project and time management, Wageningen University (2017)
- o Competence assessment (2017) & Career perspectives (2018), Wageningen University

External training at a foreign research institute

- o "Tailoring the interface of porous graphite granules and electroactive biofilms for efficient bioelectrochemical systems", Institut des Sciences Chimiques de Rennes (2016)
- o PhD study trip to Tsinghua University, Chinese Academy of Sciences, Tongji University and others, China (2016)

Selection of Management and Didactic Skills Training

- o Supervising 5 MSc students and one BSc student with theses (2015-2018)
- o Assisting on the BSc courses 'Sustainability Transitions' (2014-2018), 'Principles of environmental sciences' (2017) and 'Introduction to Environmental Technology' (2017)
- o Member of the Lab Committee at the Environmental Technology Group (2015-2018)

Selection of Oral Presentations

- o *Characterization of single activated granules for their application in bioanodes*. 5th IWA Regional Young Water Professionals Conference Benelux, 5-7 July 2017, Ghent, Belgium
- o **Best presentation award: 3D biofilm visualization on single activated carbon granules with Magnetic Resonance Imaging**. International Society for Microbial Electrochemistry and Technology, 4th European Meeting, 12-14 September 2018, Newcastle, United Kingdom

SENSE Coordinator PhD Education

Dr. Peter Vermeulen

The research described in this thesis was financially supported by Wetsus, co-funded by the Dutch Ministry of Economic affairs, Ministry of Infrastructure and Environment, the province of Friesland and the Northern Netherlands provinces.

Financial support from both Wageningen University and Wetsus for printing this thesis is gratefully acknowledged.

Cover design by my friend, Rakel Arbizu.

Printed by ProefschriftMaken (www.proefschriftmaken.nl)

This thesis is printed on FCS certified paper.

